CARBONATE SEQUESTRATION IN THE PACIFIC, INDIAN, AND ATLANTIC OCEANS OVER THE CENOZOIC

FARANAK DALVAND

ORCID: 0009-0001-2478-4749

This thesis is submitted in fulfilment of the requirements for the degree of Doctor of Philosophy

Supervisor: A/Prof. Adriana Dutkiewicz

Associate Supervisors: Dr Nicky M. Wright & Dr Ben R. Mather

School of Geosciences
Faculty of Science

The University of Sydney
New South Wales, Australia

2026

Declaration

I declare that this thesis contains fewer than 80,000 words, exclusive of tables, figures, bibliographies, and appendices. This thesis is my own original work and has not been submitted, in whole or in part, for a higher degree at any other university or institution.

This thesis contains no material previously published or written by another person except where due reference is made in the text. Parts of this work have been presented at academic conferences. Any work undertaken in collaboration with others has been clearly acknowledged.

Copilot was used solely for language refinement purposes, including spelling correction, minor sentence restructuring, and improvements in clarity. All AI-assisted modifications were carefully reviewed to ensure accuracy, correctness, and the absence of bias.

The software, *pyBacktrack 1.4*, was used solely as a computational tool and did not generate any of the intellectual content of this thesis. All photographs and images presented in this thesis are from my personal archive, except where alternative sources are clearly acknowledged.

Signature:

Name: Faranak Dalvand

Date: February 2026

Acknowledgments

This thesis would not have been possible without the support, guidance, and encouragement of many individuals to whom I am deeply grateful.

First and foremost, I would like to express my sincere gratitude to my supervisor, A/Prof Adriana Dutkiewicz, for providing me with the invaluable opportunity to work and pursue my research aspirations under her guidance over the years. Her distinctive scientific expertise, intellectual generosity, patience, and unwavering guidance have shaped both this research and my development as an independent scientist. Without her support, I would not have come this far.

I am equally appreciative of my associate supervisor, Dr Nicky Wright, for her valuable advice, constructive discussions, and continuous support at every stage of my doctoral journey. Her exceptional expertise and thoughtful engagement significantly enhanced the scientific quality of this research.

I would also like to sincerely thank Prof Dietmar Müller for his generous guidance, insightful advice, and for developing, in collaboration with my supervisor, the methodological framework that underpins this work. His scientific vision and unique expertise have supported and enriched this research throughout its entire development. It has been a privilege to work alongside such esteemed academics and to learn from them.

I further express my sincere appreciation to Dr Ben Mather, who served as my associate supervisor during the first project on the Pacific Ocean, for his guidance, outstanding scientific insight and valuable contributions, which laid an important foundation for this thesis.

I extend my sincere thanks to the School of Geosciences and the EarthByte Group for their support and for fostering a collaborative and stimulating research environment that provided the foundation for this work. I am also grateful to colleagues and fellow researchers within the EarthByte Group for their valuable discussions, technical assistance, and collegiality.

I would also like to acknowledge the financial support provided by the Australian Research Council (ARC) grant FT190100829, which funded my scholarship and research. I also acknowledge the Faculty of Science Research Tuition Fee Scholarship and additional financial support from the School of Geosciences. The pyBacktrack and GPlates software used in this project was supported by the AuScope Simulation, Analysis and Modelling node funded by the Australian Government through the National Collaborative Research Infrastructure Strategy, NCRIS.

My sincere thanks go to my friends for their encouragement and companionship during both challenging and rewarding times throughout this journey.

Finally, I wish to express my heartfelt appreciation to my family, my parents, especially my sister Zara and her husband Mike, and my love, Sam, for their love, patience, and belief in me. Their support has been the foundation of my perseverance, and this achievement is as much theirs as it is mine.

Authorship Attribution

This thesis is structured around the following three articles:

ARTICLE 1: Dalvand, F., Dutkiewicz, A., Wright, N. M., Mather, B. R., & Müller, R. D. (2025). Regional carbonate compensation depth variability in the Pacific Ocean since the Oligocene. *Frontiers in Earth Science*, 13(1605906). (Published on 18 June 2025) DOI: https://doi.org/10.3389/feart.2025.1605906

I conceived and designed this study in collaboration with A.D., N.M.R., B.M., & R.D.M. The modelling framework was developed by R.D.M and A.D. I co-designed the study, conducted the data analysis, produced all figures and tables, and wrote the drafts of the manuscript, which were reviewed and edited by all co-authors.

This Article contains material previously published in https://doi.org/10.5281/zenodo.15116747. This material comprises all the datasets in this study, supplemental text, figures, and tables.

ARTICLE 2: Dalvand, F., Dutkiewicz, A., Wright, N. M., & Müller, R. D. (2025). Indian Ocean carbonate compensation depth since the Late Oligocene. *Geo-Marine Letters*, 45(38), 1-14. (Published on 04 November 2025) DOI: https://doi.org/10.1007/s00367-025-00825-5

I conceived and designed this study in collaboration with A.D., N.M.R., & R.D.M. The modelling framework was developed by R.D.M and A.D. I co-designed the study, conducted the data analysis, produced all figures and tables, and wrote the drafts of the manuscript, which were reviewed and edited by all co-authors.

This Article contains material previously published in https://doi.org/10.5281/zenodo.17232379. This material comprises all the datasets in this study, supplemental text, figures, and tables.

ARTICLE 3: Dalvand, F., Dutkiewicz, A., Wright, N. M., & Müller, R. D. (2026). Cretaceous to Cenozoic Carbonate Burial Variability Across the Atlantic, Pacific and Indian Oceans. (Submitted to the Journal of *Marine Geology* in February 2026)

I conceived and designed this study in collaboration with A.D., N.M.R., & R.D.M. I co-designed the study, conducted the data analysis, produced all figures and tables, and wrote the drafts of the manuscript, which were reviewed and edited by all co-authors.

This Article contains material previously published in https://doi.org/10.5281/zenodo.18755594. This material comprises all the datasets in this study, supplemental text, figures, and tables.

In addition to the authorship attribution statements above, in cases where I am not the corresponding author of a published item, permission to include the published material has been granted by the corresponding author.

Faranak Dalvand, February 2026

As supervisor for the candidature upon which this thesis is based, I can confirm that the authorship attribution statements above are correct.

Adriana Dutkiewicz, February 2026

Abstract

Deep-sea carbonate records serve as essential archives for reconstructing long-term global carbon cycle dynamics, providing direct evidence of variations in ocean chemistry, carbon sequestration, and climate evolution through geological time. The distribution of pelagic carbonates is primarily governed by the carbonate compensation depth (CCD), the depth at which carbonate supply from the surface equals its dissolution. Therefore, the CCD acts as a sensitive proxy for oceanic carbonate saturation state, surface productivity, and deep-water chemistry. However, regional CCD reconstructions across the Pacific and Indian oceans remain poorly constrained due to limited data coverage and methodological constraints in previous studies.

This thesis addresses these limitations by reconstructing the evolution of the CCD across the Pacific and Indian oceans on regional scales during the Cenozoic. A comprehensive dataset, including lithology core logs, age-depth relationships, and carbonate contents and dry bulk density data, was compiled using drill sites of the Deep Sea Drilling Project (DSDP), Ocean Drilling Program (ODP), and International Ocean Discovery Program (IODP) expeditions. Variations in CCD were estimated using linear reduced major-axis regressions of carbonate accumulation rate (CAR) versus paleo-water depth at 0.5 Ma intervals. Paleo-water depths were reconstructed using *pyBacktrack 1.4 software*, accounting for both dynamic topography and eustatic sea-level changes. The Cenozoic CCD was modelled across six regions of the Pacific: western and eastern North Pacific, western tropical Pacific, eastern equatorial Pacific, and western and eastern South Pacific, and three regions of the Indian Ocean: western equatorial Indian, southeast Indian, and Southern Ocean. The results reveal pronounced regional CCD variability, with deeper CCDs in equatorial regions relative to higher latitudes, closely linked to changes in ocean circulation, gateway evolution, ice-sheet expansion, and climate transitions throughout the Cenozoic.

The results show that the Pacific CCD experienced pronounced variability of ~1–1.2 km during the Neogene period. Regional reconstructions since the early Miocene highlight the roles of Antarctic ice-sheet expansion, climate shifts, and Pacific gateway restructuring in shaping deep-water circulation and carbonate preservation. A marked west–east contrast emerges, with a distinct post-24 Ma deepening in the western Pacific linked to delayed oceanographic adjustments following West Antarctic ice-sheet expansion. The new CCD models also capture the late Miocene carbonate crash and biogenic bloom across the equatorial Pacific, with a ~1 Myr lag in the western tropical Pacific likely linked to the Panama Gateway constriction and Western Pacific Warm Pool (WPWP) dynamics. The absence of the carbonate crash in the western North Pacific underscores its predominantly equatorial expression.

In the Indian Ocean, the CCD exhibits regionally variable fluctuations of ~1–1.5 km over the past 15 Ma, with a long-term deepening from ~3.5 km in the late Oligocene to ~4.4 km by the Pliocene in the western equatorial basin. In contrast, the southeast and Southern Ocean sectors remained consistently shallower, oscillating between ~2.7–3.5 km and 3.4–4 km, respectively, reflecting latitudinal gradients in carbonate flux and seafloor bathymetry. The equatorial CCD fluctuations are variably attributed to atmospheric CO_2 changes, evolving Tethyan and Indonesian gateway dynamics, and the development of the Indo-Pacific water exchange. Elevated carbonate production aligns with the emergence of the Pacific Warm Pool and strengthened Indian monsoon circulation since the middle Miocene, culminating in the late Miocene biogenic bloom.

This research further presents the first basin-specific synthesis of CAR for the Atlantic, Pacific, and Indian oceans since the Cretaceous, providing a first-order reconstruction of global

carbonate flux maps derived from basin-based computations. This approach addresses a significant gap in earlier global assessments, which largely overlooked inter-basin variability. The Cretaceous CAR analysis reveals an unstable, spatially heterogeneous pelagic carbonate system that could reflect a greenhouse-world climate, episodic volcanic CO_2 inputs, and repeated carbon-cycle disruptions. Although constrained by sparse site coverage, particularly in the Pacific and Indian oceans, the sedimentary records reflect elevated mid-Cretaceous carbonate accumulation across the Atlantic and Pacific, followed by reductions in burial rates in the Late Cretaceous linked to major Ocean Anoxic Events (OAEs) and transient CCD shoaling. Basin-specific differences in CAR underscore contrasting oceanographic states: the Atlantic and Indian sectors display late-Cretaceous increases associated with emerging Southern Hemisphere deep-water formation and improved basin ventilation, whereas the Pacific remains persistently undersaturated and characterized by muted carbonate burial. Collectively, these patterns highlight the sensitivity of pelagic carbonate burial to rapid changes in ocean chemistry and circulation, reflecting the broader transition towards a more ventilated, carbonate-preserving global ocean system near the end of the Cretaceous period.

The Cenozoic deep-sea records reveal a fundamental shift from the heterogeneous carbonate burial patterns of the Cretaceous to a more stabilized Cenozoic system shaped by major gateway reorganizations and the establishment of modern thermohaline circulation. Although global CARs remained relatively stable, basin-specific trajectories diverged substantially. The Pacific shows the strongest and most sustained rise in carbonate burial since the early Oligocene, coinciding with widespread deepening of the CCD. The Atlantic Ocean shows two distinct peaks: one in the late Eocene, associated with Northern Component Water (NCW)–driven enhancement, and a second spanning the middle Miocene to early Pliocene, linked to Antarctic reglaciation, intensified North Atlantic Deep Water (NADW) formation, and the biogenic bloom. The Indian Ocean exhibits a pronounced intensification during the Neogene, driven by evolving Indo-Pacific circulation and Indonesian Seaway constriction, and the onset of a modern-like South Asian Monsoon. Across all major oceans, a coherent global rise in CAR between ~15 and ~5 Ma reflects the combined effects of major reorganizations in ocean circulation, Antarctic ice sheet expansion, and declining atmospheric CO_2. This interval is followed by a pervasive reduction in CAR since the Pliocene, most strongly aligned with the termination of the biogenic bloom and amplified by late Neogene-Quaternary reorganisations in ocean circulation and the onset of Northern Hemisphere glaciation. These results confirm that Cenozoic pelagic carbonate burial was shaped by strong inter-basin contrasts and sensitivity to tectonic evolution, water-mass ventilation, and major climatic transitions, rather than by a simple progressive increase through time.

This global synthesis of deep-sea carbonate accumulation rates provides an integrated perspective on how tectonic evolution, water-mass circulation, and productivity regimes have jointly regulated long-term variations in pelagic carbonate flux and CCD across the major ocean basins. Together, the results offer the most comprehensive view of the evolution of the deep-sea carbonate reservoir through geological time. By delivering basin-resolved constraints on carbonate burial and CCD dynamics, this study significantly advances the quantitative framework for reconstructing long-term oceanic carbon storage and establishes a robust foundation for evaluating how pelagic carbonate processes modulate Earth’s climate system over deep time.

Table of Contents

Declaration ii
Acknowledgments iii
Authorship Attribution iv
Abstract v
List of Abbreviations viii
1. Introduction 1
1.1. Background: Earth's long-term carbon cycle and marine carbonate burial 1
1.2. The carbonate compensation depth (CCD) 1
1.3. Carbonate burial, global and basin heterogeneity 2
1.4. Deep-sea carbonate burial shifts and spatiotemporal CCD variability 3
1.5. Advances in CCD reconstructions 5
1.6. Thesis motivation and significance 6
1.7. Thesis overview 7
1.8. Methodological framework and thesis approach 9
2. Article 1 10
Dalvand, F., Dutkiewicz, A., Wright, N. M., Mather, B. R. & Müller, R. D. Regional carbonate compensation depth variability in the Pacific Ocean since the Oligocene
3. Article 2 27
Dalvand, F., Dutkiewicz, A., Wright, N. M. & Müller, R. D. Indian Ocean carbonate compensation depth since the Late Oligocene
4. Article 3 42
Dalvand, F., Dutkiewicz, A., Wright, N. M. & Müller, R. D. Cretaceous to Cenozoic Carbonate Burial Variability Across the Atlantic, Pacific and Indian Oceans
5. Discussion 74
5.1. Global and basin-wide carbonate burial variability over the Cretaceous 74
5.2. Cenozoic carbonate burial transition: Paleogene CCD and basin-specific CAR variabilities 76
5.3. Neogene carbonate system and CCD shifts 79
5.4. Significance and future research 84
6. Conclusions 85
References 87
Appendix A 102
Supplement to Article 1
Appendix B 109
Supplement to Article 2
Appendix C 118
Supplement to Article 3

List of Abbreviations

CAR	Carbonate Accumulation Rate
CCD	Carbonate Compensation Depth
CO_2	Carbon Dioxide
DSDP	Deep Sea Drilling Project
EOT	Eocene–Oligocene Transition
IODP	International Ocean Discovery Program/Integrated Ocean Drilling Program
K-Pg	Cretaceous–Paleogene
MCO	Miocene Climatic Optimum
NADW	North Atlantic Deep Water
NCW	Northern Component Water
OAE	Ocean Anoxic Event
ODP	Ocean Drilling Program
PETM	Palaeocene–Eocene Thermal Maximum
SAM	South Asian Monsoon
WPWP	Western Pacific Warm Pool

1 | Introduction

1.1. Background: Earth's long-term carbon cycle and marine carbonate burial

The long-term evolution of Earth's climate is governed by the exchange of carbon among the atmosphere, oceans, biosphere, and solid Earth. Central to this system is the deep carbon cycle, which transfers carbon between Earth's surface and interior through subduction-related ingassing and volcanism-dependent degassing, thereby exerting first-order control over atmospheric carbon dioxide (CO_2) concentrations, ocean chemistry, and long-term climate stability across geological timescales (Dasgupta, 2013; Isson et al., 2020; Müller et al., 2022; Sleep & Zahnle, 2001). Variations in atmospheric CO_2 reflect the dynamic redistribution of carbon among interconnected reservoirs, including deep-sea sediments, the oceanic lithosphere, and the mantle, which collectively regulate the balance between long-term carbon sources and sinks (Berner, 2004; Müller et al., 2022; Omta et al., 2018; Wong et al., 2019; Zhang et al., 2024a).

Sediments entering subduction zones show pronounced compositional and stratigraphic heterogeneity, ranging from calcareous and siliceous ooze to clay-rich and terrigenous sediments, and exhibit substantial variations in thickness along downgoing plates (Dutkiewicz et al., 2017; Dutkiewicz et al., 2016). Among these lithologies, pelagic carbonate overwhelmingly dominates the subducting carbon inventory (Clift, 2017; Müller et al., 2022; Plank & Manning, 2019; Ridgwell & Hargreaves, 2007), contributing ~277 Mt C yr^{-1} to the total present-day deep carbon input of ~311 Mt C yr^{-1} through the oceanic plate settings (Müller et al., 2022). Pelagic carbonate is produced in the surface ocean (euphotic zone) primarily by planktonic calcifiers (e.g., coccolithophores and planktonic foraminifera) and exported to depth as particulate calcium carbonate ($CaCO_3$), commonly known as "carbonate rain" (Honjo, 1976; Honjo et al., 2008). A fraction of this exported carbonate is ultimately preserved in sediments that enter the Earth's interior; the remainder dissolves in the water column or at the sediment–water interface, returning carbon and alkalinity to the ocean (Archer, 1996; Ridgwell & Zeebe, 2005).

1.2. The carbonate compensation depth (CCD)

A primary control on deep-sea carbonate preservation is the CCD, which governs the balance between $CaCO_3$ dissolution and accumulation, and thus acts as a negative feedback that buffers changes in ocean alkalinity and atmospheric CO_2 over timescales of ~10^3–10^5 years (Broecker & Peng, 1987; Cartapanis et al., 2018; Dutkiewicz et al., 2018; Omta et al., 2018). The CCD is defined as the water depth at which the supply of carbonate to the seafloor equals its rate of dissolution, such that carbonate is absent from sediments below this level (Figure 1) (Lyle, 2003; Rae et al., 2021; van Andel, 1975). Changes in the position of the CCD integrate long-term interactions among multiple components of the Earth system, including the carbonate saturation state of the ocean, biological productivity and export, alkalinity input from weathering, deep-water circulation, climate and sea-level change (Boss & Wilkinson, 1991; Boudreau et al., 2019; Dutkiewicz et al., 2016; Komar & Zeebe, 2021; Stuecker & Zeebe, 2010; van Andel, 1975; Xiao et al., 2024). CCD reconstructions, therefore, provide a critical parameter for exploring the dynamics of the deep carbon reservoir and the functioning of the global carbon cycle across geological timescales.

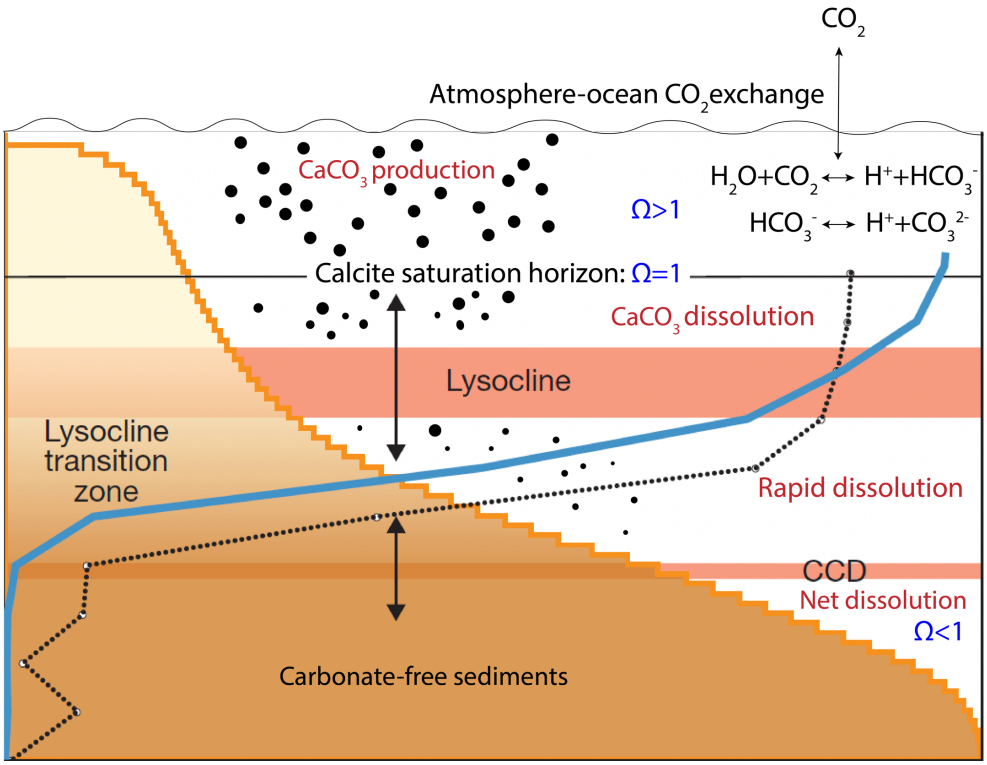

Figure 1: Schematic of the carbonate compensation depth (CCD) modified after Pälike et al. (2012), illustrating interplay between atmospheric CO_2 and ocean carbonate chemistry on ocean saturation state, and on $CaCO_3$ preservation and dissolution. The blue line represents the carbonate accumulation rate, whereas the dotted black line shows the $CaCO_3$ content of sediments. Ω denotes the carbonate saturation state, where $\Omega > 1$ indicates supersaturated conditions favourable for $CaCO_3$ precipitation /preservation, $\Omega = 1$ represents saturation equilibrium, and $\Omega < 1$ indicates undersaturated conditions favourable for carbonate dissolution.

1.3. Carbonate burial, global and basin heterogeneity

The marine carbonate system is regulated by the interplay between dissolved inorganic carbon (DIC) and seawater alkalinity, which together determine carbonate ion concentrations and the distribution of carbon species (CO_2, HCO_3^-, and CO_3^{2-}), and thereby determine the carbonate saturation state (Ω). This saturation state controls the thermodynamic stability of marine carbonates, such that calcium carbonate tends to precipitate when $\Omega > 1$ and dissolve when $\Omega < 1$ (Figure 1) (Rae et al., 2021; Ridgwell & Zeebe, 2005; Zeebe & Wolf-Gladrow, 2001). Deep waters have lower carbonate ion concentrations due to accumulated respired CO_2, creating a vertical saturation gradient (Broecker & Peng, 1982). This gradient establishes the lysocline, the depth marking a sharp transition to elevated carbonate dissolution rates due to reduced carbonate saturation, above the CCD, where carbonate supply and dissolution become balanced (Broecker, 2003). The position of the CCD therefore reflects integrated effects of surface productivity, organic carbon remineralisation, deep-water chemistry, and alkalinity supply. Xiao et al. (2024) provide a synthetic review of Cenozoic CCD evolution and its driving mechanisms, noting a general deepening trend across the major oceans (Atlantic, Pacific and Indian) over the Cenozoic. The authors argue that CCD variations reflect the combined effects of productivity, shallow–basin carbonate fractionation, alkalinity input and pelagic calcifier evolution. However, questions remain about the evolution of the CCD and carbonate burial linked to the major identified drivers.

On multimillion-year timescales, ocean alkalinity is regulated primarily by continental silicate weathering, which delivers bicarbonate and Ca^{2+} to the oceans, promoting carbonate precipitation and burial (Berner et al., 1983; Walker et al., 1981). Tectonic processes such as mountain building, continental uplift, and volcanism modulate weathering fluxes, thereby influencing ocean alkalinity and CCD depth (Kent & Muttoni, 2013; Wallmann, 2001). However, Cenozoic studies show that on orbital to multi-million year timescales, CCD trends can be decoupled from silicate weathering and even from global carbonate burial, because ocean circulation, organic matter remineralisation, and shelf–basin partitioning modulate deep-sea carbonate saturation (Boudreau et al., 2019; Cartapanis et al., 2018; Greene et al., 2019; Kerr et al., 2017; Komar & Zeebe, 2021). This contrasts with earlier assumptions of a tight link between CCD variability and weathering.

Furthermore, the extent to which the partitioning of carbonate burial between shallow platforms and the deep ocean controls the long-term evolution of the global carbonate system remains unresolved. Earlier works have proposed a progressive, monotonic increase in deep-sea carbonate accumulation throughout the Cenozoic, often grounded in globally averaged compilations (e.g., Hay, 1999; Kump & Arthur, 1997; Mackenzie & Morse, 1992; Opdyke & Wilkinson, 1988). Recent quantitative modelling advances a regime-based framework in which carbonate burial dynamics are governed by the coupled evolution of alkalinity input and shallow-platform accommodation space (Salles et al., 2025). In this framework, major palaeoceanographic reorganisations may trigger inverse responses between neritic and pelagic burial, implying a dynamic reallocation of carbonate sinks rather than uniform global change. By comparison, newly developed bias-adjusted reconstructions indicate that pelagic sediment burial rates were considerably lower and characterised by strong regional variability rather than a uniform global trend (Renaudie & Lazarus, 2025). The proposed regime-shift framework, therefore, has yet to be rigorously evaluated using basin-scale empirical records, as such constraints are not adequately represented in current datasets.

From an evolutionary perspective, Suchéras-Marx and Henderiks (2014) highlight the importance of calcareous nannoplankton evolution for carbonate burial, in addition to oceanographic and climatic influences. Later Suchéras-Marx et al. (2019) contend that after the Late Cretaceous peak in speciation, calcareous nannoplankton entered an establishment phase characterised by elevated raw nannofossil accumulation rates but reduced species richness, a pattern interpreted as consistent with the rise in carbonate burial during the Cenozoic. Nevertheless, reassessing the relationship between pelagic calcifier evolutionary dynamics and carbonate burial trajectories over the Cenozoic is essential, as discrepancies between biological production indicators and sedimentary accumulation records may indicate that increased calcifier proliferation does not necessarily translate into proportional gains in long-term carbonate sequestration. Such offsets highlight the decisive influence of preservation thresholds, dissolution intensity, and basin-scale redistribution processes in modulating the transfer of biogenic carbonate to the sedimentary archive. Moreover, because preservation conditions are spatially heterogeneous, controlled by basin-specific water-mass chemistry, circulation structure, and saturation state through time (e.g., Archer, 1996; Bostock et al., 2011; Feely et al., 2004; Gerhardt & Henrich, 2001; Li et al., 2022; Ridgwell & Zeebe, 2005; Sulpis et al., 2018), interpretations derived from globally integrated biological datasets require systematic re-evaluation within a basin-resolved framework.

1.4. Deep-sea carbonate burial shifts and spatiotemporal CCD variability

From the Cretaceous to the Cenozoic, Earth underwent a major climatic transformation, shifting from a high-CO_2 greenhouse world to a Cenozoic icehouse state marked by the onset of Antarctic glaciation (Foster et al., 2017; Zachos et al., 2001; Zachos et al., 2008). This

transition involved large-scale reorganisation of ocean circulation, gateway evolution, and a shift in deep-water formation from low-latitude to high-latitude sources, thereby driving substantial changes in carbonate saturation state and CCD depth (e.g., Cramer et al., 2009; Dutkiewicz et al., 2019; Friedrich et al., 2012; Zachos et al., 2001). With the progression of tectonic reconfiguration and climatic transition, deep-sea carbonates evolved to constitute the principal long-term reservoir of oceanic carbon, reshaping ocean alkalinity budgets and contributing to atmospheric CO_2 variability within the broader framework of long-term carbon cycle feedbacks (e.g., Müller et al., 2022; Poulsen et al., 2001; Scotese et al., 2025; Wallmann, 2001). Importantly, pelagic carbonate evolution was not uniform worldwide. Distinct circulation patterns, productivity gradients, and sedimentary regimes across the Atlantic, Pacific, and Indian oceans (e.g., Chiarella et al., 2017; Ladant et al., 2020; Michel et al., 2018) likely generated substantial spatial heterogeneity in carbonate burial budgets within and between these basins.

Over the Cenozoic, most studies infer an overall global CCD deepening of ~1–2 km across major ocean basins, punctuated by large transient shoaling and deepening events (e.g., Berger, 1973; Boss & Wilkinson, 1991; Dutkiewicz & Müller, 2022; Komar & Zeebe, 2021; Peterson & Backman, 1990; Sclater et al., 1977; van Andel, 1975). However, the CCD can differ substantially between major ocean basins and within a single basin due to contrasts in oceanographic characteristics (Campbell et al., 2018; Dutkiewicz & Müller, 2022; Pälike et al., 2012; Rea et al., 1995; van Andel, 1975). Observations demonstrate substantial inter-basin variability in CCD depth at present. The Pacific Ocean, characterised by older, more CO_2-rich deep waters, generally exhibits a shallower CCD than the Atlantic, which receives younger, more alkaline deep waters formed in the North Atlantic (Broecker & Peng, 1982; Feely et al., 2004). Intra-basin variability further complicates the picture. Latitudinal productivity gradients, distinct water-mass circulation pathways and characteristics, and regional variations in alkalinity generate spatially variable CCD within individual basins, often deviating markedly from a single basin-wide mean CCD (e.g., Dutkiewicz & Müller, 2022; Lyle, 2003; Pälike et al., 2012; Peterson & Backman, 1990; Rea et al., 1995; Rea & Leinen, 1986; Sclater et al., 1977; van Andel, 1975).

These observations indicate that treating the mean CCD as a basin-wide representative (van Andel, 1975) does not capture the substantial regional variability that exists within individual ocean basins. In the equatorial Pacific, high-resolution records suggest a ~1.8 km of CCD deepening since the Eocene, broadly tracking Cenozoic global cooling and enhanced silicate weathering, but also significant CCD fluctuations, ranging from ~3 km to ~4.8 km, that require explanation by multiple interacting oceanographic drivers (Pälike et al., 2012). Regionally resolved CCD reconstructions from the northern, central, and southern Atlantic reveal pronounced spatial variability of approximately 1.5 km, with depths generally oscillating between ~3 and 4.5 km since the early Cenozoic (Dutkiewicz & Müller, 2022). These basin-scale fluctuations correspond to a ~2.5-fold increase in carbon sequestered in pelagic carbonate during this period. South Atlantic CCD reconstructions, corrected for dynamic topography and eustatic sea-level, indicate ~500 m of deepening between the Late Cretaceous and early Cenozoic, followed by ~200 m of deepening to the present, when these components are explicitly incorporated (Dutkiewicz & Müller, 2021). Regional CCD variability throughout the Cenozoic has been attributed to the interplay of multiple climatic and basin-specific oceanographic forcings, including global atmospheric CO_2 perturbations, progressive global cooling and Antarctic glaciation, oceanic gateway reconfigurations, and shifts in deep-water formation and large-scale ocean circulation patterns (e.g., Dutkiewicz & Müller, 2022; Komar & Zeebe, 2021; Pälike et al., 2012; Taylor et al., 2023).

Short-term CCD variability provides further insights into the mechanisms governing its evolution. Late Palaeocene–early Eocene (58–49 Ma) pelagic carbonate compilations show that, despite >3 °C global warming within this period, CCD deepening was modest, implying partial decoupling of CCD from temperature and underscoring the roles of ocean circulation and organic carbon respiration in masking a simple weathering–CCD relationship (Greene et al., 2019). Across the Indian Ocean, CCD changes are comparable in timing and magnitude to those in the Atlantic and Pacific records during specific events, such as the Palaeocene–Eocene Thermal Maximum (PETM) and the early Eocene Climatic Optimum (Greene et al., 2019; Penman et al., 2016; Slotnick et al., 2015). Slotnick et al. (2015) show that the CCD was deep between ~59 and 52 Ma, followed by rapid shoaling at ~51–50 Ma, marked by a decline in carbonate accumulation and a shift from calcareous ooze to clay accumulation. This event is interpreted as reflecting a major reduction in ^{13}C-depleted carbon flux and a significant reorganisation of exogenic carbon cycling. During the PETM, CCD modelling reveals pronounced shoaling at the onset of the event, followed by a post-event overshoot (over-deepening) in the North Atlantic, interpreted as evidence for intense silicate weathering and excess calcite burial above and below the pre-event CCD during recovery (Penman et al., 2016; Ridgwell, 2007). Using high-resolution depth-transect records from the Pacific and South Atlantic, Taylor et al. (2023) document a short-lived (~300 kyr) CCD shoaling across the Eocene–Oligocene transition, associated with a negative carbon isotope excursion, followed by rapid two-stage deepening, including transient overdeepening beyond 5 km, linked to Antarctic glaciation and a major reorganisation of global seawater chemistry. Lyle et al. (2019) differentiate productivity-driven dilution from genuine dissolution across five Pliocene–Pleistocene low-$CaCO_3$ intervals, and caution that reliance on simple $CaCO_3$ thresholds can misinterpret productivity fluctuations as CCD shoaling (Lyle et al., 2019; Preiss-Daimler et al., 2021). These findings underscore the importance of resolving CCD variability across both short-term perturbations and long-term geological evolution, as only regionally constrained, basin-specific CCD reconstructions can accurately capture the spatial heterogeneity and temporal dynamics necessary to interpret carbonate burial patterns and their role in the global carbon cycle.

1.5. Advances in CCD reconstructions

Early global and basin-scale CCD reconstructions collectively indicate that large-amplitude Cenozoic CCD shifts are fundamentally linked to major climate transitions, reflecting changes in ocean chemistry, circulation, and carbonate burial efficiency (e.g., Berger, 1973; Boss & Wilkinson, 1991; Peterson & Backman, 1990; Sclater et al., 1977; van Andel, 1975). As geochemical and stratigraphic datasets expanded, CCD variability became increasingly interpreted as a proxy for long-term changes in ocean carbonate saturation and burial efficiency, highlighting the need to integrate CCD reconstructions with quantitative constraints on carbonate accumulation (Delaney & Boyle, 1988). Further work by Boss and Wilkinson (1991) linked CCD behaviour to biological evolution and sea-level–driven shifts between shallow- and deep-marine carbonate deposition, underscoring the combined influence of biotic and physical processes on pelagic carbonate burial since the Mesozoic. These reconstructions established the CCD as a first-order integrator of Earth-system change, responding to long-term cooling, evolving weathering fluxes, and shifts between shallow- and deep-marine carbonate burial. However, early syntheses implicitly assumed broad spatial coherence, limiting their ability to resolve regional variability in carbonate preservation and dissolution.

Subsequent quantitative regional compilations demonstrated that carbonate accumulation rates and CCD evolution can vary substantially within individual ocean basins, underscoring that basin-wide or global averages obscure pronounced spatial heterogeneity (Lyle, 2003). Pälike et al. (2012) subsequently produced a high-resolution Cenozoic equatorial Pacific CCD

transect that quantitatively links CCD deepening and large-amplitude Eocene fluctuations to changes in weathering fluxes and organic-carbon burial, demonstrating how integrated core data and Earth system modelling can constrain the mechanisms driving long-term CCD evolution. Improvements in regionally resolved CCD reconstructions that integrate carbonate accumulation data with paleobathymetric backtracking further illustrate that vertical seafloor motions, driven by tectonic subsidence, sediment compaction, dynamic topography, and eustatic sea-level change, exert first-order control on inferred CCD histories (Campbell et al., 2018; Dutkiewicz & Müller, 2021) and have enabled more robust regional CCD reconstructions with improved constraints on deep-sea carbonate sequestration and long-term deep carbon-cycle budgets (Dutkiewicz & Müller, 2022).

1.6. Thesis motivation and significance

Recent high-resolution reconstructions demonstrating pronounced regional variability in the CCD throughout the Cenozoic fundamentally challenge the long-standing reliance on globally averaged representations of carbonate system evolution. These may imply that extrapolating regional CCD reconstructions and basin-specific carbonate burial estimates to global scales introduces significant uncertainty into long-term carbon flux calculations and carbon cycle models. This thesis is founded on the premise that carbonate burial and CCD evolution must be treated as spatially dynamic, process-sensitive proxies rather than globally uniform thresholds. Resolving this complexity requires basin-resolved, depth-stratified carbonate analyses capable of capturing inter-basin contrasts and intra-basin heterogeneity. Many global syntheses infer a steady Cenozoic increase in pelagic burial from globally averaged carbonate budgets (e.g., Hay, 1999; Kump & Arthur, 1997; Mackenzie & Morse, 1992; Opdyke & Wilkinson, 1988), in contrast to the recent finding of the Cenozoic subdued and spatially heterogeneous deep-sea sediment accumulation history (Renaudie & Lazarus, 2025) and non-monotonic calcareous nannoplankton evolutionary records since the Cretaceous (Suchéras-Marx et al., 2019). Thus, a critical uncertainty remains about how pelagic carbonate burial evolved within and among ocean basins from the Cretaceous to the present. Motivated by this need, I present the first systematic computation of basin-scale carbonate burial rates across the Atlantic, Pacific, and Indian oceans from the Cretaceous to the present.

Furthermore, while regionally resolved CCD frameworks are relatively well developed in the Atlantic (Dutkiewicz & Müller, 2022), equivalent reconstructions for the Pacific and Indian oceans remain limited. The Pacific and Indian oceans together represent a large fraction of Earth's ocean surface and play central roles in ocean circulation, climate dynamics, and deep-sea carbon cycling. Occupying approximately 46% of the present-day ocean surface, the Pacific Ocean is the largest ocean basin and constitutes a key component of the Earth system, playing a central role in regulating global heat distribution and deep-water circulation, and thereby influencing long-term climate dynamics and global climate variability (Lyle et al., 2008). The equatorial Pacific constitutes one of the most productive regions of the modern ocean, with new production of the order of 1×10^{15} g C yr^{-1}, accounting for roughly 18–56% of modern global production (Chavez & Barber, 1987). This exceptional productivity underpins the Pacific's critical role as a major carbon sink in the global carbon cycle (Lyle et al., 2008). The Pacific exhibits strong latitudinal and longitudinal heterogeneity in productivity, upwelling, and carbonate preservation, and pronounced regional variability in carbonate accumulation patterns (e.g., Gray et al., 2018; Lyle, 2003; Ma et al., 2018; Pennington et al., 2006; Yin et al., 2022). Compilation of Neogene carbonate mass accumulation rates shows that changes in Pacific carbonate deposition are both regionally heterogeneous and globally influential, with latitude-dependent productivity and dissolution patterns tightly linked to CCD structure and evolution (Lyle, 2003). Despite its significance and extensive drilling history, CCD reconstructions in the Pacific have often been dominated by records from the eastern

equatorial region (e.g., Campbell et al., 2018; Komar & Zeebe, 2021; Pälike et al., 2012; Rea & Lyle, 2005; Taylor et al., 2023), and poorly resolved reconstructions in the northwestern Pacific (Rea et al., 1995) and the southeastern Pacific (Rea & Leinen, 1986). Consequently, the extent to which existing CCD curves capture variability across the wider basin remains unclear.

The Indian Ocean is particularly important because it forms an essential part of Earth system climate feedbacks via its tropical warm pool and acts as a key conduit within the global thermohaline circulation, facilitating interbasin exchange of water masses between the Atlantic and Pacific via the Southern Ocean (Piotrowski et al., 2009; Schott et al., 2009). Spanning a broad tropical domain and dynamically linked to the eastern tropical Pacific (Valsala et al., 2020), the Indian Ocean is a key component of the low-latitude ocean system. It also has comparatively high concentrations of dissolved inorganic carbon relative to other major ocean basins (Sarma et al., 2007), a feature that exerts significant influence on global carbon cycling and oceanic carbon storage. This basin marks meridional gradients in hydrochemical characteristics, carbonate saturation state and circulation properties (e.g., Kolla et al., 1976; Phillips et al., 2021; Sabine et al., 2002; Wyrtki, 1973; Zhang et al., 2022b), which requires robust regional carbonate synthesis. Nevertheless, CCD reconstructions in the Indian Ocean remain limited in both spatial coverage and temporal resolution. Apart from the early Paleogene record derived from the Ninetyeast Ridge (Slotnick et al., 2015), most existing reconstructions are restricted to the equatorial sector (Campbell et al., 2018; Peterson & Backman, 1990) and remain far less comprehensive than those available for the Atlantic and equatorial Pacific. This limitation partly reflects the basin's complex and heterogeneous sedimentary settings, including substantial siliciclastic and terrigenous inputs and the widespread occurrence of turbidite systems, which complicate the extraction of continuous pelagic carbonate records (Davies et al., 1995; Kolla et al., 1976). As a result, the basin-scale Indian Ocean contribution to deep-sea carbonate sequestration remains relatively under-constrained.

This thesis, therefore, addresses these gaps by presenting the first systematic regional CCD reconstructions of the Pacific and Indian oceans. By integrating CCD evolution with carbonate accumulation records, this study establishes a quantitative framework to reassess key hypotheses concerning long-term pelagic carbonate evolution, shelf–basin partitioning, alkalinity supply controls, and the role of pelagic calcifier evolution in regulating carbonate export and preservation. Through this basin-spanning approach, the CCD reconstructions will help better constrain long-term carbon-cycle models while also advancing a more mechanistic understanding of deep-time carbonate-system dynamics.

1.7. Thesis overview

This thesis comprises three chapters (presented as journal articles) on CCD reconstruction and the evaluation of deep-sea carbonate accumulation rates (CARs). The first chapter (Article 1, published in *Frontiers in Earth Science*) quantifies regional CCD variability in the Pacific Ocean across six regions and evaluates how CCD evolution relates to Pacific oceanographic structure and climate variability. The second chapter (Article 2, published in *Geo-Marine Letters*) advances CCD modelling in the Indian Ocean across three regions over the Neogene. This article addresses a major gap in basin coverage and tests the extent to which regional hydrographic domains require distinct CCD histories. The third chapter (Article 3 under review in *Marine Geology*) integrates basin-resolved CAR datasets into a single global compilation spanning the Atlantic, Pacific, and Indian oceans over the last ~120 Myr. It quantifies temporal trends, spatial evolution, and depth-dependent burial regimes, providing the first unified empirical framework for evaluating inter-basin heterogeneity and comparing competing interpretations of global pelagic carbonate burial evolution.

Article 1

Article 1 reconstructs the CCD across six regions of the Pacific Ocean, including the western and eastern North Pacific, the western tropical and eastern equatorial Pacific, and the western and eastern South Pacific during the Neogene. The Pacific is the largest ocean basin and exhibits pronounced spatial heterogeneity in productivity, circulation, and carbonate preservation. Yet CCD reconstructions for this basin have historically relied on a small number of records from the eastern equatorial Pacific. These reconstructions are often assumed to represent the basin as a whole, despite growing evidence of strong regional variability.

In this article, the Pacific Ocean is subdivided into distinct oceanographic regions based on latitudinal and longitudinal gradients in carbonate production and deep-water structure. New CCD reconstructions are developed for each region using a consistent backtracking and regression framework, enabling direct comparison of CCD evolution within the basin. By quantifying spatio-temporal CCD variability across the Pacific Ocean, I investigate how regional CCD histories diverge from commonly used equatorial reconstructions. The results establish a spatially resolved baseline for Pacific carbonate preservation and demonstrate that basin-wide carbonate burial estimates require regionally explicit CCD constraints. I find Neogene CCD fluctuations of ~1–1.2 km across the Pacific, with distinct regional responses to major climate and oceanographic shifts. Early Miocene West Antarctic ice-sheet growth and ocean reorganisation resulted in pronounced western tropical Pacific CCD deepening after ~24 Ma, which was not mirrored in the eastern equatorial Pacific. Both the late Miocene carbonate crash and biogenic bloom are evident across equatorial Pacific regions, with a ~1 Myr lag in the western equatorial CCD likely tied to Panama Gateway constriction and Western Pacific Warm Pool (WPWP) shifts. This paper presents a new, spatially explicit CCD framework for the Pacific that can be used to evaluate the evolution of deep-sea carbonate burial and its coupling to climate, ocean circulation, and carbon cycling on geological timescales.

Article 2

Article 2 extends CCD reconstructions to the Indian Ocean, an ocean that exerts a significant influence on global thermohaline circulation yet remains comparatively underrepresented in quantitative CCD studies. This article presents new CCD reconstructions for selected regions of the Indian Ocean that preserve reliable pelagic carbonate records, including the western equatorial Indian Ocean, the southeast Indian Ocean, and the Southern Ocean. By expanding spatial coverage beyond a small number of localised sites and extending temporal constraints wherever possible, Article 2 addresses a major gap in global CCD coverage. The resulting regional CCD models are used to assess how ocean circulation patterns, water-mass properties, and basin geometry influence carbonate preservation in the Indian Ocean, and how these controls vary regionally.

The results indicate that the Indian Ocean CCD exhibits pronounced regional variability, with several hundred meters of deepening and shoaling associated with major Cenozoic climate and oceanographic events, including the growth of Antarctic ice sheets, reorganization of deep-water masses driven by gateway closures and openings (e.g., loss of Tethyan connections, changes in Pacific and Southern Ocean inflow), and intervals of intensified continental weathering and riverine input. The CCD reconstruction captures a pronounced middle–late Miocene shoaling linked to the global carbonate crash, followed by later deepening episodes as circulation and carbonate burial patterns adjusted. By applying a similar conceptual and quantitative framework to that used in Article 1 to a different basin, the analysis provides a comparative test of CCD reconstruction approaches, strengthens the thesis' broader argument that regional CCD histories are key to understanding how the deep-sea carbonate reservoir

interacts with climate and ocean circulation on million-year timescales, and establishes a quantitative basis for future carbon-cycle modelling.

Article 3

Article 3 integrates basin-resolved CAR datasets from the Atlantic, Pacific, and Indian oceans into a unified global synthesis spanning the last ~120 million years. Building on the CCD reconstructions developed in Articles 1 and 2 and on existing Atlantic work of Dutkiewicz and Müller (2022), this chapter provides a comprehensive assessment of the distribution of deep-sea carbonate across the global oceans over deep time. I compiled CAR records from 335 deep-sea drill sites and used a consistent temporal framework to evaluate long-term trends in pelagic carbonate burial within and between ocean basins. The analysis explicitly incorporates a paleobathymetry assessment of carbonate accumulation across shallow, intermediate, and deep oceanic regimes. This approach enables a direct evaluation of how the vertical structure of carbonate burial evolved through major climatic transitions and oceanographic reorganisations.

My results suggest that the Cretaceous carbonate system was highly heterogeneous and variable, whereas the Cenozoic evolved towards a more stable carbonate burial regime across the three ocean basins. I further find that pelagic carbonate burial exhibits strongly basin-differentiated patterns rather than a monotonic increase through the Cenozoic. In the Cenozoic, the Pacific responded most strongly to the Eocene–Oligocene transition (EOT); the Atlantic showed late Eocene and the late Miocene–early Pliocene maxima tied to Northern Component Water (NCW) and North Atlantic Deep Water (NADW) impacts; and the Indian Ocean's largest CAR increase occurred after ~20 Ma, linked to CCD deepening, monsoon intensification and gateway reorganisations. By resolving basin-scale and depth-dependent patterns, Article 3 provides the first comprehensive empirical framework for reconciling competing interpretations of global pelagic carbonate burial evolution.

1.8. Methodological framework and thesis approach

In this thesis, I used a large set of drill sites (92 in Article 1, 70 in Article 2, and 335 in Article 3) from the Deep Sea Drilling Project (DSDP), the Ocean Drilling Program (ODP), and both phases of the IODP, the Integrated Ocean Drilling Program and the International Ocean Discovery Program. I extracted lithology, carbonate contents ($CaCO_3$ wt%) and dry bulk densities from the expeditions' archives for multiple depths for each of these drill sites, comprising a large dataset of thousands of points. The datasets are available as digital supplements with each journal article via the Zenodo archive. In addition, the age–depth models utilised in these compilations are primarily sourced from the Neptune Sandbox Berlin (NSB; https://nsb.mfn-berlin.de/, Renaudie et al., 2020; accessed January–March 2023). Where unavailable, age-depth models are derived from initial/preceding expedition reports, and Lyle's (2002) dataset, and all are calibrated to the Gradstein et al. (2020) timescale.

The overall framework comprises the following steps. First, drill sites are backtracked to reconstruct paleo-water depth through time using *pyBacktrack 1.4 software* (Müller et al., 2018), which accounts for sediment decompaction and tectonic subsidence (Sclater et al., 1985; Stein & Stein, 1992), dynamic topography (Braz et al., 2021)**,** and eustatic sea-level change (Miller et al., 2024). Backtracking involves lithology-specific decompaction of the sediment column at 10 m or less intervals for each drill site. Second, I calculate CAR at each drill site by multiplying the $CaCO_3$ weight % of a sample by its dry bulk density and the linear sedimentation rate (Lyle, 2003), and then partitioned into 1 Myr-wide moving windows with 0.5 Myr time steps, balancing temporal resolution and data coverage. Third, the CCD is quantified from CAR vs paleo-water depth relationships, assuming that CAR extrapolates to zero (Lyle, 2003) and using a reduced major axis regression with explicit outlier detection to

reduce bias from localised processes such as downslope transport or atypical productivity (Articles 1 & 2). Finally, basin-scale CAR datasets are synthesised into a global compilation to quantify temporal trends and spatial evolution (including plate reconstructions via pyGPlates software), and further depth-resolved analysis (Article 3). Comprehensive methodological descriptions, datasets and full citation details are provided in Articles 1–3.

2 | Article 1

Regional carbonate compensation depth variability in the Pacific Ocean since the Oligocene

Faranak Dalvand, Adriana Dutkiewicz, Nicky M. Wright, Ben R. Mather & R. Dietmar Müller

EarthBythe Group, School of Geosciences, University of Sydney, NSW, Australia

Published in *Frontiers in Earth Science* (2025), DOI: https://doi.org/10.3389/feart.2025.1605906

frontiers | Frontiers in Earth Science

TYPE Original Research
PUBLISHED 18 June 2025
DOI 10.3389/feart.2025.1605906

OPEN ACCESS

EDITED BY
Claudia Belviso,
National Research Council (CNR), Italy

REVIEWED BY
Felipe Toledo,
University of São Paulo, Brazil
Kaustubh Hakim,
KU Leuven, Belgium

*CORRESPONDENCE
Faranak Dalvand,
faranak.dalvand@sydney.edu.au

RECEIVED 04 April 2025
ACCEPTED 30 May 2025
PUBLISHED 18 June 2025

CITATION
Dalvand F, Dutkiewicz A, Wright NM, Mather BR and Müller D (2025) Regional carbonate compensation depth variability in the Pacific Ocean since the Oligocene. *Front. Earth Sci.* 13:1605906. doi: 10.3389/feart.2025.1605906

Regional carbonate compensation depth variability in the Pacific Ocean since the Oligocene

Faranak Dalvand*, Adriana Dutkiewicz, Nicky M. Wright, Ben R. Mather and Dietmar Müller

EarthByte Group, School of Geosciences, University of Sydney, Sydney, NSW, Australia

Deep-sea carbonates constitute the primary deep carbon reservoir, playing a critical role in regulating the long-term global carbon cycle. Reconstructing the temporal evolution of carbonate flux to the seafloor requires estimating the changes in carbonate compensation depth (CCD), a key proxy, revealing the depth where the rate of calcium carbonate supply from biogenic ooze equals the rate of dissolution. However, regional CCD estimates across the Pacific, the deepest and largest ocean basin, remain poorly constrained, except for the eastern equatorial region. Here, we present six new regional reconstructions of the CCD across the Pacific Ocean, using a linear reduced major-axis regression of the carbonate accumulation rate (CAR) versus paleo-water depth, that include the effects of dynamic topography and eustasy. The CCDs show significant fluctuations of ~1–1.2 km across the Pacific over the Neogene. Regional CCD models since the early Miocene suggest the influence of climate perturbations, Antarctic ice-sheet growth, and Pacific gateway reorganization on Pacific deep-water circulation and carbonate production. The western Pacific CCD shows a distinct deepening after ~24 Ma, not seen in the eastern tropical Pacific, which we interpret as a delayed consequence of changes in deep water circulation in response to the expansion of the West Antarctic ice sheet into the marine realm at ~26 Ma. Our models also reveal two significant late Miocene events, the carbonate crash and biogenic bloom, across both the western and eastern equatorial Pacific. However, a ~1 Ma lag is noted for both events in the western tropical CCD, likely attributed to the successive effects of Panama Gateway constriction and shifts in the Western Pacific Warm Pool, respectively. The absence of the carbonate crash event from the western North Pacific reflects the regional nature of this event, predominantly influencing the Pacific equatorial region. Our analysis offers new insights into regional CCD variability across the Pacific Ocean and can be used to evaluate the evolution of deep-sea carbonate carbon reservoirs in the context of the long-term carbon cycle.

KEYWORDS

Pacific Ocean, Neogene, carbonate compensation depth, carbon cycle, paleowater depth, carbonate accumulation

1 Introduction

The burial of marine planktic organism remains on the seafloor represents the capture and storage of carbon from the atmosphere, and a significant component of the long-term carbon cycle (Ridgwell and Hargreaves, 2007). A recent study indicates that carbon sequestered through pelagic sediments has become the dominant source of the deep carbon cycle since the early Cenozoic, peaking at ~277 Mt C/yr of carbonate carbon flux at present, out of a total deep carbon input of 311 Mt C/yr across the oceanic plate system (Müller et al., 2022). These computations are based on the global carbonate compensation depth (CCD) estimates of Boss and Wilkinson (1991). The CCD is defined as the water depth at which the supply of carbonate is balanced by its dissolution, leading to the absence of carbonate-bearing sediments below the CCD (Lyle, 2003; Rea and Lyle, 2005). The amount of carbonate deposited in deep-sea sediments over time is critically linked to CCD variations over geological time because the position of the CCD determines the area of seafloor available for carbonate sedimentation (Dutkiewicz et al., 2018). Factors affecting carbonate burial, such as ocean saturation state and alkalinity feedback, the biological pump, and atmospheric CO_2, exhibit strong links to CCD shifts (Xiao et al., 2024). All these factors result in significant variability of the CCD between ocean basins (e.g., Campbell et al., 2018; van Andel, 1975; Xiao et al., 2024). For example, Campbell et al.'s (2018) results indicate that the CCD has varied by ~300 m in the equatorial Pacific Ocean since the Pliocene, whereas the equatorial Indian Ocean has experienced fluctuations of ~1 km during the same period. Recent reconstructions of regional CCDs within the Atlantic Ocean demonstrate that the CCD can differ contemporaneously by as much as 1.2 km even within a single ocean basin due to regional variabilities in productivity and ocean chemistry (Dutkiewicz and Müller, 2022). This highlights the importance of regional CCD reconstructions for robust calculations of deep-sea carbonate storage across the global ocean, which provide significantly more accurate inputs for solid Earth carbon cycle modeling (e.g., Müller et al., 2022). To date, such detailed computations have only been carried out for the Atlantic Ocean (Dutkiewicz and Müller, 2022).

The Pacific occupies a vast area of the Earth's total surface covered by oceans, and plays a critical role in the recycling of carbon *via* its associated network of subduction zones (Müller et al., 2022). Yet, despite its latitudinally-variable accumulation of carbonate (Lyle, 2003) related to productivity (Pennington et al., 2006), upwelling (Gray et al., 2018), oceanic gateway configurations (Straume et al., 2020), geochemistry (Ma et al., 2018) and deep water circulation (Yin et al., 2022), our understanding of regional long-term variations of the CCD and carbonate flux throughout the Pacific is incomplete. The eastern equatorial Pacific is the only region that has been extensively studied (e.g., Campbell et al., 2018; Komar and Zeebe, 2021; Leon-Rodriguez and Dickens, 2010; Pälike et al., 2012; Rea and Lyle, 2005; van Andel, 1975), exhibiting slightly divergent CCD reconstructions for this region spanning the Cenozoic. Limited low-resolution CCD reconstructions based on a small number of deep-sea drill sites also exist for the northwestern Pacific (Rea et al., 1995) and the southeastern Pacific (Rea and Leinen, 1986). However, in the absence of regional CCDs, the high-resolution CCD of Pälike et al. (2012) in an unusually high-productivity region of the eastern equatorial is usually taken to represent the entire Pacific. Here, we present new CCD reconstructions for six regions of the Pacific spanning the Neogene and examine the influence of climate and oceanography changes on carbonate burial and CCD variability over time. The new CCD models will improve constraints on deep carbon cycling computation across the Pacific Ocean.

2 Methods and procedure

2.1 Drill sites and data sources

Our analysis uses 92 scientific ocean drilling sites from the Pacific Ocean (Figure 1), comprising 44 Deep Sea Drilling Project (DSDP) sites, 40 sites from Ocean Drilling Program (ODP) and 8 sites from Integrated Ocean Drilling Program (IODP). Drill sites are primarily located on oceanic crust, with nine sites on continental crust at water depths greater than 1,100 m (Supplementary Material, Table 1). These were chosen based on complete data availability consisting of good core recovery, reliable age-depth models, $CaCO_3$ content, and dry bulk density measurements from http://deepseadrilling.org/, http://www-odp.tamu.edu/ and http://web.iodp.tamu.edu/LORE/ databases (accessed November 2022–July 2023). Age-depth models were obtained from the Neptune Sandbox Berlin (NSB; https://nsb.mfn-berlin.de/, Renaudie et al., 2020; accessed January–March 2023). The NSB data are also available as an archive at https://zenodo.org/records/10057363. For drill sites where the NSB database lacked age-depth models, age-depth plots from Lyle (2002) and initial reports were used. All age-depth models were converted to the Gradstein et al. (2020) timescale. All input data files are available *via* https://doi.org/10.5281/zenodo.15116747 and the digital supplement.

Significant portions of the South Pacific and central North Pacific have not been sampled because scientific ocean drilling expeditions predominantly focus on deep basins with high probable carbonate content (Wade et al., 2020). Hence, our study includes relatively few deep-sea drill sites from these regions.

2.2 CCD reconstruction

In order to reconstruct the regional CCDs, we split the Pacific Ocean into six regions (western North Pacific, eastern North Pacific, western tropical Pacific, eastern equatorial Pacific, western South Pacific and eastern South Pacific; Figure 1) following Lyle's (2003) approach based on careful considerations of north-south and west-east oceanographic variations such as carbonate productivity and the thermocline. This approach aligns with our assessment of regional CCD reconstructions, ensuring a division of the Pacific into sub-regions based on distinct oceanographic domains.

For computing the CCD through time, we use the workflow developed by Dutkiewicz and Müller (2021), age-depth models and lithological data from each drill site, and pyBacktrack 1.4 software (Müller et al., 2018) to backtrack each site and compute the paleowater depth (Supplementary Material, Figure 1). Paleobathymetry is computed by isostatically decompacting the

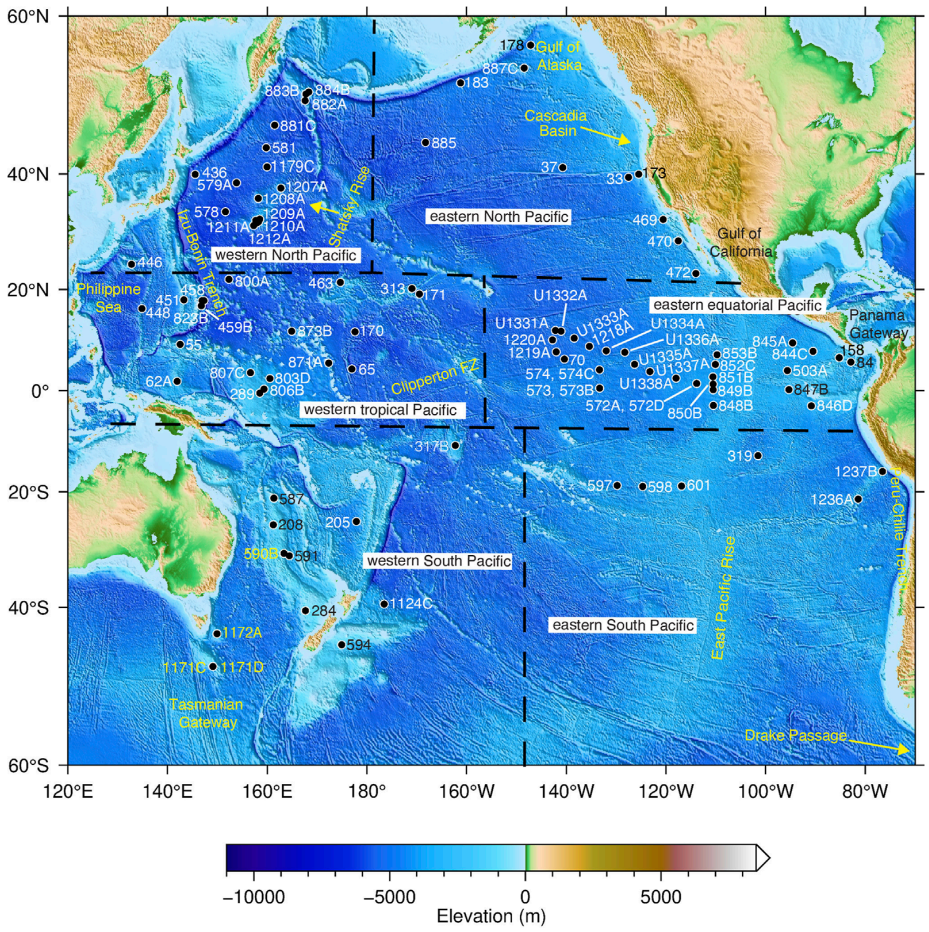

FIGURE 1
Location of 92 sites drilled by the Deep Sea Drilling Project (DSDP), the Ocean Drilling Program (ODP), and the Integrated Ocean Drilling Program (IODP) in the Pacific Ocean used in this study. Black dashed lines define six regions for which we reconstruct the carbonate compensation depth (CCD). Elevation from ETOPO1 global relief model (https://www.ngdc.noaa.gov/mgg/global/; Amante and Eakins, 2009). Mercator projection.

sediment column for each drill site while considering the effects of tectonic subsidence (Sclater et al., 1985) on both oceanic and continental crusts, time-dependent dynamic topography (Braz et al., 2021) and eustatic sea level (Haq et al., 1987) as modified by Miller et al. (2005), following Braz et al. (2021). Lithology-specific decompaction of the sediment column was carried out in 10 m intervals or less in order to capture lithology variations using the lithology library in pyBacktrack 1.4 (Müller et al., 2018).

We combine the paleowater depths with computations of carbonate accumulation rates (CAR) from multiple drill sites in each region to reconstruct the CCD through time. For each drill site, the CAR value is computed by multiplying the weight % of $CaCO_3$ of a sample by its dry bulk density and the linear sedimentation rate (Lyle, 2003). All data on carbonate content (with an average error of <0.8%) and dry bulk density are provided in Supplementary Material. For each drill site, the CAR values are partitioned into 1 Myr-wide moving window and 0.5 Myr time steps. For times where data points are sparse, the CAR values are averaged into a 1 Myr-wide moving window with 1 Myr time steps. We follow Campbell et al. (2018) method and use a linear reduced major axis regression on the CAR values *versus* paleo-water depth, while also detecting using GMT 6.4.0 *gmtregress* (https://docs.generic-mapping-tools.org/6.4/gmtregress.html; Wessel et al., 2019) to define the CCD for each time step, at 95% confidence. It is essential to exclude statistical outliers when combining data from many sediment cores across broad oceanic regions. Since the CCD is inferred as the depth at which CAR approaches zero, the presence of anomalously high CAR values at great depths, or small accumulation rates at shallow depths, produce outliers which can bias the slope and intercept of regression models, resulting in unrealistic or physically implausible CCD estimates. Outliers often reflect local rather than regional processes. These may include enhanced or anomalously low carbonate productivity or reworking

TABLE 1 Comparison of published present-day CCD reconstructions and this study.

Region	CCD (m) at 0.5 Ma (this study)	CCD at 0 Ma (this study)	CCD at 0 Ma (Sulpis et al., 2018)	CCD at 0 Ma (Zhang et al., 2022)	CCD at 0 Ma (Bostock et al., 2011)	CCD at 0 Ma
western North Pacific	3,624 ± 174	3,688 ± 377	n.d.	4,000 ± 300	n.d.	~2,400[a]
eastern North Pacific	4,473 ± 230	4,384 ± 142	4,422 ± 990	n.d.	n.d.	n.d.
western tropical Pacific	4,499 ± 568	n.d.	4,671 ± 400	4,500 ± 400	4,500 ± 300	n.d.
eastern equatorial Pacific	4,225 ± 161	4,192 ± 326	central: 4,432 ± 386 eastern: 3,895 ± 377	5,100 ± 400	4,600 ± 100	~4,600[b] 4650[c] ~4,550[d] ~4,400[e]
western South Pacific	4,357 ± 54	n.d.	4,320 ± 308	n.d.	~3700–4800[f]	n.d.
eastern South Pacific	3,670 ± 499	n.d.	4,036 ± 195	n.d.	n.d.	~4,000[g]

Note: Computation of the present-day CCD in the western tropical Pacific and western and eastern South Pacific is not possible due to disturbed or missing core tops at older drill sites. Therefore, for these regions, the CCD at 0.5 Ma is taken as the closest estimate. n.d., not determined.
[a]Variable CCD values across the western South Pacific.
[b]Rea et al. (1995).
[c]Lyle (2003).
[d]Pälike et al. (2012).
[e]Campbell et al. (2018).
[f]Komar and Zeebe (2021).
[g]Rea and Leinen (1986).

of sediments. Their exclusion from regional analyses is important to avoid violating assumptions of regional environmental homogeneity and erroneous generalizations about basin-scale CCD evolution.

To estimate the CCD, we assume that CAR approaches zero due to a progressive increase in dissolution below the lysocline (Lyle, 2003). Therefore, the y-intercept of the regression line determines the CCD at each time step (Figure 2). However, it should be noted that the variability in the shape of the lysocline over time, driven by changes in rates of surface carbonate productivity (Broecker, 2008) and dissolution (Broecker, 2008; Pälike et al., 2012), remains poorly understood. For instance, Broecker (2008) highlighted a greater offset between the carbonate undersaturation and saturation horizons at higher carbonate burial rates compared to the smoother transition of the saturation horizon at lower carbonate deposition rates. Furthermore, determining carbonate dissolution rates in deep-sea sediments presents challenges due to insufficient knowledge of the different factors involved, such as the hydrodynamic boundary layer's (bottom water layer) role in resisting seafloor dissolution and the duration over which carbonate can resist dissolution on the seafloor. Thus, our computations follow the simple linear regression approach of Pälike et al. (2012) and Campbell et al. (2018).

Linear reduced major axis regression analysis is employed to account for uncertainties both in the CAR value and in the paleowater depth. The primary uncertainty in CCD reconstruction arises from paleobathymetry computations, while additional sources of uncertainty include sediment decompaction, the presence of unconformities, and carbonate measurements (Dutkiewicz et al., 2018). The total uncertainty resulting from regression analysis for each reconstruction time and sub-region reflects various error sources such as age-depth errors, carbonate content, and sedimentation rates (see also Dutkiewicz et al., 2018; van Andel et al., 1975). Additionally, following a similar approach to Dutkiewicz and Müller (2022), we consider a cutoff for CAR values of <1,500 mg/cm^2/kyr for paleo-water depths <2.5 km (i.e., water depth above the mid-ocean ridge). CAR values exceeding 2,000 mg/cm^2/kyr at paleo-water depths >4.5 km are also excluded following the approach of Dutkiewicz and Müller (2022), because they represent anomalies related to processes such as downslope transport of carbonate sediments.

We perform a linear regression on CAR values *versus* paleo-water depth (Figure 2) using three approaches, incorporating two recently published dynamic topography methods. The first approach uses the "D10" dynamic topography model (Braz et al., 2021) combined with eustatic sea level from Haq et al. (1987) with modifications by Miller et al. (2005). The second approach uses the "M6" model, which is a dynamic topography model from which long-term sea-level fluctuations are computed (Müller et al., 2018), while the third approach excludes the effects of dynamic topography and sea level. Our preferred model, D10 (a compressible mantle flow model) was used because it accounts for mantle plumes, which are essential for Pacific dynamic topography estimations due to the significant mantle upwelling in the Pacific.

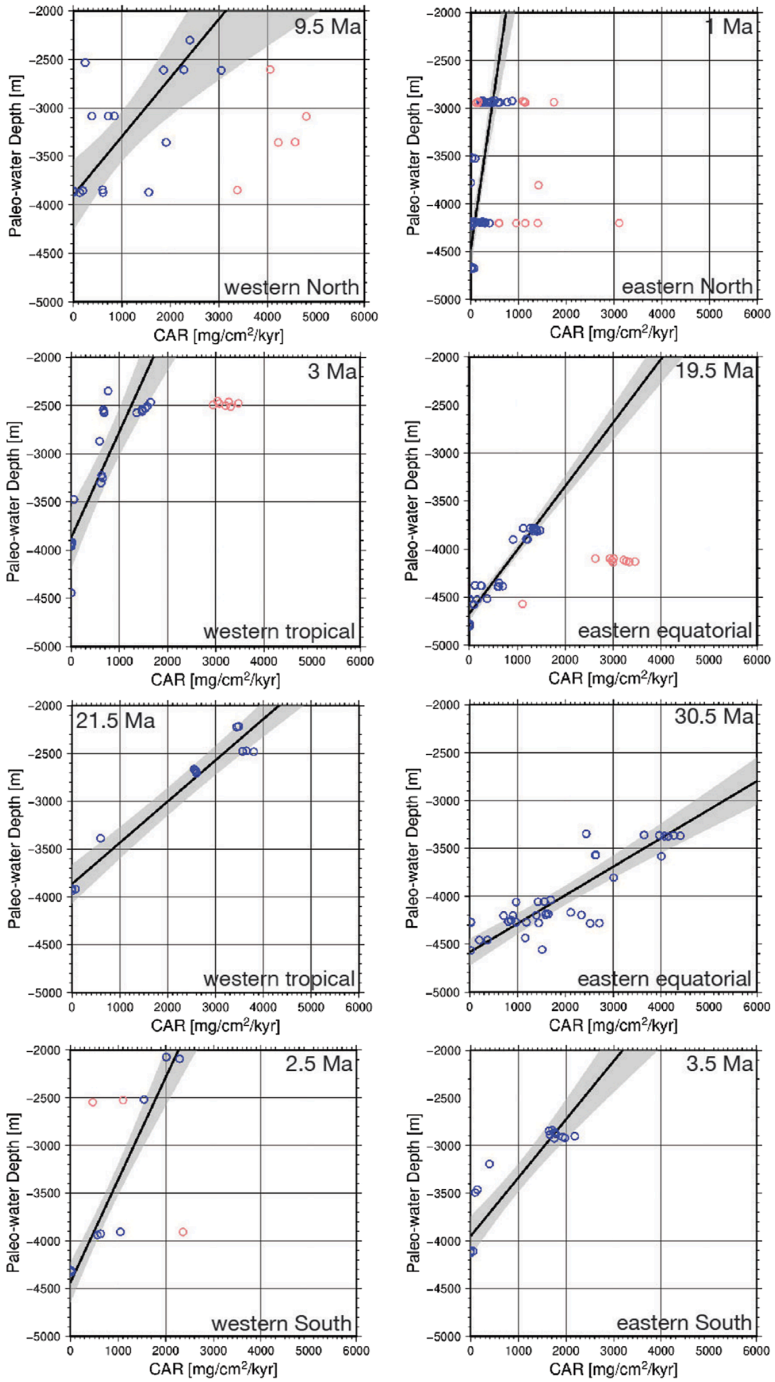

FIGURE 2
Examples of CCD computations using linear reduced major-axis regression analysis with outlier detection. This regression analysis includes the dynamic topography model D10 (Braz et al., 2021). The CCD is defined by the carbonate accumulation rate (CAR) values extrapolating to zero as a function of the paleowater depth (i.e., the y-intercept). Data points (blue and red circles) represent multiple drill sites at each time interval. Red circles represent outliers. Gray band indicates 95% confidence envelope. Note that the slope of the line is only used to determine the location of the CCD. Multiple times have been excluded from the analysis due to insufficient data to generate regression plots. Our robust regression approach detects outliers based on the mean of the squared residuals across three thresholds: the standard approach identifies outliers for the absolute value of standardized residuals >2.5, with two narrower thresholds set at >1.5 and >0.5. We also examine the standard regression analysis without identifying outliers, particularly in cases of oddly distributed sparse data points, where three thresholds of outlier detection result in incorrectly identified outliers

(*Continued*)

FIGURE 2 (Continued)
(by visual inspection). For example, during the time interval centered at 19.5 Ma in the eastern equatorial region, regression analysis identified drill sites DSDP 70, 574 (and 574-hole C) as outliers due to deviations in CAR values from the standardized residuals (>2.5). Sites 574 and 574C exhibited anomalously high CAR values exceeding 2,600 mg/cm^2/k.y at a paleowater depth of ~4.2 km. These anomalies fell outside the CAR value cutoff for exclusion through the computational analysis. Site 70 is represented at this time by two distinct CAR values: CAR value 99 mg/cm^2/k.y at a paleowater depth of 4,580 m and CAR value 1,109 mg/cm^2/k.y at a paleowater depth of 4,571 m, with the latter value reflecting a notable CAR anomaly considering the relatively similar paleowater depth at the same sampling window with the CCD located at a paleowater depth of ~4.6 km. While these sites were consistently flagged as outliers in earlier intervals before 19.5 Ma, only site 574 continued to exhibit anomalies after 19.5 Ma. Site 574 (and 574C) exhibited higher CAR values during the early Miocene despite being located farther from the narrow equatorial high-productivity zone compared to other drill sites, such as site 573 (with significantly lower CAR values < 1,100 mg/cm^2/k.y at a shallower paleowater depth ~3.8 km). The anomalously high CAR values at these drill sites during this time period may be attributable to downslope carbonate transport processes. The regression analysis without accounting for outliers at this time interval resulted in a ~100 m shallower CCD.

3 Results: regional CCD reconstructions in the Pacific

The Pacific CCD of van Andel et al. (1975) over the Cenozoic generally tracks the global CCD variations (e.g., Boss and Wilkinson, 1991; Delaney and Boyle, 1988). Van Andel et al. (1975) described the CCD in the equatorial Pacific as distinct from the entire Pacific CCD since 50 Ma, primarily in terms of the magnitude of fluctuations (~500 m deeper), which aligns with the overall trend of the equatorial Pacific CCD of Berger (1973). However, our results show significant regional variability in the CCD fluctuations across the entire Pacific Ocean, highlighting the shortcomings of a single representative CCD over the entire Pacific (Figures 3, 4, 6). However, given that the eastern equatorial CCD is the most detailed and intensely studied CCD in the Pacific (Campbell et al., 2018; Lyle, 2003; Pälike et al., 2012), and is also well-defined in our reconstructions, we explore regional CCD changes in the Pacific in relation to the CCD model of the eastern equatorial area.

3.1 North Pacific CCD modeling

3.1.1 Eastern North Pacific

Due to data scarcity, our CCD reconstruction in the eastern north area cannot extend before the middle Miocene, as the regression analysis fails to provide the CCD estimates. During the late middle Miocene, considering the associated errors of ~±100–700 m, rarely exceeding ~1 km, the CCD in this region is relatively shallow, between ~3.2 and 3.9 km (Figure 3A), compared to the much deeper CCD of ~4.4–4.8 km observed in the eastern equatorial region during this interval (Figure 4A). However, the CCD of ~3.5 km at ~8.5 Ma gradually deepens, reaching a maximum depth of ~4.5 km in the Pliocene in this region. Since 4.5 Ma, the CCD model exhibits a lower level of uncertainties (<±400 m) compared to uncertainties of earlier segments (~±700 m and occasionally > ±1 km). The CCD has remained relatively stable between ~4.3 and ~4.4 km since 4 Ma. The present-day CCD in the eastern North Pacific, at ~4.3 km, is comparable with the modern CCD of ~4.4 km determined by Sulpis et al. (2018) for this region (Table 1).

3.1.2 Western North Pacific

In the western North Pacific, our model estimates the CCD at ~4.2 km by ~19 Ma, which gradually shoals to ~3.4 km during the middle Miocene, as also indicated by Rea et al. (1995), Figure 3B. The middle Miocene shallow CCD is followed by a series of smaller deepening and shoaling episodes (ranging between ~3.5–4 km) towards the Pliocene, which broadly correlates with the shoaling trend of the CCD observed by Rea et al. (1995) for this region within this period. The western North Pacific CCD remains at ~3.8–3.9 km between 12 Ma and 8.5 Ma, with no evidence for the sharp CCD shoaling attributed to well-known carbonate crash of the late Miocene in the eastern equatorial region (e.g., Lyle et al., 1995). The CCD has remained shallow since the Pliocene, varying between ~3.4 and 3.7 km, with smaller uncertainties (<±200 m) than prior to the Pliocene (up to ~±700 m). In this study, the present-day CCD of the western North region, at ~3.6 km, appears to be the shallowest modern CCD modeled in all the regions of the Pacific. This is consistent with Zhang et al.'s (2022) findings of a shallower CCD (~4 km) in this region compared to a CCD of ~5.1 km and ~4.5 km in the western and central equatorial Pacific, respectively (Table 1). The shallow CCD from our model is much deeper (~1.2 km) than Rea et al.'s (1995) estimate of present-day CCD of ~2.4 km in the western North Pacific.

3.2 Eastern equatorial Pacific CCD modeling

The CCD across the eastern equatorial Pacific has been the subject of multiple reconstructions (e.g., Campbell et al., 2018; Lyle, 2003; Pälike et al., 2012). Our eastern equatorial CCD spans 35 Ma to 0 Ma and exhibits a comparable long-term trend with that of Berger (1973), van Andel (1975), Lyle (2003), Pälike et al. (2012) and Campbell et al. (2018), with some differences in short-term fluctuations (Figure 4A). Our regression analysis indicates the early Oligocene CCD deepening from ~4 km at ~35 Ma to ~4.6 km at ~31.5 Ma. The deep CCD throughout the Oligocene experiences some modest fluctuations (~300 m) up to the early Miocene. The CCD shoaling between 19 and 16 Ma (Figure 4A), agrees with that modeled by Pälike et al. (2012) and Lyle (2003). After 16 Ma, the CCD deepens to ~4.8 km by 12 Ma, the deepest Cenozoic CCD in this region. In the latest Neogene, the CCD shallows to ~4 km. Previously modeled shallow CCD maxima in the latest Neogene (e.g., Campbell et al., 2018; Lyle et al., 1995; Pälike et al., 2012) are observed in our model at 10–9 Ma and 7–6.5 Ma, along with the shoaling episode in the Pliocene-Pleistocene (reaching ~3.9 km by 2.5 Ma).

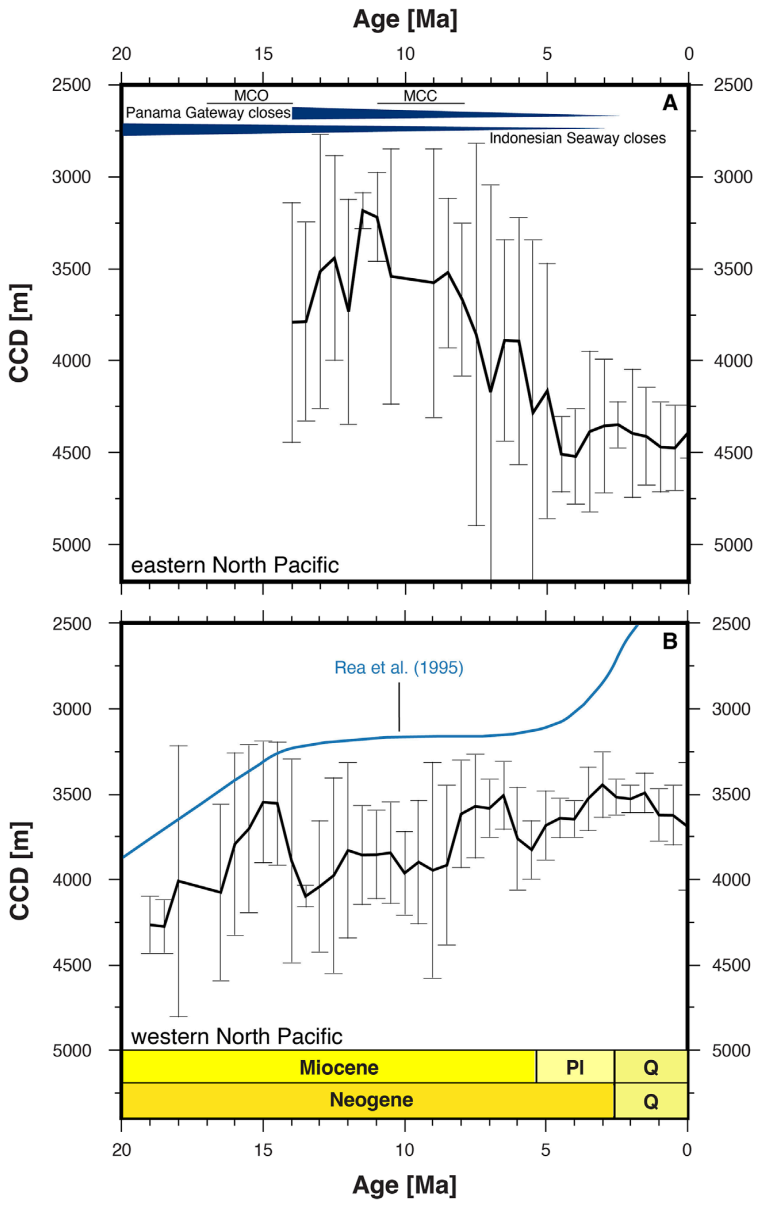

FIGURE 3
CCD reconstructions for the North Pacific spanning the last 20 Ma, covering the regions defined in Figure 1, including **(A)** eastern North Pacific and **(B)** western North Pacific. The northwest Pacific CCD curve from Rea et al. (1995) is shown in **(B)**. Solid black line is the portion of the CCD reconstructed using regression analysis, and error bars indicate uncertainty represented by the gray envelope as shown in Figure 2. The timing of Miocene Climate Optimum (MCO) from Westerhold et al. (2020) and the Miocene Carbonate Crash (MCC) in the equatorial Pacific from Lyle et al. (1995). Timing of ocean gateway closing from Schmittner et al. (2004) for the Panama Gateway, and from Bahr et al. (2023) and Kuhnt et al. (2004) for the Indonesian Seaway.

Our present-day CCD of ~4.2 km in the eastern equatorial region is in good agreement with independent estimates such as ~4.4 km for the central equatorial Pacific from Sulpis et al. (2018), ~4.6 km from Bostock et al. (2011), and ~4.6 km from Pälike et al. (2012) (Table 1).

3.2.1 Reproducibility of the eastern equatorial CCD reconstruction

The CCD reconstruction of Pälike et al. (2012) for the eastern equatorial region extending back to the early Eocene is extremely detailed and shows major and frequent fluctuations on

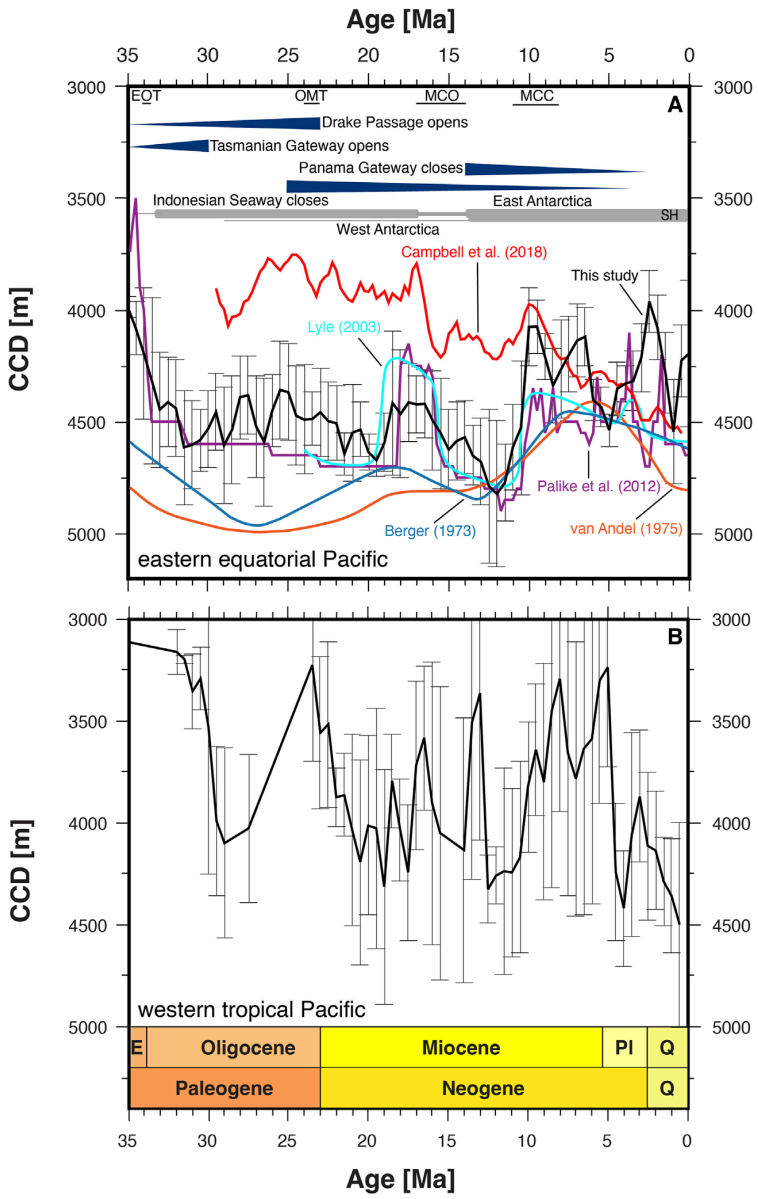

FIGURE 4
CCD reconstructions for the equatorial Pacific spanning the last 35 Ma, covering the regions defined in Figure 1, including **(A)** eastern equatorial Pacific and **(B)** western tropical Pacific. Regional CCD curves from published studies are shown in **A**. Solid black line is the portion of the CCD reconstructed using regression analysis, and error bars indicate uncertainty represented by the gray envelope as shown in Figure 2. The timing of Eocene/Oligocene Transition (EOT), Oligocene/Miocene Transition (OMT), Miocene Climate Optimum (MCO), and the Southern Hemisphere (SH) glaciation from Westerhold et al. (2020). Approximate timing of the Miocene Carbonate Crash (MCC) in the equatorial Pacific from Lyle et al. (1995). Timing of ocean gateway opening and closing from Eagles and Jokat (2014) for the Drake Passage, from Straume et al. (2020) for the Tasmanian Gateway, from Schmittner et al. (2004) for the Panama Gateway, and from Bahr et al. (2023) and Kuhnt et al. (2004) for the Indonesian Seaway.

250 kyr timescales. However, their analysis does not include a computation of uncertainties, which prohibits an evaluation of the true significance of some of these fluctuations. Because the Pälike et al. (2012) reconstruction used a similar approach to ours we are able to reproduce their CCD and show that their errors are large and comparable to those in our model, which includes a subset of drill sites used in the Pälike et al. (2012) dataset. In order to assess the associated errors in Pälike et al's. (2012) model, we reconstruct the CCD based on the authors' dataset. We use our preferred regression analysis, together with three alternative

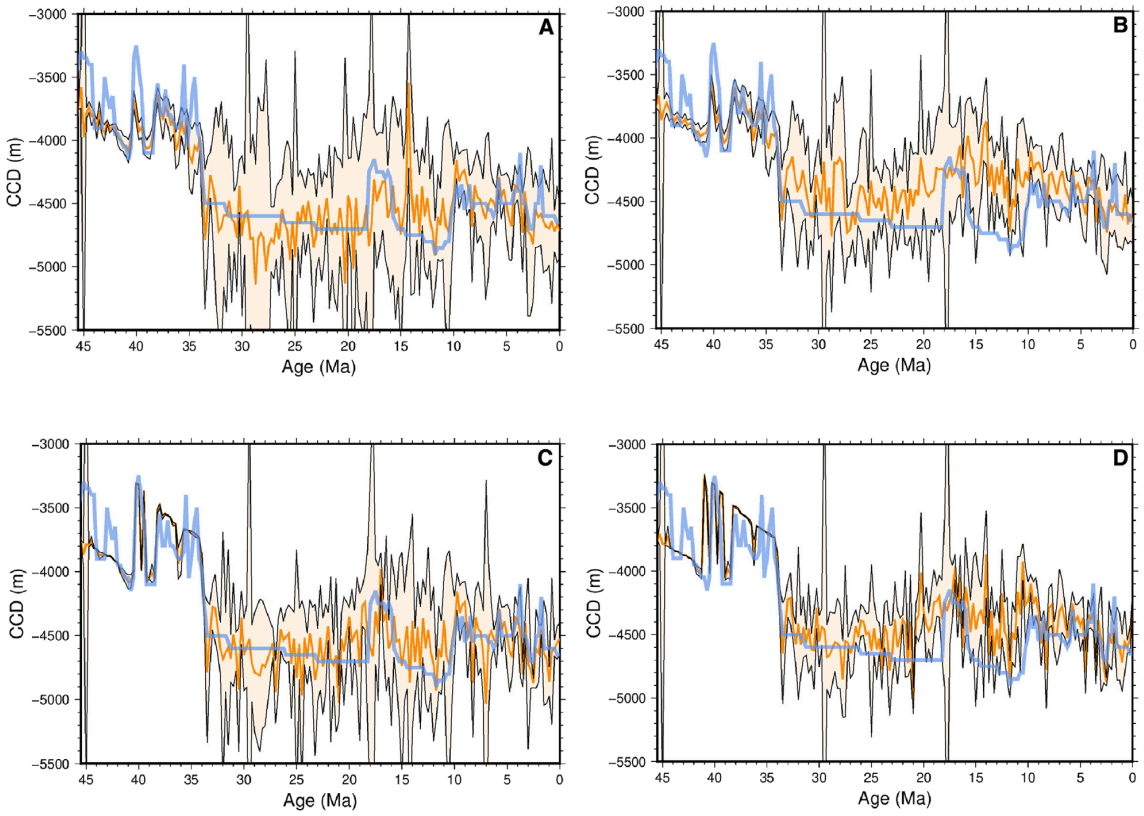

FIGURE 5
Assessment of uncertainties in the eastern equatorial Pacific CCD model of Pälike et al. (2012), which was reported without errors (blue curve) and without details of their regression method. Our re-assessment is based on carbonate accumulation data (CAR) and paleo-water depths used by Pälike et al. (2012) and applies four different regression methods to produce a CCD curve (orange line) with an uncertainty envelope (light orange). **(A)** LSR—least squares with reduced axis regression calculating errors on the x-axis (CAR) and the y-axis (paleo-water depth), **(B)** LSY method—least squares regression computing errors on the y-axis, **(C)** LWR—weighted least squares with reduced axis regression and outlier detection, **(D)** LWY—weighted least squares with outlier detection and error computation on the y-axis. Note that LWR results in the best match to the published curve of Pälike et al. (2012) with a large error envelope between 33 Ma and 0 Ma. Smaller errors prior to 33 Ma reflect fewer data points used in the regression.

methods (Figure 5) to find the regression method that best fits the Pälike et al. (2012) CCD curve because the exact method that they used is not described. Similar to Campbell et al. (2018), we were not able to reproduce the Pälike et al. (2012) CCD exactly using their dataset, but we find a close match with the published curve using the least squares with reduced axis regression (LSR; Figure 5A) and the standard least squares regression with y-axis errors only (LWR; Figure 5C). However, the uncertainties are substantial for the period 33–0 Ma, ranging between ±100 m and ±1,783 m (mean = ±490 m) for LSR, and ±35 m to ±1,750 m (mean = ±355 m) for LWR. The LSY method produces a relatively poor match with the published curve and relatively large errors (Figure 5B), while the LWY regression (Figure 5D) produces smaller errors but worse fit than either LSR and LWR. The uncertainties for older times are smaller because fewer data points are used in the regression, resulting in tighter fits to sparse data. However, this does not imply that the model is more accurate, as regressions based on sparse data points reduce the confidence in resulting interpretations, which should be used with caution.

Our eastern equatorial CCD broadly tracks Pälike et al's. (2012) CCD, with a slight divergence from the Oligocene to the early Miocene and a notable decoupling between the late Pliocene and the Pleistocene (Figure 4A). The disparity in these results can be attributed to a larger dataset of drill sites used in our CCD model *versus* that of Pälike et al. (2012) for this region. However, the uncertainties in our CCD are generally smaller (±75–345 m; mean = ±184 m) than those calculated for the Pälike et al. (2012) CCD. Our results illustrate that CCD fluctuations over timescales less than ~0.5 million years are typically within the errors of the data used for this purpose, even if high-resolution stratigraphic data are used, and irrespective of the type of regression analysis.

3.3 Western tropical Pacific CCD modeling

In the western tropical region, the CCD between 32 Ma and 29 Ma is inferred to have deepened from ~3.2 to 3.9 km within this period (Figure 4B). The CCD drop at the beginning of the

Oligocene shows a delay of ~2 Ma in the western tropical region compared to the eastern equatorial area. The CCD of ~3.2 km during the latest Oligocene deepens to ~4 km toward the early Miocene. Compared to other regions of the Pacific, the western tropical area has experienced significant CCD fluctuations during the Neogene, although the uncertainties are quite large (up to ~±700 m). Throughout the Miocene, the western tropical Pacific exhibits various CCD fluctuations, marking a significant deepening between 12.5 Ma and 10.5 Ma, succeeded by a lowered CCD in the late Miocene. Notably, an ~0.5–1 km shallower CCD compared to the eastern equatorial Pacific is evident in this region during the latest Miocene. This is followed by a CCD deepening in the early Pliocene and a shallower CCD during the latest Pliocene. Since the Pleistocene, there has been a gradual deepening of the CCD to ~4.5 km at 0.5 Ma. The 0.5 Ma CCD from our study is comparable with the present-day CCDs of ~4.5–4.6 km from Sulpis et al. (2018), Zhang et al. (2022), and Bostock et al. (2011) across this region (Table 1).

3.4 South Pacific CCD modeling

3.4.1 Eastern South Pacific

Data limitation makes it challenging to compute the CCD prior to the middle Miocene using regression analysis. The CCD in the eastern South Pacific has remained above ~4 km since the middle Miocene (uncertainties are generally < ±300 m, Figure 6A). Similar to the CCD shoaling of the eastern equatorial region, this area shows a shallower CCD between 19.5 Ma and 17 Ma (~3.5–3.6 km) compared to the middle Miocene segment, followed by a significant shoaling to ~3.2 km at 10.5 Ma. The CCD deepening reconstructed between 15 Ma to 11 Ma across the equatorial region (Lyle, 2003; Pälike et al., 2012; and this study; Figure 4A) correlates with the CCD shoaling (~700 m) in this region. While the data are insufficient between 10.5 Ma to 8.5 Ma to generate regression plots, interpolation suggests a deepening CCD, reaching around 4 km by 8.5 Ma. The CCD has remained shallow since the late Neogene, ranging between ~3.6 and 3.9 km, with minor fluctuations, consistent with the CCD of Rea and Leinen (1986). Our modern CCD at 0.5 Ma is ~400 m shallower than the present-day CCD of Sulpis et al. (2018) and Rea and Leinen (1986) estimated to be ~4 km (Table 1).

3.4.2 Western South Pacific

Owing to the complexity of the seafloor topography and deep ocean circulation in the western South Pacific over time (Bostock et al., 2011), it would be advantageous to reconstruct the CCD at sub-basin scales in this region. However, sparse data coverage only allows us to model the CCD for the entire western South Pacific. Our CCD model is confined to the late Neogene (Figure 6B). The late Miocene CCD is between ~4.1 and 4.2 km, with no evidence of shoaling that is associated with the eastern equatorial Pacific between ~12 Ma and 8 Ma (Figure 4A). A brief CCD rise of ~300 m from 7.5 Ma to 6.5 Ma coincides with a shoaling episode of the eastern equatorial Pacific (Figures 4A, 6B). A CCD of ~4.3 km at 0.5 Ma is significantly deeper than that of the eastern south region (~3.6 km).

4 Causes of regional CCD variations in the Pacific over the Neogene

Our CCD reconstructions provide new insights into regional CCD variations across the Pacific since the early Miocene, particularly in the equatorial region that includes the first CCD model for the western tropical Pacific. Distinct CCD fluctuations in the western and eastern equatorial regions of the Pacific (Figures 4A,B) highlight the importance of longitudinal CCD variability beyond the previously discussed latitudinal gradient (Lyle, 2003). Previous studies (Campbell et al., 2018; Lyle, 2003; Pälike et al., 2012) have documented the eastern equatorial Pacific CCD evolution in detail. However, our complementary western tropical CCD model represents a new CCD reconstruction in this region (Figure 4B), revealing two significant (~1 km) CCD deepening pulses from the early Oligocene to the early Miocene not seen in the eastern equatorial region. The first deepening, from ~3.2 km at 30.5 Ma to ~4 km at 29 Ma, remains enigmatic. It cannot be linked to regional gateway modifications due to a lack of any significant changes in tropical Pacific gateways before the Miocene (Lyle et al., 2008), nor to the early Oligocene East Antarctic glaciation, as this continental glaciation did not lead to deep ocean circulation changes or associated cooling (Lear et al., 2000; Mackensen, 2004). Further constraints from additional drill sites with reliable age models covering the earliest Oligocene, which are currently not available, are essential to determine whether this shift represents a regional response to primary carbonate productivity (e.g., Lyle et al., 2008; Moore Jr et al., 2004; Van Andel and Moore Jr, 1974).

The second CCD deepening in this region, from ~3.2 km at 23.5 Ma to ~4.1 km at 20.5 Ma following a gradual rise, may be associated with the significant growth of West Antarctic Ice Sheet (WAIS) at this time. A recent study by Klages et al. (2024) based on Earth system and ice sheet models, utilizing multiproxy data from both terrestrial and marine microfossils from West Antarctica's Pacific margin, revealed that the West Antarctic ice sheet initially expanded into the marine realm at ~26 Ma, lagging the East Antarctic glaciation by ~7–8 Ma. A delayed response to this late Oligocene growth in Antarctic ice sheet has also been observed in ocean cooling of ~1°C after ~24 Ma based on geochemical proxies (Billups and Schrag, 2002). Thus, the western tropical CCD deepening after ~24 Ma may be ascribed to the ocean's delayed cooling in response to the late Oligocene WAIS, coinciding with a notable decrease in atmospheric CO_2 during the earliest Miocene (Hönisch et al., 2023). Our results suggest that the early Miocene Antarctic Bottom Water (AABW) formation (Woodruff and Savin, 1989), following the expansion of the WAIS and its northward flow along the western South Pacific, may have impacted the western tropical Pacific during the earliest Miocene. This glacial cooling may be incorporated with low sea surface temperature (SST) affected by the distributed Western Pacific Warm Pool (WPWP) to the Indian Ocean during this time, resulting in this early Miocene CCD deepening. Episodes of higher nutrient concentration favoring carbonate productivity (small-size coccolith production) in the western tropical Pacific over the Miocene correspond to cooling and a shallower thermocline affected by the Western Pacific Warm Pool (WPWP) dynamics

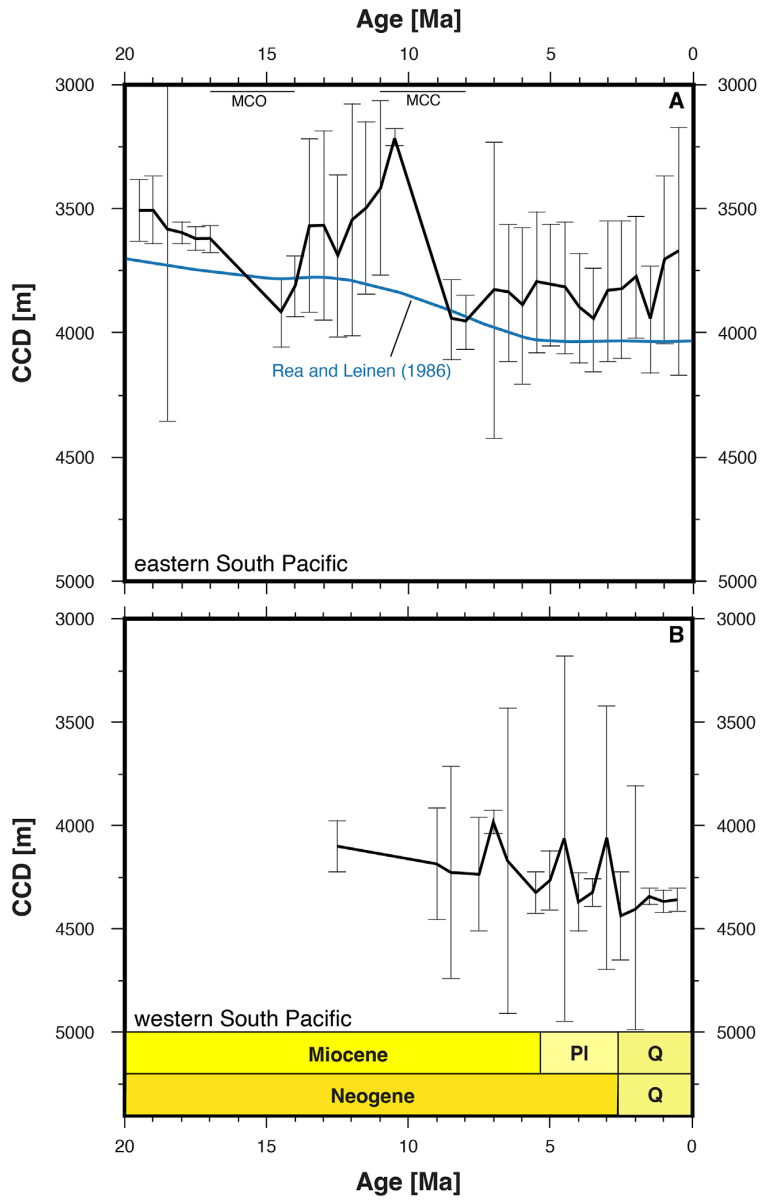

FIGURE 6
CCD reconstructions for the South Pacific spanning the last 20 Ma, covering the regions defined in Figure 1, including **(A)** eastern South Pacific and **(B)** western South Pacific. The southeast Pacific CCD curve from Rea and Leinen (1986) is shown in **A**. Solid black line is the portion of the CCD reconstructed using regression analysis, and error bars indicate uncertainty represented by the gray envelope as shown in Figure 2. The timing of Miocene Climate Optimum (MCO) from Westerhold et al. (2020) and the Miocene Carbonate Crash (MCC) in the equatorial Pacific from Lyle et al. (1995).

(Imai et al., 2015; Yuwono and Sato, 2020). During the early Miocene, when the Indonesian Seaway was still open, the Indo-Pacific water exchange and westward WPWP flow to the Indian Ocean created a shallow thermocline across the western tropical region (Von Der Heydt and Dijkstra, 2011), which could possibly contribute to carbonate accumulation. The role of the thermocline in calcareous biogenic productivity across the western tropical and western North Pacific during the Miocene and Pliocene (Imai et al., 2015; Pratiwi and Sato, 2016) suggests that it may have played a major role in driving CCD variations in the western tropical Pacific since the Miocene. For instance, the cooling and shoaling of the thermocline and enhanced water mixing across the western tropical Pacific since 4 Ma, with intensified episodes between ~3.1 Ma and ~0.7 Ma (Dang et al., 2024), agree with our modelled CCD

deepening from ~3.8 km at 3 Ma to ~4.5 km at 0.5 Ma in this region. The western tropical Pacific thermocline and its vertical changes, affected by the East Antarctic glaciation and the progressively reduced Indo-Pacific water exchange through the Indonesian Seaway constriction during the Miocene (Gallagher et al., 2009; Gasperi and Kennett, 1993; Nathan and Leckie, 2009), and its effect on the CCD variability of this region require further investigation.

Although Imai et al. (2015) described a similar effect of the thermocline changes on carbonate production in the western North Pacific over the Neogene, the inferred timing by the authors (e.g., shoaling of the thermocline since 5 Ma) does not exhibit a clear pattern correlative with our western North Pacific CCD fluctuations. In the middle Miocene, a CCD shoaling in the western North Pacific, peaking at ~3.5 km between 15 Ma and 14.5 Ma (Figure 3B), could be associated with the Miocene Climate Optimum (MCO: 17–14 Ma; Westerhold et al., 2020). Holbourn et al. (2014) used benthic foraminiferal isotope signatures from the eastern equatorial Pacific during the MCO combined with astronomically tuned $\delta^{18}O$ and $\delta^{13}C$ proxies from the southeast and northwest Pacific covering the same interval from an earlier study (Holbourn et al., 2007) to suggest that the Southern Hemisphere warming led to an ~5 °C increase in Pacific deep ocean temperature between 15.7 and 14.7 Ma, which in turn resulted in enhanced deep-sea carbonate dissolution and a CCD rise. According to the authors, carbonate preservation recovered during the next cooling phase at ~13.8 Ma, associating with Antarctic ice sheet expansion, which correlates with a reduction in atmospheric CO_2 (Hönisch et al., 2023). This pattern and subsequent recovery are reflected in a CCD shoaling within MCO, peaking at ~3.5 km between~15 and ~14.5 Ma, followed by a deepening to ~4 km at 13.5 Ma in our model from the western North region. A recent study by Holbourn et al. (2024) based on a multi-proxy record from Site U1490 in the western equatorial Pacific shows an increased carbonate accumulation over the MCO followed by a decrease during the Middle Miocene Climate Transition (MMCT). These excursions agree with our CCD model for the western tropical Pacific (Figure 4B), which shows a CCD deepening from ~3.6 km at ~16.5 Ma to ~4.1 km at its end, followed by a short-lived CCD shallowing to 3.5 km at the start of the MMCT. Holbourn et al. (2024) attribute the carbonate accumulation high during the MCO to increased primary productivity, possibly related to an increase in weathering (Bolton et al., 2016; Si and Rosenthal, 2019), which compensated for increased carbonate dissolution related to the increased formation and northward expansion of corrosive deep waters in the western tropical Pacific. During the MMCT, carbonate preservation improved due to reduced CO_2 uptake at deep-water formation sites in the Southern Ocean, while carbonate accumulation decreased (Holbourn et al., 2024) suggesting that primary productivity also decreased at this time.

Since the late Miocene, the CCD fluctuated between ~3.4 km and ~3.9 km in the western North Pacific (Figure 3B), which could be linked to the impact of the Panama Gateway constriction on the deep-water chemistry of the Pacific. At present, the Pacific deep water is becoming enriched in dissolved silica, while displaying relatively low carbonate ion concentrations as deep water flows and ages toward the North Pacific (Zhang et al., 2022). This northward silica gradient across the Pacific mirrors the late Miocene pattern, following the formation of AABW and its northward flow to the North Pacific (Woodruff and Savin, 1989). This silica gradient is triggered by reduced Atlantic-Pacific water exchange through the restriction of the Panama Gateway and enhanced nutrient concentration and productivity across the eastern equatorial Pacific (Schneider and Schmittner, 2006). Productivity increases result in opal sedimentation due to faster rain of opal and its higher preservation compared to carbonate (Lyle and Baldauf, 2015). Recycling and dissolution of biogenic opal before complete burial (Ragueneau et al., 2000) could result in enhanced dissolved silica (DSi) toward the North Pacific. Additionally, Panama Gateway constriction enhanced the North Atlantic Deep Water (NADW) production (Butzin et al., 2011; Schneider and Schmittner, 2006) and accompanied by Antarctic cooling, led to an increased AABW flow to the Pacific enriched in dissolved silica (Keller and Barron, 1983), triggering the DSi pool to the North Pacific (Cortese et al., 2004). All these occurrences have resulted in enhanced silica burial in the western North Pacific over the late Neogene (Barron, 1998; Rea et al., 1995), which is reflected in the overall shoaling trend of our CCD model since the late Miocene. We interpret this CCD rise in relation to silica flux because diatom productivity surpasses coccolith accumulation under relatively high nutrient supply conditions (Litchman, 2007), and higher silica productivity intervals coincide with carbonate dissolution (Lyle and Baldauf, 2015), which leads to a shoaling trend of the CCD. This is supported by the stratigraphy of ODP sites 881, 882, 883 and 884 from the western North region (Figure 1), which is dominated by post-late Miocene diatom ooze. In addition, our CCD reconstruction in the western North Pacific shows shoaling peaks at 6.5 Ma and 3 Ma, which correlate with two notable peaks of silica accumulation (at ~6 Ma and ~3 Ma) in this region (Rea et al., 1995).

Our eastern equatorial CCD model shows two shallowing pulses in relation to two major events of the late Miocene, encompassing the carbonate crash and biogenic bloom, in this region (Figure 4A). The first shoaling, with an onset at ~11.5 Ma, corresponds to the carbonate crash event recognized by Lyle et al. (1995) in different parts of the eastern equatorial Pacific between 11 and 8 Ma. Lyle and Baldauf (2015) determined that this event occurred between 13.2 and 8 Ma in the Pacific eastern equatorial region. Our CCD reconstructions suggest that the peak of the carbonate crash occurred between 10.5 and 9 Ma over a regional scale across the eastern equatorial Pacific, coinciding with the lowest carbonate preservation of ~9.7 Ma from Lyle et al. (2019). This event is reflected in the CCD shoaling of ~800 m from ~4.8 km at 12 Ma to ~4 km at 10 Ma in our model, ~300 m shallower than the value computed by Pälike et al. (2012) for this period (Figure 4A). The carbonate crash may be explained as a consequence of the Panama Gateway constriction by enhanced carbonate dissolution due to intensified AABW flow and corrosive water circulation to the Pacific (Lyle et al., 1995; Roth et al., 2000). Furthermore, in the western tropical Pacific, the CCD shoals by ~900 m, from ~4.2 km at ~11 Ma to ~3.2 km at ~8 Ma (Figure 4B), indicating the occurrence of the carbonate crash event in this region. This marked shift further suggests that the equatorial region of the Pacific has experienced a substantial response to the carbonate crash event during the late Miocene. Based on our CCD data, we propose the initiation of carbonate crash in the eastern equatorial Pacific at ~11.5 Ma and in the western tropical Pacific at ~10.5 Ma. Additionally, the CCD shallowing corresponding to the carbonate crash peaks at ~8 Ma in the western tropical region, compared to that of the eastern equatorial of

~10–9.5 Ma. These patterns may offer the east-west lag in the onset and intensification of the carbonate crash. Nathan and Leckie (2009) described a ~1 Ma delay in the initiation of the carbonate crash event from the Caribbean to the eastern equatorial Pacific, which we argue may have further extended into the western tropical region of the Pacific. However, considering the 0.5 Ma resolution of our analysis, this interpretation should be regarded with caution. We also note a signal of this event in our model for the eastern South Pacific expressed by a rise of the CCD from ~3.5 to ~3.2 km between 12 and 10.5 Ma (Figure 6A). The carbonate crash event was also inferred in the eastern South Pacific by Preiss-Daimler et al. (2021) based on a carbonate accumulation decline at ~11 Ma. The occurrence of the carbonate crash event in the eastern South Pacific suggests that the oceanographic effect of the Panama Gateway constriction extended beyond the Pacific equatorial region. However, our findings indicate that the carbonate crash may not have occurred as a basin-wide event across the Pacific Ocean. The spatially variable expression of the carbonate crash within the Pacific broadly corresponds to the carbonate crash signals observed in the low-to mid-latitude Atlantic and Indian Oceans (Lübbers et al., 2019; Preiss-Daimler et al., 2021). Notably, our CCD model reveals no evidence of this occurrence in the western North Pacific, where the CCD remained relatively stable between ~3.9 and ~3.8 km from ~12 to ~8.5 Ma (Figure 3B). Moreover, examining core sediments from deep-sea drill sites in this region, like those from the Shatsky Rise (Figure 1), which extend into the middle Miocene, demonstrate well-preserved carbonate sequences predominantly composed of nannofossil ooze, with $CaCO_3$ concentrations averaging ~60–70% during this interval.

The subsequent CCD shallowing in the eastern equatorial region of the latest Miocene, peaking between ~7 and ~6.5 Ma (Figure 4A), corresponds to the late Miocene biogenic bloom event of the eastern equatorial Pacific, which may be another response to the Panama Gateway constriction and the resulting differentiation in Atlantic-Pacific deep water (Farrell et al., 1995; Lyle and Baldauf, 2015; Lyle et al., 2019; Pillot et al., 2023). The occurrence of the biogenic bloom from our model is coeval with the late Miocene carbon isotope shift between 7.7 and 6.4 Ma (Drury et al., 2017). While the underlying mechanisms of the late Miocene biogenic bloom remain debated, Pillot et al. (2023) argue that the heterogeneous distribution of biogenic bloom (with peak intensity at ~7 Ma) across the global ocean may be driven by the strengthening of thermohaline circulation or intensified wind-driven upwelling on a global scale, both influenced by climate variability and gateway dynamics. Here, our CCD record correlates with the highest biogenic opal accumulation rates recorded between 7.1 and 6.4 Ma from Lyle and Baldauf (2015), and between 7 and 6.5 Ma from Lyle et al. (2019) in the eastern equatorial region. Lyle et al. (2019) suggest that despite high carbonate burial since 14 Ma (apart from the carbonate crash interval), enhanced diatom productivity during the biogenic bloom was accompanied by reduced carbonate accumulation across the equatorial high-productivity region of the Pacific. Supporting this, Lyle et al.'s (2019) data indicate that an average of ~20% increase in biogenic opal wt% corresponded with a ~20% decrease in $CaCO_3$ wt% between ~7 and ~6.5 Ma at drill site U1338, which is part of a cluster of eight drill sites, identified within the biogenic bloom manifestation zone in the eastern equatorial Pacific (Pillot et al., 2023). Within this period, opal wt% peaked at ~39%, while carbonate content declined to ~44%, representing a ~35% reduction from ~7.5 Ma. These observations may suggest that enhanced opal accumulation is captured in our CCD model by a peak of shoaling (~7–6.5 Ma) across the eastern equatorial region. However, in the western tropical region, CCD shoaling reached its peak between ~5.5 and ~5 Ma (~3.3–3.2 km), when the eastern equatorial CCD deepened to ~4.5 km by ~5 Ma (Figures 4A,B). The observed offset in CCD trends between the western and eastern equatorial Pacific until ~4 Ma may reflect perturbations between biogenic opal production and carbonate accumulation, modulated by thermocline variability across the equator. The thermocline shifts, influenced by the Pacific warm pool dynamics, contributed to longitudinal asymmetry in species distribution across the equatorial Pacific during the late Miocene (Nathan and Leckie, 2009). Our results also represent a subsequent relative convergence of CCD patterns across the western tropical and eastern equatorial regions between ~4 Ma and ~1 Ma, which coincides with a diminished west-east thermocline gradient (Wara et al., 2005) and the disappearance of a nannofossil content gradient across the equatorial Pacific during this interval (Bolton et al., 2010). Nevertheless, a more comprehensive understanding of the interplay between CCD variability, Pacific warm pool fluctuations, and the differential contributions of opal and carbonate productivity across the equatorial Pacific necessitates further examination of high-resolution proxy data.

5 Conclusions

We present new models of the CCD across the entire Pacific Ocean, split into six regions (western North Pacific, eastern North Pacific, western tropical Pacific, eastern equatorial Pacific, western South Pacific, and eastern South Pacific). Our results demonstrate distinct regional variability in CCD fluctuations across the Pacific, which differ from the reconstructed average CCD that characterizes the overall Pacific basin. We find the deepest CCD in the eastern equatorial area, ranging between ~3.7 and ~4.7 km prior to the middle Miocene. In contrast, the western North Pacific region features a relatively shallow CCD (~2.3–4 km) over the majority of the Neogene, rarely exceeding 4 km. Coupled with the diverse CCD changes between the eastern equatorial and western tropical regions of the Pacific, our CCD models highlight substantial latitude-longitude heterogeneity in carbonate flux across the Pacific Ocean over the late Cenozoic. We interpret the CCD changes across the Pacific regions to reflect the effect of climate variability, the Antarctic glaciation, and the configurations of the Indonesian and the Panama gateways on regional carbonate productivity across the Pacific over the Neogene. Our model of the western tropical Pacific CCD, the first of its kind, demonstrates a distinct drop at the earliest Miocene that may be related to marine West Antarctic ice sheet growth at 26 Ma (Klages et al., 2024), suggesting a delayed deep ocean cooling after ~2 Ma. We propose the peaks of CCD shoaling ~10–9.5 Ma and ~7–6.5 Ma corresponding to the carbonate crash and biogenic bloom events, respectively, in the eastern equatorial Pacific. These occurrences are also observed in the western tropical region from our CCD models, which may imply these events are characterized over the equatorial region of the Pacific.

Our study provides constraints on CCD perturbations on regional scales. The particularly deeper CCD of the eastern equatorial Pacific, compared to the western tropical and western North regions during the Miocene, offers a caution against the common practice of using the eastern equatorial CCD to represent the entire Pacific (e.g., Bogumil et al., 2024; Boudreau and Luo, 2017) in long-term carbon cycle modeling. However, there is a vital need for future drilling targeting oceanic crust older than 60 Ma in the western Pacific to gain deeper insights into CCD behavior during the warm intervals of the Cretaceous and Paleogene. Additionally, future research could focus on better constraining the CCD and carbonate accumulation in other regions of the global ocean, noting that their evolution is poorly-defined in the Indian and Southern oceans.

Data availability statement

Data supporting the results of this study can be found online at https://doi.org/10.5281/zenodo.15116747.

Author contributions

FD: Data curation, Formal Analysis, Investigation, Visualization, Writing – original draft. AD: Conceptualization, Formal Analysis, Funding acquisition, Methodology, Supervision, Writing – review and editing. NW: Formal Analysis, Supervision, Writing – review and editing. BM: Formal Analysis, Supervision, Writing – review and editing. DM: Conceptualization, Formal Analysis, Methodology, Supervision, Writing – review and editing.

Funding

The author(s) declare that financial support was received for the research and/or publication of this article. This research was supported by an Australian Research Council (ARC) PhD scholarship to FD and an ARC Future Fellowship to AD via grant FT190100829. NW was supported by BHP through the Spatio TEmporaL expLorAtion for Resources "STELLAR" project and an ARC Early Career Industry Fellowship via grant IE230100098. BM and DM were also supported by the "STELLAR" project, and by the AuScope Simulation, Analysis and Modelling node funded by the Australian Government through the National Collaborative Research Infrastructure Strategy, NCRIS.

Acknowledgments

We thank the reviewers for their thoughtful and constructive feedback, which greatly enhanced the quality of this article.

Conflict of interest

The authors declare that the research was conducted in the absence of any commercial or financial relationships that could be construed as a potential conflict of interest.

Generative AI statement

The author(s) declare that no Generative AI was used in the creation of this manuscript.

Publisher's note

All claims expressed in this article are solely those of the authors and do not necessarily represent those of their affiliated organizations, or those of the publisher, the editors and the reviewers. Any product that may be evaluated in this article, or claim that may be made by its manufacturer, is not guaranteed or endorsed by the publisher.

Supplementary material

The Supplementary Material for this article can be found online at: https://www.frontiersin.org/articles/10.3389/feart.2025.1605906/full#supplementary-material

References

Amante, C., and Eakins, B. W. (2009). *ETOPO1 arc-minute global relief model: procedures, data sources and analysis*. Boulder, CO: National Geophysical Data Center, NOAA, NOAA Technical Memorandum NESDIS NGDC-24. Available online at: https://repository.library.noaa.gov/view/noaa/1163.

Bahr, A., Kaboth-Bahr, S., and Karas, C. (2023). The opening and closure of oceanic seaways during the Cenozoic: pacemaker of global climate change? *Straits and seaways: controls, processes and implications in modern and ancient systems*. Editors V. M. Rossi, S. G. Longhitano, C. Olario, and F. L. Chiocci (London, UK: Geological Society, London, Special Publication), 523, 141–171. doi:10.1144/SP523-2021-54

Barron, J. A. (1998). Late Neogene changes in diatom sedimentation in the North Pacific. *J. Asian Earth Sci.* 16 (1), 85–95. doi:10.1016/S0743-9547(97)00046-9

Berger, W. H. (1973). Cenozoic sedimentation in the eastern tropical Pacific. *Geol. Soc. Am. Bull.* 84 (6), 1941–1954. doi:10.1130/0016-7606(1973)84<1941:CSITET>2.0.CO;2

Billups, K., and Schrag, D. P. (2002). Paleotemperatures and ice volume of the past 27 Myr revisited with paired Mg/Ca and $^{18}O/^{16}O$ measurements on benthic foraminifera. *Paleoceanography* 17 (1), 3-1-3-11. doi:10.1029/2000PA000567

Bogumil, M., Mittal, T., and Lithgow-Bertelloni, C. (2024). The effects of bathymetry on the long-term carbon cycle and CCD. *Earth, Atmos. Planet. Sci.* 121 (21), e2400232121. doi:10.1073/pnas.2400232121

Bolton, C. T., Gibbs, S. J., and Wilson, P. A. (2010). Evolution of nutricline dynamics in the equatorial Pacific during the late Pliocene. *Paleoceanogr. Paleoclimatology* 25 (1). doi:10.1029/2009PA001821

Bolton, C. T., Hernández-Sánchez, M. T., Fuertes, M., González-Lemos, S., Abrevaya, L., Mendez-Vicente, A., et al. (2016). Decrease in coccolithophore calcification and CO_2 since the middle Miocene. *Nat. Commun.* 7 (10284), 10284. doi:10.1038/ncomms10284

Boss, S. K., and Wilkinson, B. H. (1991). Planktogenic/eustatic control on cratonic/oceanic carbonate accumulation. *J. Geol.* 99 (4), 497–513. doi:10.1086/629513

Bostock, H. C., Hayward, B. W., Neil, H. L., Currie, K. I., and Dunbar, G. B. (2011). Deep-water carbonate concentrations in the southwest Pacific. *Deep Sea Res. Part I Oceanogr. Res. Pap.* 58 (1), 72–85. doi:10.1016/j.dsr.2010.11.010

Boudreau, B. P., and Luo, Y. (2017). Retrodiction of secular variations in deep-sea $CaCO_3$ burial during the Cenozoic. *Earth Planet. Sci. Lett.* 474, 1–12. doi:10.1016/j.epsl.2017.06.005

Braz, C., Zahirovic, S., Salles, T., Flament, N., Harrington, L., and Müller, R. D. (2021). Modelling the role of dynamic topography and eustasy in the evolution of the Great Artesian Basin. *Basin Res.* 33 (6), 3378–3405. doi:10.1111/bre.12606

Broecker, W. S. (2008). A need to improve reconstructions of the fluctuations in the calcite compensation depth over the course of the Cenozoic. *Paleoceanography* 23 (1), PA1204. doi:10.1029/2007PA001456

Butzin, M., Lohmann, G., and Bickert, T. (2011). Miocene ocean circulation inferred from marine carbon cycle modeling combined with benthic isotope records. *Paleoceanogr. Paleoclimatology* 26 (1). doi:10.1029/2009PA001901

Campbell, S. M., Moucha, R., Derry, L. A., and Raymo, M. E. (2018). Effects of dynamic topography on the Cenozoic carbonate compensation depth. *Geochem. Geophys. Geosystems* 19 (4), 1025–1034. doi:10.1002/2017GC007386

Cortese, G., Gersonde, R., Hillenbrand, C.-D., and Kuhn, G. (2004). Opal sedimentation shifts in the world ocean over the last 15 myr. *Earth Planet. Sci. Lett.* 224 (3-4), 509–527. doi:10.1016/j.epsl.2004.05.035

Dang, H., Ren, Y., Peng, N., Ma, X., Liu, F., Luo, L., et al. (2024). Long-term changes in the Western Pacific Warm Pool upper-water structure over the last 4 Ma. *Palaeogeogr. Palaeoclimatol. Palaeoecol.* 651, 112396. doi:10.1016/j.palaeo.2024.112396

Delaney, M. L., and Boyle, E. A. (1988). Tertiary paleoceanic chemical variability: unintended consequences of simple geochemical models. *Paleoceanogr.Paleoclimatology* 3 (2), 137–156. doi:10.1029/PA003i002p00137

Drury, A. J., Westerhold, T., Frederichs, T., Tian, J., Wilkens, R., Channell, J. E., et al. (2017). Late miocene climate and time scale reconciliation: accurate orbital calibration from a deep-sea perspective. *Earth Planet. Sci. Lett.* 475, 254–266. doi:10.1016/j.epsl.2017.07.038

Dutkiewicz, A., and Müller, R. D. (2021). The carbonate compensation depth in the South Atlantic Ocean since the late cretaceous. *Geology* 49 (7), 873–878. doi:10.1130/G48404.1

Dutkiewicz, A., and Müller, R. D. (2022). The history of Cenozoic carbonate flux in the Atlantic Ocean constrained by multiple regional carbonate compensation depth reconstructions. *Geochem. Geophys. Geosystems* 23 (11), e2022GC010667. doi:10.1029/2022GC010667

Dutkiewicz, A., Müller, R. D., Cannon, J., Vaughan, S., and Zahirovic, S. (2018). Sequestration and subduction of deep-sea carbonate in the global ocean since the Early Cretaceous. *Geology* 47 (1), 91–94. doi:10.1130/G45424.1

Eagles, G., and Jokat, W. (2014). Tectonic reconstructions for paleobathymetry in Drake passage. *Tectonophysics* 611, 28–50. doi:10.1016/j.tecto.2013.11.021

Farrell, J. W., Raffi, I., Janecek, T. R., Murray, D. W., Levitan, M., Dadey, K. A., et al. (1995). "35. Late Neogene sedimentation patterns in the eastern equatorial Pacific Ocean," Editors N. G. Pisias, L. A. Mayer, T. R. Janecek, A. Palmer-Julson, and T. H. van Andel (College Station, TX: Ocean Drilling Program), 138, 2419–2426. doi:10.2973/odp.proc.sr.138.143.1995*Proc. Ocean Drill. Program, Sci. Results*

Gallagher, S. J., Wallace, M. W., Li, C. L., Kinna, B., Bye, J. T., Akimoto, K., et al. (2009). Neogene history of the West Pacific warm pool, Kuroshio and Leeuwin currents. *Paleoceanogr. Paleoclimatology* 24 (1), 1–27. doi:10.1029/2008PA001660

Gasperi, J. T., and Kennett, J. P. (1993). Vertical thermal structure evolution of Miocene surface waters: western equatorial Pacific DSDP Site 289. *Mar. Micropaleontol.* 22 (3), 235–254. doi:10.1016/0377-8398(93)90046-Z

Gradstein, F. M., Ogg, J. G., Schmitz, M. D., and Ogg, G. M. (2020). *Geologic time scale 2020, 1*. Netherlands: Elsevier. doi:10.1016/C2020-1-02369-3

Gray, W. R., Rae, J. W. B., Wills, R. C. J., Shevenell, A. E., Taylor, B., Burke, A., et al. (2018). Deglacial upwelling, productivity and CO_2 outgassing in the North Pacific ocean. *Nat. Geosci.* 11 (5), 340–344. doi:10.1038/s41561-018-0108-6

Haq, B. U., Hardenbol, J., and Vail, P. R. (1987). Chronology of fluctuating sea levels since the Triassic. *Science* 235 (4793), 1156–1167. doi:10.1126/science.235.4793.1156

Holbourn, A., Kuhnt, W., Kulhanek, D. K., Mountain, G., Rosenthal, Y., Sagawa, T., et al. (2024). Re-Organization of Pacific overturning circulation across the Miocene climate Optimum. *Nat. Commun.* 15 (8135), 8135. doi:10.1038/s41467-024-52516-x

Holbourn, A., Kuhnt, W., Lyle, M., Schneider, L., Romero, O., and Andersen, N. (2014). Middle Miocene climate cooling linked to intensification of eastern equatorial Pacific upwelling. *Geology* 42 (1), 19–22. doi:10.1130/G34890.1

Holbourn, A., Kuhnt, W., Schulz, M., Flores, J.-A., and Andersen, N. (2007). Orbitally-paced climate evolution during the middle Miocene "Monterey" carbon-isotope excursion. *Earth Planet. Sci. Lett.* 261 (3-4), 534–550. doi:10.1016/j.epsl.2007.07.026

Hönisch, B., Royer, D. L., Breecker, D. O., Polissar, P. J., Bowen, G. J., Henehan, M. J., et al. (2023). Toward a Cenozoic history of atmospheric CO_2. *Science* 382 (6675), eadi5177. doi:10.1126/science.adi5177

Imai, R., Farida, M., Sato, T., and Iryu, Y. (2015). Evidence for eutrophication in the northwestern Pacific and eastern Indian oceans during the Miocene to Pleistocene based on the nannofossil accumulation rate, Discoaster abundance, and coccolith size distribution of Reticulofenestra. *Mar. Micropaleontol.* 116, 15–27. doi:10.1016/j.marmicro.2015.01.001

Keller, G., and Barron, J. A. (1983). Paleoceanographic implications of Miocene deep-sea hiatuses. *Geol. Soc. Am. Bull.* 94 (5), 590–613. doi:10.1130/0016-7606(1983)94<590:PIOMDH>2.0.CO;2

Klages, J. P., Hillenbrand, C.-D., Bohaty, S. M., Salzmann, U., Bickert, T., Lohmann, G., et al. (2024). Ice sheet–free West Antarctica during peak early Oligocene glaciation. *Science* 385, 322–327. doi:10.1126/science.adj3931

Komar, N., and Zeebe, R. E. (2021). Reconciling atmospheric CO_2, weathering, and calcite compensation depth across the Cenozoic. *Sci. Adv.* 7 (4), eabd4876. doi:10.1126/sciadv.abd4876

Kuhnt, W., Holbourn, A., Hall, R., Zuvela, M., and Käse, R. (2004). "Neogene history of the Indonesian throughflow," in *Continent-Ocean interactions within east asian marginal seas, geophysical monograph*. Editors P. Clift, W. Kuhnt, P. Wang, and D. Hayes, (Washington, DC: American Geophysical Union), 149, 299–320. doi:10.1029/149GM16

Lear, C. H., Elderfield, H., and Wilson, P. A. (2000). Cenozoic deep-sea temperatures and global ice volumes from Mg/Ca in benthic foraminiferal calcite. *Science* 287 (5451), 269–272. doi:10.1126/science.287.5451.269

Leon-Rodriguez, L., and Dickens, G. R. (2010). Constraints on ocean acidification associated with rapid and massive carbon injections: the early paleogene record at ocean drilling program site 1215, equatorial Pacific Ocean. *Palaeogeogr. Palaeoclimatol. Palaeoecol.* 298 (3-4), 409–420. doi:10.1016/j.palaeo.2010.10.029

Litchman, E. (2007). "Resource competition and the ecological success of phytoplankton," in *Evolution of primary producers in the seas*. Editors P. G. Falkowski, and A. H. Knoll (Burlington, MA: Elsevier), 351–375. doi:10.1016/B978-012370518-1/50017-5

Lübbers, J., Kuhnt, W., Holbourn, A. E., Bolton, C. T., Gray, E., Usui, Y., et al. (2019). The middle to late Miocene "carbonate crash" in the equatorial Indian ocean. *Paleoceanogr. Paleoclimatology* 34 (5), 813–832. doi:10.1029/2018PA003482

Lyle, M. (2002). "Age-depth profiles for Pacific DSDP and ODP drillsites," in *Center for geophysical investigation of the shallow subsurface*. Boise, Idaho: Boise State University.

Lyle, M. (2003). Neogene carbonate burial in the Pacific Ocean. *Paleoceanogr. Paleoclimatology* 18 (3). doi:10.1029/2002PA000777

Lyle, M., and Baldauf, J. (2015). Biogenic sediment regimes in the Neogene equatorial Pacific, IODP Site U1338: burial, production, and diatom community. *Palaeogeogr. Palaeoclimatol. Palaeoecol.* 433, 106–128. doi:10.1016/j.palaeo.2015.04.001

Lyle, M., Barron, J., Bralower, T. J., Huber, M., Olivarez Lyle, A., Ravelo, A. C., et al. (2008). Pacific Ocean and cenozoic evolution of climate. *Rev. Geophys.* 46 (2). doi:10.1029/2005RG000190

Lyle, M., Dadey, K. A., and Farrell, J. W. (1995). "42. The late Miocene (11–8 Ma) eastern Pacific carbonate crash: evidence for reorganization of deep-water circulation by the closure of the Panama gateway," *Proceedings of the ocean drilling program, scientific results*. Editors N. G. Pisas, L. A. Mayer, T. R. Janecek, Palmer-Julson and T. H. van Andel (College Station, TX: Ocean Drilling Program), 138, 821–838. doi:10.2973/odp.proc.sr.138.157.1995

Lyle, M., Drury, A. J., Tian, J., Wilkens, R., and Westerhold, T. (2019). Late Miocene to Holocene high-resolution eastern equatorial Pacific carbonate records: stratigraphy linked by dissolution and paleoproductivity. *Clim. Past* 15 (5), 1715–1739. doi:10.5194/cp-15-1715-2019

Ma, X., Tian, J., Ma, W., Li, K., and Yu, J. (2018). Changes of deep Pacific overturning circulation and carbonate chemistry during middle Miocene East Antarctic ice sheet expansion. *Earth Planet. Sci. Lett.* 484, 253–263. doi:10.1016/j.epsl.2017.12.002

Mackensen, A. (2004). Changing Southern Ocean palaeocirculation and effects on global climate. *Antarct. Sci.* 16 (4), 369–386. doi:10.1017/S0954102004002202

Miller, K. G., Kominz, M. A., Browning, J. V., Wright, J. D., Mountain, G. S., Katz, M. E., et al. (2005). The Phanerozoic record of global sea-level change. *Science* 310 (5752), 1293–1298. doi:10.1126/science.1116412

Moore Jr, T. C., Backman, J., Raffi, I., Nigrini, C., Sanfilippo, A., Pälike, H., et al. (2004). Paleogene tropical Pacific: clues to circulation, productivity, and plate motion. *Paleoceanogr. Paleoclimatology* 19 (3). doi:10.1029/2003PA000998

Müller, R. D., Cannon, J., Williams, S., and Dutkiewicz, A. (2018). PyBacktrack 1.0: a tool for reconstructing paleobathymetry on oceanic and continental crust. *Geochem. Geophys. Geosystems* 19 (6), 1898–1909. doi:10.1029/2017GC007313

Müller, R. D., Mather, B., Dutkiewicz, A., Keller, T., Merdith, A., Gonzalez, C. M., et al. (2022). Evolution of Earth's tectonic carbon conveyor belt. *Nature* 605 (7911), 629–639. doi:10.1038/s41586-022-04420-x

Nathan, S. A., and Leckie, R. M. (2009). Early history of the Western Pacific Warm Pool during the middle to late Miocene (~13.2–5.8 Ma): role of sea-level change and implications for equatorial circulation. *Palaeogeogr. Palaeoclimatol. Palaeoecol.* 274 (3-4), 140–159. doi:10.1016/j.palaeo.2009.01.007

Pälike, H., Lyle, M. W., Nishi, H., Raffi, I., Ridgwell, A., Gamage, K., et al. (2012). A Cenozoic record of the equatorial Pacific carbonate compensation depth. *Nature* 488, 609–614. doi:10.1038/nature11360

Pennington, J. T., Mahoney, K. L., Kuwahara, V. S., Kolber, D. D., Calienes, R., and Chavez, F. P. (2006). Primary production in the eastern tropical Pacific: a review. *Prog. Oceanogr.* 69 (2-4), 285–317. doi:10.1016/j.pocean.2006.03.012

Pillot, Q., Suchéras-Marx, B., Sarr, A. C., Bolton, C., and Donnadieu, Y. (2023). A global reassessment of the spatial and temporal expression of the Late Miocene Biogenic Bloom. *Paleoceanogr. Paleoclimatology* 38 (3), e2022PA004564. doi:10.1029/2022PA004564

Pratiwi, S. D., and Sato, T. (2016). Reconstruction of paleoceanography significance in the Western Pacific and Atlantic oceans during the Neogene based on calcareous nannofossil productivity and size variations, related to the global tectonic events. *Open J. Geol.* 6 (8), 931–943. doi:10.4236/ojg.2016.68070

Preiss-Daimler, I., Zarkogiannis, S. D., Kontakiotis, G., Henrich, R., and Antonarakou, A. (2021). Paleoceanographic perturbations and the marine carbonate system during the middle to late Miocene carbonate crash—a critical review. *Geosciences* 11 (2), 94. doi:10.3390/geosciences11020094

Ragueneau, O., Tréguer, P., Leynaert, A., Anderson, R. F., Brzezinski, M. A., DeMaster, D. J., et al. (2000). A review of the Si cycle in the modern ocean: recent progress and missing gaps in the application of biogenic opal as a paleoproductivity proxy. *Glob. Planet. Change* 26 (4), 317–365. doi:10.1016/S0921-8181(00)00052-7

Rea, D. K., Basov, I. A., and Krissek, L. A. (1995). "Scientific results of drilling the North Pacific transect," *Proceedings of the Ocean Drilling Program, scientific results*. Editors D. K. Rea, I. A. Basov, D. W. Scholl, and J. F. Allan (College Station, TX: Ocean Drilling Program), 145, 577–596. doi:10.2973/odp.proc.sr.145.1995

Rea, D. K., and Leinen, M. (1986). "Crustal subsidence and calcite deposition in the South Pacific ocean," *Initial reports of the Deep Sea Drilling project*. Editors M. Leinen, and D. K. Rea (Washington, U.S: Government. Printing Office), 92, 299–303. doi:10.2973/dsdp.proc.92.112.1986

Rea, D. K., and Lyle, M. W. (2005). Paleogene calcite compensation depth in the eastern subtropical Pacific: answers and questions. *Paleoceanogr. Paleoclimatology* 20 (1), 1–9. doi:10.1029/2004PA001064

Renaudie, J., Lazarus, D. B., and Diver, P. (2020). NSB (Neptune Sandbox Berlin): an expanded and improved database of marine planktonic microfossil data and deep-sea stratigraphy. *Palaeontol. Electron.* 23 (1), 1–28. doi:10.26879/1032

Ridgwell, A., and Hargreaves, J. C. (2007). Regulation of atmospheric CO_2 by deep-sea sediments in an Earth system model. *Glob. Biogeochem. Cycles* 21 (2), 1–14. doi:10.1029/2006GB002764

Roth, J. M., Droxler, A. W., and Kameo, K. (2000). "The Caribbean carbonate crash at the middle to late Miocene transition: linkage to the establishment of the modern global ocean conveyor," in *Proceedings of the Ocean Drilling Program, scientific results*. Editors R. M. Leckie, H. Sigurdsson, G. D. Acton, and G. Draper (College Station, TX: Ocean Drilling Program), 165. doi:10.2973/odp.proc.sr.165.013.2000

Schmittner, A., Sarnthein, N., Kinkel, H., Bartoli, G., Bickert, T., Crucifix, M., et al. (2004). Global impact of the Panamanian seaway closure. *Eos, Trans. AGU* 85 (49), 526. doi:10.1029/2004EO490010

Schneider, B., and Schmittner, A. (2006). Simulating the impact of the Panamanian seaway closure on ocean circulation, marine productivity and nutrient cycling. *Earth Planet. Sci. Lett.* 246 (3-4), 367–380. doi:10.1016/j.epsl.2006.04.028

Sclater, J. G., Meinke, L., Bennett, A., and Murphy, C. (1985). "The depth of the ocean through the Neogene," in *The Miocene ocean: paleoceanography and biogeography*. Editor J. P. Kennett (Geological Society of America Memoirs), 163, 1–20. doi:10.1130/MEM163-p1

Si, W., and Rosenthal, Y. (2019). Reduced continental weathering and marine calcification linked to late Neogene decline in atmospheric CO_2, *Nat. Geosci.* 12, 833–838. doi:10.1038/s41561-019-0450-3

Straume, E. O., Gaina, C., Medvedev, S., and Nisancioglu, K. H. (2020). Global Cenozoic paleobathymetry with a focus on the Northern Hemisphere oceanic gateways. *Gondwana Res.* 86, 126–143. doi:10.1016/j.gr.2020.05.011

Sulpis, O., Boudreau, B. P., Mucci, A., Jenkins, C., Trossman, D. S., Arbic, B. K., et al. (2018). Current $CaCO_3$ dissolution at the seafloor caused by anthropogenic CO_2. *Proc. Natl. Acad. Sci. U. S. A.* 115 (46), 11700–11705. doi:10.1073/pnas.1804250115

van Andel, T. H. (1975). Mesozoic/Cenozoic calcite compensation depth and the global distribution of calcareous sediments. *Earth Planet. Sci. Lett.* 26 (2), 187–194. doi:10.1016/0012-821X(75)90086-2

van Andel, T. H., Heath, G. R., Moore, J., and Theodore, C. (1975). "Cenozoic history and paleoceanography of the central equatorial Pacific Ocean," *Cenozoic history and paleoceanography of the central equatorial Pacific Ocean*. Editors T. H. van Andel, G. R. Heath, J. Moore, and T. Carlton (Boulder, CO: Geological Society of America Memoris), 143, 1–223. doi:10.1130/MEM143-p1

Van Andel, T. H., and Moore, J. , T. (1974). Cenozoic calcium carbonate distribution and calcite compensation depth in the central equatorial Pacific Ocean. *Geology* 2 (2), 87–92. doi:10.1130/0091-7613(1974)2<87:CCCDAC>2.0.CO;2

Von Der Heydt, A. S., and Dijkstra, H. A. (2011). "The impact of ocean gateways on ENSO variability in the Miocene," *The SE asian gateway: history and tectonics of the australia-asia collision*. Editors R. Hall, M. A. Cottam, and M. E. J. Wilson (London, UK: Geological Society, London, Special Publications), 355, 305–318. doi:10.1144/SP355.15

Wade, B. S., O'Neill, J. F., Phujareanchaiwon, C., Ali, I., Lyle, M., and Witkowski, J. (2020). Evolution of deep-sea sediments across the Paleocene-Eocene and Eocene-Oligocene boundaries. *Earth-Science Rev.* 211, 103403. doi:10.1016/j.earscirev.2020.103403

Wara, M. W., Ravelo, A. C., and Delaney, M. L. (2005). Permanent el niño-like conditions during the Pliocene warm period. *Science* 309 (5735), 758–761. doi:10.1126/science.1112596

Wessel, P., Luis, J. F., Uieda, L., Scharroo, R., Wobbe, F., Smith, W. H. F., et al. (2019). The generic mapping tools version 6. *Geochem. Geophys. Geosystems* 20 (11), 5556–5564. doi:10.1029/2019GC008515

Westerhold, T., Marwan, N., Drury, A. J., Liebrand, D., Agnini, C., Anagnostou, E., et al. (2020). An astronomically dated record of Earth's climate and its predictability over the last 66 million years. *Science* 369 (6509), 1383–1387. doi:10.1126/science.aba6853

Woodruff, F., and Savin, S. M. (1989). Miocene deepwater oceanography. *Paleoceanogr. Paleoclimatology* 4 (1), 87–140. doi:10.1029/PA004i001p00087

Xiao, K., Hu, X., Jiang, J., and Wang, J. (2024). Unraveling the Cenozoic carbon cycle by reconstructing carbonate compensation depth (CCD). *Sci. China Earth Sci.* 67 (6), 1743–1758. doi:10.1007/s11430-023-1291-5

Yin, S., Hernández-Molina, F. J., Jutzeler, M., and Li, J. (2022). Progressive intensification of Pacific deep water circulation since the early Pliocene. *Geophys. Res. Lett.* 49 (9), e2022GL098051. doi:10.1029/2022GL098051

Yuwono, F. S., and Sato, T. (2020). Miocene Sea surface dynamics in the western equatorial pacific based on calcareous nannofossil records. *IOP Conf. Ser. Earth Environ. Sci.* 618, 012006. Paper presented at the IOP Conference Series: Earth and Environmental Science. doi:10.1088/1755-1315/618/1/012006

Zhang, H., Che, H., Xia, J., Cheng, Q., Qi, D., Cao, J., et al. (2022). Sedimentary $CaCO_3$ accumulation in the deep west Pacific Ocean. *Front. Earth Sci.* 10 (857260), 1–8. doi:10.3389/feart.2022.857260

3| Article 2

Indian Ocean carbonate compensation depth since the Late Oligocene

Faranak Dalvand, Adriana Dutkiewicz, Nicky M. Wright & R. Dietmar Müller
EarthBythe Group, School of Geosciences, University of Sydney, NSW, Australia

Published in *Geo-Marine Letters* (2025), DOI: https://doi.org/10.1007/s00367-025-00825-5

Geo-Marine Letters (2025) 45:38
https://doi.org/10.1007/s00367-025-00825-5

RESEARCH

Indian Ocean carbonate compensation depth since the Late Oligocene

Faranak Dalvand[1] · Adriana Dutkiewicz[1] · Nicky M. Wright[1] · R. Dietmar Müller[1]

Received: 2 July 2025 / Accepted: 13 October 2025 / Published online: 4 November 2025

Abstract

The carbonate compensation depth (CCD), defined as the depth in the ocean where the supply rate of pelagic carbonate is balanced by its dissolution, provides an important parameter for estimating the amount of calcium carbonate-bound carbon that is stored in deep-sea sediments. The CCD is reasonably well-constrained across the Atlantic and Pacific oceans; however, our understanding of the regional CCD evolution across the Indian Ocean is limited to very broad relationships and a tightly confined region of the western equatorial sector. Here, we reconstruct the evolution of the CCD since the late Oligocene in three key regions of the Indian Ocean: the western equatorial Indian Ocean, the southeast Indian Ocean, and the Southern Ocean. We find that the CCD shows region-specific fluctuations of ~1–1.5 km over the last 15 Ma, marked by a long-term deepening pattern from ~3.5 km in the late Oligocene to ~4.4 km in the Pliocene across the western equatorial region, which was at its shallowest (~3.6 km) by ~27.5 Ma, and at its deepest (~4.4 km) by ~7.5–7 and ~4.5 Ma. In comparison, the southeast Indian and Southern oceans maintained relatively shallower CCDs, fluctuating between ~2.7 and 3.5 km and 3.4 and 4 km, respectively, since the late Miocene, consistent with the latitudinal gradient in carbonate flux and seafloor bathymetry. We propose that CCD variability across the equatorial Indian Ocean is driven by atmospheric CO_2 fluctuations, the dynamics of the Tethyan and Indonesian seaways, and the development of the Indo-Pacific water exchange since the late Oligocene. Peaks in carbonate productivity align with the establishment of the Pacific warm pool and the intensification of the Indian monsoons since the middle Miocene, with peak intensity contributing to the biogenic bloom interval of the late Miocene. The new regional CCD models provide a foundation for estimating the evolution of deep-sea carbonate carbon reservoirs across the Indian Ocean within the framework of the long-term global carbon cycle.

Introduction

Deep-sea carbonate records are critical archives for reconstructing the long-term dynamics of the global carbon cycle, offering direct evidence of variations in oceanic chemistry, carbon sequestration, and climate evolution over geological timescales. As the dominant long-term sink of carbon, deep-sea carbonates facilitate the transfer of surface carbon into the Earth's interior via the carbon conveyor belt (Müller et al. 2022). The distribution of pelagic carbonates is primarily controlled by the carbonate compensation depth (CCD) (e.g., Dutkiewicz et al. 2019; Woosley 2016), a dynamic boundary that reflects the equilibrium between the supply of carbonate and its dissolution. This means that the CCD represents the depth in the ocean below which the rate of carbonate dissolution exceeds the rate of accumulation (Lyle 2003), making it a sensitive indicator of changes in oceanic carbonate saturation state, surface productivity, and deep-water chemistry (e.g., Ridgwell and Zeebe 2005). Thus, the robust reconstruction of the CCD in global ocean basins over time is fundamental to advancing the quantification of long-term deep-ocean carbon storage.

Significant advances have been achieved in understanding CCD variations throughout the Cenozoic in both the Atlantic and Pacific oceans, where extensive ocean drilling efforts and high-resolution datasets have facilitated the development of regional CCD models (e.g., Dalvand et al. 2025; Dutkiewicz and Müller 2022; Pälike et al. 2012). In contrast, the Indian Ocean remains relatively understudied despite its crucial role in global thermohaline circulation by facilitating water mass exchange between the Atlantic and Pacific oceans (Piotrowski et al. 2009), and its major contribution to the climate system through its tropical warm pool (Schott et al. 2009),

✉ Faranak Dalvand
faranak.dalvand@sydney.edu.au

[1] EarthByte Group, School of Geosciences, University of Sydney, Sydney, Australia

making it a particularly sensitive domain for investigating carbon-climate feedbacks. Previous CCD reconstructions for the Indian Ocean have focused on limited drilling records distributed across the basin, providing generalised basin-wide CCD trends (Sclater et al. 1977; van Andel 1975). However, the Indian Ocean exhibits pronounced latitudinal variability in carbonate saturation states (Sabine et al. 2002) and regional changes in water mass properties (e.g., age, source, chemistry) and carbonate distribution (e.g., Kolla et al. 1976; Zhang et al. 2022), requiring CCD assessments at regional scales. Existing regional CCD studies are restricted to localised sites, such as the early Paleogene CCD from Ninetyeast Ridge (Slotnick et al. 2015) and the late Cenozoic from Ocean Drilling Program (ODP) Leg 115 drill sites in the western equatorial Indian (Campbell et al. 2018; Peterson and Backman 1990), collectively representing a small portion of the Indian basin.

Our objective in this study is to advance CCD modelling by broadening the spatial scope of the analysis within the western equatorial Indian Ocean, incorporating multiple locations in this region to refine the CCD model in previously underexplored areas, and extending temporal resolution back to the Oligocene. We also provide a new assessment of CCD variability in the southeast Indian Ocean and the Southern Ocean over the Neogene. The outcomes of this research will support the development of more accurate models of long-term carbon sequestration and enhance understanding of global carbon cycle mechanisms.

Data and methods

Data compilation

To optimise regional spatial coverage while ensuring data reliability, we identified three key regions for CCD modelling: the western equatorial Indian Ocean, the southeast Indian Ocean, and the Southern Ocean. These regions are defined based on the distribution of drill sites reliable for pelagic carbonate system studies, and are representative of broader oceanographic and latitudinal gradients. The CCD modelling in the northern Indian Ocean (Bay of Bengal and Arabian Basin) and the southwestern Indian region is hindered by complex stratigraphic sequences dominated by terrigenous and siliciclastic influx, turbidites, and reworked sediments throughout the Cenozoic (see also Davies et al. 1995; Kolla et al. 1976). Such depositional complexities obscure primary pelagic carbonate records, compromise the reliability of carbonate accumulation estimates, and constrain the use of regression analysis. Thus, we excluded these regions from our analysis and limited our CCD reconstruction to parts of the Indian Ocean with deep-sea drill sites containing undisturbed, well-preserved pelagic sequences. Similarly, the eastern equatorial region is excluded from this study due to the lack of drill cores suitable for regression analysis. In addition, CCD modelling for the early Cenozoic is constrained by poor Paleogene core recovery, along with the presence of unconformities, tectonic disruption, and bottom-water erosion, resulting in discontinuous and disturbed sediment records across the Indian Ocean (Davies et al. 1995; Peterson et al. 1992). Our criteria to define the southeast Indian Ocean, spanning from ~10°S to the southern Australian margin, is based on consistent regional hydrochemical characteristics, such as temperature, oxygen, and nutrient distributions, within the subtropical gyre between the hydrochemical front (~10–15°S) and the Antarctic Polar Front (~53°S) across the eastern Indian Ocean (Phillips et al. 2021; Wyrtki 1973). Drill sites within this region (including the Ninetyeast Ridge, Broken Ridge, the northwestern Australian region, the Great Australian Bight, and the South Australian margin) are bathed in intermediate-depth waters, sourced primarily from Antarctic Intermediate Water (AAIW) (Glaubke et al. 2024), with additional contributions from locally formed Subantarctic Mode Water (SAMW) (e.g., Li et al. 2021; Sallée et al. 2010). The latter originates through convective overturning near the Subantarctic Front south of Australia and subsequently spreads westward into the southeast Indian Ocean (Sallée et al. 2010). These intermediate waters are further influenced by Pacific-derived water circulation (through the Indonesian Throughflow and Tasman leakage), sharing a similar oceanographic regime distinct from the Southern Ocean setting (e.g., Phillips et al. 2021; Speich et al. 2002; van Sebille et al. 2014).

We utilised 70 deep-sea drill holes from the three defined regions selected for data availability, including lithology core logs, age-depth relationship, and carbonate and dry bulk density data (Fig. 1 and Supplementary Table 1). The drill sites span expeditions from the Deep Sea Drilling Project (DSDP), Ocean Drilling Program (ODP), and International Ocean Discovery Program (IODP). All data (available at https://doi.org/10.5281/zenodo.15780673) were sourced from the expeditions databases (http://deepseadrilling.org/, http://www-odp.tamu.edu/ and http://web.iodp.tamu.edu/LORE/), with age-depth models from initial/proceeding reports and Neptune Sandbox Berlin (NSB; https://nsb.mfn-berlin.de/, Renaudie et al. 2020; accessed February 2021), which are calibrated to the Gradstein et al. (2020) timescale. An archived version of the NSB dataset is also available at https://zenodo.org/records/10057363.

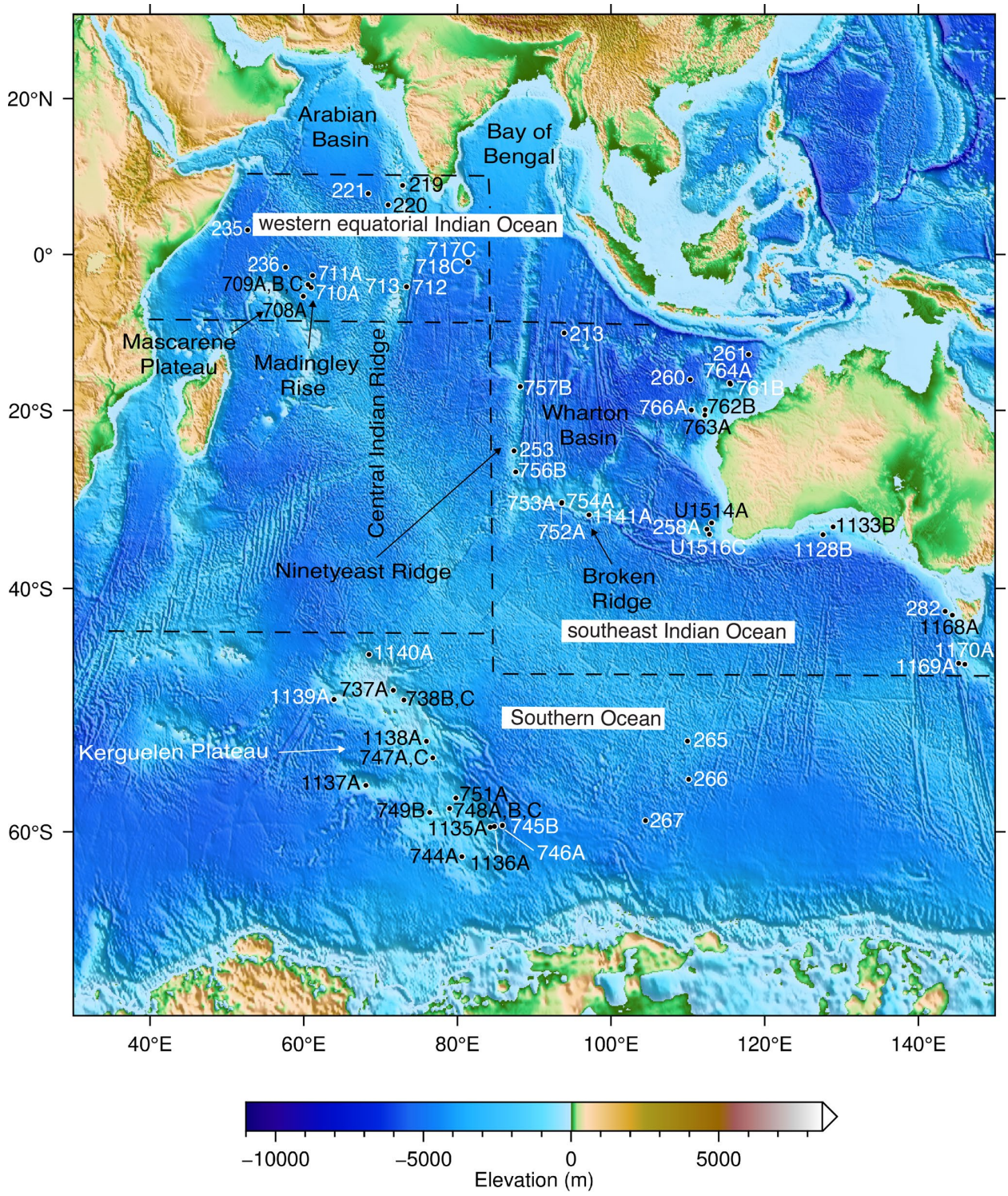

Fig. 1 Map of the Indian Ocean showing the location of 70 drill holes used in this study from the Deep Sea Drilling Project (DSDP), the Ocean Drilling Program (ODP), and the International Ocean Discovery Program (IODP) expeditions. Three regions for carbonate compensation depth (CCD) modelling are outlined by black dashed lines. Elevation shown is from ETOPO1 global relief model (https://www.ngdc.noaa.gov/mgg/global/; Amante and Eakins 2009). Mercator projection

Reconstructing the carbonate compensation depth (CCD)

We compute the CCD following the method employed in Dutkiewicz and Müller (2021) and Dalvand et al. (2025). Specifically, we use pyBacktrack 1.4 (Müller et al. 2018) to perform drill site backtracking and determine paleo-water depth through time, including changes in dynamic topography (Braz et al. 2021) and eustatic sea level (Miller et al. 2024). Within pyBacktrack 1.4, the paleobathymetry reconstruction on oceanic and continental crusts involves isostatic decompaction of sediment columns at each drill site, accounting for the effects of tectonic subsidence (Sclater et al. 1985; Stein and Stein 1992). For backtracking, we examine paleo-water depth computation using two age-depth relationships from Stein and Stein (1992)–GDH-1–and from Richards et al. (2018) along with estimates of oceanic lithosphere temperature and plate thickness. Although GDH-1 underestimates the subsidence of old oceanic lithosphere compared to areas of oceanic lithosphere unaffected by intraplate volcanism, it is more appropriate for paleodepth reconstruction in regions like the Indian Ocean, which features numerous oceanic plateaus, hotspot tracks, and seamounts associated with thermal rejuvenation and uplift. These areas bias the empirical data used in model fitting, leading to enhanced flattening in the age-depth relationship for ages older than 80 Myr. Thus, GDH-1 is utilised as the most appropriate model for backtracking the paleodepth of the ocean floor in this study. For backtracking, we also perform lithology-specific decompaction of the sediment column (from DSDP/ODP/IODP initial and proceeding reports) at 10 m intervals or finer using the lithology library in pyBacktrack 1.4, for which proportional estimates were applied to mixed lithologies (Müller et al. 2018).

At each drill site, carbonate accumulation rates (CARs) are calculated following Lyle (2003) by multiplying the weight% of $CaCO_3$ in a sample by its dry bulk density and the linear sedimentation rate. CAR values from multiple drill sites, partitioned into 1 Myr-wide moving windows and 0.5 Myr time steps, are integrated with computed paleo-water depths to reconstruct the CCD in the three regions. The CCD is quantified based on the assumption that the CAR value extrapolates to zero (Lyle 2003) below the lysocline, a depth at which a noticeable increase in $CaCO_3$ dissolution occurs (Broecker 2003), given the variability in lysocline shape over time (Broecker 2008). At each time step, following Campbell et al.'s (2018) approach, we perform a linear reduced major axis regression of CAR values against paleo-water depth to define the CCD (the y-intercept of the regression line, Fig. 2 and Supplementary Fig. 1) at 95% confidence, following the methodology of Dutkiewicz et al. (2019). Outliers are detected using GMT 6.4.0 *gmtregress* (https://docs.generic-mapping-tools.org/6.4/gmtregress.html; Wessel et al. 2019). Additionally, adopting the approach of Dutkiewicz and Müller (2022), we apply cutoffs to exclude CAR values < 1500 mg/cm²/kyr at paleo-water depths < 2.5 km (above the mid-ocean ridges) and values > 2000 mg/cm²/kyr at depths > 4.5 km, thereby reducing the influence of anomalous local signals such as dilution by non-carbonate or detrital material and downslope carbonate transport.

Fig. 2 Examples of regression analysis for CCD computation accounting for outliers, which incorporates the dynamic topography model from Braz et al. (2021) and the eustatic sea-level model from Miller et al. (2024). The paleo-water depth at which the carbonate accumulation rate (CAR) values become negligible (approach zero) with increasing depth determines the CCD, corresponding to the y-intercept. The regression plots highlight the evolution of the CCD across the western equatorial Indian Ocean since the latest Oligocene. Blue and red data points within each time window display data from multiple drill sites, with red circles indicating identified outliers. The 95% confidence envelope is depicted as a grey band. Regression plots from the southeast Indian Ocean and Southern Ocean are provided in the Supplementary Fig. 1

Results and discussion: CCD variability since the late Oligocene across the Indian Ocean

The incorporation of the GDH-1 age-depth relationship from Stein and Stein (1992) for backtracking the paleodepth of the ocean floor yields higher estimates of paleo-water depths and CCD compared to the Richards et al. (2018) model (see Data and Methods section). This difference reaches up to ~220 m in older intervals back to ~30.5 Ma across the western equatorial Indian region (Fig. 3). The GDH-1 model suggests comparatively greater depths for older oceanic lithosphere, relative to other age-depth relationships, such as that of Richards et al. (2018), partly due to its accounting for thermally rejuvenated seafloor, particularly in regions influenced by hotspot volcanism. However, the southeast region and the Southern Ocean demonstrate negligible deepening up to ~50 m in the middle Miocene intervals.

Our CCD reconstructions, which include the first CCD models in the southeast Indian and Southern oceans, reveal notable regional variation across the Indian Ocean, with comparatively shallower CCDs in these southern regions relative to the deeper estimates in the western equatorial Indian Ocean since the late Miocene (Fig. 4b–d). These patterns suggest substantial regional changes in carbonate flux throughout the Indian Ocean, primarily driven by surface and deep-water circulation, which appears to be the dominant control on the carbonate system within this ocean basin at present (Zhang et al. 2022). Here, we investigate the evolution of the CCD across the Indian Ocean in three

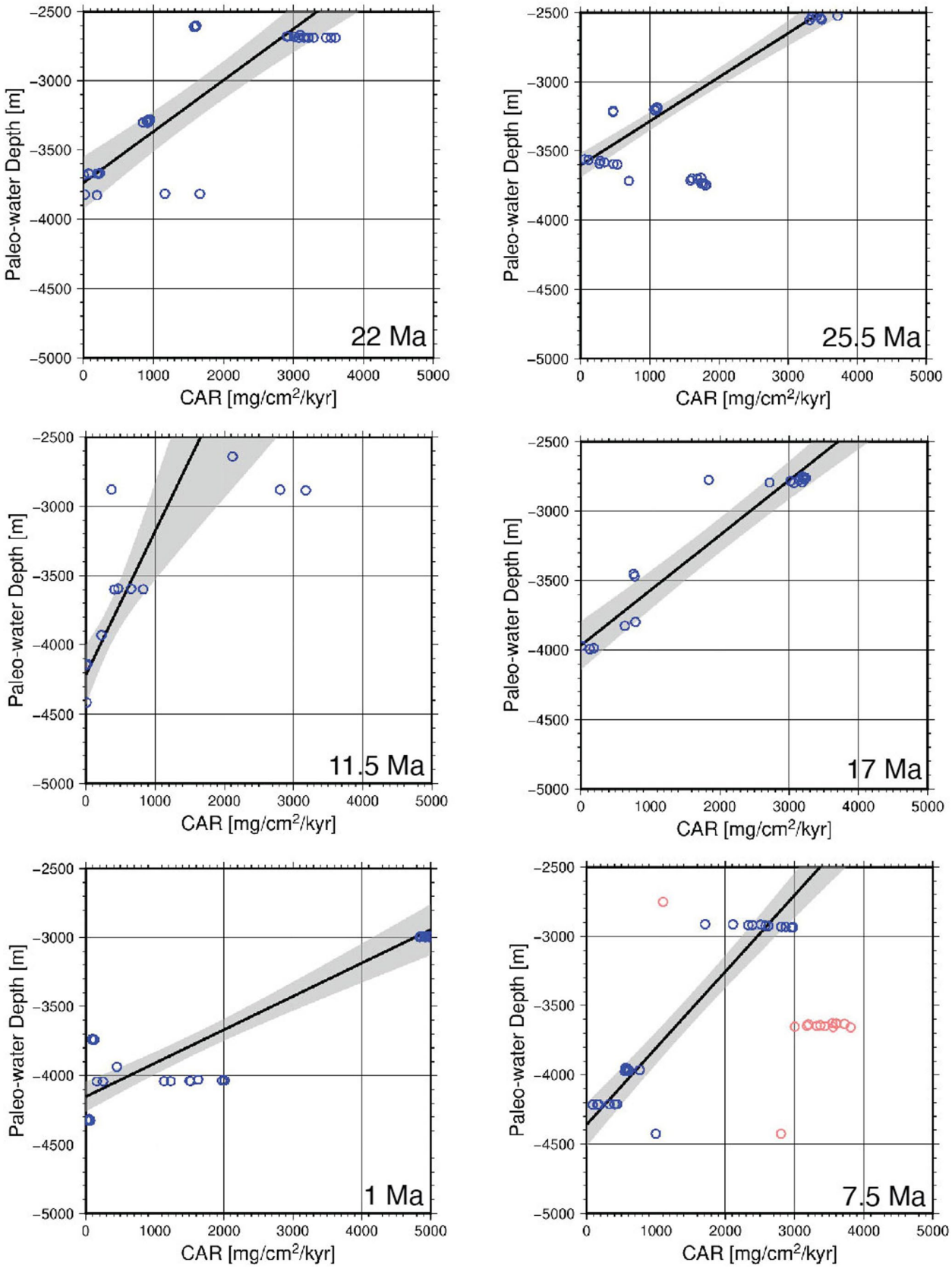
Paleo-water Depth [m]
CAR [mg/cm²/kyr]
22 Ma
25.5 Ma
11.5 Ma
17 Ma
1 Ma
7.5 Ma

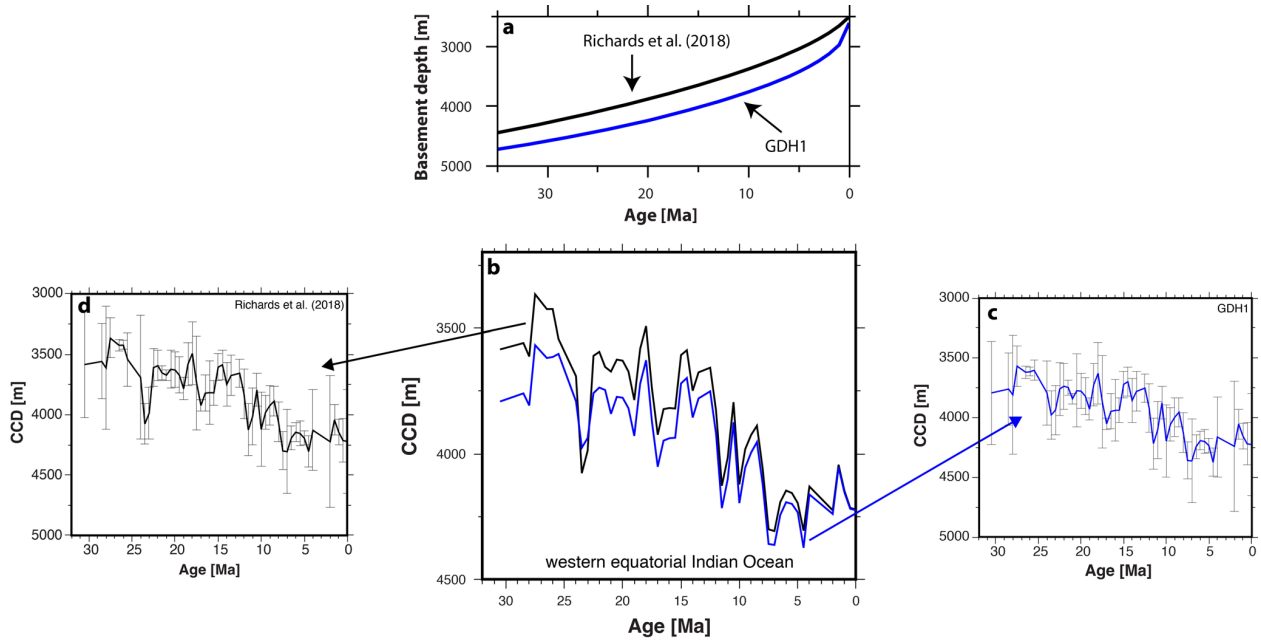

Fig. 3 Comparison of the CCD reconstructions in the western equatorial Indian Ocean using two oceanic basement age-depth relationships: GDH-1 model from Stein and Stein (1992), and the model of Richards et al. (2018) shown in (**a**). (**b**) CCD reconstructions for the western equatorial Indian Ocean using GDH-1 (blue line) and Richards et al. (2018) (black line). (**c**) and (**d**) CCD reconstructions with associated uncertainties using GDH-1 and Richards et al. (2018), respectively

main episodes since 30.5 Ma. Given the greater spatial and temporal coverage of drill sites from the western equatorial Indian Ocean, our discussion primarily focuses on the Oligocene and Miocene history of the CCD this region. Our discussion of CCD variability in the southeast Indian and Southern oceans is restricted to the late Miocene due to limited data coverage and higher associated uncertainties.

Late Oligocene to early Miocene

The Oligocene is marked by a major deepening of the carbonate compensation depth (CCD) by as much as 1–1.5 km, linked to global cooling, the onset of Antarctic glaciation, and changes in the carbon cycle (e.g., Taylor et al. 2023; van Andel and Moore Jr 1974; Zhifei et al. 2004). However, our CCD reconstruction in the western equatorial region shows that the CCD was relatively shallow (~3.6–4 km; Fig. 4b) during the latest Oligocene. Peterson and Backman (1990) estimated the CCD to be ~4.2 km for the same interval (Fig. 4b) but regarded this estimate as uncertain due to insufficient data. The shallow nature of our CCD can be explained by examining the subsidence history of each drill site used in the CCD reconstruction. Backtracking of the western equatorial sites shows that the latest Oligocene paleo-water depths are on average ~300–400 m shallower than those inferred in Peterson and Backman's (1990) reconstruction. Campbell et al. (2018) also demonstrated that drill sites were consistently offset to shallower depths, by approximately 400–800 m, relative to estimates derived from backtracking using Sclater et al.'s (1985) now outdated subsidence model. Because these sites were at relatively shallow water depths (between ~2.2–3.5 km; Supplementary Fig. 2), they invariably yield a relatively shallow CCD meaning that the seafloor at the sites may have been above the CCD. Therefore, the CCD in our model should be regarded as a minimum for this time (see dashed line in Fig. 4b).

At the earliest Miocene, the western equatorial Indian CCD shoals by ~300 m, from ~4 km at ~23.5 to ~3.7 km at ~20 Ma (Fig. 4b). While this shoaling has uncertainties up to ±280 m, it is consistent with previously documented CCD variations in the entire Indian Ocean CCD (van Andel 1975) and the western equatorial CCD (Peterson and Backman 1990) (Fig. 4b). This CCD change coincides with the late Oligocene–early Miocene transition (OMT; ~23.7–22.7 Ma), as documented in the northern Indian Ocean. In this record, the OMT spans a glaciation phase (~23.7–23 Ma) followed by deglaciation after ~23 Ma, and is recognized as a transient boundary marked by enhanced terrigenous flux and reduced carbonate preservation linked to the South Asian proto-monsoon (Beasley et al. 2021). The early Miocene CCD shoaling also correlates with the rise in atmospheric CO_2 (Hönisch et al. 2023; Fig. 4a), and is associated with reduced carbonate accumulation rates, driven by the relative

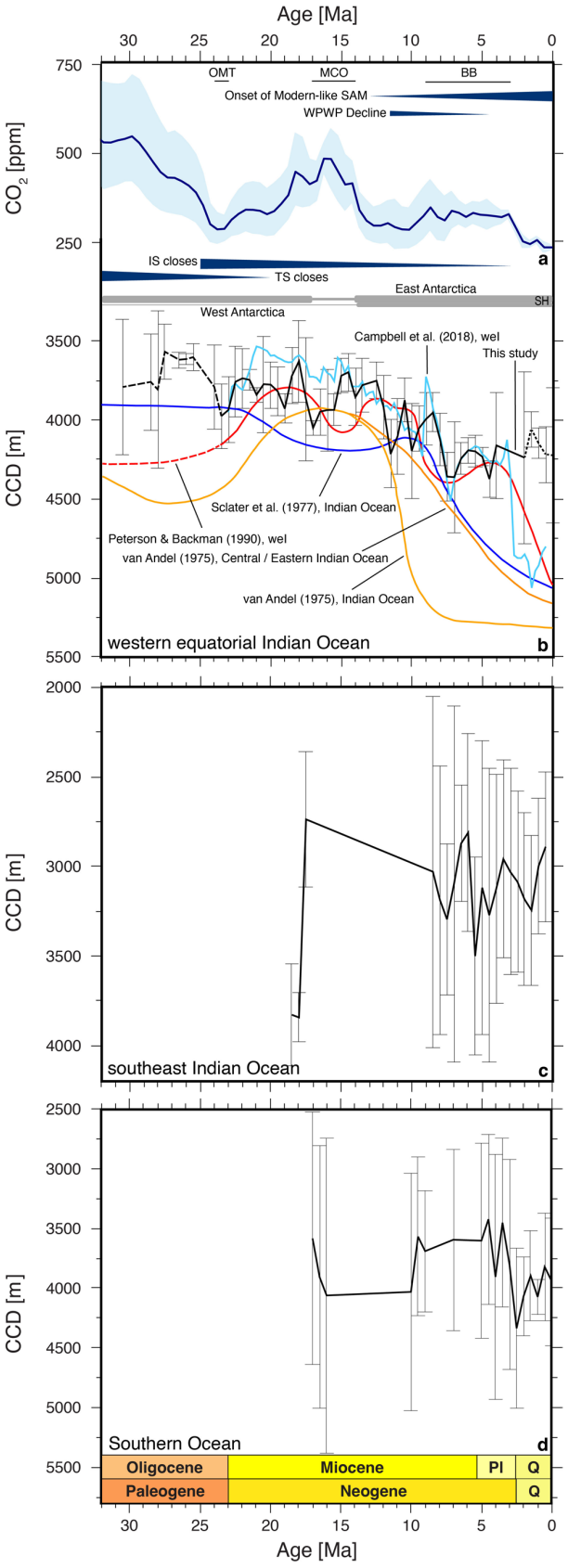

Fig. 4 (**a**) Atmospheric CO_2 estimates and error bars with 95% confidence intervals, shown at 500-kyr mean resolution since ~32 Ma from Hönisch et al. (2023). (**b**–**d**) Modelled CCDs within the Indian regions, as specified in Fig. 1, including (**b**) the western equatorial Indian Ocean, also showing earlier CCD reconstructions, (**c**) the southeast Indian Ocean, and (**d**) the Southern Ocean. Regression-derived CCD estimates from this study are shown as solid black lines. Each curve is accompanied by error bars indicating the range of uncertainty (derived from the grey envelope in Fig. 2). The timing of the Oligocene/Miocene transition (OMT), Miocene Climate Optimum (MCO) and the Southern Hemisphere (SH) glaciation from Westerhold et al. (2020), the Tethyan Seaway closure from Straume et al. (2024), and the Indonesian Seaway closure from Bahr et al. (2023) and Kuhnt et al. (2004). Approximate timing of the late Miocene-early Pliocene biogenic bloom (BB) in the equatorial Indian Ocean from Dickens and Owen (1999), the onset of the modern-like South Asian monsoon (SAM) from Gupta et al. (2015), and the Western Pacific Warm Pool (WPWP) decline from Nathan and Leckie (2009). The wel refers to the western equatorial region of the Indian Ocean, and IS and TS indicate the Indonesian and Tethyan seaways, respectively. The dashed portions of the CCD curve in the late Oligocene (panel b) from Peterson and Backman (1990) and from this study represent a minimum CCD, reflecting the shallower paleowater depths of the drill sites within this period. The Quaternary interval is also shown with a distinct dashed line, indicating the discrepancy with earlier studies. Considering the large associated uncertainties (±430 m at present), this portion should be interpreted with caution

influence of carbonate dissolution, reduced carbonate productivity, and winnowing of fine carbonates (corresponding to vigorous intermediate water circulation) in this region (Peterson et al. 1992). The early Miocene reduction in carbonate burial has been attributed to the intrusion of warm, saline Tethyan waters into the Indian Ocean (Woodruff and Savin 1989) along with the presence of well-oxygenated intermediate and deep water masses across the equatorial Indian Ocean during the early to middle Miocene (Boersma 1990). Circulation of Tethyan-derived waters influenced the western equatorial Indian Ocean (Bialik et al. 2019) until the closure of the deep Tethyan Seaway at ~20–19 Ma (Straume et al. 2024, 2025), despite a temporary re-flooding during the early middle Miocene through the shallow Mesopotamian Seaway, until its full closure at ~13.8 Ma (Bialik et al. 2019; Straume et al. 2024). Moreover, the initial Arabia-Eurasia collision at ~27 Ma (McQuarrie and van Hinsbergen 2013) led to enhanced terrigenous input to the northwestern Indian Ocean between ~24 and 21 Ma (Torfstein and Steinberg 2020). A comparable signal is observed across the western equatorial Indian Ocean, evidenced by increased clay accumulation and a concurrent reduction in carbonate content at drill sites such as DSDP Leg 24 Site 235, ODP Leg 115 Sites 709, 710, and 711 during this time.

The early Miocene CCD shallows further to ~3.6 km at ~18 Ma, before deepening to ~4.1 km at ~17 Ma (uncertainties ±90 to 250 m). This shallow interval (~19–18 Ma) coincides with a period of reduced carbonate flux and a shallower CCD in the equatorial Pacific, described as "carbonate famine" by Lyle (2003) linked to lowered carbonate

productivity and increased dissolution, which likely reflects Indo-Pacific water exchange due to the wide Indonesian Seaway before ~14 Ma (Gourlan et al. 2008).

Middle to late Miocene

Between ~17 and 14.5 Ma, the CCD shoals from ~4.1 km to ~3.7 km (uncertainties up to ±120 m, increasing to ±260 m at ~16 Ma, Fig. 4b), potentially reflecting a response to the climate shift over the Miocene Climate Optimum (MCO: 17–14 Ma; Westerhold et al. 2020), associated with elevated atmospheric CO_2 concentrations (Hönisch et al. 2023; Fig. 4a). The Monterey Excursion (carbon isotope maxima; Vincent and Berger 1985) between ~16.5 and 13.5 Ma across the eastern equatorial Indian Ocean is marked by a shift from carbonate deposition to siliceous productivity peaks at ~15.6 Ma, recorded by Kochhann et al. (2021). However, drill sites in the western equatorial Indian Ocean show increased clay deposition and a simultaneous decrease in carbonate burial during the CCD shoaling related to the MCO (peaking at ~3.7 km between ~15 and ~14.5 Ma), with no evidence of silica burial.

The CCD deepening from ~3.6 km at ~14.5 Ma to ~4.2 km at ~11.5 Ma (with uncertainties of ±110–210 m)—including a pronounced drop between ~12.5 and 11.5 Ma—indicates a transitional phase in carbonate flux in the western equatorial Indian Ocean, likely driven by multiple concurrent processes (Fig. 4b). This transition followed the surface and deep-water cooling and resulting thermocline shoaling, from ~14.7 Ma across the equatorial Indian, attributed to the constriction of the Indonesian Seaway (Podder et al. 2024). However, Podder et al. (2024) highlight the significant water mass change by ~12.9 Ma, linked to the initiation of the modern-like South Asian monsoon (SAM) at this time (Gupta et al. 2015), which coincided with the expansion of the Indian oxygen minimum zone (Betzler et al. 2016) and a significant $\delta^{13}C$ decline (Zachos et al. 1992). The onset of the modern-like SAM intensified upwelling and productivity in the western Indian Ocean (Sarr et al. 2022), with further contributions from global cooling and enhanced formation of Antarctic Bottom Water (AABW) and Northern Component Water (NCW), leading to increased foraminifera productivity in this region (Smart et al. 2007). Moreover, the primary evolution of the Western Pacific Warm Pool (WPWP) following the Middle Miocene Climate Transition (MMCT) is attributed to the progressive constriction of the Indonesian Seaway, which reduced Indo-Pacific water exchange and, in turn, promoted regional cooling and enhanced surface productivity in the eastern equatorial Indian Ocean (Sosdian and Lear 2020). The post-MMCO development of the WPWP may have potentially influenced the western equatorial Indian Ocean, as suggested by comparable water mass characteristics in these regions between ~14 Ma and ~3 Ma, supported by similar Nd isotope signatures (Gourlan et al. 2008). However, we argue that the major influence of the WPWP decline on the western equatorial Indian Ocean at ~11.5 Ma is reflected in a marked CCD drop (to ~4.2 km), coinciding with the stabilisation of the WPWP position across the equatorial Pacific by ~11.6 Ma (Nathan and Leckie 2009). This is consistent with the stepwise CCD shoaling observed after ~11.5 Ma across the equatorial Pacific (Dalvand et al. 2025). Dalvand et al. (2025) recorded a peak of CCD deepening across the eastern equatorial Pacific at ~12 Ma and in the western tropical Pacific at ~12.5 Ma– patterns not mirrored in other Pacific sectors. A contemporaneous CCD drop across the western equatorial Indian Ocean suggests a broader equatorial response spanning the Pacific and Indian oceans. Nevertheless, we believe that the post–12 Ma CCD shoaling in the equatorial Pacific (Dalvand et al. 2025) reflects the WPWP stabilisation at ~11.6 Ma in the Pacific, while the coeval peak of CCD deepening in the western equatorial Indian Ocean may signal a diminishing WPWP influence in this region.

The deep CCD of ~4.2 km at ~11.5 Ma in the western equatorial region was interrupted by subsequent shoaling to ~3.8 km at 10.5 Ma (with uncertainties of ±130–300 m, Fig. 4b), likely linked to the carbonate crash globally occurring between ~11 and 10 Ma (Torfstein and Steinberg 2020). While the carbonate crash in the equatorial Indian Ocean has been constrained to ~13.5–8.2 Ma, peaking between ~11.5 and 10 Ma, based on records from a single site IODP-U1443 located above the regional CCD in the eastern equatorial Indian Ocean (Lübbers et al. 2019), our regional model from the western equatorial sector reveals only a short-lived CCD shoaling episode culminating at ~10.5 Ma, followed by a recovery to ~4.1 km at ~10 Ma.

Since the latest Miocene

Tha western equatorial Indian Ocean involved a~500 m deepening from ~3.9 km at ~8.5 Ma to ~4.4 km by ~7 Ma, with associated uncertainties of ±120–160 m. Subsequently, the CCD exhibits modest variability between ~4.1 and 4.3 km before stabilising at its modern depth of ~4.2 km (Fig. 4b). The overall deepening trend since ~8.5 Ma corresponds to enhanced carbonate flux in this region within this time (Peterson and Backman 1990; Peterson et al. 1992). This transition also aligns with the onset of modern deep-water circulation in the Indian Ocean during this time (Woodruff and Savin 1989), consistent with the global increase in deep-sea carbonate flux driven by intensified continental weathering and alkalinity input to pelagic realms (van der Ploeg et al. 2019). We also suggest that the

Central American Seaway (CAS) constriction may have played a role in the late Miocene CCD shift. Prabhat et al. (2022) linked changes in deep-water circulation in the western North Indian Ocean to CAS narrowing, documenting a shift from Pacific-derived water mass (PDW) prior to ~9 Ma to an increasing influence from North Atlantic Deep Water (NADW) and NCW post-9 Ma, associated with CAS constriction, based on neodymium isotopic records. This transition signifies a substantial reorganisation of the Indian Ocean deep-water regime, increasingly dominated by AABW and NCW between 9 and 6 Ma. Synchronous CCD deepening after ~9 Ma in the central North and South Atlantic (Dutkiewicz and Müller 2022) further supports the role of CAS constriction and NADW formation in regulating inter-basin carbonate dynamics.

We propose that the major Neogene CCD deepening of ~400 m between ~9 and 7 Ma (peaking at ~7.5–7 Ma) in the western equatorial Indian Ocean may be linked to the Indian biogenic bloom event. The occurrence of the biogenic bloom across the western Indian Ocean, resulting from enhanced marine productivity and carbonate accumulation between ~7.6 and 7 Ma, is marked by a decline in foraminiferal $\delta^{13}C$ at ~7.6 Ma (Diester-Haass et al. 2006). This elevated productivity has been attributed to the strengthening of the East Asian monsoon, enhanced continental weathering, and increased nutrient flux to the oceans (Bolton et al. 2022; Filippelli 1997), likely driven by Antarctic glaciation and climate cooling (Holbourn et al. 2018). This phase also coincides with a sustained decline in sea surface temperature (SST) from ~7.5 to ~5.8 Ma across the equatorial Indian Ocean (Martinot et al. 2022), attributed to reduced atmospheric CO_2 levels (Tanner et al. 2020).

We further suggest that the subsequent modest CCD shoaling of ~200 m from ~7 Ma to ~5 Ma, with a maximum shoaling during ~6–5.5 Ma (~4.4–4.2 km, considering uncertainties up to ±120 m) in this region may reflect the influence of the late Miocene-early Pliocene biogenic bloom (Bolton et al. 2022; Dickens and Owen 1999; Karatsolis et al. 2022; Pillot et al. 2023). The occurrence of biogenic bloom in the Indian Ocean is recorded between ~9 and ~3.5 Ma, peaking at ~6–5 Ma (Dickens and Owen 1999), corresponding to enhanced carbonate and silica productivity and supply of organic carbon at various drill sites in the western Indian Ocean (Baldauf et al. 1992; Dickens and Owen 1999; Mikkelsen 1990; Peterson et al. 1992). Dickens and Owen (1999) associated enhanced carbonate production of the biogenic bloom in the western equatorial Indian Ocean with an expanded oxygen minimum zone. However, the biogenic bloom period was also accompanied by intensified carbonate dissolution driven by elevated organic carbon flux due to higher productivity intensification in this region (Dickens and Owen 1999; Peterson et al. 1992), which is reflected in the brief shallowing at ~6.5–5 Ma (peaking at ~6–5.5 Ma) in our CCD model. Lyle et al. (1995) examined the relationship between productivity levels and CCD variability across the eastern Pacific. He argued that an initial enhancement of productivity promotes carbonate burial and CCD deepening. However, with further intensification of productivity, the associated rise in organic carbon flux enhances carbonate dissolution, ultimately leading to CCD shoaling. Dalvand et al. (2025) also reported a peak in CCD shoaling between ~7 and ~6.5 Ma (following a CCD deepening at ~8.5 Ma), which they interpreted to correspond to reduced carbonate burial alongside enhanced silica production during the biogenic bloom in the eastern equatorial Pacific. In the western equatorial Indian Ocean, Dickens and Owen (1999) identified late Miocene–early Pliocene biogenic bloom signals comparable to those in the Pacific. Evidence from ODP Leg 115 in this region shows reduced carbonate burial at deep drill sites (708, 710, and 711) between ~6 and ~5 Ma, subsequent to an earlier phase of enhanced productivity and carbonate burial between ~9 and ~7 Ma. Dickens and Owen (1999) further discussed a productivity peak during ~6–5 Ma, coincident with diminished carbonate burial at these sites, attributed to elevated organic carbon flux and intensified carbonate dissolution(see also Peterson and Backman 1990). Pillot et al. (2023) also recorded a peak in carbonate accumulation at ~7±0.25 Ma, followed by a decline at ~5.5±0.25 Ma in the western equatorial Indian Ocean. We therefore suggest that this CCD shoaling was largely driven by carbonate dissolution triggered by intensified productivity and organic carbon input during the latest Miocene-early Pliocene biogenic bloom. This interval also corresponds with diatom-rich sedimentation observed between ~6 and 4.5 Ma in the western equatorial Indian Ocean (Mikkelsen 1990). Thus, based on the biogenic bloom interval of ~9–3 Ma identified by Dickens and Owen (1999), we interpret the major CCD deepening between ~8 and ~7 Ma, followed by the shoaling to ~4.5 Ma, as a regional manifestation of this event in our CCD model. These variations likely represent differential CCD responses to elevated carbonate and siliceous productivity, coupled with modest carbonate dissolution. This pattern closely correlates with the CCD trends modelled by Peterson and Backman (1990) and Campbell et al. (2018) during the same interval, highlighting a strong agreement between the biogenic bloom records and observed CCD variability. Karatsolis et al. (2022) estimates the biogenic bloom to span ~5.5 to ~4.2 Ma in the Indian Ocean, with its termination (~4.6–4.4 Ma globally) attributed to nutrient input decline triggered by the weakening of the East Asian monsoon, rather than the reduction of upwelling intensity and ocean circulation variability affected by tectonic activities and reconfiguration of oceanic gateways, as dominant

controls on the biogenic bloom occurrence (Pillot et al. 2023).

Additionally, the apparent CCD deepening of ~800 m between ~5.5 and ~4 Ma in the southeast Indian Ocean (south of 15°S), a region generally characterized by low productivity (Hermoyian and Owen 2001; Peirce et al. 1989), should be interpreted with caution given the associated uncertainties in the reconstruction (±500–700 m; Fig. 4c). Nonetheless, its timing aligns with the late Miocene–early Pliocene biogenic bloom records across the Ninetyeast and Broken ridges (Dickens and Owen, 1999; Hermoyian and Owen 2001), supporting the interpretation that this signal may represent a broader regional expression of this occurrence and a noteworthy focus for further studies in the southeast Indian Ocean. The records of biogenic bloom in this region have been linked to monsoon intensity and the expansion of the oxygen minimum zone in this region, which promoted enhanced foraminifera productivity and carbonate accumulation. Hermoyian and Owen (2001) highlight the extension of the biogenic bloom into the low-productivity region of the southeast Indian Ocean, supporting its recognition as a potentially global phenomenon.

Since the late Miocene, the western equatorial Indian Ocean has exhibited a deeper CCD (~3.9–4.4 km; Fig. 4b) compared to the relatively shallower CCDs in the southeast Indian Ocean (~2.7–3.5 km; Fig. 4c) and the Southern Ocean (~3.4–4 km; Fig. 4d). This pattern correlates with the current latitudinal gradient in seawater calcite saturation (Sabine et al. 2002) and increased carbonate accumulation towards the equator of the Indian Ocean (e.g., Kolla et al. 1976). North of the hydrochemical front, a chemical transition zone marking shifts in nutrient levels and oxygen content between the subtropical regions and the northern gyres of the Indian Ocean (~10–15°S; Wyrtki 1973), elevated nutrient supply supports high productivity across the equatorial Indian Ocean (Phillips et al. 2021). In contrast, the low-productivity area of the southeast Indian Ocean is affected by corrosive AABW and carbonate dilution, leading to intensified dissolution and reduced carbonate flux (Kolla et al. 1976). At present, carbonate preservation decreases from the Southern Indian Ocean toward the northern region due to a decline in deep water CO_3^{-2} (from ~115 µmol/kg south of 40°S to ~80 µmol/kg in Central Indian and Wharton Basin) (Zhang et al. 2022). A similar pattern likely existed since the late Miocene, coinciding with the establishment of a modern-like ocean circulation (e.g., Prabhat et al. 2022; Woodruff and Savin 1989; Wright et al. 1991). Our relatively shallow CCD estimates in in this region reflect that most sites from the Great Australian Bight, the Nintyeast Ridge, and Broken Ridge were located at relatively shallow depths during the Neogene (e.g., Feary et al. 2000; Lyu et al. 2023; Peirce et al. 1989). Paleowater depths for these sites range between ~1600 m to ~3500 m from the late Oligocene to the present (Supplementary Fig. 3). Our modelled present-day CCD is therefore biased by the lack of relatively deep sites below the CCD. This biases our CCD estimates for recent times towards shallow depths. In contrast, the Southern Ocean exhibits better carbonate preservation due to younger water mass flow (Zhang et al. 2022). However, it is also marked by high biogenic opal productivity (Honjo et al. 2008), experiencing a significant transition to enhanced opal accumulation during the late Miocene cooling around the Kerguelen Plateau (Bohrmann and Ehrmann 1991).

Our CCD model for the western equatorial Indian Ocean yields a present-day CCD of ~4.2 km (±430 m), which is shallower than earlier estimates, such as ~4.8 ± 0.13 km at ~0.5 Ma computed by Campbell et al. (2018) and ~5 km calculated by Peterson and Backman (1990). It is also shallower than the present-day CCD of ~4.9 km computed by Zhang et al. (2022) in the Central Indian Basin, and the Arabian and Somali basins using a simple carbonate accumulation model. However, a recent compilation by Panchang and Ambokar (2021) shows that the present-day CCD varies between >5.1 km and 3.9 km across the Indian Ocean. It is difficult to compare results from vastly different methodologies. The difference between our and Campbell et al.'s (2018) Quaternary CCD based on similar methodology and sites may be due to different CAR computations, which are dependent on the computed sedimentation rates and hence the age-depth model used. Campbell et al. (2018) used CAR values from Peterson and Backman (1990), whereas we used updated age-depth models from NSB calibrated to the Gradstein et al. (2020) timescale. However, given the discrepancy between the various CCD estimates and the errors in our Quaternary CCD (Fig. 4b), we suggest that the 2–0 Ma segment of the CCD should be viewed with caution pending re-evaluation of the CCD should relevant data become available in the future.

Conclusions

This study offers distinct CCD models for three defined regions of the Indian Ocean: the western equatorial, the southeast Indian, and the Southern oceans. Spatial-temporal variability in CCD estimates across the Indian Ocean, fluctuating by ~1–1.5 km, suggests the intricate influence of global and regional controls on carbonate productivity, including shifts in atmospheric CO_2, ocean water mass chemistry, circulation, and reorganisation as well as paleobathymetry since the late Oligocene. The relatively deeper CCD between ~3.5 and ~4.4 km in the western equatorial Indian Ocean since the late Oligocene, compared to the other two regions, correlates with enhanced carbonate

burial across the equatorial Indian Ocean. The CCD pattern in this region has been influenced by the development of the Indo-Pacific water exchange and the evolution of the Indian monsoon system, both of which have been modulated by the progressive constriction of the Indonesian Seaway throughout the Neogene. Since the middle Miocene, the intensification and reorganisation of the South and East Asian monsoons have influenced the Indian pelagic carbonate dynamics, contributing to the deepening of the CCD across the equatorial region of the Indian Ocean.

Our results provide a basis for evaluating deep carbon reservoirs across the Indian Ocean. Nevertheless, achieving robust CCD estimates for long-term carbon computations extending into the earliest Cenozoic in the Indian Ocean requires advanced databases including improved core recovery and extended age models from well-preserved deep-sea records.

Supplementary Information The online version contains supplementary material available at https://doi.org/10.1007/s00367-025-00825-5.

Acknowledgements We thank Editor Qian Yu and the three anonymous reviewers for their thoughtful and constructive feedback, which greatly enhanced the quality of this article.

Author contributions Faranak Dalvand: Writing – original draft, Formal analysis, Data curation, Visualisation, Investigation. Adriana Dutkiewicz: Writing – review & editing, Methodology, Conceptualisation, Formal analysis, Funding acquisition, Supervision. Nicky M. Wright: Writing – review & editing, Formal analysis, Supervision. R. Dietmar Müller: Writing – review & editing, Methodology, Conceptualisation, Formal analysis, Supervision.

Funding This research was supported by an Australian Research Council (ARC) PhD scholarship to F.D. and an ARC Future Fellowship to A.D. via grant FT190100829. N.M.W. was supported by an ARC grant IE230100098. R.D.M. was supported by the AuScope Simulation, Analysis & Modelling node funded by the Australian Government through the National Collaborative Research Infrastructure Strategy, NCRIS.

Data availability Data supporting the results of this study can be found online at https://doi.org/10.5281/zenodo.17232379

Declarations

Competing interests The authors declare no competing interests.

References

Amante C, Eakins BW (2009) ETOPO1 arc-minute global relief model: procedures, data sources and analysis. National Geophysical Data Center, NOAA, NOAA Technical Memorandum NESDIS NGDC-24. https://repository.library.noaa.gov/view/noaa/1163

Bahr A, Kaboth-Bahr S, Karas C (2023) The opening and closure of oceanic seaways during the Cenozoic: pacemaker of global climate change? In V. M. Rossi, S. G. Longhitano, C. Olario, & F. L. Chiocci (Eds.), Straits and Seaways: Controls, Processes and Implications in Modern and Ancient Systems 523:141–171: Geological Society, Londen, Special Publication. https://doi.org/10.1144/SP523-2021-54

Baldauf J, Barron J, Ehrmann W, Hempel P, Murray D (1992) Biosiliceous sedimentation patterns for the Indian Ocean during the last 45 million years. In R. A. Duncan, D. K. Rea, R. B. Kidd, U. v. Rad, & J. K. Weissel (Eds.), In Synthesis of Results from Scientific Drilling in the Indian Ocean (Vol. 70, pp. 335–349). Geophysical Monograph Series. https://doi.org/10.1029/GM070p0335

Beasley C, Kender S, Giosan L, Bolton CT, Anand P, Leng MJ et al (2021) Evidence of a South Asian proto-monsoon during the Oligocene-Miocene transition. Paleoceanogr Paleoclimatol 36(9):e2021PA004278. https://doi.org/10.1029/2021PA004278

Betzler C, Eberli GP, Kroon D, Wright JD, Swart PK, Nath BN et al (2016) The abrupt onset of the modern South Asian monsoon winds. Sci Rep 6(1):29838. https://doi.org/10.1038/srep29838

Bialik OM, Frank M, Betzler C, Zammit R, Waldmann ND (2019) Two-step closure of the Miocene Indian Oboth the Atlanticcean gateway to the Mediterranean. Sci Rep 9(1):8842. https://doi.org/10.1038/s41598-019-45308-7

Boersma A (1990) Late Oligocene to late Pliocene benthic foraminifers from depth traverses in the central Indian Ocean. In R. Duncan, J. Backman, & L. C. Peterson (Eds.), Proceedings of the Ocean Drilling Program, Scientific Results (Vol. 115, pp. 315–379). College Station, TX: Ocean Drilling Program. https://doi.org/10.2973/odp.proc.sr.115.146.1990

Bohrmann G, Ehrmann WU (1991) Analysis of sedimentary facies using bulk mineralogic characteristics in Cretaceous to Quaternary sediments from the Kerguelen Plateau: Sites 737, 738, and 744. In J. Barron & B. Larsen (Eds.), Proceedings of the Ocean Drilling Program: Scientific Results College Station, TX: Ocean Drilling Program 119:211–223). https://doi.org/10.2973/odp.proc.sr.119.122.1991

Bolton CT, Gray E, Kuhnt W, Holbourn AE, Lübbers J, Grant K et al (2022) Secular and orbital-scale variability of equatorial Indian Ocean summer monsoon winds during the late Miocene. Clim Past 18(4):713–738. https://doi.org/10.5194/cp-18-713-2022

Braz C, Zahirovic S, Salles T, Flament N, Harrington L, Müller RD (2021) Modelling the role of dynamic topography and eustasy in the evolution of the Great Artesian Basin. Basin Res 33(6):3378–3405. https://doi.org/10.1111/bre.12606

Broecker WS (2003) The oceanic $CaCO_3$ cycle. In: Holland HD, Turekian KK (eds) Treatise on geochemistry. Elsevier, pp 529–549. https://doi.org/10.1016/B0-08-043751-6/06119-3

Broecker WS (2008) A need to improve reconstructions of the fluctuations in the calcite compensation depth over the course of the Cenozoic. Paleoceanography. https://doi.org/10.1029/2007PA001456

Campbell SM, Moucha R, Derry LA, Raymo ME (2018) Effects of dynamic topography on the Cenozoic carbonate compensation depth. Geochem Geophys Geosyst 19(4):1025–1034. https://doi.org/10.1002/2017GC007386

Dalvand F, Dutkiewicz A, Wright NM, Mather BR, Müller RD (2025) Regional carbonate compensation depth variability in the Pacific Ocean since the Oligocene. Front Earth Sci 13:1605906. https://doi.org/10.3389/feart.2025.1605906

Davies TA, Kidd RB, Ramsay ATS (1995) A time-slice approach to the history of Cenozoic sedimentation in the Indian Ocean. Sed Geol 96(1–2):157–179. https://doi.org/10.1016/0037-0738(94)00131-D

Dickens GR, Owen RM (1999) The latest Miocene–early Pliocene biogenic bloom: a revised Indian Ocean perspective. Mar Geol 161(1):75–91. https://doi.org/10.1016/S0025-3227(99)00057-2

Diester-Haass L, Billups K, Emeis KC (2006) Late Miocene carbon isotope records and marine biological productivity: was there a (dusty) link? Paleoceanography. https://doi.org/10.1029/2006PA001267

Dutkiewicz A, Müller RD (2021) The carbonate compensation depth in the South Atlantic Ocean since the Late Cretaceous. Geology 49(7):873–878. https://doi.org/10.1130/G48404.1

Dutkiewicz A, Müller RD (2022) The history of Cenozoic carbonate flux in the Atlantic Ocean constrained by multiple regional carbonate compensation depth reconstructions. Geochem Geophys Geosyst 23(11):e2022GC010667. https://doi.org/10.1029/2022GC010667

Dutkiewicz A, Müller RD, Cannon J, Vaughan S, Zahirovic S (2019) Sequestration and subduction of deep-sea carbonate in the global ocean since the early Cretaceous. Geology 47(1):91–94. https://doi.org/10.1130/G45424.1

Feary DA, Hine AC, Malone MJ, Andres M, Betzler C, Brooks GR et al (2000) 1. Leg 182 Summary: Great Australian Bight—Cenozoic cool-water carbonates. In D. A. Feary, A. C. Hine, M. J. Malone, M. Andres, C. Betzler, G. R. Brooks, C. A. Brunner, M. Fuller, R. S. Molina Garza, & A. E. Holbourn (Eds.), Proceedings of the Ocean Drilling Program. Initial Reports. College Station, TX: Ocean Drilling Program vol. 182. https://doi.org/10.2973/odp.proc.ir.182.101.2000

Filippelli GM (1997) Intensification of the Asian monsoon and a chemical weathering event in the late Miocene–early Pliocene: implications for late Neogene climate change. Geology 25(1):27–30. 1997)025%3C0027%3AIOTAMA%3E2.3.CO%3B2 https://doi.org/10.1130/0091-7613

Glaubke RH, Wagner AJ, Sikes EL (2024) Characterizing the stable oxygen isotopic composition of the Southeast Indian Ocean. Mar Chem 262:104397. https://doi.org/10.1016/j.marchem.2024.104397

Gourlan AT, Meynadier L, Allègre CJ (2008) Tectonically driven changes in the Indian Ocean circulation over the last 25 Ma: neodymium isotope evidence. Earth Planet Sci Lett 267(1–2):353–364. https://doi.org/10.1016/j.epsl.2007.11.054

Gradstein FM, Ogg JG, Schmitz MD, Ogg GM (2020) Geologic time scale 2020, vol vol 1. Elsevier, Netherlands. https://doi.org/10.1016/C2020-1-02369-3

Gupta AK, Yuvaraja A, Prakasam M, Clemens SC, Velu A (2015) Evolution of the South Asian monsoon wind system since the late middle Miocene. Palaeogeogr Palaeoclimatol Palaeoecol 438:160–167. https://doi.org/10.1016/j.palaeo.2015.08.006

Hermoyian CS, Owen RM (2001) Late Miocene-early Pliocene biogenic bloom: evidence from low-productivity regions of the Indian and Atlantic Oceans. Paleoceanogr Paleoclimatol 16(1):95–100. https://doi.org/10.1029/2000PA000501

Holbourn AE, Kuhnt W, Clemens SC, Kochhann KG, Jöhnck J, Lübbers J, Andersen N (2018) Late Miocene climate cooling and intensification of Southeast Asian winter monsoon. Nat Commun 9(1):1584. https://doi.org/10.1038/s41467-018-03950-1

Hönisch B, Royer DL, Breecker DO, Polissar PJ, Bowen GJ, Henehan MJ et al (2023) Toward a Cenozoic history of atmospheric CO_2. Science 382(6675):eadi5177. https://doi.org/10.1126/science.adi5177

Honjo S, Manganini SJ, Krishfield RA, Francois R (2008) Particulate organic carbon fluxes to the ocean interior and factors controlling the biological pump: a synthesis of global sediment trap programs since 1983. Prog Oceanogr 76(3):217–285. https://doi.org/10.1016/j.pocean.2007.11.003

Karatsolis BT, Lougheed BC, De Vleeschouwer D, Henderiks J (2022) Abrupt conclusion of the late Miocene-early Pliocene biogenic bloom at 4.6–4.4 Ma. Nat Commun 13(1):353. https://doi.org/10.1038/s41467-021-27784-6

Kochhann KGD, Kuhnt W, Holbourn AE, Usui Y, Lübbers J, Beil S, Andersen N (2021) Impacts of the middle Miocene climatic transition on deep-water carbonate preservation and oxygenation in the equatorial Indian Ocean. Palaeogeogr Palaeoclimatol Palaeoecol 576:110511. https://doi.org/10.1016/j.palaeo.2021.110511

Kolla V, Bé AW, Biscaye PE (1976) Calcium carbonate distribution in the surface sediments of the Indian Ocean. J Phys Res 81(15):2605–2616. https://doi.org/10.1029/JC081i015p02605

Kuhnt W, Holbourn A, Hall R, Zuvela M, Käse R (2004) Neogene history of the Indonesian throughflow. In P. Clift, W. Kuhnt, P. Wang, & D. Hayes (Eds.), Continent-Ocean Interactions Within East Asian Marginal Seas: Geophysical Monograph Series 149:299–320. https://doi.org/10.1029/149GM16

Li Z, England MH, Groeskamp S, Cerovečki I, Luo Y (2021) The origin and fate of subantarctic mode water in the Southern Ocean. J Phys Oceanogr 51(9):2951–2972. https://doi.org/10.1175/JPO-D-20-0174.1

Lübbers J, Kuhnt W, Holbourn AE, Bolton CT, Gray E, Usui Y et al (2019) The middle to late Miocene "Carbonate Crash" in the equatorial Indian Ocean. Paleoceanogr Paleoclimatol 34(5):813–832. https://doi.org/10.1029/2018PA003482

Lyle M (2003) Neogene carbonate burial in the Pacific Ocean. Paleoceanogr Paleoclimatol 18(3):1–19. https://doi.org/10.1029/2002PA000777

Lyle M, Dadey KA, Farrell JW (1995) 42. The late Miocene (11–8 Ma) eastern Pacific Carbonate Crash: evidence for reorganization of deep-water circulation by the closure of the Panama Gateway. In N. G. Pisas, L. A. Mayer, T. R. Janecek, Palmer-Julson, & T. H. van Andel (Eds.), Proceedings of the Ocean Drilling Program, Scientific Results. College Station, TX: Ocean Drilling Program 138:821–838. https://doi.org/10.2973/odp.proc.sr.138.157.1995

Lyu J, Auer G, Bialik OM, Christensen B, Yamaoka R, De Vleeschouwer D (2023) Astronomically-paced changes in paleoproductivity, winnowing, and mineral flux over Broken Ridge (Indian Ocean) since the early Miocene. Paleoceanogr Paleoclimatol 38(12):e2023PA004761. https://doi.org/10.1029/2023PA004761

Martinot C, Bolton CT, Sarr AC, Donnadieu Y, Garcia M, Gray E, Tachikawa K (2022) Drivers of late Miocene tropical sea surface cooling: a new perspective from the equatorial Indian Ocean. Paleoceanogr Paleoclimatol 37(10):e2021PA004407. https://doi.org/10.1029/2021PA004407

McQuarrie N, van Hinsbergen DJ (2013) Retrodeforming the Arabia-Eurasia collision zone: Age of collision versus magnitude of continental subduction. Geology 41(3):315–318. https://doi.org/10.1130/G33591.1

Mikkelsen N (1990) Cenozoic diatom biostratigraphy and paleoceanography of the western equatorial Indian Ocean. In R. A. Duncan, J. Backman, & L. C. Peterson (Eds.), Proceedings of the Ocean Drilling Program, Scientific Results. College Station, TX: Ocean Drilling Program vol. 115. https://doi.org/10.2973/ODP.PROC.SR.115.157.1990

Miller KG, Schmelz WJ, Browning JV, Rosenthal Y, Hess AV, Kopp RE, Wright JD (2024) Global mean and relative sea-level changes over the past 66 myr: implications for early Eocene ice sheets. Earth Sci Syst Soc 4(1):10091. https://doi.org/10.3389/esss.2023.10091

Müller RD, Cannon J, Williams S, Dutkiewicz A (2018) Pybacktrack 1.0: A tool for reconstructing paleobathymetry on oceanic and continental crust. Geochem Geophys Geosyst 19(6):1898–1909. https://doi.org/10.1029/2017GC007313

Müller RD, Mather B, Dutkiewicz A, Keller T, Merdith A, Gonzalez CM et al (2022) Evolution of earth's tectonic carbon conveyor belt. Nature 605(7911):629–639. https://doi.org/10.1038/s41586-022-04420-x

Nathan SA, Leckie RM (2009) Early history of the Western Pacific Warm Pool during the middle to late Miocene (~ 13.2–5.8 Ma): role of sea-level change and implications for equatorial circulation. Palaeogeogr Palaeoclimatol Palaeoecol 274(3–4):140–159. https://doi.org/10.1016/j.palaeo.2009.01.007

Pälike H, Lyle MW, Nishi H, Raffi I, Ridgwell A, Gamage K et al (2012) A Cenozoic record of the equatorial Pacific carbonate compensation depth. Nature 488:609–614. https://doi.org/10.1038/nature11360

Panchang R, Ambokar M (2021) Ocean acidification in the Northern Indian Ocean: a review. J Asian Earth Sci 219:104904. https://doi.org/10.1016/j.jseaes.2021.104904

Peirce J, Weissel J, Taylor E, Alt J (1989) 1. Leg 121, Background and objectives, shipboard scientific party In J. Peirce, J. Weissel, E. Taylor, & J. Alt (Eds.), Proceedings of the Ocean Drilling Program, Initial Reports. College Station, TX: Ocean Drilling Program vol 121. https://doi.org/10.2973/odp.proc.ir.121.101.1989

Peterson L, Backman J (1990) Late Cenozoic carbonate accumulation and the History of the carbonate compensation depth in the Western Equatorial Indian Ocean. In: Duncan RA, Backman J, Peterson L (eds) *Proceedings of the Ocean Drilling Program, Scientific Results*, vol Vol. 115. Ocean Drilling Program, College Station, TX, pp 467–507. https://doi.org/10.2973/odp.proc.sr.115.163.1990

Peterson LC, Murray DW, Ehrmann WU, Hempel P (1992) Cenozoic carbonate accumulation and compensation depth changes in the Indian Ocean. In R. A. Duncan, D. K. Rea, R. B. Kidd, U. v. Rad, & J. K. Weissel (Eds.), In Synthesis of Results from Scientific Drilling in the Indian Ocean. Geophysical Monograph Series 70:311–333. https://doi.org/10.1029/GM070p0311

Phillips HE, Tandon A, Furue R, Hood R, Ummenhofer CC, Benthuysen JA et al (2021) Progress in understanding of Indian Ocean circulation, variability, air–sea exchange, and impacts on biogeochemistry. Ocean Sci 17(6):1677–1751. https://doi.org/10.5194/os-17-1677-2021

Pillot Q, Suchéras-Marx B, Sarr AC, Bolton C, Donnadieu Y (2023) A global reassessment of the spatial and temporal expression of the late Miocene biogenic bloom. Paleoceanography Paleoclimatology 38(3):e2022PA004564. https://doi.org/10.1029/2022PA004564

Piotrowski AM, Banakar VK, Scrivner AE, Elderfield H, Galy A, Dennis A (2009) Indian Ocean circulation and productivity during the last glacial cycle. Earth Planet Sci Lett 285(1–2):179–189. https://doi.org/10.1016/j.epsl.2009.06.007

Podder RSIS, Gupta AK, Clemens S, Sanyal P, Panigrahi MK (2024) Changes in the Indian Ocean surface hydrography driven by the seaway closure and monsoonal circulation since the late Oligocene. Glob Planet Change 232:104335. https://doi.org/10.1016/j.gloplacha.2023.104335

Prabhat P, Rahaman W, Lathika N, Tarique M, Mishra R, Thamban M (2022) Modern-like deep water circulation in Indian Ocean caused by central American seaway closure. Nat Commun 13(1):7561. https://doi.org/10.1038/s41467-022-35145-0

Renaudie J, Lazarus DB, Diver P (2020) NSB (Neptune sandbox Berlin): an expanded and improved database of marine planktonic microfossil data and deep-sea stratigraphy. Palaeontologia Electronica 23(1):1–28. https://doi.org/10.26879/1032

Richards FD, Hoggard MJ, Cowton LR, White NJ (2018) Reassessing the thermal structure of oceanic lithosphere with revised global inventories of basement depths and heat flow measurements. J Geophys Research: Solid Earth 123(10):9136–9161. https://doi.org/10.1029/2018JB015998

Ridgwell A, Zeebe RE (2005) The role of the global carbonate cycle in the regulation and evolution of the Earth system. Earth Planet Sci Lett 234(3–4):299–315. https://doi.org/10.1016/j.epsl.2005.03.006

Sabine CL, Key RM, Feely RA, Greeley D (2002) Inorganic carbon in the Indian Ocean: distribution and dissolution processes. Glob Biogeochem Cycles 16(4):15–11. https://doi.org/10.1029/2002GB001869

Sallée J-B, Speer K, Rintoul S, Wijffels S (2010) Southern Ocean thermocline ventilation. J Phys Oceanogr 40(3):509–529. https://doi.org/10.1175/2009JPO4291.1

Sarr A-C, Donnadieu Y, Bolton CT, Ladant J-B, Licht A, Fluteau F et al (2022) Neogene South Asian monsoon rainfall and wind histories diverged due to topographic effects. Nat Geosci 15(4):314–319. https://doi.org/10.1038/s41561-022-00919-0

Schott FA, Xie SP, McCreary JP Jr (2009) Indian Ocean circulation and climate variability. Rev Geophys. https://doi.org/10.1029/2007RG000245

Sclater JG, Abbott D, Thiede J (1977) Paleobathymetry and sediments of the Indian Ocean. In J. R. Heirtzler, H. M. Bolli, T. A. Davies, J. B. Saunders, & J. G. Sclater (Eds.), Indian Ocean Geology and Biostratigraphy: Studies Following Deep-Sea Drilling Legs. Special Publications 9:25–59. https://doi.org/10.1029/SP009p0025

Sclater JG, Meinke L, Bennett A, Murphy C (1985) The depth of the ocean through the Neogene. In: Kennett JP (ed) The Miocene ocean: paleoceanography and biogeography. Geological Society of America Memoirs 163:1–20. https://doi.org/10.1130/MEM163-p1

Slotnick BS, Lauretano V, Backman J, Dickens GR, Sluijs A, Lourens L (2015) Early Paleogene variations in the calcite compensation depth: new constraints using old borehole sediments from across Ninetyeast Ridge, central Indian Ocean. Clim Past 11(3):473–493. https://doi.org/10.5194/cp-11-473-2015

Smart CW, Thomas E, Ramsay ATS (2007) Middle–late Miocene benthic foraminifera in a Western Equatorial Indian Ocean depth transect: paleoceanographic implications. Palaeogeogr Palaeoclimatol Palaeoecol 247(3–4):402–420. https://doi.org/10.1016/j.palaeo.2006.11.003

Sosdian SM, Lear CH (2020) Initiation of the Western Pacific Warm Pool at the middle Miocene climate transition? Paleoceanogr Paleoclimatol 35(12):e2020PA003920. https://doi.org/10.1029/2020PA003920

Speich S, Blanke B, de Vries P, Drijfhout S, Döös K, Ganachaud A, Marsh R (2002) Tasman leakage: A new route in the global ocean conveyor belt. Geophys Res Lett 29(10):55. https://doi.org/10.1029/2001GL014586

Stein CA, Stein S (1992) A model for the global variation in oceanic depth and heat flow with lithospheric age. Nature 359(6391):123–129. https://doi.org/10.1038/359123a0

Straume EO, Faccenna C, Becker TW, Steinberger B, Licht A, Sembroni A et al (2025) Collision, mantle convection and Tethyan closure in the Eastern Mediterranean. Nat Rev Earth Environ 6:299–317. https://doi.org/10.1038/s43017-025-00653-2

Straume EO, Steinberger B, Becker TW, Faccenna C (2024) Impact of mantle convection and dynamic topography on the Cenozoic paleogeography of central Eurasia and the West Siberian seaway. Earth Planet Sci Lett 630:118615. https://doi.org/10.1016/j.epsl.2024.118615

Tanner T, Hernández-Almeida I, Drury AJ, Guitián J, Stoll H (2020) Decreasing atmospheric CO_2 during the late Miocene cooling. Paleoceanogr Paleoclimatol 35(12):e2020PA003925. https://doi.org/10.1029/2020PA003925

Taylor VE, Westerhold T, Bohaty SM, Backman J, Dunkley Jones T, Edgar K et al (2023) Transient shoaling, over-deepening and settling of the calcite compensation depth at the Eocene-Oligocene transition. Paleoceanogr Paleoclimatol 38(6):e2022PA004493. https://doi.org/10.1029/2022PA004493

Torfstein A, Steinberg J (2020) The Oligo–Miocene closure of the Tethys Ocean and evolution of the proto-Mediterranean Sea. Sci Rep 10(1):13817. https://doi.org/10.1038/s41598-020-70652-4

van Andel TH (1975) Mesozoic/Cenozoic calcite compensation depth and the global distribution of calcareous sediments. Earth Planet Sci Lett 26(2):187–194. https://doi.org/10.1016/0012-821X(75)90086-2

Van Andel TH, Moore TC Jr (1974) Cenozoic calcium carbonate distribution and calcite compensation depth in the central equatorial Pacific Ocean. Geology 2(2):87–92. (1974)2%3C87%3ACCCDAC%3E2.0.CO%3B2 https://doi.org/10.1130/0091-7613

van der Ploeg R, Boudreau BP, Middelburg JJ, Sluijs A (2019) Cenozoic carbonate burial along continental margins. Geology 47(11):1025–1028. https://doi.org/10.1130/G46418.1

van Sebille E, Sprintall J, Schwarzkopf FU, Sen Gupta A, Santoso A, England MH et al (2014) Pacific-to-Indian Ocean connectivity: Tasman leakage, Indonesian Throughflow, and the role of ENSO. J Geophys Res Oceans 119(2):1365–1382. https://doi.org/10.1002/2013JC009525

Vincent E, Berger WH (1985) Carbon dioxide and polar cooling in the Miocene: the Monterey hypothesis. In S. E.T & W. S. Broecker (Eds.), The carbon cycle and atmospheric CO_2: Natural variations Archean to present: Geophysical Monograph Series 32:455–468. https://doi.org/10.1029/GM032p0455

Wessel P, Luis JF, Uieda L, Scharroo R, Wobbe F, Smith WHF, Tian D (2019) The generic mapping tools version 6. Geochem Geophys Geosyst 20(11):5556–5564. https://doi.org/10.1029/2019GC008515

Westerhold T, Marwan N, Drury AJ, Liebrand D, Agnini C, Anagnostou E et al (2020) An astronomically dated record of earth's climate and its predictability over the last 66 million years. Science 369(6509):1383–1387. https://doi.org/10.1126/science.aba6853

Woodruff F, Savin SM (1989) Miocene deepwater oceanography. Paleoceanogr Paleoclimatol 4(1):87–140. https://doi.org/10.1029/PA004i001p00087

Woosley RJ (2016) Carbonate Compensation Depth. In: White W (eds) Encyclopedia of Geochemistry. Encyclopedia of Earth Sciences Series. Springer, Cham. https://doi.org/10.1007/978-3-319-39193-9_85-1

Wright JD, Miller KG, Fairbanks RG (1991) Evolution of modern deepwater circulation: evidence from the late Miocene Southern Ocean. Paleoceanogr Paleoclimatol 6(2):275–290. https://doi.org/10.1029/90PA02498

Wyrtki K (1973) Physical oceanography of the Indian Ocean. In: Zeitzschel B, Gerlach SA (eds) The biology of the Indian Ocean, vol 3. Ecological Studies, Springer, Berlin, Heidelberg, pp 18–36. https://doi.org/10.1007/978-3-642-65468-8_3

Zachos JC, Rea DK, Seto K, Nomura R, Niitsuma N (1992) Paleogene and early Neogene deep water paleoceanography of the Indian Ocean as determined from benthic foraminifer stable carbon and oxygen isotope records. In R. A. Duncan, D. K. Rea, R. B. Kidd, U. v. Rad, & J. K. Weissel (Eds.), In Synthesis of Results from Scientific Drilling in the Indian Ocean. Geophysical Monograph Series 70:351–385. https://doi.org/10.1029/GM070p0351

Zhang H, Luo Y, Yu J, Zhang L, Xiang R, Yu Z, Huang H (2022) Indian Ocean sedimentary calcium carbonate distribution and its implications for the glacial deep ocean circulation. Q Sci Rev 284:107490. https://doi.org/10.1016/j.quascirev.2022.107490

Zhifei L, Shouting T, Quanhong Z, Xinrong C, Wei H (2004) Deep-water earliest Oligocene glacial maximum (EOGM) in South Atlantic. Chin Sci Bull 49(20):2190–2197. https://doi.org/10.1007/BF03185787

4 | Article 3

Cretaceous to Cenozoic carbonate burial variability across the Atlantic, Pacific and Indian Oceans

Faranak Dalvand, Adriana Dutkiewicz, Nicky M. Wright & R. Dietmar Müller

EarthBythe Group, School of Geosciences, University of Sydney, NSW, Australia

Submitted to the Journal of *Marine Geology* in February 2026

Cretaceous to Cenozoic carbonate burial variability across the Atlantic, Pacific and Indian Oceans

Faranak Dalvand[1], Adriana Dutkiewicz[1], Nicky M. Wright[1], R. Dietmar Müller[1]

[1]EarthByte Group, School of Geosciences, University of Sydney, Sydney, Australia

Corresponding Author:

Faranak Dalvand (faranak.dalvand@sydney.edu.au)

Keywords: Carbonate accumulation rates, Cretaceous, Cenozoic, Atlantic Ocean, Pacific Ocean, Indian Ocean

Abstract

Marine carbonate burial is the primary long-term process that regulates ocean carbon and alkalinity, yet how carbonate accumulation rates (CARs) vary across different ocean basins is still not well understood. We present the first global synthesis of deep-sea CAR from 120 Ma to the present, combining records from 335 DSDP/ODP/IODP drill sites in the Atlantic, Pacific, and Indian oceans with paleobathymetric models. The results reveal stark differences in carbonate accumulation patterns between the Cretaceous and the Cenozoic. The Cretaceous is marked by highly heterogeneous and variable carbonate burial, reflecting greenhouse climate conditions, episodic volcanic CO_2 inputs, evolving deep-water formation, and limited connectivity among ocean basins. The Atlantic shows pronounced mid-Cretaceous peaks in CAR, followed by Ocean Anoxic Event (OAE)-linked reductions; the Indian Ocean remains carbonate-poor until a Late Cretaceous rise tied to enhanced Southern Ocean influence; and the Pacific is persistently undersaturated with respect to calcium carbonate, with suppressed CAR into the early Paleogene. During the Cenozoic, CAR evolves toward a more stable but strongly differentiated system. The Pacific records the most pronounced response to the Eocene–Oligocene transition through a major deep-water CAR increase, whereas the Atlantic features late Eocene and late Miocene–early Pliocene maxima associated with strengthened Northern Component Water (NCW) and later North Atlantic Deep Water (NADW) formation. The Indian Ocean exhibits its largest CAR increase after ~20 Ma, linked to CCD deepening, monsoon intensification, and gateway reorganisations. A late Miocene–early Pliocene biogenic bloom enhanced carbonate burial in the Atlantic and Indian oceans more than in the Pacific, and all basins show declining CAR in the Plio-Quaternary as global circulation reorganised and the Northern Hemisphere glaciation initiated. These basin-resolved trends revise earlier assumptions of a monotonic Cenozoic increase in pelagic carbonate burial and provide a quantitative foundation for future carbon-cycle modelling.

Introduction

Carbonate burial in marine sediments is the primary long-term mechanism by which carbon is removed from the ocean, exerting first-order control over the buffering capacity of the marine carbon reservoir, atmospheric CO_2 levels, and Earth's climate state over millions of years (Broecker & Peng, 1982; Ridgwell & Zeebe, 2005; Zeebe & Westbroek, 2003). The rate at which carbonate accumulates on the seafloor records the dynamic interplay among biological productivity, ocean chemistry and circulation, the atmosphere-ocean carbon balance, and the calcite compensation depth (CCD) (Broecker, 2003; Broecker & Peng, 1982; Dutkiewicz et al., 2016; Ridgwell & Zeebe, 2005; Xiao et al., 2024). Understanding the spatial and temporal

evolution of marine carbonate accumulation is therefore essential for reconstructing past carbon-cycle dynamics and constraining the feedbacks that regulate Earth's climate system across greenhouse-to-icehouse states.

The Cretaceous through Cenozoic interval encompasses one of the most profound climate transitions in Earth's history, from extreme greenhouse conditions with atmospheric CO_2 concentrations 3–5 times those of modern levels and a nearly ice-free world, to the bipolar glaciated icehouse of the Quaternary (Foster et al., 2017; Zachos et al., 2001; Zachos et al., 2008). This long-term transition was accompanied by fundamental reorganisations of ocean circulation, progressive opening and closure of oceanic gateways, major shifts in the loci of deep-water formation from low-latitude Tethyan sources to high-latitude Southern and Northern Component Waters, and dramatic changes in carbonate saturation states and CCD depths (e.g., Cramer et al., 2009; Dutkiewicz et al., 2019; Friedrich et al., 2012; Zachos et al., 2001). As Earth evolved from a greenhouse climate with vigorous tectonism and restricted gateways to an icehouse state characterised by continental collision, mountain building, and more efficient thermohaline circulation, pelagic carbonate sediments became the dominant long-term carbon reservoir (e.g., Abelson & Erez, 2017; Müller et al., 2022; Poulsen et al., 2001; Scotese et al., 2025; Wallmann, 2001; Zhang et al., 2011). Together, these processes fundamentally altered carbonate sequestration, with profound implications for ocean alkalinity budgets and Earth's long-term CO_2 regulation. Furthermore, this global transition is expected to vary markedly across the Atlantic, Pacific, and Indian Oceans due to basin-specific differences in ocean circulation, carbonate saturation state, and productivity, and sedimentation regimes (e.g., Chiarella et al., 2017; Katavouta & Williams, 2021; Ladant et al., 2020; Michel et al., 2018), potentially leading to basin-scale heterogeneity in carbonate sequestration. Carbonate compensation depth (CCD) reconstructions suggest that the CCD can differ by as much as ~1.5 km between major ocean basins owing to regional contrasts in productivity, water-mass chemistry, and deep-ocean circulation (e.g., Campbell et al., 2018; Dalvand et al., 2025a; Dalvand et al., 2025b; Dutkiewicz & Müller, 2022; van Andel, 1975), underscoring the need for basin-resolved carbonate analyses.

Despite decades of research on marine carbonate systems, a fundamental gap remains in quantifying how pelagic carbonate accumulation evolved within and between ocean basins throughout the Cretaceous and Cenozoic. Existing global compilations largely infer a progressive Cenozoic increase in pelagic carbonate burial from aggregated budgets (e.g., Hay, 1999; Kump & Arthur, 1997; Mackenzie & Morse, 1992; Opdyke & Wilkinson, 1988), proposing proportional evolution between shallow and basin carbonate accumulation (Kump & Arthur, 1997; Salles et al., 2025; van der Ploeg et al., 2019). In contrast, a recent bias-corrected study suggests a far more muted and spatially heterogeneous pelagic accumulation history (Renaudie & Lazarus, 2025). Evolutionary syntheses of calcareous nannoplankton also document complex, non-monotonic accumulation histories, with peak richness and size during the Late Cretaceous followed by stabilised accumulation rates toward the present (Suchéras-Marx et al., 2019). These inconsistencies between inferred monotonic increases in global budgets and muted or non-monotonic trends in bias-corrected and evolutionary records underscore the need for basin-resolved quantitative constraints on pelagic carbonate accumulation to reconcile global burial models with evolutionary and oceanographic evidence.

Additionally, the role of the relative distribution of carbonate burial between the shallow platform and the deep ocean in governing global carbonate system evolution remains debated, largely due to the absence of a comprehensive, quantitative synthesis of basin-scale variability in deep-marine carbonate burial through deep time. Recent modelling work by Salles et al. (2025) proposes that deep-time carbonate burial regimes are regulated by the interplay between alkalinity supply and shallow-platform accommodation, predicting inverse behavior between

neritic and pelagic carbonate burial during major paleoceanographic reorganisations. Yet this regime-switching hypothesis requires testing against basin-resolved, depth-stratified records using direct measurements that existing datasets do not capture. A robust assessment of these predictions demands (1) basin-resolved records capable of distinguishing globally coherent signals from regional oceanographic responses, (2) depth-stratified data to quantify vertical carbonate variability over time, particularly during major climatic transitions, and (3) temporally continuous coverage spanning both greenhouse and icehouse states to capture long-term carbonate accumulation regime shifts. Global estimates lack depth resolution and basin-scale specificity by averaging carbonate burial across the global ocean, and Cenozoic studies generally focus on relatively small regions and/or short time periods (e.g., Cartapanis et al., 2018; Carter et al., 2000; Cornuault et al., 2023; Drury et al., 2021; Hagelberg et al., 1995; Hodell et al., 2001; Kasuya et al., 2024; Lyle, 2003), leaving a critical gap in our understanding of deep-time basin-wide carbonate burial dynamics.

Here, we present the first CAR synthesis spanning all major ocean basins and quantify depth-dependent changes in carbonate burial at 1 Myr resolution across the Atlantic, Pacific, and Indian oceans over the last 120 Myr. By synthesizing an extensive compilation of deep-sea sediment cores and applying a consistent quantitative framework, we construct basin-specific temporal trends and carbonate flux maps, and identify depth-dependent changes in carbonate burial. This study provides the first empirical framework for evaluating how deep-sea carbonate burial responded to large-scale global and regional forcing and for assessing the extent to which oceanographic processes governed long-term carbonate system evolution. More broadly, this framework enables future quantitative assessments of platform–basin carbonate partitioning within a unified, basin-scale perspective.

Methods

Data Compilation and Computing Carbonate Accumulation Rates

This study synthesizes carbonate accumulation rate (CAR) records from a total of 318 globally distributed scientific ocean drilling sites spanning the Pacific (117 sites), Atlantic (107 sites), and Indian Oceans (94 sites) (Figure 1, Supplementary Tables 1 to 3). The dataset integrates CAR computations for the Atlantic Ocean (Dutkiewicz & Müller, 2022), the Pacific Ocean (Dalvand et al., 2025a), and the Indian Ocean (Dalvand et al., 2025b), which together provide basin-resolved coverage of pelagic carbonate burial over the past 120 Ma. These sites include expeditions from the Deep Sea Drilling Project (DSDP), Ocean Drilling Program (ODP), and both phases of the IODP, the Integrated Ocean Drilling Program and the International Ocean Discovery Program. Carbonate accumulation rates were calculated in the basin-specific studies cited above, following the methodological workflow developed by Dutkiewicz and Müller (2021) and employing Lyle's (2003) carbonate accumulation formulation. CAR was computed at each site by combining the $CaCO_3$ content and dry bulk density of sediment at a given depth in the drill core, and the linear sedimentation rate from age-depth models at each site, using the relationship from Lyle (2003):

$$CAR = (CaCO_3\%/100)(\rho_{dry})(S),$$

where $CaCO_3$% is carbonate content, ρ_{dry} is dry bulk density, and S is linear sedimentation rate. Paleobathymetric reconstruction and sediment decompaction were performed using pyBacktrack 1.4 software (Müller et al., 2018), accounting for tectonic subsidence (Sclater et al., 1985; Stein & Stein, 1992), dynamic topography (Braz et al., 2021), and eustatic sea-level change (Miller et al., 2024). Site-level CAR time series were aggregated into 1 Myr-wide moving windows with 0.5 Myr step increments, producing temporally continuous basin-scale

and global CAR reconstructions from 120 Ma to the present. All input data files are available via: https://doi.org/10.5281/zenodo.18755594.

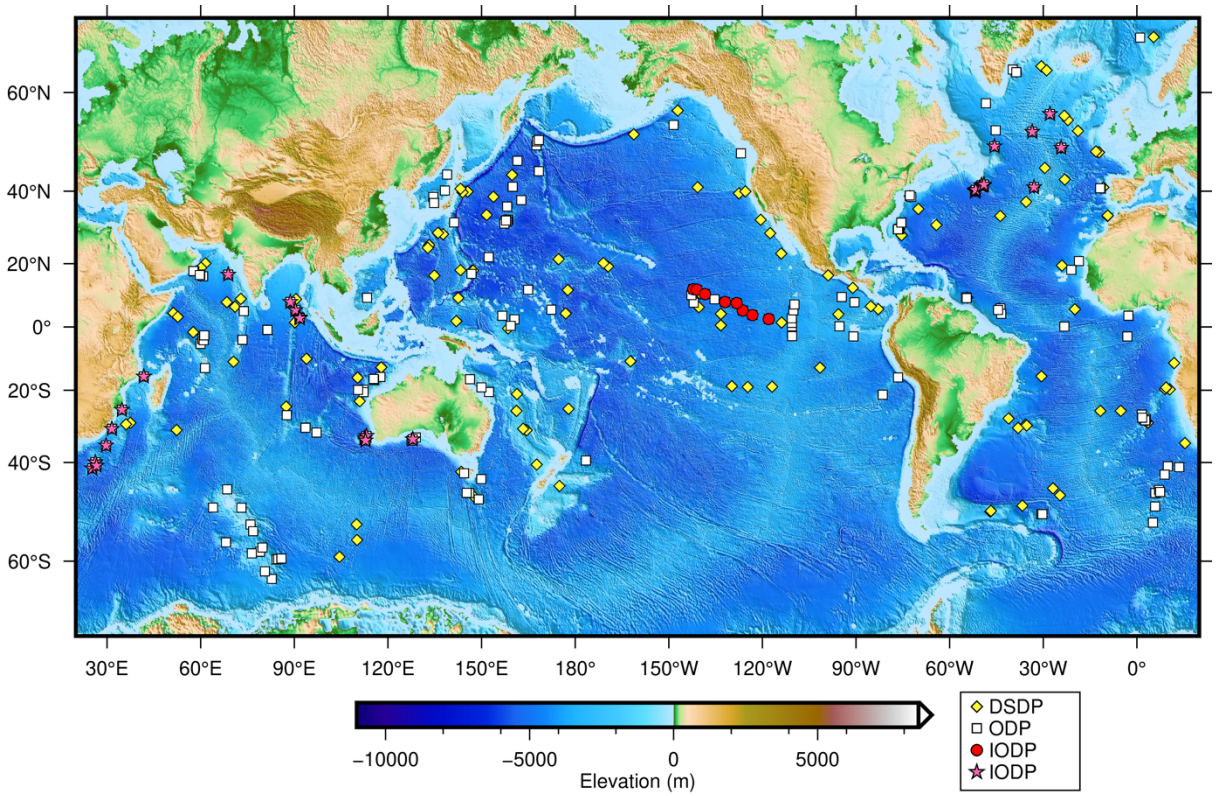

Figure 1: Global distribution of 335 drill sites used in this study from the DSDP, ODP, and IODP (red circles for Integrated Ocean Drilling Program and pink stars for International Ocean Discovery Program) expeditions. The map incorporates elevation from the ETOPO1 global relief model (https://www.ngdc.noaa.gov/mgg/global/; Amante & Eakins, 2009). More detailed maps of the drill sites are provided in the Supplementary Figures 1 to 3. Mercator projection.

Spatiotemporal Mapping and Pattern Analysis of CAR

To investigate spatial patterns of carbonate burial evolution through time, site-specific CAR time series were merged with paleo-coordinates reconstructed from a plate-tectonic model of Zahirovic et al. (2022) to produce reconstructed CAR maps for individual sites (Figures 2 and 3, Supplementary video). To quantify long-term trends and explore inter-basin variability in CAR, we conducted a series of statistical analyses. CAR values were grouped into 5 Myr bins to generate boxplots summarising the median, interquartile range, whiskers, and outliers for each ocean basin over the past 120 Ma (Figures 4). To assess how carbonate accumulation varied with bathymetry within basin-scale oceanographic regimes, CAR data were further binned at 1 Myr intervals to compute median CAR values and 10th–90th percentile spreads for three water-depth classes: <2000 m (shallow), 2000–3500 m (intermediate), and >3500 m (deep) (Figure 5).

Results

Our new compilation of carbonate data spans the mid-Cretaceous to the present across the Atlantic, Pacific, and Indian Ocean basins. Analysis of the Cretaceous interval (120–66 Ma) requires caution due to spatially uneven drill-site coverage and temporally fragmented drilling records compared to the Cenozoic (Figures 2 & 3).

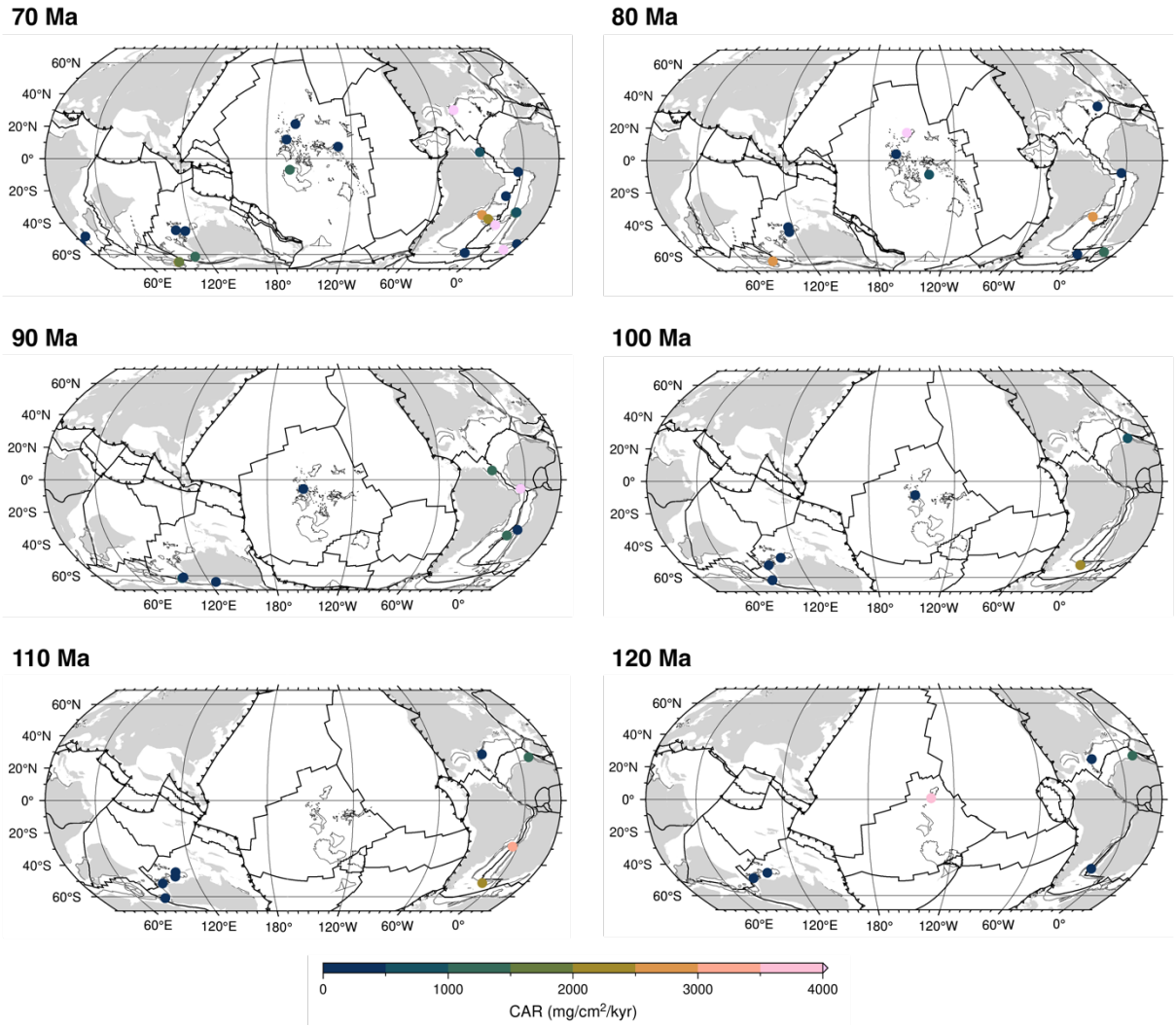

Figure 2: Carbonate accumulation rate (CAR) across the Atlantic, Pacific, and Indian Oceans from 120 Ma to 70 Ma at 10 Ma intervals, generated by merging site-specific CAR measurements from DSDP, ODP, and IODP drill sites with reconstructed paleo-coordinates based on the plate-tectonic model of Zahirovic et al. (2022). For each panel, CAR values correspond to the nearest sample within a 1 Myr bin. Black lines show reconstructed plate boundaries, with toothed segments indicating subduction zones and convergence direction. Grey lines exhibit reconstructed continent–ocean boundaries. Igneous provinces are represented by outlines. Robinson projection.

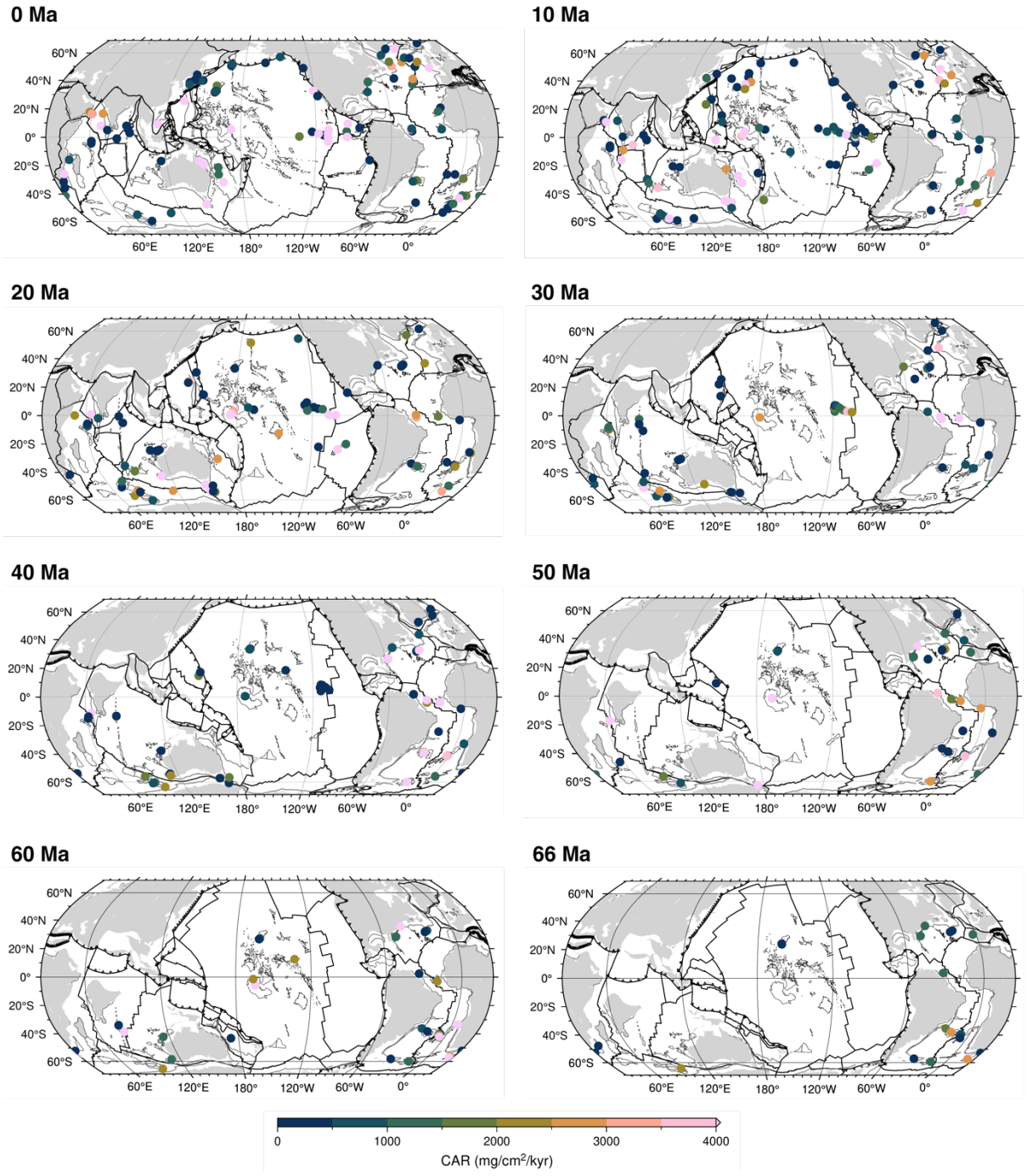

Figure 3: Carbonate accumulation rate (CAR) across the Atlantic, Pacific, and Indian Oceans from 66 Ma to 0 Ma at 10 Ma intervals. See Figure 2 for details. Robinson projection.

Atlantic Ocean

The Atlantic Ocean CAR record demonstrates a long-term transition from highly heterogeneous carbonate accumulation during the Cretaceous to a more uniform and stable depositional regime through the Cenozoic (Figure 2). Despite sparse coverage, the Cretaceous data reveal pronounced variability, with 5 Myr median CAR values ranging from < 500 to ~4000 mg cm^{-2} kyr^{-1} and 10th–90th percentiles, extending to ~8000 mg cm^{-2} kyr^{-1}. Major spikes occur during the mid-Late Cretaceous, including a distinct rise in CAR to ~4000 mg cm^{-2} kyr^{-1} at 105–100 Ma, followed by a continuous decline to ~1500 mg cm^{-2} kyr^{-1} at ~95–90 Ma. CAR maps for this interval point to a basin-wide reduction in carbonate burial,

particularly in the North Atlantic (Figure 2; Supplemental video). Depth-resolved 1-Myr analyses show that the most pronounced CAR declines at ~100–95 Ma occur in shallow settings (<2000 m), whereas intermediate depths (2000–3500 m) retain comparatively elevated burial fluxes until ~95 Ma (Figure 5). After a modest Late Cretaceous recovery, median CAR stabilises at moderate levels, fluctuating between ~2000 and ~1200 mg cm^{-2} kyr^{-1} up to the Cretaceous–Paleogene boundary. Violin plots show broad, often skewed distributions and multimodality, reflecting strong spatial heterogeneity and episodic depositional pulses in the pre-Cenozoic Atlantic (Supplementary Figure 4); CAR maps confirm large regional contrasts in carbonate accumulation (Supplemental video).

During the Cenozoic (66–0 Ma), Atlantic median CAR values are more moderate and temporally stable, generally between ~1000 and 2000 mg cm^{-2} kyr^{-1}. Percentile envelopes narrow markedly relative to the Cretaceous, with the 10th–90th percentiles mostly confined to ~3500–7500 mg cm^{-2} kyr^{-1} (Figure 4), and violin plots indicate predominantly unimodal, narrower distributions (Supplementary Figure 4), implying more homogeneous basin-scale accumulation. Two broad Cenozoic maxima occur at ~40–35 Ma and 10–5 Ma, where median CAR approaches ~2500 mg cm^{-2} kyr^{-1}. Depth-resolved analyses indicate that the late Eocene increase in CAR is dominated by shallow and intermediate sites, whereas the late Miocene enhancement is expressed across all depth classes (Figure 5). Regional CCD reconstructions indicate that the CCD remained below ~4 km across the North and Central Atlantic during the late Miocene (Dutkiewicz & Müller, 2022). When integrated with the spatial distribution of CAR (Supplemental video), this pattern suggests that the late Miocene CAR increase in the South Atlantic may have been driven by enhanced shallow-water carbonate burial, while in the Central and North Atlantic, the enhancement extended to deeper depositional environments. This correlates with the lower seafloor area above the CCD across the South Atlantic during the Miocene (Dutkiewicz & Müller, 2022). Thereafter, median CAR decreases from ~2200 mg cm^{-2} kyr^{-1} at 10–5 Ma to ~1200 mg cm^{-2} kyr^{-1} in the 5–0 Ma bin (Figure 4), a decline expressed consistently in shallow, intermediate, and deep settings and aligned with late Pliocene CCD shoaling (Dutkiewicz & Müller, 2022).

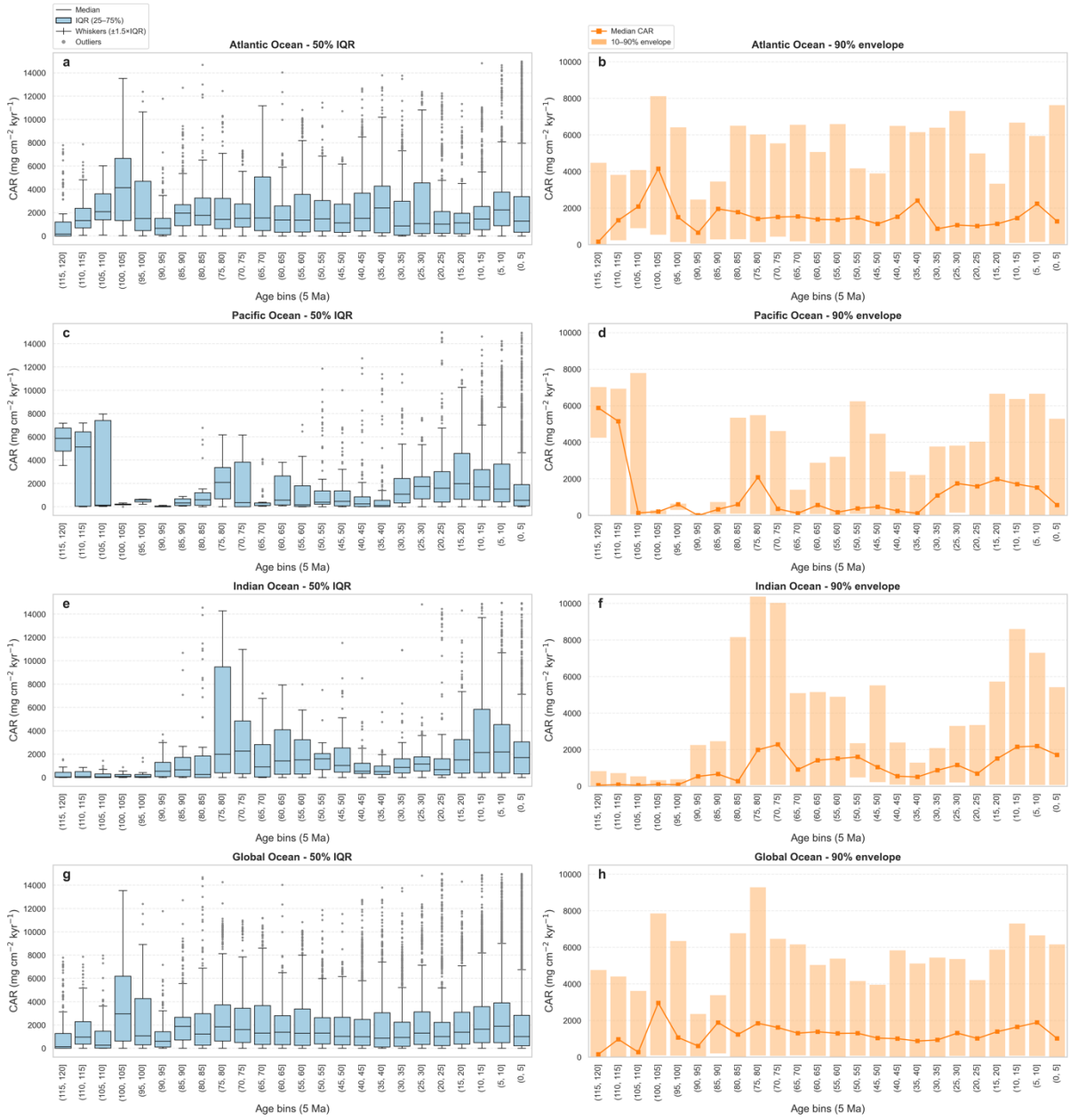

Figure 4: Statistical distributions of carbonate accumulation rates (CAR) across the Atlantic, Pacific, Indian, and the global ocean over the past 120 Myr. For each ocean basin, panels a, c, e, and g display 5 Myr boxplots of CAR values, illustrating the full distribution of measurements within each time bin, including the median, interquartile range (25th–75th percentile), whiskers (±1.5×IQR), and outliers. Panels b, d, f, and h show the corresponding 10th–90th percentile of CAR ranges (vertical bars) and median CAR trajectories (orange line) for the same 5 Myr bins, illustrating the central tendency and variability of carbonate accumulation through time.

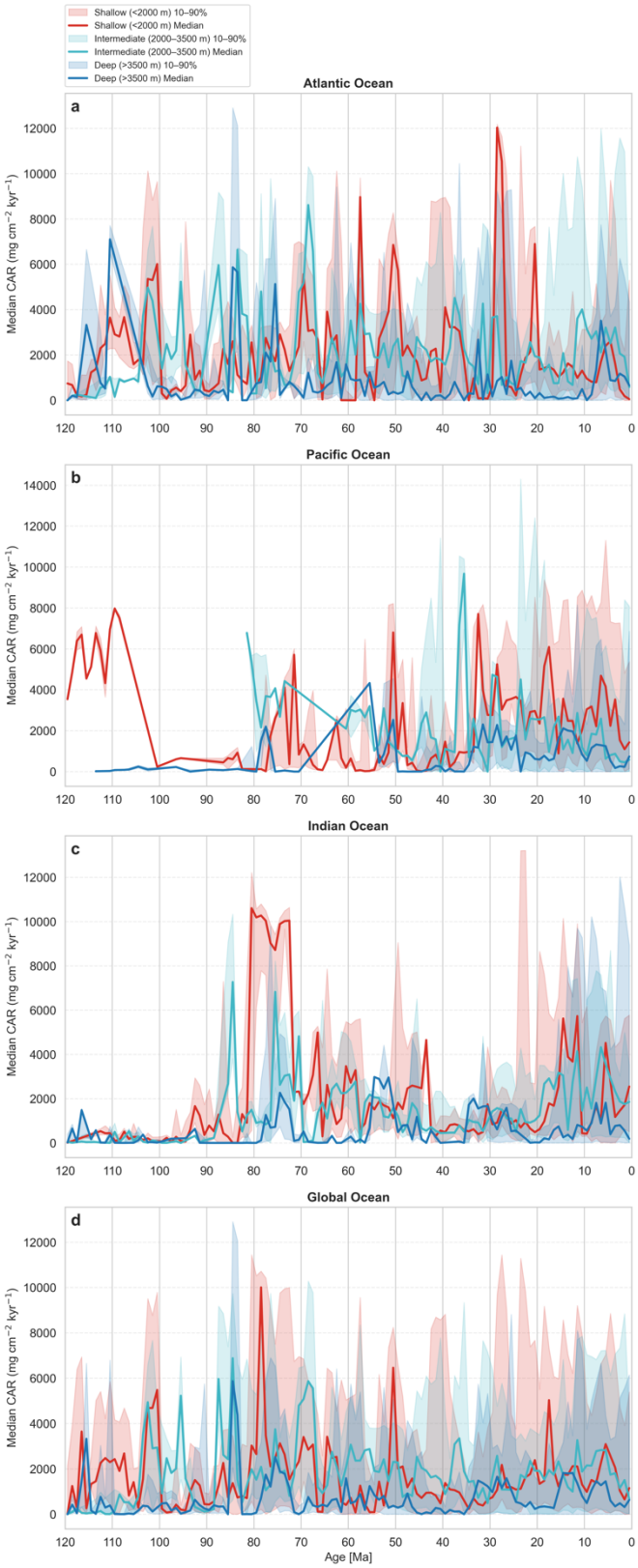

Figure 5: Carbonate accumulation rates (CAR) across the Atlantic (a), Pacific (b), Indian (c), and global ocean (d) since ~120 Ma at different water depths. The figure illustrates median CAR binned at 1 Myr intervals, partitioned into three paleowater depth categories: shallow (<2000 m, red), intermediate (2000–3500 m, teal), and deep (>3500 m, blue), for each ocean basin and globally. For each depth class, the shaded regions represent the 10th–90th percentile CAR range, and the solid lines denote the median CAR within 1 Myr bins.

Pacific Ocean

Cretaceous CAR patterns in the Pacific are strongly influenced by limited, spatially restricted sampling, with sites concentrated in the central Pacific (Figure 2). Within these constraints, median CAR values range from <500 to ~6000 mg cm^{-2} kyr^{-1} (Figure 4), with a prominent peak (~6000 mg cm^{-2} kyr^{-1}) in the 120–110 Ma bins, followed by sharp declines to <500 mg cm^{-2} kyr^{-1} in subsequent intervals. These large excursions should be interpreted with caution, as they may reflect genuine local variability and/or central Pacific sampling bias. A more moderate rise to ~2000 mg cm^{-2} kyr^{-1} at ~80–75 Ma points to localized enhancement of carbonate burial, but CAR then declines toward persistently low values (<500 mg cm^{-2} kyr^{-1}) into the latest Cretaceous (Figure 4). Cretaceous violin plots also display broad, often highly skewed distributions with long upper tails, which may reflect pronounced episodic and spatially restricted carbonate accumulation, in contrast to the Cenozoic distributions, which are narrower and more unimodal, indicating reduced variability in carbonate accumulation rates through time (Supplementary Figure 4).

The Cenozoic Pacific is characterised by a long-term recovery and stabilisation of CAR beginning in the late Eocene–early Oligocene. From ~65 to 35 Ma, median CAR remains low (<~800 mg cm^{-2} kyr^{-1}), with relatively modest temporal variability, indicating broadly suppressed carbonate burial. Occasional widening of the 10th–90th percentile to ~6000 mg cm^{-2} kyr^{-1} (Figure 4), particularly in the central and western equatorial Pacific (Figure 3), indicates intermittent local accumulation despite low basin-wide means. A major transition occurs across the late Eocene–early Oligocene, when median CAR rises from <500 mg cm^{-2} kyr^{-1} in the 40–35 Ma bin to ~1000 mg cm^{-2} kyr^{-1} in the early Oligocene, then remains at moderate levels (~1000–2000 mg cm^{-2} kyr^{-1}) through much of the Neogene. Depth-resolved 1-Myr analysis shows that deep-water sites (>3500 m) respond most strongly during the late Eocene-early Oligocene transition: median CAR increases from ~100 mg cm^{-2} kyr^{-1} at ~35 Ma to >1200 mg cm^{-2} kyr^{-1} by ~33 Ma, fluctuating between ~500 and 2000 mg cm^{-2} kyr^{-1} thereafter (Figure 5). This shift is consistent with early Oligocene CCD deepening and a fundamental reorganisation of deep-water ventilation and carbonate preservation in the Pacific (e.g., Dalvand et al., 2025a; Pälike et al., 2012; van Andel, 1975).

Neogene CAR evolution is spatially complex. Between 20 and 15 Ma, median CAR approaches ~2000 mg cm^{-2} kyr^{-1}, with maps showing enhanced accumulation in the equatorial and southern Pacific, largely at shallow depths (Figure 5; Supplemental video). The mid–late Miocene is also marked by elevated CAR, especially in the western equatorial and South Pacific. However, between ~11 and 9 Ma, CAR declines sharply at intermediate and deep sites while remaining high in shallow settings (Figure 5). This pattern corresponds to the Pacific "carbonate crash" (Lyle et al., 1995), with reduced accumulation in the eastern–central equatorial Pacific and relatively stronger burial in the western equatorial and South Pacific (Figure 3). We infer shallower preservation conditions in the western Pacific compared with enhanced dissolution in deeper eastern equatorial regions during this interval, where dissolution was intensified within this interval (Lyle et al., 1995). Median Pacific CAR decreases from ~1600 mg cm^{-2} kyr^{-1} in the 10–5 Ma interval to ~500 mg cm^{-2} kyr^{-1} in the 5–0 Ma bin, mirroring the late Neogene–Quaternary decline observed in the Atlantic. Throughout the Cenozoic, the North Pacific remains characterised by consistently lower carbonate accumulation than lower-latitude regions (Supplemental video).

Indian Ocean

The Indian Ocean CAR record shows a subdued yet distinctive Cretaceous evolution, with sites restricted to the southern Indian Ocean along the western Australian margin (Figure 3). The

available records indicate that between ~120 and 95 Ma, the median CAR remains consistently low (<500 mg cm^{-2} kyr^{-1}), and the 10th–90th percentile is generally <~2000 mg cm^{-2} kyr^{-1} (Figure 5), reflected in narrow, truncated violin plots (Supplementary Figure 4). A major increase occurs between ~80 and 70 Ma, when the median CAR rises to ~2000 mg cm^{-2} kyr^{-1} and the 10th–90th percentile expands dramatically, with maxima approaching 10,000 mg cm^{-2} kyr^{-1}. Depth-resolved analyses indicate that this enhancement is expressed at intermediate and deep sites, but the largest excursions in the upper envelope are associated with very high shallow-water (<2000 m) accumulation (Figure 5).

During the Cenozoic, the Indian Ocean exhibits higher and more variable CAR (Figure 4). Paleocene–Eocene median CAR ranges from ~1000 to ~1800 mg cm^{-2} kyr^{-1}, then declines to ~500 mg cm^{-2} kyr^{-1} in the late Eocene. A progressive increase begins in the Oligocene and continues into the Neogene, with median CAR fluctuating from ~1000 to ~2200 mg cm^{-2} kyr^{-1}. This long-term rise broadly tracks regional CCD deepening in the Indian Ocean since the early Oligocene (Dalvand et al., 2025b; Peterson & Backman, 1990; van Andel, 1975). Two Cenozoic median CAR minima occur between ~45–35 Ma (~500 mg cm^{-2} kyr^{-1}) and 25–20 Ma (~800 mg cm^{-2} kyr^{-1}), with the latter briefly interrupting the general upward trajectory beginning in the early Oligocene. The highest CAR values occur in the Late Neogene (~15 Ma to 5 Ma), when median CAR approaches ~2200 mg cm^{-2} kyr^{-1} and the 10th–90th percentile reaches ~8500 mg cm^{-2} kyr^{-1}.

Depth-resolved CAR patterns show that maximum CAR values are commonly associated with shallow–intermediate depths (<3500 m) in the Indian Ocean over the Cenozoic (Figure 4). However, notable intervals of exceptionally high deep-water accumulation occur between ~55–50 Ma and ~35–30 Ma, when median deep-water CAR (>3500 m) reaches ~2000 mg cm^{-2} kyr^{-1}, while shallow and intermediate sites are comparatively suppressed. In the late Neogene, elevated median CAR reflects high accumulation in shallow to intermediate settings, accompanied by a modest deep-water increase between 10 and 5 Ma (Figure 5). The Indian Ocean also exhibits a reduction in carbonate accumulation during the latest Cenozoic, with median CAR decreasing by ~400 mg cm^{-2} kyr^{-1} in the 5–0 Ma bin, from ~2200 mg cm^{-2} kyr^{-1} in the 10–5 Ma bin. However, the magnitude of this decline is notably smaller than the contemporaneous decreases observed in both the Atlantic and Pacific Oceans, indicating a comparatively more subdued late Cenozoic reduction in carbonate burial across the Indian Ocean.

Global Ocean

The global CAR record integrates signals from the Atlantic, Pacific, and Indian Oceans, reflecting regional heterogeneity in carbonate productivity and preservation. The analysis of CAR variability on the global scale from the Cretaceous to the present reveals a fundamental shift from a Cretaceous dominated by high-magnitude, extreme median CAR variability to the Cenozoic, characterized by moderate, persistent median accumulation and a more stable CAR regime (Figure 4). Global CAR during the pre-Cenozoic is marked by large inter-basin contrasts, with 5-Myr median values ranging from <500 to ~3000 mg cm^{-2} kyr^{-1}, and 10th–90th percentiles extending beyond ~8000 mg cm^{-2} kyr^{-1}. The early lowest global rates occur between ~120 Ma and 105 Ma (<1000 mg cm^{-2} kyr^{-1}), followed by a sharp increase between ~105 and ~100 Ma, when the median CAR rises to ~3000 mg cm^{-2} kyr^{-1} and the 10th–90th percentile widens considerably to ~7800 mg cm^{-2} kyr^{-1}, indicating a major, sustained enhancement of global burial. CAR values decline sharply in the 95–90 Ma bin to below 1000 mg cm^{-2} kyr^{-1}. During the Late Cretaceous (~90 Ma to 65 Ma bins), there is modest fluctuation with a moderate median CAR between ~1500–2000 mg cm^{-2} kyr^{-1}. Given limited Indian and Pacific data coverage, the great variability in the global ocean budget during the pre-Cenozoic

is primarily driven by the Atlantic Ocean, which is represented by more data points (Figure 2) and more continuous temporal coverage.

In contrast, the Cenozoic record shows progressive stabilisation, with global median values typically between ~1000 and 2000 mg cm^{-2} kyr^{-1} and a wide stable percentile (spanning ~4000-7000 mg cm^{-2} kyr^{-1}) across the entire Cenozoic record. The Atlantic Ocean maintains moderate medians (~1000–2300 mg cm^{-2} kyr^{-1}) over the Cenozoic (Figure 4). The Pacific and Indian Oceans exert an increasing regional influence after ~35 Ma, rising from lower earlier values, and contributing to elevated Neogene carbonate. At the global scale, the highest Cenozoic median CARs (~1600–2000 mg cm^{-2} kyr^{-1}) occur between ~20 and 5 Ma, with a peak at ~5–10 Ma (Figure 4), followed by a decline in the subsequent age bin.

Discussion

This synthesis presents novel insights into the temporal evolution of marine carbonate accumulation across the Cretaceous and Cenozoic, revealing two fundamentally distinct CAR regimes. Given the limitations of our Cretaceous dataset, our interpretation is tentative. The available Cretaceous records exhibit pronounced temporal heterogeneity, with irregular, high-amplitude fluctuations in median CAR values and spatially variable carbonate flux, reflecting a carbonate system influenced by climatic and tectonic changes. In contrast, the Cenozoic CAR record demonstrates a transition toward comparatively stable carbonate burial with reduced temporal variability, yet strongly basin-differentiated regimes.

Cretaceous Carbonate System: Temporal and Spatial Heterogeneity

First-order insights from the Cretaceous CAR data, constrained by limited core recovery and incomplete stratigraphic coverage, show pronounced interbasin heterogeneity and high temporal variability, reflecting strong spatial contrasts and frequent fluctuations in carbonate accumulation rates across basins, even under broadly greenhouse climate conditions. Across all basins, CARs fluctuate strongly throughout the mid–Late Cretaceous, indicating distinct basin-specific trajectories rather than a coherent global signal (Figure 4). We argue that the Cretaceous CAR records reflect the interplay between sustained greenhouse forcing, while their pronounced variability arises from basin-specific modulation by ocean circulation, and episodic perturbations such as Oceanic Anoxic Events (OAEs). Elevated atmospheric CO_2, driven by intensified volcanism and crustal decarbonation, promoted high pelagic carbonate production during the mid-Cretaceous greenhouse (Lee et al., 2013; Steuber et al., 2023). However, this carbonate production was repeatedly disrupted by globally OAEs, which induced transient acidification, lowered carbonate saturation, and widespread CCD shoaling (Jenkyns, 2018; Jones et al., 2023).

In the Atlantic, the decline in CAR from ~100–90 Ma (Figure 4) likely reflects a compound response to OAE-related chemical perturbations and to contemporaneous reorganisation of deep-water circulation. During the Late Cretaceous, vigorous southern deep-water formation (Donnadieu et al., 2016) and the progressive replacement of Tethyan-sourced deep waters by southern-sourced water masses across the Early–Late Cretaceous transition (Liu et al., 2023), fundamentally reorganized Atlantic deep-water circulation. This reorganization was aided by strengthened interbasin connectivity following the opening of the Equatorial Atlantic Gateway between ~100 and 90 Ma (Dummann et al., 2023), which altered carbonate saturation states and preservation patterns across the Atlantic Ocean. The depth-dependent decline in shallow Atlantic CAR (<2000 m) across this interval (Figure 5) is consistent with intensified upper-ocean acidification and planktonic ecosystem disruption, and with suppressed shallow carbonate preservation during OAE1d documented in the western North Atlantic (Watkins et

al., 2005). By contrast, the comparatively buffered intermediate-water CAR suggests that OAE1 burial suppression was dominated by shallow-water dissolution, consistent with enhanced deep-water carbonate preservation reported for Cretaceous dissolution intervals (Roth & Krumbach, 1986).

The intensified decline in Atlantic CAR from ~95–90 Ma (median ~800 mg cm^{-2} kyr^{-1}) likely corresponds to OAE2, reflecting widespread volcanic CO_2 outgassing, transient acidification, and reduced carbonate burial (Jenkyns, 2018; Jenkyns et al., 2017; Leckie et al., 2002). Post-90 Ma, CAR values recover as atmospheric CO_2 declines and enhanced silicate weathering stabilises ocean carbonate chemistry (Blättler et al., 2011; Núñez-Useche et al., 2020; Paris et al., 2016). By the Late Cretaceous, Atlantic CAR stabilises at moderate levels, likely reflecting improved carbonate preservation associated with progressive cooling, stronger export of Southern Component Water into the basin (Friedrich et al., 2012), and reduced Pacific deep-water input after ~80 Ma (Moiroud et al., 2016). This interval is also marked by the proliferation of oceanic red beds, particularly in the Atlantic Ocean, indicating enhanced deep-ocean oxygenation and strengthened meridional circulation (Ladant et al., 2020; Robinson et al., 2010; Wang et al., 2011), conditions favourable for pelagic carbonate deposition (Mansour & Wagreich, 2022; Wang et al., 2011).

The Indian Ocean record, derived from sites located in the southern Indian Ocean, reflects similar forcing but with additional regional modulation. Persistently low mid-Cretaceous CARs (Figure 4) likely record the cumulative imprint of multiple OAEs operating on timescales finer than our binning resolution. Evidence from the southwest Australia basin indicates marked reductions in carbonate accumulation during these OAE-related acidification events, consistent with globally observed declines in deep-sea carbonate burial (Jones et al., 2023; Petrizzo et al., 2022). Since the middle Cretaceous, the proto-Indian Ocean shared common intermediate and deep-water masses with the South Atlantic, implying strong inter-basin connectivity and circulation between the South Atlantic and Indian sectors (Moiroud et al., 2016). However, the proximity of the Indian Ocean to volcanic and hydrothermal activity associated with the Kerguelen Plateau, which underwent major emplacement during the mid-Cretaceous (Coffin et al., 2002; Duncan, 2002; Frey et al., 2000), likely imposed local perturbations to seawater chemistry that suppressed carbonate burial. The subsequent rise in Indian CAR between ~80–70 Ma parallels Atlantic recovery and is consistent with strengthened deep-water connectivity between the South Atlantic and Indian Oceans (Moiroud et al., 2016).

The Pacific exhibits persistently low CAR throughout much of the Cretaceous. Suppressed carbonate accumulation from ~110–85 Ma, followed by a modest recovery between ~85 and 75 Ma, is also evident in the Indian Ocean, likely reflecting the global post-OAE rebound in pelagic carbonate production (Wang et al., 2011). Nonetheless, Pacific CARs remain markedly lower than coeval Atlantic and Indian values throughout the Late Cretaceous, consistent with inherently lower carbonate saturation in Pacific deep waters, a condition that persists today (Archer, 1996). Limited southern-sourced deep-water influence and the dominance of older, less saturated Pacific water masses maintained low carbonate saturation and enhanced dissolution relative to the Atlantic and Indian Oceans (Ladant et al., 2020; Roth, 1989). Strengthened Southern Ocean deep-water export preferentially ventilated the Atlantic–Indian system while reducing Pacific inflow to the Atlantic (Moiroud et al., 2016), amplifying interbasin contrasts in carbonate burial. Our Pacific dataset also captures a sharp CAR decline (<200 mg cm^{-2} kyr^{-1}) across the Cretaceous–early Paleogene boundary (~70–65 Ma), reflecting reduced productivity and enhanced dissolution, likely linked to Deccan Traps volcanism and associated environmental stress, resulting in diminished carbonate burial during this period, as recorded in tropical Pacific sediments (Dameron et al., 2017; Jouini et al., 2023). A

contemporaneous CAR decline in the Indian Ocean may suggest a coordinated response across basins interconnected by intermediate- and deep-water flow at this time (Ladant et al., 2020).

Cenozoic Carbonate System: Stabilisation and Basin-Scale Divergence

Our compilation reveals that the Cenozoic carbonate burial system is relatively stable compared to the Cretaceous, yet strongly differentiated among ocean basins. At the global scale, median CAR remains modest throughout the Paleogene, increases in the late Neogene, and declines towards the present. Critically, this aggregate trajectory does not exhibit an order-of-magnitude increase in pelagic carbonate burial toward the present. Instead, the apparent long-term trend masks pronounced basin-scale divergence. While Opdyke and Wilkinson (1988) inferred an approximately eightfold increase in pelagic carbonate accumulation from the latest Cretaceous to the present, our site-based reconstruction indicates a more moderate global rise (Figure 4), with much of the variability arising from differences in how the Atlantic, Pacific, and Indian basins responded to Cenozoic climatic and gateway forcing. These varied responses influence the global budget differently than a steady increase in global carbonate production.

In the Atlantic, we identified the first major Cenozoic CAR peak in the late Eocene, which likely reflects intensified Northern Component Water (NCW) formation. Coxall et al. (2018) linked the late Eocene strengthening of NCW to tectonic reorganisation of subarctic basins, which enhanced weathering and nutrient delivery and exported well-oxygenated deep-water southward ~1–2 Myr before the onset of Antarctic glaciation. Consistent with this, Dutkiewicz and Müller (2022) inferred elevated carbonate carbon fluxes in the Atlantic at ~38 Ma, preceding the opening of major Southern Ocean gateways (Straume et al., 2020) and the onset of global cooling and Antarctic glaciation (Westerhold et al., 2020).

Across the Pacific, which maintained the lowest CAR among the three basins during the Paleocene–Eocene, we record the clearest expression of the EOT reorganisation, as evidenced by pronounced intensification of carbonate burial (CAR) during this interval. Recent high-resolution paleoceanographic reconstructions by Wade et al. (2020) provide critical context for interpreting this Pacific transformation. The authors synthesized global deep-sea lithofacies distributions across key Paleogene climate boundaries, documenting a striking expansion of calcareous sediment deposition across the equatorial Pacific during the early Oligocene, where our data coverage is primarily concentrated. Their lithofacies compilations indicate that Pacific regions previously dominated by pelagic clay and siliceous ooze transitioned to widespread carbonate-rich deposition across the EOT, whereas the Atlantic and Indian Oceans retained more persistent carbonate-rich sedimentation with minor spatial adjustments. According to Wade et al. (2020), this pattern is consistent with pronounced deepening of the Pacific CCD at the EOT (e.g., Dalvand et al., 2025a; Pälike et al., 2012; Taylor et al., 2023; van Andel, 1975), and comparatively subdued CCD changes in the other basins. This pattern aligns with findings of Renaudie and Lazarus (2025), who document a strong increase in pelagic accumulation rates in the Pacific, a more subdued increase in the Indian Ocean, and no detectable shift in sedimentation rates during the early Oligocene. Our CAR estimates further provide rate-based support for this framework: throughout the Paleogene, the Atlantic and Indian Oceans maintain higher CARs (~1500–2000 and ~500–1800 mg cm^{-2} kyr^{-1}, respectively), while the Pacific remains strongly suppressed (<500 mg cm^{-2} kyr^{-1}) until the latest Eocene (Figure 4). The early Oligocene (~35–30 Ma) CAR jump to ~1200 mg cm^{-2} kyr^{-1} in the Pacific, therefore, represents the most pronounced Paleogene change among the major basins and captures the strongest expression of EOT-related influence in our dataset. Our depth-resolved Pacific results reveal a strong increase in deep-water CAR during the early Oligocene (~34 Ma), a pattern also observed in the Indian Ocean, albeit at slightly lower intensity (Figure 5).

The early Miocene marks a more modest yet globally coherent inflection in carbonate accumulation. Our compilation reveals a synchronous reduction in median CAR across the Pacific and Indian Oceans between ~25–20 Ma, briefly interrupting the long-term Oligocene rise (Figure 4). This pattern aligns with the Pacific basin-wide early Miocene declines in CAR documented by Lyle (2003), who attributed this reduction, and the contemporaneous CCD shoaling (also observed globally), to early Neogene warming, deglaciation, and brief sea-level rise (Lear et al., 2000; Miller et al., 2020; van Andel, 1975). In contrast, the Atlantic preserves broadly stable median CAR from the early Oligocene through the early Miocene, though with wide percentile ranges indicative of greater spatial heterogeneity (Figure 4; Supplemental video). Our depth-binned analyses further substantiate the depth dependence of this signal, showing that the early Miocene CAR decline is most pronounced in deep-water settings (>3500 m) across all three basins (Figure 5). The Atlantic, however, offsets this deep-water decline through substantial increases in shallow and intermediate CAR, resulting in an overall stable median CAR during this transitional interval. These observations correlate with early Miocene climate–ocean adjustments, suggesting weakened deep-water carbonate preservation and reduced deep carbonate burial, while simultaneously promoting expanded shallow-water carbonate production under rising sea level (e.g., Miller et al., 2005; Tcherepanov et al., 2008).

From the middle Miocene through the early Pliocene (~15–5 Ma), our results document a globally coherent rise in CAR across all three ocean basins, despite inter-basin variability, followed by a decline thereafter (Figure 4). In the Atlantic, median CAR rises from ~15 Ma, reaching its second Cenozoic maximum between ~10 and 5 Ma. Depth-resolved patterns indicate that this enhancement is most pronounced at intermediate water depths after ~13 Ma (Figure 5). We interpret this pattern to be consistent with southeast Atlantic records reported by Drury et al. (2021), who attribute intensified carbonate burial to enhanced deep-water ventilation and cooling associated with Antarctic reglaciation, following elevated carbonate dissolution during the Miocene Climate Optimum (MCO: 17–14 Ma; Westerhold et al., 2020). The mid- to late Miocene rise in Atlantic CAR further coincided with strengthened North Atlantic Deep Water (NADW) formation driven by Greenland ice-sheet expansion (Pillot et al., 2022), and with the gradual constriction of the Panama Gateway from ~14 Ma (Schneider & Schmittner, 2006).

The MCO interval (~17–14 Ma) in the Pacific appears to have been moderated by spatial heterogeneity in carbonate-ion concentrations, with regional variability in [CO_3^{2-}] offsetting localized dissolution during the MCO (Holbourn et al., 2024), likely preventing basin-scale CAR collapse in our ~20–15 Ma record (Figure 4). Following the MCO, Pacific CARs remain relatively high, consistent with evidence for Antarctic ice-sheet expansion, global cooling, and improved deep-water ventilation (e.g., Holbourn et al., 2024; Sutherland et al., 2022). By contrast, the Indian Ocean displays a stronger and more sustained post-MCO increase in carbonate burial. This trend aligns with documented overall CCD deepening in the equatorial Indian Ocean since the middle Miocene (Dalvand et al., 2025b), driven by multiple interconnected forcing mechanisms. These include the evolution of the Western Pacific Warm Pool (WPWP), reduced Indo-Pacific water exchange associated with Indonesian Seaway constriction, which together promoted cooler surface and deep-water conditions, as well as the initiation of a modern-like South Asian Monsoon (SAM), and the strengthening of AABW and NCW influence (e.g., Gupta et al., 2015; Podder et al., 2024; Sarr et al., 2022; Smart et al., 2007; Sosdian & Lear, 2020). Together, these processes appear to have created especially favourable conditions for carbonate burial in the Indian Ocean, explaining the systematic offset toward higher Indian CAR relative to the Pacific between ~15 and 5 Ma.

Superimposed on these long-term trends is the globally recognized late Miocene–early Pliocene biogenic bloom, during which both carbonate and silica accumulation increased (e.g.,

Bolton et al., 2022; Lyle & Baldauf, 2015; Pillot et al., 2023). However, the proportional enhancement of calcareous versus siliceous accumulation varied substantially across ocean basins and even within individual regions (e.g., Cornuault et al., 2023; Dickens & Owen, 1999; Drury et al., 2021; Jianru et al., 2002; Lyle et al., 1995; Lyle et al., 2019; Mora, 2002). Our results capture this event as a strong CAR increase between ~10 and 5 Ma in all three basins, yet with distinct amplitude and character. The Atlantic and Indian Oceans display the highest CARs during this interval, whereas the Pacific shows a more muted response and even a slight decline relative to the preceding 15–10 Ma interval. When considered alongside the regionally heterogeneous sedimentological evidence from this period, such as enhanced carbonate burial in the southwest Pacific (Sutherland et al., 2022), increased biogenic silica fluxes in the North Pacific (Rea et al., 1995), and spatially variable opal-to-carbonate ratios in the eastern equatorial Pacific (e.g., Lyle & Baldauf, 2015; Lyle et al., 2019), these observations suggest that the Pacific biogenic bloom was likely expressed as a disproportionately higher silica contribution relative to carbonate burial at the basin scale. By contrast, the Atlantic and Indian Oceans show regional evidence of intensified carbonate accumulation during the biogenic bloom interval (e.g., Cornuault et al., 2023; Dickens & Owen, 1999; Drury et al., 2021; Peterson & Backman, 1990), helping to explain the comparatively subdued Pacific CAR response during the ~10–5 Ma interval (Figure 4).

The contrasting Pacific response likely reflects gateway-driven reorganisation of global ocean circulation, particularly the progressive restriction of the Central American Seaway, which reduced Atlantic–Pacific exchange and altered deep-water mass pathways (Lyle et al., 1995; Roth et al., 2000; Schneider & Schmittner, 2006). This promoted the development of a northward silica gradient in the Pacific through enhanced influence of silica-rich deep waters and circulation of Antarctic Bottom Water, which carries elevated dissolved silica into the Pacific basin (Cortese et al., 2004; Keller & Barron, 1983; Woodruff & Savin, 1989; Zhang et al., 2022a). Additional recycling and dissolution of biogenic opal further contributed to dissolved silica enrichment toward the North Pacific (Ragueneau et al., 2000), favouring diatom productivity over carbonate producers (Litchman, 2007; Lyle & Baldauf, 2015). As a result, biogenic production was preferentially partitioned into opal rather than carbonate, suppressing carbonate accumulation despite high overall productivity. In contrast, the Atlantic and Indian oceans, characterised by different circulation regimes and lower silica supply, maintained more carbonate-favourable conditions during the biogenic bloom interval.

Our compilation also shows a major decline in global CAR between ~5 Ma and 0 Ma, expressed across all three ocean basins (Figure 4). Regional records document a gradual decline in carbonate burial from the Pliocene through the Quaternary, following the biogenic bloom peak (e.g., Cornuault et al., 2023; Dickens & Owen, 1999; Lyle & Baldauf, 2015; Lyle et al., 2019; Sutherland et al., 2022), superimposed on glacial–interglacial variability (e.g., Cornuault et al., 2023; Farrell & Prell, 1989; Gröger et al., 2003; Hodell et al., 2001). This downturn coincides with the weakening of NADW and Atlantic Meridional Overturning Circulation (AMOC) during the early Pliocene (Pillot et al., 2023) and with the subsequent intensification of Northern Hemisphere glaciation after ~2.7 Ma (Haug et al., 1999), which correlates with a sustained reduction in global marine productivity since the Pliocene (Karatsolis et al., 2022). The progressive shoaling and final closure of the Panama Gateway between ~4.6 and 2.5 Ma represents a key tectonic driver of these changes, fundamentally reorganising inter-basin exchange of water masses and carbonate saturation states (Bartoli et al., 2005; Haug & Tiedemann, 1998). Initial Panama Gateway shoaling between ~4.6 and 4.2 Ma reduced Pacific–Atlantic communication and established modern-day contrasts—with higher carbonate saturation and burial in the Atlantic and relatively corrosive conditions in the Pacific (e.g., Cannariato & Ravelo, 1997; Haug & Tiedemann, 1998; Haug et al., 2001). Our CAR data

reflect this divergence over the 5–0 Ma interval, the Atlantic median CAR (~1300 mg cm^{-2} kyr^{-1}, with 10th–90th percentiles extending to ~7500 mg cm^{-2} kyr^{-1}) far exceeds the Pacific median (~500 mg cm^{-2} kyr^{-1}). Additionally, the initiation of the Northern Hemisphere Glaciation (NHG), facilitated by the final closure of the Panama Gateway between ~3 and 2.5 Ma (Bartoli et al., 2005), enhanced meridional temperature gradients and upwelling, driving a shift toward a more "Pacific-like" ocean state characterised by elevated silica preservation and nutrient regimes favouring opal export over carbonate, thereby constraining calcareous nannoplankton productivity to only the most ecophysiologically competitive taxa (Cortese et al., 2004; Suchéras-Marx et al., 2019). The associated long-term reduction in CAR recorded in our compilation thus reflects the combined effects of gateway-driven circulation changes, the transition to a bipolar glaciated climate, and a productivity regime unfavourable for pelagic carbonate burial.

Global Implications

Our reconstruction reveals a previously unresolved reorganisation of the global carbonate burial system from the mid-Cretaceous to the present, challenging first-order assumptions of a monotonic, order-of-magnitude intensification of Cenozoic pelagic carbonate burial (Boss & Wilkinson, 1991; Hay, 1999; Opdyke & Wilkinson, 1988). This global pattern has been linked to proportional shallow–deep carbonate differentiation (Boss & Wilkinson, 1991; Dutkiewicz et al., 2019; Opdyke & Wilkinson, 1988; Pohl et al., 2020; Salles et al., 2025), sea-level fall (Miller et al., 2005), calcareous plankton evolution (Hay, 2004; Komar & Zeebe, 2021; Suchéras-Marx et al., 2019; Wilkinson & Walker, 1989), changes in ocean chemistry and weathering input, and CCD shifts (Boudreau et al., 2019; Dutkiewicz et al., 2019; Komar & Zeebe, 2021; van der Ploeg et al., 2019). Kump and Arthur (1997) argued for shallow–deep partitioning as the primary control on Cenozoic carbonate burial, estimating an approximately eightfold fractionation between shallow and deep accumulation rates since the Oligocene (Figure 6a), with alkalinity supply exerting a secondary influence. More recently, Salles et al. (2025) reframed this evolution as an alkalinity-driven reorganisation of the carbonate system, whereby excess alkalinity exceeded shallow-platform accommodation, promoting redistribution toward pelagic settings and modulating CCD fluctuations.

In contrast to shallow-carbonate productivity estimates of Salles et al. (2025) which indicate a sharp decline during the Paleocene–Eocene, our global pelagic CAR record remains comparatively steady across this interval and instead exhibits a progressive, modest increase from the early Oligocene through the Pliocene (Figure 6: a & e). This trend is broadly consistent with independent deep-sea carbonate accumulation compilations (Figure 6b), which show a long-term increase punctuated by variability through the Cenozoic (Hay et al., 1988), and with sediment accumulation patterns (Figure 6c), which indicate a general decline from the Late Cretaceous into the Cenozoic (Renaudie and Lazarus, 2025). Crucially, our basin-resolved synthesis demonstrates pronounced Paleocene inter-ocean divergence, showing that global carbonate accumulation rates emerge from integrating heterogeneous regional responses to common climatic and geochemical forcings. During the Paleocene–Eocene interval of shallow-platform collapse, the Atlantic and Indian Oceans maintain higher pelagic CARs, whereas the Pacific persistently exhibits the lowest carbonate accumulation. This muted Pacific response implies partial inter-basin compensation that buffers the global burial signal—a pattern also evident across the Eocene–Oligocene transition, when intensified deep-sea carbonate burial in the Pacific and Indian Oceans coincides with steadier Atlantic rates and only modest increases in global CAR. Together, these results indicate that although alkalinity-driven reorganisation defines the first-order structure of the Cenozoic carbonate system, it did not generate a

monotonic intensification of deep-sea carbonate burial at the global scale, as previously suggested (Opdyke & Wilkinson, 1988). Basin-scale contrasts in median CARs (Figure 6f) further emphasise that this evolution was strongly non-uniform, with asynchronous intensification across the Atlantic, Pacific, and Indian Oceans. Our results highlight basin-specific oceanographic controls—including circulation pathways, carbonate saturation gradients, and gateway evolution—that govern the long-term partitioning of alkalinity and carbonate burial between ocean basins.

Nannoplankton evolutionary patterns provide additional constraints on the relative roles of biological production in governing carbonate burial. Although partial correlation exists between nannofossil evolution from Suchéras-Marx et al. (2019) and our global CAR (Figure 6d), several intervals exhibit clear decoupling between biological innovation and carbonate burial intensity. Peaks in nannofossil accumulation during the Late Cretaceous coincide with highly variable global CARs, which we interpret as reflecting the dominance of basin-specific preservation conditions over production. The pronounced CAR reduction at ~95–90 Ma persists despite elevated nannoplankton abundance, suggesting that acidification and circulation-driven dissolution suppress carbonate burial at this time. While Cretaceous diversification established the potential for pelagic carbonate production, major shifts in the global record appear to be unaligned with evolutionary thresholds before the Neogene. The Cenozoic provides clear evidence for basin-scale intensification of deep-sea carbonate accumulation to occur during the nannoplankton “establishment phase”. During this phase, evolutionary innovation (invasion and specialization) was muted, and global CARs remained relatively stable, pointing to regional oceanographic forcing as the primary control. Similarly, a synchronous global decline in CARs at 5–0 Ma contrasts with contemporaneous increases in nannofossil accumulation, underscoring a fundamental decoupling between biological productivity and carbonate burial.

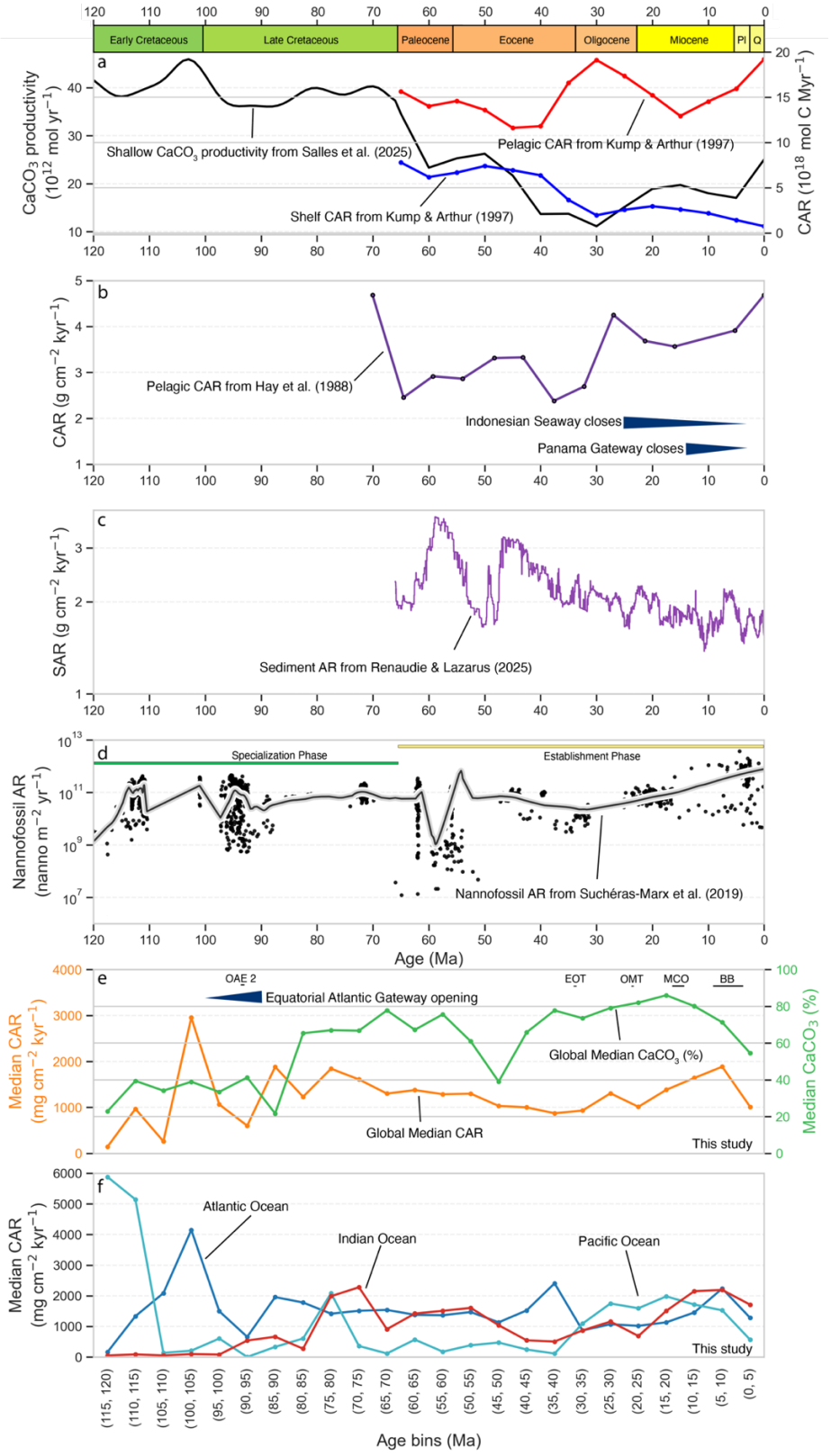

Figure 6: Evolution of shallow and pelagic carbonate burial, sediment accumulation, and nannofossil production over the last 120 Ma. **(a)** Global $CaCO_3$ production estimates, showing shallow-water carbonate production derived from model-based alkalinity and platform-area reconstructions (black; Salles et al., 2025), alongside deep-sea and shelf carbonate accumulation rates estimated using geochemical mass-balance modelling from Kump and Arthur (1997). **(b)** Deep-sea carbonate accumulation rates compiled from sediment-core measurements and mass-

accumulation calculations from Hay et al. (1988). **(c)** Measured sediment accumulation rates from Renaudie and Lazarus (2025). **(d)** Nannofossil accumulation rates (AR) from Suchéras-Marx et al. (2019), shown as individual data points smoothed with LOWESS (SF=0.1). **(e)** Global median deep-sea carbonate accumulation rates (orange), plotted together with median carbonate content ($CaCO_3$ %) (green) calculated within 5 Myr bins across all sites in this study. **(f)** Median carbonate accumulation rates for the Atlantic, Pacific, and Indian Oceans, computed within 5 Myr bins from this study. The timing of the Oceanic Anoxic Event 2 (OAE 2) is from Jenkyns (2018), the Eocene/Oligocene transition (EOT), the Oligocene/Miocene transition (OMT), and the Miocene Climate Optimum (MCO) are from Westerhold et al. (2020), the Equatorial Atlantic Gateway opening is from Dummann et al. (2023), the Indonesian Seaway closure is from Bahr et al. (2023) and Kuhnt et al. (2004), and the Panama Gateway closure is from Schmittner et al. (2004). Approximate span of the late Miocene-early Pliocene biogenic bloom (BB) across the global oceans is from Pillot et al. (2023).

Conclusions

This study presents a comprehensive, basin-resolved synthesis of pelagic carbonate accumulation rates across the Atlantic, Pacific, and Indian Oceans from the mid-Cretaceous to the present. We present the first large-scale, basin-specific reconstruction of marine carbonate burial, providing new constraints on the long-term evolution of the Earth system, including connections between the carbon cycle, ocean circulation, and climate. Our results delineate two contrasting modes of carbonate accumulation: a highly dynamic, environmentally volatile Cretaceous regime associated with greenhouse conditions, and a comparatively stabilised but strongly differentiated Cenozoic regime shaped by tectonic reorganisation, climate cooling, and the evolution of ocean gateways.

Beyond documenting regional variability, our findings carry global implications for understanding long-term climate sensitivity, shelf-basin carbonate fractionation, biological evolution, and carbon sequestration. The transition from greenhouse to icehouse conditions is reflected in systematic basin-wide shifts in carbonate burial patterns, with direct consequences for oceanic carbon storage and atmospheric CO_2 regulation. These results highlight the central role of basin-scale carbonate burial in modulating the global carbon cycle, demonstrating how spatial differences in ocean chemistry, biological productivity, and deep-water circulation propagate into global carbon fluxes over geological timescales.

Our synthesis revises earlier conceptual models that invoked a uniformly increasing global carbonate burial through time. Instead, we show that long-term carbonate accumulation emerges from complex, asynchronous interactions between ocean basins, tectonic events, and climatic transitions. Distinct basin-specific responses, such as Late Cretaceous instability in the Pacific and pronounced Oligocene intensification in the Pacific and Indian Oceans, contrast with regime changes in the Atlantic, underscoring the spatial heterogeneity of marine carbon sinks and their sensitivity to deep-time oceanographic-climate reorganisations. This framework demonstrates that the long-term trajectory of pelagic carbonate burial is neither monotonic nor spatially coherent. These findings underscore the need for next-generation carbon cycle models to explicitly incorporate inter-basin heterogeneity, with implications for reconstructing past climate states and anticipating future responses of the ocean–carbon system to anthropogenic forcing.

Credit authorship contribution statement

Faranak Dalvand: Writing – original draft, Formal analysis, Data curation, Visualisation, Investigation. **Adriana Dutkiewicz:** Writing – review & editing, Methodology, Conceptualisation, Formal analysis, Funding acquisition, Supervision. **Nicky M. Wright:** Writing – review & editing, Formal analysis, Supervision. **R. Dietmar Müller:** Writing – review & editing, Methodology, Conceptualisation, Formal analysis, Visualisation, Supervision.

Declaration of competing interest

The authors declare that they have no known competing financial interests or personal relationships that could have appeared to influence the work reported in this paper.

Data statement

Data supporting the results of this study can be found online at https://doi.org/10.5281/zenodo.18755594.

Funding declaration

This research was supported by an Australian Research Council (ARC) PhD scholarship to F.D. and an ARC Future Fellowship to A.D. via grant FT190100829. N.M.W. was supported by ARC grant IE230100098. R.D.M. was supported by the AuScope Simulation, Analysis & Modelling node funded by the Australian Government through the National Collaborative Research Infrastructure Strategy, NCRIS.

Appendix A. Supplementary data

Supplementary data to this article can be found online at https://doi/.org/XXXX.

References

Abelson, M., & Erez, J. (2017). The onset of modern-like Atlantic meridional overturning circulation at the Eocene-Oligocene transition: Evidence, causes, and possible implications for global cooling. *Geochemistry, Geophysics, Geosystems, 18*(6), 2177-2199. https://doi.org/10.1002/2017GC006826

Amante, C., & Eakins, B. W. (2009). *ETOPO1 arc-minute global relief model: procedures, data sources and analysis*. Retrieved from National Geophysical Data Center, NOAA: https://repository.library.noaa.gov/view/noaa/1163

Archer, D. (1996). An atlas of the distribution of calcium carbonate in sediments of the deep sea. *Global Biogeochemical Cycles, 10*(1), 159-174. https://doi.org/10.1029/95GB03016

Bahr, A., Kaboth-Bahr, S., & Karas, C. (2023). The opening and closure of oceanic seaways during the Cenozoic: pacemaker of global climate change? In V. M. Rossi, S. G. Longhitano, C. Olario, & F. L. Chiocci (Eds.), *Straits and Seaways: Controls, Processes and Implications in Modern and Ancient Systems* (Vol. 523, pp. 141-171): Geological Society, Londen, Special Publication. https://doi.org/10.1144/SP523-2021-54

Bartoli, G., Sarnthein, M., Weinelt, M., Erlenkeuser, H., Garbe-Schönberg, D., & Lea, D. W. (2005). Final closure of Panama and the onset of northern hemisphere glaciation. *Earth and Planetary Science Letters, 237*(1-2), 33-44. https://doi.org/10.1016/j.epsl.2005.06.020

Blättler, C. L., Jenkyns, H. C., Reynard, L. M., & Henderson, G. M. (2011). Significant increases in global weathering during Oceanic Anoxic Events 1a and 2 indicated by calcium isotopes. *Earth and Planetary Science Letters, 309*(1-2), 77-88. https://doi.org/10.1016/j.epsl.2011.06.029

Bolton, C. T., Gray, E., Kuhnt, W., Holbourn, A. E., Lübbers, J., Grant, K., et al. (2022). Secular and orbital-scale variability of equatorial Indian Ocean summer monsoon winds during the late Miocene. *Climate of the Past, 18*(4), 713-738. https://doi.org/10.5194/cp-18-713-2022

Boss, S. K., & Wilkinson, B. H. (1991). Planktogenic/eustatic control on cratonic/oceanic carbonate accumulation. *The Journal of Geology, 99*(4), 497-513. https://doi.org/10.1086/629513

Boudreau, B. P., Middelburg, J. J., Sluijs, A., & van der Ploeg, R. (2019). Secular variations in the carbonate chemistry of the oceans over the Cenozoic. *Earth and Planetary Science Letters, 512*, 194-206. https://doi.org/10.1016/j.epsl.2019.02.004

Braz, C., Zahirovic, S., Salles, T., Flament, N., Harrington, L., & Müller, R. D. (2021). Modelling the role of dynamic topography and eustasy in the evolution of the Great Artesian Basin. *Basin Research, 33*(6), 3378-3405. https://doi.org/10.1111/bre.12606

Broecker, W. S. (2003). The oceanic $CaCO_3$ cycle. In H. D. Holland & K. K. Turekian (Eds.), *Treatise on Geochemistry* (pp. 529–549): Elsevier. https://doi.org/10.1016/B0-08-043751-6/06119-3

Broecker, W. S., & Peng, T.-H. (1982). *Tracers in the Sea* (Vol. 690): Lamont-Doherty Geological Observatory, Columbia University Palisades, New York. https://doi.org/10.1017/S0033822200005221

Campbell, S. M., Moucha, R., Derry, L. A., & Raymo, M. E. (2018). Effects of dynamic topography on the Cenozoic carbonate compensation depth. *Geochemistry, Geophysics, Geosystems, 19*(4), 1025-1034. https://doi.org/10.1002/2017GC007386

Cannariato, K. G., & Ravelo, A. C. (1997). Pliocene-Pleistocene evolution of eastern tropical Pacific surface water circulation and thermocline depth. *Paleoceanography and Paleoclimatology, 12*(6), 805-820. https://doi.org/10.1029/97PA02514

Cartapanis, O., Galbraith, E. D., Bianchi, D., & Jaccard, S. L. (2018). Carbon burial in deep-sea sediment and implications for oceanic inventories of carbon and alkalinity over the last glacial cycle. *Climate of the Past, 14*(11), 1819-1850. https://doi.org/10.5194/cp-14-1819-2018

Carter, L., Neil, H. L., & McCave, I. N. (2000). Glacial to interglacial changes in non-carbonate and carbonate accumulation in the SW Pacific Ocean, New Zealand. *Palaeogeography, Palaeoclimatology, Palaeoecology, 162*(3-4), 333-356. https://doi.org/10.1016/S0031-0182(00)00137-1

Chiarella, D., Longhitano, S. G., & Tropeano, M. (2017). Types of mixing and heterogeneities in siliciclastic-carbonate sediments. *Marine and Petroleum Geology, 88*, 617-627. https://doi.org/10.1016/j.marpetgeo.2017.09.010

Coffin, M. F., Pringle, M. S., Duncan, R. A., Gladczenko, T. P., Storey, M., Müller, R. D., & Gahagan, L. A. (2002). Kerguelen hotspot magma output since 130 Ma. *Journal of petrology, 43*(7), 1121-1137. https://doi.org/10.1093/petrology/43.7.1121

Cornuault, P., Westerhold, T., Pälike, H., Bickert, T., Baumann, K.-H., & Kucera, M. (2023). Nature and origin of variations in pelagic carbonate production in the tropical ocean since the Mid Miocene (ODP Site 927). *Biogeosciences, 20*(3), 597-618. https://doi.org/10.5194/bg-20-597-2023

Cortese, G., Gersonde, R., Hillenbrand, C.-D., & Kuhn, G. (2004). Opal sedimentation shifts in the World Ocean over the last 15 Myr. *Earth and Planetary Science Letters, 224*(3-4), 509-527. https://doi.org/10.1016/j.epsl.2004.05.035

Coxall, H. K., Huck, C. E., Huber, M., Lear, C. H., Legarda-Lisarri, A., O'regan, M., et al. (2018). Export of nutrient rich Northern Component Water preceded early Oligocene Antarctic glaciation. *Nature Geoscience, 11*(3), 190-196. https://doi.org/10.1038/s41561-018-0069-9

Cramer, B. S., Toggweiler, J. R., Wright, J. D., Katz, M. E., & Miller, K. G. (2009). Ocean overturning since the Late Cretaceous: Inferences from a new benthic foraminiferal isotope compilation. *Paleoceanography and Paleoclimatology, 24*(4). https://doi.org/10.1029/2008PA001683

Dalvand, F., Dutkiewicz, A., Wright, N. M., Mather, B. R., & Müller, R. D. (2025a). Regional carbonate compensation depth variability in the Pacific Ocean since the Oligocene. *Frontiers in Earth Science, 13*(1605906). https://doi.org/10.3389/feart.2025.1605906

Dalvand, F., Dutkiewicz, A., Wright, N. M., & Müller, R. D. (2025b). Indian Ocean carbonate compensation depth since the Late Oligocene. *Geo-Marine Letters, 45*(38), 1-14. https://doi.org/10.1007/s00367-025-00825-5

Dameron, S. N., Leckie, R. M., Clark, K., MacLeod, K. G., Thomas, D. J., & Lees, J. A. (2017). Extinction, dissolution, and possible ocean acidification prior to the Cretaceous/Paleogene (K/Pg) boundary in the tropical Pacific. *Palaeogeography, Palaeoclimatology, Palaeoecology, 485*, 433-454. https://doi.org/10.1016/j.palaeo.2017.06.032

Dickens, G. R., & Owen, R. M. (1999). The latest Miocene–early Pliocene biogenic bloom: a revised Indian Ocean perspective. *Marine Geology, 161*(1), 75-91. https://doi.org/10.1016/S0025-3227(99)00057-2

Donnadieu, Y., Pucéat, E., Moiroud, M., Guillocheau, F., & Deconinck, J.-F. (2016). A better-ventilated ocean triggered by Late Cretaceous changes in continental configuration. *Nature Communications, 7*(1), 10316. https://doi.org/10.1038/ncomms10316

Drury, A. J., Liebrand, D., Westerhold, T., Beddow, H. M., Hodell, D. A., Rohlfs, N., et al. (2021). Climate, cryosphere and carbon cycle controls on Southeast Atlantic orbital-scale carbonate deposition since the Oligocene (30–0 Ma). *Climate of the Past 17*(5), 2091-2117. https://doi.org/10.5194/cp-17-2091-2021

Dummann, W., Hofmann, P., Herrle, J. O., Frank, M., & Wagner, T. (2023). The early opening of the Equatorial Atlantic gateway and the evolution of Cretaceous peak warming. *Geology, 51*(5), 476-480. https://doi.org/10.1130/G50842.1

Duncan, R. A. (2002). A time frame for construction of the Kerguelen Plateau and Broken Ridge. *Journal of Petrology, 43*(7), 1109-1119. https://doi.org/10.1093/petrology/43.7.1109

Dutkiewicz, A., & Müller, R. D. (2021). The carbonate compensation depth in the South Atlantic Ocean since the Late Cretaceous. *Geology, 49*(7), 873-878. https://doi.org/10.1130/G48404.1

Dutkiewicz, A., & Müller, R. D. (2022). The history of Cenozoic carbonate flux in the Atlantic Ocean constrained by multiple regional carbonate compensation depth reconstructions. *Geochemistry, Geophysics, Geosystems, 23*(11), e2022GC010667. https://doi.org/10.1029/2022GC010667

Dutkiewicz, A., Müller, R. D., Cannon, J., Vaughan, S., & Zahirovic, S. (2019). Sequestration and subduction of deep-sea carbonate in the global ocean since the Early Cretaceous. *Geology, 47*(1), 91-94. https://doi.org/10.1130/G45424.1

Dutkiewicz, A., O'callaghan, S., & Müller, R. D. (2016). Controls on the distribution of deep-sea sediments. *Geochemistry, Geophysics, Geosystems, 17*(8), 3075-3098. https://doi.org/10.1002/2016GC006428

Farrell, J. W., & Prell, W. L. (1989). Climatic change and $CaCO_3$ preservation: An 800,000 year bathymetric reconstruction from the central equatorial Pacific Ocean. *Paleoceanography and Paleoclimatology, 4*(4), 447-466. https://doi.org/10.1029/PA004i004p00447

Foster, G. L., Royer, D. L., & Lunt, D. J. (2017). Future climate forcing potentially without precedent in the last 420 million years. *Nature Communications, 8*(1), 14845. https://doi.org/10.1038/ncomms14845

Frey, F. A., Coffin, M. F., Wallace, P. J., Weis, D., Zhao, X., Wise Jr, S. W., et al. (2000). Origin and evolution of a submarine large igneous province: the Kerguelen Plateau

and Broken Ridge, southern Indian Ocean. *Earth and Planetary Science Letters, 176*(1), 73-89. https://doi.org/10.1016/S0012-821X(99)00315-5

Friedrich, O., Norris, R. D., & Erbacher, J. (2012). Evolution of middle to Late Cretaceous oceans—A 55 m.y. record of Earth's temperature and carbon cycle. *Geology, 40*(2), 107-110. https://doi.org/10.1130/G32701.1

Gröger, M., Henrich, R., & Bickert, T. (2003). Glacial–interglacial variability in lower North Atlantic deep water: inference from silt grain-size analysis and carbonate preservation in the western equatorial Atlantic. *Marine Geology, 201*(4), 321-332. https://doi.org/10.1016/S0025-3227(03)00263-9

Gupta, A. K., Yuvaraja, A., Prakasam, M., Clemens, S. C., & Velu, A. (2015). Evolution of the South Asian monsoon wind system since the late Middle Miocene. *Palaeogeography, Palaeoclimatology, Palaeoecology, 438*, 160-167. https://doi.org/10.1016/j.palaeo.2015.08.006

Hagelberg, T. K., Pisias, N. G., Mayer, L. A., Shackleton, N. J., & Mix, A. C. (1995). Spatial and temporal variability of late Neogene equatorial Pacific carbonate: Leg 138. In N. G. Pisias, L. A. Mayer, T. R. Janecek, A. Palmer-Julson, & T. H. van Andel (Eds.), *Proc. ODP, Sci Results* (Vol. 138, pp. 321–336). College Station, TX: Ocean Drilling Program. https://doi:10.2973/odp.proc.sr.138.116.1995

Haug, G. H., Sigman, D. M., Tiedemann, R., Pedersen, T. F., & Sarnthein, M. (1999). Onset of permanent stratification in the subarctic Pacific Ocean. *Nature, 401*(6755), 779-782. https://doi.org/10.1038/44550

Haug, G. H., & Tiedemann, R. (1998). Effect of the formation of the Isthmus of Panama on Atlantic Ocean thermohaline circulation. *Nature, 393*(6686), 673-676. https://doi.org/10.1038/31447

Haug, G. H., Tiedemann, R., Zahn, R., & Ravelo, A. C. (2001). Role of Panama uplift on oceanic freshwater balance. *Geology, 29*(3), 207-210. https://doi.org/10.1130/0091-7613(2001)029<0207:ROPUOO>2.0.CO;2

Hay, W. W. (1999). Carbonate sedimentation through the late Precambrian and Phanerozoic. *Zentralblatt für Geologie und Paläontologie/Teil 1, 1998*(5-6), 435-445.

Hay, W. W. (2004). Carbonate fluxes and calcareous nannoplankton. In H. R. Thierstein & J. R. Young (Eds.), *Coccolithophores: from molecular processes to global impact* (pp. 509-528). Berline, Heidelberg: Springer. https://doi.org/10.1007/978-3-662-06278-4_19

Hay, W. W., Sloan, J. L., & Wold, C. N. (1988). Mass/age distribution and composition of sediments on the ocean floor and the global rate of sediment subduction. *Journal of Geophysical Research: Solid Earth, 93*(B12), 14933-14940. https://doi.org/10.1029/JB093iB12p14933

Hodell, D. A., Charles, C. D., & Sierro, F. J. (2001). Late Pleistocene evolution of the ocean's carbonate system. *Earth and Planetary Science Letters, 192*(2), 109-124. https://doi.org/10.1016/S0012-821X(01)00430-7

Holbourn, A., Kuhnt, W., Kulhanek, D. K., Mountain, G., Rosenthal, Y., Sagawa, T., et al. (2024). Re-organization of Pacific overturning circulation across the Miocene Climate Optimum. *Nature Communications, 15*(8135). https://doi.org/10.1038/s41467-024-52516-x

Jenkyns, H. C. (2018). Transient cooling episodes during Cretaceous Oceanic Anoxic Events with special reference to OAE 1a (Early Aptian). *Philosophical Transactions of the Royal Society A: Mathematical, Physical and Engineering Sciences, 376*(2130), 20170073. https://doi.org/10.1098/rsta.2017.0073

Jenkyns, H. C., Dickson, A. J., Ruhl, M., & Van den Boorn, S. H. (2017). Basalt-seawater interaction, the Plenus Cold Event, enhanced weathering and geochemical change:

deconstructing Oceanic Anoxic Event 2 (Cenomanian–Turonian, Late Cretaceous). *Sedimentology, 64*(1), 16-43. https://doi.org/10.1111/sed.12305

Jianru, L. i., Rujian, W., & Baohua, L. i. (2002). Variations of opal accumulation rates and paleoproductivity over the past 12 Ma at ODP Site 1143, southern South China Sea. *Chinese Science Bulletin, 47*(7), 596-598. https://doi.org/10.1360/02tb9137

Jones, M. M., Sageman, B. B., Selby, D., Jacobson, A. D., Batenburg, S. J., Riquier, L., et al. (2023). Abrupt episode of mid-Cretaceous ocean acidification triggered by massive volcanism. *Nature Geoscience, 16*(2), 169-174. https://doi.org/10.1038/s41561-022-01115-w

Jouini, A., Paris, G., Caro, G., Bartolini, A., & Gardin, S. (2023). Constraining oceanic carbonate chemistry evolution during the Cretaceous-Paleogene transition: Combined benthic and planktonic calcium isotope records from the equatorial Pacific Ocean. *Earth and Planetary Science Letters, 619*, 118305. https://doi.org/10.1016/j.epsl.2023.118305

Karatsolis, B. T., Lougheed, B. C., De Vleeschouwer, D., & Henderiks, J. (2022). Abrupt conclusion of the late Miocene-early Pliocene biogenic bloom at 4.6-4.4 Ma. *Nature Communications, 13*(1), 353. https://doi.org/10.1038/s41467-021-27784-6

Kasuya, T., Okazaki, Y., Iwasaki, S., Nagashima, K., Kimoto, K., Lamy, F., et al. (2024). Orbital timescale CaCO3 burial and dissolution changes off the Chilean margin in the subantarctic Pacific over the past 140 kyr. *Progress in Earth and Planetary Science, 11*(56). https://doi.org/10.1186/s40645-024-00657-4

Katavouta, A., & Williams, R. G. (2021). Ocean carbon cycle feedbacks in CMIP6 models: contributions from different basins. *Biogeosciences, 18*(10), 3189-3218. https://doi.org/10.5194/bg-18-3189-2021

Komar, N., & Zeebe, R. E. (2021). Reconciling atmospheric CO2, weathering, and calcite compensation depth across the Cenozoic. *Science Advances, 7*(4), eabd4876.

Kuhnt, W., Holbourn, A., Hall, R., Zuvela, M., & Käse, R. (2004). Neogene history of the Indonesian throughflow. In P. Clift, W. Kuhnt, P. Wang, & D. Hayes (Eds.), *Continent-Ocean Interactions within East Asian Marginal Seas, Geophysical Monograph* (Vol. 149, pp. 299-320). https://doi.org/10.1029/149GM16

Kump, L. R., & Arthur, M. A. (1997). Global chemical erosion during the Cenozoic: Weatherability balances the budgets. In W. F. Ruddiman (Ed.), *Tectonic uplift and climate change* (pp. 399-426). Boston, MA: Springer. https://doi.org/10.1007/978-1-4615-5935-1_18

Ladant, J.-B., Poulsen, C. J., Fluteau, F., Tabor, C. R., MacLeod, K. G., Martin, E. E., et al. (2020). Paleogeographic controls on the evolution of Late Cretaceous ocean circulation. *Climate of the Past, 16*(3), 973-1006. https://doi.org/10.5194/cp-16-973-2020

Lear, C. H., Elderfield, H., & Wilson, P. A. (2000). Cenozoic deep-sea temperatures and global ice volumes from Mg/Ca in benthic foraminiferal calcite. *science, 287*(5451), 269-272. https://doi.org/10.1126/science.287.5451.269

Leckie, R. M., Bralower, T. J., & Cashman, R. (2002). Oceanic anoxic events and plankton evolution: Biotic response to tectonic forcing during the mid-Cretaceous. *Paleoceanography and Paleoclimatology, 17*(3), 13-11-13-29. https://doi.org/10.1029/2001PA000623

Lee, C.-T. A., Shen, B., Slotnick, B. S., Liao, K., Dickens, G. R., Yokoyama, Y., et al. (2013). Continental arc–island arc fluctuations, growth of crustal carbonates, and long-term climate change. *Geosphere, 9*(1), 21-36. https://doi.org/10.1130/GES00822.1

Liu, S., Hernández-Molina, F. J., Rodrigues, S., & Van Rooij, D. (2023). Deep-water circulation in the northeast Atlantic during the mid-and Late Cretaceous. *Geology, 51*(6), 515-520. https://doi.org/10.1130/G50886.1

Lyle, M. (2003). Neogene carbonate burial in the Pacific Ocean. *Paleoceanography and Paleoclimatology, 18*(3), 1-19. https://doi.org/10.1029/2002PA000777

Lyle, M., & Baldauf, J. (2015). Biogenic sediment regimes in the Neogene equatorial Pacific, IODP Site U1338: Burial, production, and diatom community. *Palaeogeography, Palaeoclimatology, Palaeoecology, 433*, 106-128. https://doi.org/10.1016/j.palaeo.2015.04.001

Lyle, M., Dadey, K. A., & Farrell, J. W. (1995). 42. The Late Miocene (11–8 Ma) Eastern Pacific Carbonate Crash: evidence for reorganization of deep-water Circulation by the closure of the Panama Gateway. In N. G. Pisas, L. A. Mayer, T. R. Janecek, Palmer-Julson, & T. H. van Andel (Eds.), *Proceedings of the Ocean Drilling Program, Scientific Results* (Vol. 138, pp. 821-838). College Station, TX: Ocean Drilling Program. https://doi.org/10.2973/odp.proc.sr.138.157.1995

Lyle, M., Drury, A. J., Tian, J., Wilkens, R., & Westerhold, T. (2019). Late Miocene to Holocene high-resolution eastern equatorial Pacific carbonate records: stratigraphy linked by dissolution and paleoproductivity. *Climate of the Past, 15*(5), 1715-1739. https://doi.org/10.5194/cp-15-1715-2019

Mackenzie, F. T., & Morse, J. W. (1992). Sedimentary carbonates through Phanerozoic time. *Geochimica et Cosmochimica Acta, 56*(8), 3281-3295. https://doi.org/10.1016/0016-7037(92)90305-3

Mansour, A., & Wagreich, M. (2022). Earth system changes during the cooling greenhouse phase of the Late Cretaceous: Coniacian-Santonian OAE3 subevents and fundamental variations in organic carbon deposition. *Earth-Science Reviews, 229*, 104022. https://doi.org/10.1016/j.earscirev.2022.104022

Michel, J., Borgomano, J., & Reijmer, J. J. G. (2018). Heterozoan carbonates: When, where and why? A synthesis on parameters controlling carbonate production and occurrences. *Earth-Science Reviews, 182*, 50-67. https://doi.org/10.1016/j.earscirev.2018.05.003

Miller, K. G., Browning, J. V., Schmelz, W. J., Kopp, R. E., Mountain, G. S., & Wright, J. D. (2020). Cenozoic sea-level and cryospheric evolution from deep-sea geochemical and continental margin records. *Science Advances, 6*(20), eaaz1346. https://doi.org/10.1126/sciadv.aaz1346

Miller, K. G., Kominz, M. A., Browning, J. V., Wright, J. D., Mountain, G. S., Katz, M. E., et al. (2005). The Phanerozoic record of global sea-level change. *Science, 310*(5752), 1293-1298. https://doi.org/10.1126/science.1116412

Miller, K. G., Schmelz, W. J., Browning, J. V., Rosenthal, Y., Hess, A. V., Kopp, R. E., & Wright, J. D. (2024). Global mean and relative sea-level changes over the past 66 Myr: implications for early Eocene ice sheets. *Earth Science, Systems and Society, 4*(1), 10091. https://doi.org/10.3389/esss.2023.10091

Moiroud, M., Pucéat, E., Donnadieu, Y., Bayon, G., Guiraud, M., Voigt, S., et al. (2016). Evolution of neodymium isotopic signature of seawater during the Late Cretaceous: Implications for intermediate and deep circulation. *Gondwana Research, 36*, 503-522. https://doi.org/10.1016/j.gr.2015.08.005

Mora, G. (2002). 11. Variations in the Accumulation of Marine Organic Matter and Carbonates at Leg 186 Sites. In K. Suyehiro, I. S. Sacks, G. D. Acton, & M. Oda (Eds.), *Proceedings of the Ocean Drilling Program, Scientific Results* (Vol. 186, pp. 1-17): Ocean Drilling Program. https://doi.org/10.2973/odp.proc.sr.186.116.2003

Müller, R. D., Cannon, J., Williams, S., & Dutkiewicz, A. (2018). PyBacktrack 1.0: A tool for reconstructing paleobathymetry on oceanic and continental crust. *Geochemistry, Geophysics, Geosystems, 19*(6), 1898-1909. https://doi.org/10.1029/2017GC007313

Müller, R. D., Mather, B., Dutkiewicz, A., Keller, T., Merdith, A., Gonzalez, C. M., et al. (2022). Evolution of Earth's tectonic carbon conveyor belt. *Nature, 605*(7911), 629-639. https://doi.org/10.1038/s41586-022-04420-x

Núñez-Useche, F., Barragán, R., Torres-Martínez, M. A., López-Zúñiga, P. A., Moreno-Bedmar, J. A., Chávez-Cabello, G., et al. (2020). Response of the western proto-North Atlantic margin to the early Aptian oceanic anoxic event (OAE) 1a: an example from the Cupido platform margin-Gulf of Mexico, NE Mexico. *Cretaceous Research, 113*, 104488. https://doi.org/10.1016/j.cretres.2020.104488

Opdyke, B. N., & Wilkinson, B. H. (1988). Surface area control of shallow cratonic to deep marine carbonate accumulation. *Paleoceanography and Paleoclimatology, 3*(6), 685-703. https://doi.org/10.1029/PA003i006p00685

Pälike, H., Lyle, M. W., Nishi, H., Raffi, I., Ridgwell, A., Gamage, K., et al. (2012). A Cenozoic record of the equatorial Pacific carbonate compensation depth. *Nature, 488*, 609-614. https://doi.org/10.1038/nature11360

Paris, G., Donnadieu, Y., Beaumont, V., Fluteau, F., & Goddéris, Y. (2016). Geochemical consequences of intense pulse-like degassing during the onset of the Central Atlantic Magmatic Province. *Palaeogeography, Palaeoclimatology, Palaeoecology, 441*, 74-82. https://doi.org/10.1016/j.palaeo.2015.04.011

Peterson, L., & Backman, J. (1990). Late Cenozoic Carbonate Accumulation and the History of the Carbonate Compensation Depth in the Western Equatorial Indian Ocean. In R. A. Duncan, J. Backman, & L. Peterson (Eds.), *Proceedings of the Ocean Drilling Program, Scientific Results* (Vol. 115, pp. 467-507). College Station, TX: Ocean Drilling Program. https://doi.org/10.2973/odp.proc.sr.115.163.1990

Petrizzo, M. R., Amaglio, G., Watkins, D. K., MacLeod, K. G., Huber, B. T., Hasegawa, T., & Wolfgring, E. (2022). Biotic and paleoceanographic changes across the Late Cretaceous Oceanic Anoxic Event 2 in the southern high latitudes (IODP sites U1513 and U1516, SE Indian Ocean). *Paleoceanography and Paleoclimatology, 37*(9), e2022PA004474. https://doi.org/10.1029/2022PA004474

Pillot, Q., Donnadieu, Y., Sarr, A. C., Ladant, J. B., & Suchéras-Marx, B. (2022). Evolution of ocean circulation in the North Atlantic Ocean during the Miocene: Impact of the Greenland ice sheet and the eastern Tethys seaway. *Paleoceanography and Paleoclimatology, 37*(8), e2022PA004415. https://doi.org/10.1029/2022PA004415

Pillot, Q., Suchéras-Marx, B., Sarr, A. C., Bolton, C., & Donnadieu, Y. (2023). A global reassessment of the spatial and temporal expression of the Late Miocene Biogenic Bloom. *Paleoceanography and Paleoclimatology, 38*(3), e2022PA004564. https://doi.org/10.1029/2022PA004564

Podder, R. S. I. S., Gupta, A. K., Clemens, S., Sanyal, P., & Panigrahi, M. K. (2024). Changes in the Indian Ocean surface hydrography driven by the seaway closure and monsoonal circulation since the late Oligocene. *Global and Planetary Change, 232*, 104335. https://doi.org/10.1016/j.gloplacha.2023.104335

Pohl, A., Donnadieu, Y., Godderis, Y., Lanteaume, C., Hairabian, A., Frau, C., et al. (2020). Carbonate platform production during the Cretaceous. *GSA Bulletin, 132*(11-12), 2606-2610. https://doi.org/10.1130/B35680.1

Poulsen, C. J., Barron, E. J., Arthur, M. A., & Peterson, W. H. (2001). Response of the mid-Cretaceous global oceanic circulation to tectonic and CO_2 forcings. *Paleoceanography and Paleoclimatology, 16*(6), 576-592. https://doi.org/10.1029/2000PA000579

Rea, D. K., Basov, I. A., & Krissek, L. A. (1995). Scientific results of drilling the North Pacific transect. In D. K. Rea, I. A. Basov, D. W. Scholl, & J. F. Allan (Eds.), *Proceedings of the Ocean Drilling Program, Scientific Results* (Vol. 145, pp. 577-596). College Station, TX: Ocean Drilling Program. https://doi.org/10.2973/odp.proc.sr.145.1995

Renaudie, J., & Lazarus, D. B. (2025). Cenozoic pelagic accumulation rates and biased sampling of the deep-sea record. *Biogeosciences, 22*(8), 1929-1946. https://doi.org/10.5194/bg-22-1929-2025

Ridgwell, A., & Zeebe, R. E. (2005). The role of the global carbonate cycle in the regulation and evolution of the Earth system. *Earth and Planetary Science Letters, 234*(3-4), 299-315. https://doi.org/10.1016/j.epsl.2005.03.006

Robinson, S. A., Murphy, D. P., Vance, D., & Thomas, D. J. (2010). Formation of "southern component water" in the Late Cretaceous: evidence from Nd-isotopes. *Geology, 38*(10), 871-874. https://doi.org/10.1130/G31165.1

Roth, P. H. (1989). Ocean circulation and calcareous nannoplankton evolution during the Jurassic and Cretaceous. *Palaeogeography, Palaeoclimatology, Palaeoecology, 74*(1-2), 111-126. https://doi.org/10.1016/0031-0182(89)90022-9

Roth, P. H., & Krumbach, K. R. (1986). Middle Cretaceous calcareous nannofossil biogeography and preservation in the Atlantic and Indian Oceans: implications for paleoceanography. *Marine Micropaleontology, 10*(1-3), 235-266. https://doi.org/10.1016/0377-8398(86)90031-9

Salles, T., Husson, L., Trung Nguyen, T., Vila-Concejo, A., Leonard, J., Da Silva, A. P., et al. (2025). Carbonate burial regimes, the Meso-Cenozoic climate, and nannoplankton expansion. *Proceedings of the National Academy of Sciences, 122*(49), e2516468122. https://doi.org/10.1073/pnas.2516468122

Sarr, A.-C., Donnadieu, Y., Bolton, C. T., Ladant, J.-B., Licht, A., Fluteau, F., et al. (2022). Neogene South Asian monsoon rainfall and wind histories diverged due to topographic effects. *Nature Geoscience, 15*(4), 314-319. https://doi.org/10.1038/s41561-022-00919-0

Schmittner, A., Sarnthein, N., Kinkel, H., Bartoli, G., Bickert, T., Crucifix, M., et al. (2004). Global impact of the Panamanian seaway closure. *Eos, Trans. AGU, 85*(49), 526-526. https://doi.org/10.1029/2004EO490010

Schneider, B., & Schmittner, A. (2006). Simulating the impact of the Panamanian seaway closure on ocean circulation, marine productivity and nutrient cycling. *Earth and Planetary Science Letters, 246*(3-4), 367-380. https://doi.org/10.1016/j.epsl.2006.04.028

Sclater, J. G., Meinke, L., Bennett, A., & Murphy, C. (1985). The depth of the ocean through the Neogene. In J. P. Kennett (Ed.), *The Miocene Ocean: Paleoceanography and Biogeography* (Vol. 163, pp. 1-20): Geological Society of America Memoirs. https://doi.org/10.1130/MEM163-p1

Scotese, C. R., Vérard, C., Burgener, L., Elling, R. P., & Kocsis, A. T. (2025). The Cretaceous world: plate tectonics, palaeogeography and palaeoclimate. *Geological Society, London, Special Publications, 544*(1), 31-202. https://doi.org/10.1144/SP544-2024-28

Smart, C. W., Thomas, E., & Ramsay, A. T. S. (2007). Middle–late Miocene benthic foraminifera in a western equatorial Indian Ocean depth transect: Paleoceanographic implications. *Palaeogeography, Palaeoclimatology, Palaeoecology, 247*(3-4), 402-420. https://doi.org/10.1016/j.palaeo.2006.11.003

Sosdian, S. M., & Lear, C. H. (2020). Initiation of the Western Pacific Warm Pool at the Middle Miocene Climate Transition? *Paleoceanography and Paleoclimatology, 35*(12), e2020PA003920. https://doi.org/10.1029/2020PA003920

Stein, C. A., & Stein, S. (1992). A model for the global variation in oceanic depth and heat flow with lithospheric age. *Nature, 359*(6391), 123-129. https://doi.org/10.1038/359123a0

Steuber, T., Löser, H., Mutterlose, J., & Parente, M. (2023). Biogeodynamics of Cretaceous marine carbonate production. *Earth-Science Reviews, 238*, 104341. https://doi.org/10.1016/j.earscirev.2023.104341

Straume, E. O., Gaina, C., Medvedev, S., & Nisancioglu, K. H. (2020). Global Cenozoic paleobathymetry with a focus on the Northern Hemisphere oceanic gateways. *Gondwana Research, 86*, 126-143. https://doi.org/10.1016/j.gr.2020.05.011

Suchéras-Marx, B., Mattioli, E., Allemand, P., Giraud, F., Pittet, B., Plancq, J., & Escarguel, G. (2019). The colonization of the oceans by calcifying pelagic algae. *Biogeosciences, 16*(12), 2501-2510. https://doi.org/10.5194/bg-16-2501-2019

Sutherland, R., Dos Santos, Z., Agnini, C., Alegret, L., Lam, A., Westerhold, T., et al. (2022). Neogene mass accumulation rate of carbonate sediment across northern Zealandia, Tasman Sea, southwest Pacific. *Paleoceanography and Paleoclimatology, 37*(2), e2021PA004294. https://doi.org/10.1029/2021PA004294

Taylor, V. E., Westerhold, T., Bohaty, S. M., Backman, J., Dunkley Jones, T., Edgar, K. M., et al. (2023). Transient shoaling, over-deepening and settling of the calcite compensation depth at the Eocene-Oligocene transition. *Paleoceanography and Paleoclimatology, 38*(6), e2022PA004493. https://doi.org/10.1029/2022PA004493

Tcherepanov, E. N., Droxler, A. W., Lapointe, P., & Mohn, K. (2008). Carbonate seismic stratigraphy of the Gulf of Papua mixed depositional system: Neogene stratigraphic signature and eustatic control. *Basin Research, 20*(2), 185-209. https://doi.org/10.1111/j.1365-2117.2008.00364.x

van Andel, T. H. (1975). Mesozoic/Cenozoic calcite compensation depth and the global distribution of calcareous sediments. *Earth and Planetary Science Letters, 26*(2), 187-194. https://doi.org/10.1016/0012-821X(75)90086-2

van der Ploeg, R., Boudreau, B. P., Middelburg, J. J., & Sluijs, A. (2019). Cenozoic carbonate burial along continental margins. *Geology, 47*(11), 1025-1028. https://doi.org/10.1130/G46418.1

Wade, B. S., O'Neill, J. F., Phujareanchaiwon, C., Ali, I., Lyle, M., & Witkowski, J. (2020). Evolution of deep-sea sediments across the Paleocene-Eocene and Eocene-Oligocene boundaries. *Earth-Science Reviews, 211*, 103403. https://doi.org/10.1016/j.earscirev.2020.103403

Wallmann, K. (2001). Controls on the Cretaceous and Cenozoic evolution of seawater composition, atmospheric CO_2 and climate. *Geochimica et Cosmochimica Acta, 65*(18), 3005-3025. https://doi.org/10.1016/S0016-7037(01)00638-X

Wang, C., Hu, X., Huang, Y., Wagreich, M., Scott, R., & Hay, W. (2011). Cretaceous oceanic red beds as possible consequence of oceanic anoxic events. *Sedimentary geology, 235*(1-2), 27-37. https://doi.org/10.1016/j.sedgeo.2010.06.025

Watkins, D. K., Cooper, M. J., & Wilson, P. A. (2005). Calcareous nannoplankton response to late Albian oceanic anoxic event 1d in the western North Atlantic. *Paleoceanography and Paleoclimatology, 20*(2). https://doi.org/10.1029/2004PA001097

Westerhold, T., Marwan, N., Drury, A. J., Liebrand, D., Agnini, C., Anagnostou, E., et al. (2020). An astronomically dated record of Earth's climate and its predictability over the last 66 million years. *Science, 369*(6509), 1383-1387. https://doi.org/10.1126/science.aba6853

Wilkinson, B. H., & Walker, J. C. (1989). Phanerozoic cycling of sedimentary carbonate. *American Journal of Science, 289*(4), 525-548.

Xiao, K., Hu, X., Jiang, J., & Wang, J. (2024). Unraveling the Cenozoic carbon cycle by reconstructing carbonate compensation depth (CCD). *Science China Earth Sciences, 67*(6), 1743-1758. https://doi.org/10.1007/s11430-023-1291-5

Zachos, J., Pagani, M., Sloan, L., Thomas, E., & Billups, K. (2001). Trends, rhythms, and aberrations in global climate 65 Ma to present. *Science, 292*(5517), 686-693. https://doi.org/10.1126/science.1059412

Zachos, J. C., Dickens, G. R., & Zeebe, R. E. (2008). An early Cenozoic perspective on greenhouse warming and carbon-cycle dynamics. *Nature, 451*(7176), 279-283. https://doi.org/10.1038/nature06588

Zahirovic, S., Eleish, A., Doss, S., Pall, J., Cannon, J., Pistone, M., et al. (2022). Subduction and carbonate platform interactions. *Geoscience Data Journal, 9*(2), 371-383. https://doi.org/10.1002/gdj3.146

Zeebe, R. E., & Westbroek, P. (2003). A simple model for the $CaCO_3$ saturation state of the ocean: The "Strangelove," the "Neritan," and the "Cretan" Ocean. *Geochemistry, Geophysics, Geosystems, 4*(12). https://doi.org/10.1029/2003GC000538

Zhang, Z., Nisancioglu, K. H., Flatøy, F., Bentsen, M., Bethke, I., & Wang, H. (2011). Tropical seaways played a more important role than high latitude seaways in Cenozoic cooling. *Climate of the Past, 7*(3), 801-813. https://doi.org/10.5194/cp-7-801-2011, 2011

5 | Discussion

In this thesis, I present the regional variability of the CCD across the Pacific and Indian oceans since the Oligocene. I also examine the spatiotemporal distribution of deep-sea carbonate (CAR) across three major ocean basins, the Atlantic, Pacific and Indian oceans, to investigate the long-term evolution of pelagic carbonate flux since the Late Cretaceous. These records provide new constraints on how the locus and intensity of deep-sea carbonate burial have shifted between basins. They further reveal that such reorganisations arise from the interplay of palaeoceanographic processes, including changes in deep-water circulation, ocean chemistry and saturation state, productivity regimes, and gateway configuration. The combined influence of these factors imposes persistent spatial heterogeneity on carbonate burial efficiency. Quantifying how shifts in the CCD translate into changes in carbonate accumulation is therefore essential for constraining long-term carbon fluxes, ocean alkalinity budgets, and feedback within the global carbon cycle.

This chapter synthesises the three thesis articles to develop an integrated interpretation of the evolution of the deep-sea carbonate system from the Cretaceous to the present, with particular focus on Neogene CCD variability and its coupling with CAR across the Pacific, Indian, and Atlantic oceans. By coupling CCD reconstructions with CAR synthesis, this thesis provides a mechanistic framework for interpreting carbonate-system reorganisations and for evaluating changes in burial magnitude against the physical and chemical drivers that shift saturation state. I organise the discussion around three key frameworks that integrate the results of the three thesis chapters. The first two sections explore global and basin-scale patterns in carbonate burial and CCD variability from the Cretaceous into the Cenozoic, emphasising the greenhouse–icehouse transition and its impact on the deep-sea carbonate system and inter-basin heterogeneity. The third section synthesises these results to examine Neogene carbonate-system reorganisation and CCD shifts, explicitly addressing regional asymmetry in timing and magnitude across ocean basins.

5.1. Global and basin-wide carbonate burial variability over the Cretaceous

Deep-sea carbonate burial has been the dominant long-term sink for marine carbon and alkalinity since the Late Cretaceous, with its magnitude and distribution closely coupled to variations in the CCD. Global synthesis estimates a CCD of ~3–3.5 km during the middle to Late Cretaceous, deepening towards the Cenozoic CCD (Dutkiewicz et al., 2019), which tracks the progressive enhancement of deep carbonate burial through deep time (e.g., Boss & Wilkinson, 1991; Boudreau & Luo, 2017; Ridgwell & Zeebe, 2005). The relatively shallow CCD (<~4 km), characteristic of much of the Cretaceous, has been attributed to carbonate burial dominated by extensive neritic and epicratonic platforms (Boss & Wilkinson, 1991; van Andel, 1975), with episodic shoaling during transient acidification events such as Oceanic Anoxic Event 2 (OAE2: ~94.5 Ma) driven by large CO_2 inputs that reduced deep-sea carbonate saturation and suppressed pelagic carbonate accumulation (Jones et al., 2023). Since ~80 Ma, the progressive increase in seafloor area above the CCD (Dutkiewicz et al., 2019) and the contraction of flooded shelf areas shifted carbonate burial from shelves to deep basins, thereby

preconditioning a long-term trend towards a deeper CCD (Bogumil et al., 2024; Opdyke & Wilkinson, 1988).

However, a major insight from the CAR synthesis in this thesis is that, even within the broad Cretaceous greenhouse regime, pelagic carbonate burial was neither spatially nor temporally uniform. Rather than a single coherent global trajectory, the Cretaceous record is characterised by strong inter-basin contrasts and high temporal variability, implying that regional modulation by ocean circulation and basin geometry exerted a first-order control on deep-sea carbonate preservation. This is important because it reframes the Cretaceous carbonate system not as a relatively steady baseline punctuated by OAEs, but as a dynamically partitioned system in which the capacity for carbonate preservation differed markedly among basins and changed as tectonic gateways evolved.

Model–proxy syntheses indicate that since the mid-Cretaceous, as Equatorial Atlantic Gateway (EAG) deepened and improved communication with high-latitude source regions, basins became more effectively ventilated by dense southern deep waters, favouring improved deep-sea carbonate preservation and a deeper regional CCD relative to earlier, more restricted, sluggish-circulation stages (Dummann et al., 2023; Steinig et al., 2024). In this context, the key contribution of Article 3 is to show that the timing and magnitude of increased pelagic burial were not globally synchronous but were mediated by basin-specific circulation trajectories. In particular, the Atlantic Ocean's comparatively higher mid–Late Cretaceous median CAR can be interpreted as reflecting improved ventilation and higher carbonate saturation relative to the Pacific with lower CAR, where older deep waters enriched in respired CO_2 maintained lower carbonate ion concentrations, more corrosive conditions, and suppressed carbonate preservation. This spatial structure is consistent with the modern ocean, where the Pacific's deep waters typically have lower carbonate ion concentrations than the Atlantic due to ageing along the overturning pathway (Archer, 1996; Ladant et al., 2020; Roth, 1989). The results from Article 3 highlight that analogous gradients were established, at least intermittently, during the Cretaceous as ocean circulation and basin geometry evolved.

Article 3 further indicates strongly fluctuating global CARs, with persistently low values (commonly <1000 mg cm^{-2} kyr^{-1}) between ~120 and 80 Ma, despite superimposed episodic perturbations. Importantly, this first basin-resolved synthesis of deep-sea carbonate accumulation across the Atlantic, Pacific, and Indian oceans reveals pronounced spatial and temporal heterogeneity during the mid–Late Cretaceous, as well as a fundamental contrast between Cretaceous and Cenozoic carbonate-system behaviour. The Atlantic Ocean exhibits comparatively higher CARs throughout much of the mid–Late Cretaceous, between ~800–2000 mg cm^{-2} kyr^{-1}, shaped by the reorganisation of Atlantic deep-water circulation as southern-sourced water masses replaced Tethyan-sourced deep waters (Dummann et al., 2023; Liu et al., 2023), with abrupt reductions in carbonate burial during major perturbations, most notably during OAE2. For example, median Atlantic CAR values decrease to ~800 mg cm^{-2} kyr^{-1} during the ~95–90 Ma interval, consistent with widespread carbonate dissolution and reduced preservation during OAE2 (Jenkyns, 2018; Jenkyns et al., 2017; Leckie et al., 2002). These transient declines indicate that carbonate burial in the Atlantic, despite relatively favourable preservation conditions, was highly sensitive to episodes of ocean acidification driven by volcanic CO_2 input (Steuber et al., 2023) and reduced carbonate saturation.

The Pacific Ocean maintains consistently low CARs throughout much of the Cretaceous, commonly remaining below ~500 mg cm^{-2} kyr^{-1} and declining to <200 mg cm^{-2} kyr^{-1} near the Cretaceous–Paleogene boundary. These low values reflect the long-standing corrosiveness of Pacific deep waters, driven by limited ventilation from southern-sourced deep waters and the dominance of older, low-saturation water masses (Ladant et al., 2020; Roth, 1989). This finding

supports the interpretation that older deep waters in the Pacific accumulate respired CO_2 along circulation pathways, reducing carbonate ion concentration and saturation state, and thereby promoting dissolution despite elevated surface carbonate production (Bradtmiller et al., 2010; Umling & Thunell, 2018; Yu et al., 2013). However, episodes of elevated CAR, such as ~1000 mg cm^{-2} kyr^{-1} between ~85 and 75 Ma, correlate with global pelagic carbonate recovery stages following the OAEs (Wang et al., 2011). The Pacific shows the greatest CAR decline over the Late Cretaceous, with the lowest values during the latest Cretaceous-early Paleocene, compared with the coeval higher steady-state CAR of the Atlantic. The thesis results suggest that by the Late Cretaceous, the Pacific was already predisposed to lower carbonate preservation efficiency than the Atlantic, implying that basin geometry and ocean circulation, and not just climate, determined the partitioning of carbonate burial.

The Indian Ocean shows intermediate median CAR values, ranging from <500 to 2000 mg cm^{-2} kyr^{-1}, generally lower than those in the Atlantic but higher than those in the Pacific. This reflects the Indian Ocean's partial deep-water connectivity with the Atlantic and its shared intermediate- and deep-water masses with the South Atlantic, but with regional suppression of carbonate preservation likely linked to south Indian volcanic and hydrothermal influences. In the Indian Ocean, using a dataset from the southern sector of the basin in this study (Article 2), the imprint of magmatism and hydrothermal activity associated with the Kerguelen Plateau (Coffin et al., 2002; Duncan, 2002) likely altered ocean pH, alkalinity, and dissolved carbon content, thereby generating spatially heterogeneous carbonate chemistry. These processes may have locally reduced carbonate preservation, even during intervals when improved ventilation, linked to evolving connectivity with the Atlantic, could otherwise have enhanced carbonate flux. However, the Indian Ocean records a Late Cretaceous decline in CAR values synchronous with that of the Pacific, likely reflecting exchange of intermediate and deep waters between the two basins during this interval (Ladant et al., 2020).

These highly variable Cretaceous CAR records reveal that, even under sustained greenhouse conditions with elevated atmospheric CO_2, carbonate burial followed distinct basin-specific pathways, indicating strong regional modulation by circulation dynamics and transient perturbations such as OAEs. This matters for carbon-cycle interpretation because it implies that the ocean's buffering capacity is unevenly distributed, with certain basins acting as stronger sinks during some intervals and weaker sinks during others, and that the global carbonate sink may be stabilised through compensation between basins rather than by a uniform response.

5.2. Cenozoic carbonate burial transition: Paleogene CCD and basin-specific CAR variabilities

One of the principal findings from the CAR records of this thesis is that the highly variable Cretaceous carbonate system transitioned into a Cenozoic regime characterised by greater overall stability yet pronounced inter-basin differentiation among the Atlantic, Pacific, and Indian oceans (Article 3). This transition is often framed as a long-term deepening of the CCD over the Cenozoic, attributed to changes in alkalinity distribution, carbonate burial partitioning between shelves and the deep ocean, and evolving bathymetry, which together raised deep-ocean carbonate saturation and promoted greater pelagic $CaCO_3$ accumulation (e.g., Bogumil et al., 2024; Boudreau et al., 2019; Derry, 2022; Komar & Zeebe, 2021; Salles et al., 2025). Yet, the basin-resolved reconstruction in this thesis shows that this long-term framing is incomplete when evaluated against rate-based burial evidence and spatially resolved CCD behaviour. Rather than a monotonic increase in pelagic carbonate burial and progressive deepening of the CCD, the results reveal persistently variable accumulation patterns and regionally distinct CCD evolution.

Early Cenozoic reconstructions indicate that the CCD remained relatively shallow (~3.0–3.5 km) and highly variable (Pälike et al., 2012; van Andel, 1975). Short-lived perturbations during this interval, such as the Paleocene–Eocene Thermal Maximum (~56 Ma), are known from high-resolution records to have produced rapid CCD shoaling followed by recovery through enhanced dissolution and weathering feedbacks (Zachos et al., 2005). Although such transient events occur at timescales shorter than those resolved in this study, they demonstrate the inherent sensitivity of the carbonate system to carbon-cycle disturbances. At the same time, global syntheses for the latest Paleocene–earliest Eocene suggest that, despite substantial warming, the area-weighted global CCD may have changed little in some reconstructions because regional CCD changes were offset by circulation and respiration (remineralization of sinking organic carbon) effects; models requiring >1 km CCD deepening to balance outgassing and weathering are supported only regionally (Greene et al., 2019; Komar et al., 2013; Slotnick et al., 2015). This underscores that global CCD estimates can mask compensating regional responses, and that global CCD stability may reflect spatial compensation rather than true uniformity.

During the Paleogene, the Atlantic is characterised by persistently higher median carbonate accumulation rates, generally between ~1200 and 2000 mg cm^{-2} kyr^{-1}, reflecting sustained carbonate preservation under progressively improved deep-water ventilation. This pattern correlates with the documented regional deep CCD below ~4 km across the North and South Atlantic Ocean from the latest Cretaceous to the middle Eocene (Dutkiewicz & Müller, 2022; Norris et al., 2012). The Indian Ocean shows slightly lower but still elevated accumulation, ranging from ~1000 to ~1800 mg cm^{-2} kyr^{-1}, whereas the Pacific remains strongly suppressed, with carbonate burial remaining limited until the late Eocene (<~800 mg cm^{-2} kyr^{-1}). The Indian Ocean's response is consistent with its intermediate carbonate saturation regime, which lies between the more corrosive deep waters of the Pacific and the comparatively higher saturation state of the Atlantic (Bostock et al., 2013; Sabine et al., 2002; Zeebe & Westbroek, 2003). In particular, across the Cretaceous–Paleogene (K-Pg) boundary, the end-Cretaceous mass extinction caused an abrupt collapse in pelagic carbonate production (Henehan et al., 2016; Henehan et al., 2019). The resulting reduction in pelagic carbonate export led, over the subsequent ~1 Ma, to enhanced deep-sea carbonate preservation and deepening of the CCD as ocean alkalinity and the global carbon cycle re-equilibrated (Henehan et al., 2019). Despite the substantial difference in temporal resolution between the short-lived K–Pg perturbation (~1 Myr) and the 5-Myr binning applied in this study, the coarse resolution precludes direct attribution of inter-basin carbonate burial variability to the extinction-driven collapse and recovery of pelagic carbonate production. The 5-Myr bins instead capture an integrated basin-scale signal over a broader late Maastrichtian–early Paleocene interval, within which the transient suppression and subsequent re-equilibration of the carbonate system are temporally averaged. My CAR results reveal a marked reduction in carbonate burial across the Pacific (at ~<200 mg cm^{-2} kyr^{-1}) and Indian oceans (at ~1000 mg cm^{-2} kyr^{-1}) between ~70–65 Ma, whereas the Atlantic shows no comparable response (at ~1500 mg cm^{-2} kyr^{-1}). Consistent with this pattern, CCD reconstructions from both the North and South Atlantic indicate a persistently deep CCD (~4.5–5 km) in the earliest Palaeocene (Dutkiewicz & Müller, 2022). Nevertheless, the global signal shows a relatively smooth transition, with median CAR values clustering near those of the Atlantic. This pattern suggests that comparatively steady Atlantic carbonate burial exerts a disproportionate influence on the integrated global signal during certain intervals, whereas the Pacific appears more sensitive to perturbations, thereby intensifying dissolution and reducing carbonate burial under stressed conditions.

Many studies place the major Cenozoic shift from a shallow (~3–4 km) to deep (~4.5 km) CCD at or around the Eocene–Oligocene transition (~34 Ma), broadly linked to Antarctic glaciation

and a reorganised carbon cycle (e.g., Pälike et al., 2012; Taylor et al., 2023; van Andel, 1975). However, my results show that the late Eocene–early Oligocene interval elicited strongly basin-asymmetric responses (Article 3), rather than a uniform global deepening of the CCD. In the Atlantic, the initial significant Cenozoic CAR peak (from ~1700 to ~2300 mg cm^{-2} kyr^{-1}) occurred in the late Eocene (~40–35 Ma), likely reflecting intensified NCW formation, driven by subarctic tectonic reorganisation that enhanced deep-water ventilation prior to Antarctic glaciation (Straume et al., 2020; Westerhold et al., 2020). This peak correlates with an increase in carbonate carbon flux in the Atlantic at ~38 Ma (Dutkiewicz & Müller, 2022). In contrast, the Pacific underwent the most pronounced intensification of carbonate burial in the early Oligocene, from ~<200 to ~1200 mg cm^{-2} kyr^{-1}, coincident with a shift from non-calcareous to carbonate-rich lithofacies (Wade et al., 2020).

In this framework, the Pacific emerges as a primary locus of Cenozoic deep-sea carbonate reorganisation during the greenhouse-to-icehouse transition, analogous to the reorganisation inferred across the EOT. High-resolution reconstructions by Wade et al. (2020) show a major early Oligocene expansion of carbonate deposition across the equatorial Pacific, overlapping with the most densely sampled region of my dataset. Their lithofacies synthesis documents a transition from clay- and silica-dominated sediments to widespread carbonate accumulation across the EOT in the Pacific Ocean, while the Atlantic and Indian oceans maintained comparatively continuous carbonate-rich regimes. This pattern is supported by deep-sea sedimentation-rate reconstructions of Renaudie and Lazarus (2025) and by my CAR estimates, which indicate persistently higher Paleogene CARs in the Atlantic (~1500–2000 mg cm^{-2} kyr^{-1}) and Indian (~500–1800 mg cm^{-2} kyr^{-1}) oceans, and strongly suppressed carbonate burial in the Pacific until the latest Eocene. The early Oligocene intensification of carbonate burial correlates with substantial CCD deepening in the equatorial Pacific, reflecting enhanced carbonate preservation driven by improved deep-water ventilation and cooling associated with Antarctic glaciation (Article 1, Pälike et al., 2012; van Andel, 1975). By contrast, comparatively smaller changes in the Atlantic and Indian oceans across the same interval are consistent with smaller CCD shifts (Dutkiewicz & Müller, 2022; Peterson & Backman, 1990; Sclater et al., 1977).

The observed asymmetry in carbonate burial rates across the Pacific, Atlantic, and Indian oceans during the late Eocene-early Oligocene period highlights pronounced inter-basin differences in carbonate system response to Antarctic glaciation. Rather than producing a uniform adjustment, Antarctic glaciation altered the spatial distribution of deep-sea carbonate preservation, with the strongest effects in basins that had previously been more dissolution-prone. These patterns suggest that the large-scale reorganisation of the carbonate system during the EOT was mediated by basin-specific ocean chemistry and circulation, yielding divergent carbonate burial outcomes under shared climatic forcing. These results reinforce the thesis's broader argument that the carbonate system's response to global climate transitions varies according to existing oceanographic and basin-scale boundary conditions. Basins starting in a dissolution-prone state (low saturation state) show high sensitivity to ventilation and cooling, whereas those starting in a preservation-favourable state show muted sensitivity (Crowley, 1983; Ridgwell & Zeebe, 2005). This basin-resolved perspective also reframes debates about the critical role of shallow–deep carbonate burial fractionation and alkalinity-driven reorganisation over the Cenozoic. (e.g., Armstrong McKay et al., 2016; Cartapanis et al., 2018; Salles et al., 2025; van der Ploeg et al., 2019). While enhanced alkalinity supply and changing shelf accommodation likely contribute to long-term trends (Salles et al., 2025), the spatial pattern of burial change across the EOT suggests that circulation-mediated redistribution of carbonate saturation gradients is essential to explaining where burial intensified. Therefore,

models that treat the CCD as a near-global equilibrium response to weathering may miss the core mechanism by which the CCD and carbonate burial evolve differently across basins.

5.3. Neogene carbonate system and CCD shifts

Results from the first multi-regional CCD reconstructions since the late Oligocene reveal pronounced regional variability, with ~1–1.2 km CCD fluctuations across six Pacific regions (western North Pacific, eastern North Pacific, western tropical Pacific, eastern equatorial Pacific, western South Pacific, and eastern South Pacific, Article 1) and ~1–1.5 km CCD variations across three sectors of the Indian Ocean (western equatorial, southeast Indian, and Southern Ocean sectors, Article 2). I find that CCD shifts in both the Pacific and Indian oceans are closely linked to climate perturbations, Antarctic ice-sheet growth, and reorganisations of ocean circulation associated with the opening and closure of major gateways, including the Tethyan, Indonesian, and Panama gateways, and evolving Indo-Pacific water exchange. Both basins exhibit pronounced longitudinal–latitudinal variability throughout the Neogene, with the deepest CCDs consistently developed in equatorial regions, ranging between ~3.7–4.7 km in the eastern equatorial Pacific and ~3.6–4.4 km in the western equatorial Indian Ocean.

A major implication of these reconstructions is that the Neogene CCD cannot be treated as a single curve within a single basin. In the Pacific, pronounced east–west differences across the equator show that carbonate preservation responds to zonal structure in thermocline depth, productivity patterns, and the chemistry of intermediate and deep waters, not only to the long-recognised north–south gradient. This conclusion is particularly important because much of the existing CCD framework for the Neogene Pacific is derived from eastern equatorial records (e.g., Campbell et al., 2018; Komar & Zeebe, 2021; Pälike et al., 2012; Rea & Lyle, 2005), while the western tropical Pacific has been underrepresented despite its central role in Indo-Pacific heat and water exchange (Nathan & Leckie, 2009). By providing the first CCD reconstruction for the western tropical Pacific, Article 1 demonstrates that equatorial carbonate preservation has a fundamentally zonal component, likely implying the dynamic interplay among Indonesian Throughflow history, WPWP evolution, and water-mass sourcing.

At the basin scale, the early Miocene is characterised by a synchronous decline in median CAR (~25–20 Ma age bin) in the Pacific and Indian oceans, accompanied by a pronounced suppression of deep-water (>3500 m) carbonate burial across all three basins (Article 3). This decline coincides with equatorial CCD shoaling in the Pacific (~200 m, Article 1) and the Indian oceans (~300 m, Article 2), indicating reduced preservation driven by early Neogene warming and elevated atmospheric CO_2 (Lear et al., 2000; Miller et al., 2020; van Andel, 1975). Neogene syntheses of Pacific $CaCO_3$ mass-accumulation rates highlight strong regional variability and a globally expressed decline in pelagic carbonate burial during the early Miocene, likely tied to rising sea level (Lyle, 2003). Unlike the Pacific, where early Miocene variability is often discussed primarily in terms of equatorial productivity and the global climate state, the Indian Ocean carbonate accumulation is interpreted in terms of the fate of the Tethyan Seaway, the initiation and evolution of monsoon-driven terrigenous input, and the development of oxygenated water masses (Beasley et al., 2021; Boersma, 1990; Peterson et al., 1992; Torfstein & Steinberg, 2020; Woodruff & Savin, 1989). In contrast, Atlantic median CAR values remain broadly stable across this interval, despite evidence of reduced deep-water burial, indicating compensatory increases in shallow and intermediate burial. Regional CCD reconstructions from the Atlantic show that shoaling was confined to the basin's northern sector, where a relatively deep CCD (~4.7 km) shoaled to ~4.3 km (Dutkiewicz & Müller, 2022). This thesis further extends this interpretation by showing that the reduction in carbonate burial is evident in deep-water settings across all basins in the depth-binned CAR synthesis,

which captures interbasin variability and emphasises that the primary imprint of this interval is a reduction in deep-water preservation. Nevertheless, global carbonate records indicate an overall decline of carbonate burial accumulation during the early Miocene, underscoring the importance of cross-basin interactions in regulating the global carbonate budget and the global manifestation of the early Miocene carbonate decline in the deep ocean.

However, superimposed on this broadly coherent early Miocene weakening of the deep carbonate sink, the new regional CCD reconstructions reveal strongly asymmetric behaviour that helps explain why global Neogene trends can be misleading. Across the equatorial Pacific, the first CCD reconstruction in this study, from the western tropical region, reveals pronounced east–west asymmetry, with a distinct CCD deepening from ~3.2 km at ~23.5 Ma to ~4.1 km at ~20.5 Ma in the west, not observed in the eastern Pacific. This is interpreted as a delayed response (after ~24 Ma) to West Antarctic Ice Sheet expansion at ~26 Ma (Billups & Schrag, 2002; Klages et al., 2024). The deepening of the western tropical Pacific CCD after ~24 Ma is consistent with the idea that improvements in deep-water ventilation and cooling propagated into the Pacific in a spatially structured way, potentially via strengthened southern-sourced deep-water influence along the western South Pacific margin and into the western equatorial domain (e.g., Foppert et al., 2021; Silvano et al., 2023; Sloyan et al., 2013; Yi, 2023). Importantly, this deepening occurs during the broader early Miocene interval when depth-stratified CAR synthesis indicates reduced deep-water burial at the basin scale. Similarly, Dutkiewicz and Müller (2022) document CCD deepening in the South Atlantic, from ~3.4 km to ~3.8 km over the same interval, contrasting with the shoaling observed in the North Atlantic. The coexistence of regionally varied CCD patterns in the Pacific and Atlantic, coupled with an overall reduction in deep carbonate burial, suggests that preservation changes were not uniform. Certain regions may have experienced improved deep-water saturation due to changes in ocean circulation or water-mass sourcing, while the basin-integrated deep sink weakened due to global warming, sea-level rise, and broader dissolution.

Furthermore, the interpretation of the west-east asymmetry in the equatorial Pacific in terms of carbonate accumulation and CCD variability naturally highlights the roles of upper-ocean structure and thermocline dynamics. The western tropical Pacific lies within the WPWP influence and is sensitive to shifts in thermocline depth and nutrient supply that regulate carbonate export (Nathan & Leckie, 2009; Shi et al., 2022). Episodes of enhanced nutrient concentrations favouring coccolith productivity in this region have been linked to cooling and shoaling of the thermocline associated with WPWP dynamics (Imai et al., 2015; Liang & Liu, 2018; Shi et al., 2022; Yuwono & Sato, 2020). This correlates with a shallow thermocline across the western tropical Pacific driven by a relatively open Indonesian Seaway and Indo-Pacific water exchange (Von Der Heydt & Dijkstra, 2011).

During the late early Miocene, the co-occurrence of equatorial CCD shoaling in both the Pacific and Indian oceans (Articles 1 & 2) at ~19–18 Ma is notable because it overlaps with earlier CCD reconstructions (Campbell et al., 2018; Lyle, 2003; van Andel, 1975) and Lyle's (2003) concept of a "carbonate famine" in the equatorial Pacific within this interval, attributed to reduced productivity and increased dissolution, potentially linked to wide Indonesian Seaway connectivity. In this context, the thesis suggests that Indo-Pacific exchange may have had a basin-wide effect. Vigorous intermediate-water throughflow and evolving thermocline structure during the early–middle Miocene likely influenced nutrient delivery and surface productivity in both the equatorial Pacific and Indian oceans, contributing to reduced carbonate export and elevated regional dissolution, thereby paralleling mechanisms for the later middle–late Miocene carbonate crash interval (e.g., Lübbers et al., 2019; Lyu et al., 2023; Preiss-Daimler et al., 2021). This inference remains interpretative, but it highlights the value of pairing Pacific and Indian CCD reconstructions, as similar timing of CCD shifts across basins can point

to a shared driver (e.g., Indo-Pacific exchange, global atmospheric CO_2), while differences in amplitude or sign can reveal how local circulation and productivity regimes modulated the response.

Since the middle Miocene, the integrated CCD and CAR records capture a transitional interval in which changes in climate state, ocean circulation, and biological productivity interacted within a complex framework. Regional CCD shoaling during the Miocene Climatic Optimum (MCO: 17–14 Ma; Westerhold et al., 2020) in both the Pacific and Indian oceans reflects enhanced carbonate dissolution under warmer deep-water conditions, whereas subsequent CCD deepening coincides with global cooling and the expansion of the Antarctic ice sheets (Articles 1 & 2). Previous studies indicate that the MCO in the equatorial Pacific was characterised by elevated deep-ocean temperatures and intensified carbonate dissolution, followed by progressive CCD deepening after ~16 Ma, as atmospheric CO_2 declined, and global cooling and Antarctic ice-sheet advanced (Holbourn et al., 2024; Holbourn et al., 2014; Hönisch et al., 2023). Expanding on this framework, this thesis identifies a spatially coherent phase of CCD deepening across the late MCO interval in the western North Pacific and the equatorial Pacific. A comparable deepening signal is also resolved in my CCD model for the western equatorial Indian Ocean. These observations align with previously published reconstructions from the eastern equatorial Pacific (Campbell et al., 2018; Lyle, 2003; Pälike et al., 2012), the western equatorial Indian Ocean (Campbell et al., 2018), and the central North Atlantic (Dutkiewicz & Müller, 2022). Crucially, the results presented here show that this CCD reorganisation extended beyond equatorial regions, indicating a more extensive, basin-wide restructuring of the carbonate system during the MCO.

In the Pacific and Indian oceans, my CCD models reveal pronounced post-MCO regional variability, including longitudinal asymmetry across the equator and heightened sensitivity to thermocline dynamics and silica–carbonate competition. A particularly valuable cross-basin link emerges around ~12–11.5 Ma. In the Indian Ocean, the western equatorial CCD reaches ~4.2 km at ~11.5 Ma, while in the equatorial Pacific, Article 1 documents a peak in CCD deepening around ~12 Ma in the eastern equatorial Pacific and ~12.5 Ma in the western tropical Pacific, followed by stepwise shoaling after ~11.5 Ma. Article 2 proposes that the western equatorial Indian CCD behaviour may reflect a broader equatorial response spanning the Pacific and Indian oceans, potentially linked to stabilisation of the WPWP position around ~11.6 Ma (Nathan & Leckie, 2009) and to the progressive restriction of the Indonesian Seaway and associated changes in Indo-Pacific water-mass exchange (Sosdian & Lear, 2020; Zhang et al., 2024b). Although the specific mechanism may differ between basins, with WPWP stabilisation in the Pacific versus diminishing warm-pool influence and monsoon-driven productivity in the Indian (Gupta et al., 2015; Sarr et al., 2022), the near-synchronous timing suggests that the equatorial Indo-Pacific carbonate system underwent a coordinated reorganisation in the mid–late Miocene. This interpretation is important because it provides a mechanistic bridge between the Pacific and Indian CCD curves. Rather than treating them as independent regional records, I propose that their coupled behaviour reflects the shared evolution of equatorial circulation, thermocline structure, and water-mass chemistry.

The integrated CAR and CCD analyses presented here further reveal basin-scale carbonate dynamics during this interval. CCD reconstructions indicate a pronounced deepening in the eastern equatorial Pacific, reaching ~4.8 km at ~12 Ma, the deepest equatorial Pacific CCD of the Cenozoic, consistent with estimates by Pälike et al. (2012). This deepening likely reflects enhanced Antarctic glaciation and strengthened deep-water ventilation (e.g., Holbourn et al., 2024; Sutherland et al., 2022), coupled with post-middle Miocene Climate Transition (MMCT) cooling, reduced volcanic CO_2 input from the Columbia River Basalt (Sosdian & Lear, 2020), and intensified alkalinity removal through deep-sea carbonate burial (van der Ploeg et al.,

2019). Despite this, Pacific basin-wide CAR values between ~15 and 10 Ma remain comparatively lower than those of the Indian Ocean, highlighting the dominant influence of WPWP development on carbonate budgets during this interval, beyond the effects of global climatic and tectonic drivers.

In the Indian Ocean, the post-MCO CCD evolution, characterised by progressive deepening in the western equatorial sector, closely aligns with the basin-scale CAR synthesis, which documents a sustained increase in carbonate accumulation after ~15 Ma, peaking between ~10 and 5 Ma (Articles 2 & 3). This interval encompasses the late Miocene–early Pliocene biogenic bloom (e.g., Bolton et al., 2022; Lyle & Baldauf, 2015; Pillot et al., 2023), recorded as CCD deepening in both western equatorial and eastern South Indian Ocean reconstructions, and reflects the combined influence of Indonesian Seaway constriction, strengthening Antarctic glaciation, monsoon intensification, evolution of the WPWP, and enhanced surface productivity linked to thermocline shoaling and expansion of oxygen zones (Betzler et al., 2016; Bolton et al., 2022; Dickens & Owen, 1999; Filippelli, 1997; Gupta et al., 2015; Holbourn et al., 2018; Martinot et al., 2022; Nathan & Leckie, 2009; Sarr et al., 2022). Across the Pacific, the late Miocene biogenic bloom shows pronounced regional heterogeneity, with a ~1 Myr offset between the western and eastern equatorial sectors and a complete absence in the western North Pacific (Article 1). The equatorial CCD variability across the Pacific and Indian oceans during this interval is similarly best interpreted in terms of regional circulation patterns and zonal asymmetry associated with WPWP dynamics and Indo-Pacific exchange (Articles 1 & 2).

The western North Pacific record highlights another major mechanism shaping Neogene CCD variability, reflecting silica–carbonate competition and the development of a northward silica gradient. The western North Pacific CCD has remained comparatively shallow since the mid-Miocene (typically ~2.8–4 km), owing to enhanced siliceous productivity and burial that exceeded carbonate accumulation, generating a persistent northward silica gradient across the Pacific (e.g., Cortese et al., 2004; Ragueneau et al., 2000; Woodruff & Savin, 1989; Zhang et al., 2022a). Here, my findings link this regime to gateway forcing, whereby Panama's restriction reduced Atlantic–Pacific exchange, strengthened the NADW, and influenced Antarctic Bottom Water (AABW) pathways, indirectly increasing silica delivery and preservation patterns in the North Pacific (Cortese et al., 2004; Rea et al., 1995). The observed CCD shoaling peaks at ~6.5 Ma and ~3 Ma, corresponding to known silica accumulation peaks in the region (Rea et al., 1995).

The late Miocene biogenic bloom interval further illustrates this non-linear behaviour, illustrating how CCD responses to changes in productivity diverge among basins. In the eastern equatorial Pacific, the carbonate crash (~10.5–9 Ma) represents the shallowest Neogene CCD. Subsequently, during the late Miocene (~7–6.5 Ma), a renewed phase of CCD shoaling occurred (Article 1), coinciding with elevated opal accumulation and declining $CaCO_3$ wt% at key sites, indicating intensified silica deposition and reduced carbonate preservation (Lyle & Baldauf, 2015; Lyle et al., 2019). The thesis interprets this shoaling as indicating enhanced silica productivity and reduced carbonate preservation, despite elevated overall productivity. This interpretation helps reconcile the apparent paradox that the biogenic bloom is often associated with increased biogenic production yet can coincide with reduced carbonate burial in some regions. These observations show that increased productivity does not necessarily lead to greater carbonate burial or deeper CCDs. Instead, the balance between carbonate and organic carbon fluxes, mediated by CCD position (Lyle et al., 1995), determines whether productivity enhances or suppresses long-term carbonate burial.

The Indian Ocean CCD record provides complementary evidence of the biogenic bloom and strengthens the thesis' cross-basin synthesis. In the western equatorial Indian Ocean, a major CCD deepening of ~400 m between ~9 and 7 Ma, peaking near ~7.5–7 Ma, coincides with the identified Indian biogenic bloom and the establishment of modern deep-water circulation patterns (e.g., Dickens & Owen, 1999; Prabhat et al., 2022; Woodruff & Savin, 1989; Wright et al., 1991). This deepening aligns with evidence of enhanced productivity and carbonate accumulation in the western Indian Ocean, and with broader circulation reorganisation potentially linked to Central American Seaway constriction, increasing NADW/NCW influence, and the strengthening of the East Asian monsoon (Bolton et al., 2022; Filippelli, 1997; Peterson et al., 1992; Prabhat et al., 2022). Yet, the Indian record also shows a subsequent modest shoaling (~200 m) between ~7 and 5 Ma, interpreted as reflecting intensified dissolution driven by elevated organic carbon flux during the late Miocene–early Pliocene productivity peak.

When these CCD reconstructions are integrated with the basin-resolved CAR synthesis, a clearer picture emerges. Article 3 shows that from the middle Miocene through the early Pliocene (~15–5 Ma), all three basins experienced enhanced carbonate accumulation, underscoring the global significance of the biogenic bloom interval. However, the amplitude and expression vary. The Atlantic and Indian oceans show the strongest CAR increase, whereas the Pacific response is comparatively muted and, in some intervals, even lower than in the preceding 15–10 Ma window. This pattern aligns with the CCD evidence. In the Atlantic and Indian oceans, late Miocene CCD deepening indicates enhanced preservation and higher burial efficiency (Article 2, Campbell et al., 2018; Dutkiewicz & Müller, 2022). Whereas, in the Pacific, regional CCD shoaling in equatorial sectors indicates dissolution impact and silica competition, which can suppress preserved carbonate burial even under high productivity (Article 1). This nonlinear behaviour likely represents a key feature of the late Cenozoic carbonate system and highlights the importance of integrating CCD dynamics with CAR patterns.

The latest Cenozoic evolution of carbonate systems is characterised by a basin-wide decline in CAR across all three oceans from the Pliocene to the present, with the Pacific experiencing a higher drop. This widespread decrease in carbonate accumulation rates since the Pliocene is accompanied by an overall trend of CCD shoaling across large parts of the Pacific (Article 1), Indian (Article 2) and Atlantic (Dutkiewicz & Müller, 2022) oceans. This pattern likely reflects the combined effects of ocean gateway reorganisation, changes in deep-ocean overturning linked to the Atlantic meridional overturning and Antarctic ice-sheet expansion, intensification of Northern Hemisphere glaciation, and a late Neogene reorganisation of nutrient and productivity regimes that shifted export production and burial patterns between siliceous and calcareous biota (e.g., Derry, 2022; Kerr et al., 2017; Komar & Zeebe, 2021; Preiss-Daimler et al., 2021; Qin et al., 2022; Si & Rosenthal, 2019). In this context, the thesis adds two important insights. First, the decline in carbonate accumulation is not simply a uniform suppression of carbonate production as it is accompanied by increased expression of glacial–interglacial variability and by persistent basin divergence (e.g., Atlantic remaining more carbonate-rich than the Pacific). Second, the CCD reconstructions show that late Neogene to Quaternary CCD behaviour retains large regional swings of several hundred metres to more than 1 km superimposed on the longer-term shoaling trend, consistent with glacial–interglacial shoaling–deepening cycles associated with orbital-scale changes in deep-water formation, regional ocean circulation, and the productivity/dissolution balance (e.g., Karlin et al., 1992; Lee et al., 2000; Xu et al., 2022). In the western tropical Pacific, for example, CCD deepening from ~3.8 km at ~3 Ma to ~4.5 km at ~0.5 Ma is consistent with intensified cooling, thermocline shoaling, and enhanced mixing in the region during the late Pliocene to Quaternary. This illustrates that even

as the global system shifts towards lower average burial, some regions can experience deepening due to local circulation and productivity structure.

5.4. Significance and future research

The findings presented in this thesis represent a significant contribution to the field, advancing our mechanistic understanding of the processes and feedbacks that regulate pelagic carbonate burial and the long-term evolution of the deep-sea carbonate system. My results demonstrate that regional CCD behaviour and basin-scale carbonate burial are closely coupled yet highly non-uniform across space and time, with important implications for the deep carbon cycle. In contrast to the alkalinity-driven regime framework proposed by Salles et al. (2025), which attributes Cenozoic carbonate system evolution primarily to excess alkalinity overwhelming shallow-platform accommodation and promoting progressive redistribution towards pelagic burial, our basin-resolved reconstruction reveals a more complex and spatially heterogeneous trajectory. Rather than a monotonic intensification of deep-sea carbonate accumulation, the pelagic CAR record demonstrates compensating inter-basin behaviour and temporal asymmetry, particularly during the major transition intervals. Moreover, comparisons with nannoplankton evolutionary trajectories (Suchéras-Marx et al., 2019) reveal repeated decoupling between biological innovation and carbonate burial intensity. These findings indicate that although alkalinity supply and pelagic calcifier evolution exert fundamental, first-order controls on the spatial distribution of the marine carbonate, the trajectory of long-term carbonate sequestration is strongly modulated by basin-specific ocean circulation patterns, spatial gradients in carbonate productivity and saturation state, and depth-dependent preservation thresholds.

The basin-resolved framework developed in this thesis opens several avenues for future research. First, extending regional CCD reconstructions into undersampled sectors of the global oceans will be essential for refining inter-basin contrasts and testing the robustness of the compensatory burial patterns identified here. Improved age-depth models for drill sites, together with higher-temporal-resolution carbonate system proxies (e.g., boron isotopes, foraminiferal $\delta^{11}B$, or carbonate ion reconstructions) and expanded depth transects of sediment cores spanning above and below the CCD, would provide tighter constraints on carbonate preservation thresholds and the position of the lysocline and CCD. Second, integrating basin-scale CAR reconstructions with fully coupled Earth system and carbon cycle models would enable a quantitative evaluation of how regional preservation regimes propagate into global alkalinity budgets and atmospheric CO_2 feedback. Finally, linking carbonate burial dynamics more explicitly to evolving deep-water formation patterns, silicate weathering fluxes, and calcareous nanoplankton patterns will help resolve the relative contributions of circulation, chemistry, and biological evolution to long-term carbonate sequestration. Together, these directions will advance a mechanistic, spatially explicit understanding of the deep-time evolution of the carbon cycle.

6 | Conclusions

In this thesis, based on three articles, I presented new regional reconstructions of the carbonate compensation depth (CCD) in the Pacific and Indian oceans, along with the first global carbonate burial maps over time. These results provide new quantitative constraints on the evolution of the CCD and deep-sea carbonate flux through time. I employed a consistent methodological framework that integrates large-scale drill-site compilations (from DSDP/OPD/IODP expeditions), backtracked paleo–water depth reconstructions that explicitly account for sediment compaction, tectonic subsidence, dynamic topography, and eustatic sea-level change, and regression-based CCD computation from CAR–depth relationships. This integrated strategy enables direct comparison of CCD evolution and carbonate burial across basins and through time, overcoming limitations of earlier studies based on sparse depth transects or basin-averaged assumptions.

My results demonstrate that shifts in the CCD exert a first-order control on both the magnitude and spatial distribution of pelagic carbonate burial, while the relationship between CCD variability and carbonate accumulation is regionally modulated by deep-water circulation, productivity regimes, and tectonic gateway evolution. During the Cretaceous, pelagic carbonate burial was highly unstable and spatially heterogeneous across all three ocean basins, reflecting a greenhouse-world ocean characterised by episodic perturbations, variable ventilation, and strong sensitivity to transient events such as OAEs. Basin-resolved CAR records show that elevated atmospheric CO_2 did not generate uniform carbonate burial responses across ocean basins. The Atlantic experienced comparatively higher burial rates but showed strong variation in response to shifts in circulation and saturation state. In contrast, the Pacific remained persistently undersaturated and corrosive, resulting in suppressed carbonate accumulation, while the Indian Ocean exhibited intermediate behaviour consistent with its partial connectivity to southern-sourced deep waters. These patterns indicate that effective deep-water ventilation and enhanced carbonate preservation emerged asynchronously among basins, and that global carbonate burial cannot be inferred from single-basin or globally averaged records.

Across the Cenozoic, the marine carbonate system shifted towards greater overall stability yet remained strongly differentiated between basins. Although long-term deepening of the CCD is evident, this thesis challenges the prevailing assumption of a progressive increase in pelagic carbonate burial through time. Instead, basin-specific trajectories dominate, with the Pacific exhibiting the strongest response to the Eocene–Oligocene transition and early Neogene climate change, the Atlantic showing episodic maxima linked to the development of NCW and intensified NADW formation, and the Indian Ocean recording a pronounced Neogene intensification tied to Indo-Pacific exchange, monsoon strengthening, and gateway reorganisation. The first multi-regional CCD reconstructions reveal large-amplitude Neogene variability of ~1–1.2 km across the Pacific and ~1–1.5 km across the Indian Ocean, with consistently deeper CCDs in equatorial regions and pronounced longitudinal–latitudinal asymmetry. These results demonstrate that CCD evolution is not spatially coherent even within individual basins.

My results further document the late Miocene biogenic bloom and the complex interplay among productivity, dissolution, burial, and CCD dynamics. Despite enhanced carbonate production across all basins, burial responses diverged markedly, with CCD deepening and

elevated CARs in the Atlantic and Indian oceans, whereas burial remained muted or declined in parts of the Pacific, where increased siliceous productivity and intensified dissolution offset carbonate export. The subsequent Pliocene–Recent decline in CAR across all basins was accompanied by widespread shoaling of the CCD through large portions of the Pacific, Indian, and Atlantic oceans. These results indicate that long-term carbonate burial arises from basin-scale responses that compensate and contrast, rather than from a uniform global trend. The central outcome of this thesis is that the global carbonate burial signal emerges from spatially differentiated responses to climate forcing, mediated by basin-scale oceanographic structure and evolving carbonate system dynamics. This integrated framework highlights the importance of considering the spatial distribution of carbonate burial among ocean basins in regulating long-term carbon sequestration in the ocean and the global carbon cycle, and provides a revised perspective on how tectonic and climatic boundary conditions control the deep-sea carbonate system through time.

References

Archer, D. (1996). An atlas of the distribution of calcium carbonate in sediments of the deep sea. *Global Biogeochemical Cycles, 10*(1), 159-174. https://doi.org/10.1029/95GB03016

Armstrong McKay, D. I., Tyrrell, T., & Wilson, P. A. (2016). Global carbon cycle perturbation across the Eocene-Oligocene climate transition. *Paleoceanography and Paleoclimatology, 31*(2), 311-329. https://doi.org/10.1002/2015PA002818

Beasley, C., Kender, S., Giosan, L., Bolton, C. T., Anand, P., Leng, M. J., et al. (2021). Evidence of a South Asian proto-monsoon during the Oligocene-Miocene transition. *Paleoceanography and Paleoclimatology, 36*(9), e2021PA004278. https://doi.org/10.1029/2021PA004278

Berger, W. H. (1973). Cenozoic sedimentation in the eastern tropical Pacific. *Geological Society of America Bulletin, 84*(6), 1941-1954. https://doi.org/10.1130/0016-7606(1973)84<1941:CSITET>2.0.CO;2

Berner, R. A. (2004). *The Phanerozoic carbon cycle: CO_2 and O_2*. New York: Oxford University Press https://doi.org/10.1093/oso/9780195173338.001.0001

Berner, R. A., Lasaga, A. C., & Garrels, R. M. (1983). Carbonate-silicate geochemical cycle and its effect on atmospheric carbon dioxide over the past 100 million years. *Am. J. Sci.;(United States), 283*(7). https://doi.org/10.2475/ajs.283.7.641

Betzler, C., Eberli, G. P., Kroon, D., Wright, J. D., Swart, P. K., Nath, B. N., et al. (2016). The abrupt onset of the modern South Asian Monsoon winds. *Scientific reports, 6*(1), 29838. https://doi.org/10.1038/srep29838

Billups, K., & Schrag, D. P. (2002). Paleotemperatures and ice volume of the past 27 Myr revisited with paired Mg/Ca and $^{18}O/^{16}O$ measurements on benthic foraminifera. *Paleoceanography, 17*(1), 3-1-3-11. https://doi.org/10.1029/2000PA000567

Boersma, A. (1990). Late Oligocene to late Pliocene benthic foraminifers from depth traverses in the central Indian Ocean. In R. Duncan, J. Backman, & L. C. Peterson (Eds.), *Proceedings of the Ocean Drilling Program, Scientific Results* (Vol. 115, pp. 315-379). College Station, TX: Ocean Drilling Program. https://doi.org/10.2973/odp.proc.sr.115.146.1990

Bogumil, M., Mittal, T., & Lithgow-Bertelloni, C. (2024). The effects of bathymetry on the long-term carbon cycle and CCD. *Proceedings of the National Academy of Sciences, 121*(21), e2400232121. https://doi.org/10.1073/pnas.2400232121

Bolton, C. T., Gray, E., Kuhnt, W., Holbourn, A. E., Lübbers, J., Grant, K., et al. (2022). Secular and orbital-scale variability of equatorial Indian Ocean summer monsoon winds during the late Miocene. *Climate of the Past, 18*(4), 713-738. https://doi.org/10.5194/cp-18-713-2022

Boss, S. K., & Wilkinson, B. H. (1991). Planktogenic/eustatic control on cratonic/oceanic carbonate accumulation. *The Journal of Geology, 99*(4), 497-513.

Bostock, H. C., Hayward, B. W., Neil, H. L., Currie, K. I., & Dunbar, G. B. (2011). Deep-water carbonate concentrations in the southwest Pacific. *Deep Sea Research Part I: Oceanographic Research Papers, 58*(1), 72-85. https://doi.org/10.1016/j.dsr.2010.11.010

Bostock, H. C., Mikaloff Fletcher, S. E., & Williams, M. J. M. (2013). Estimating carbonate parameters from hydrographic data for the intermediate and deep waters of the Southern Hemisphere oceans. *Biogeosciences, 10*(10), 6199-6213. https://doi.org/10.5194/bg-10-6199-2013, 2013

Boudreau, B. P., & Luo, Y. (2017). Retrodiction of secular variations in deep-sea $CaCO_3$ burial during the Cenozoic. *Earth and Planetary Science Letters, 474*, 1-12.

Boudreau, B. P., Middelburg, J. J., Sluijs, A., & van der Ploeg, R. (2019). Secular variations in the carbonate chemistry of the oceans over the Cenozoic. *Earth and Planetary Science Letters, 512*, 194-206. https://doi.org/10.1016/j.epsl.2019.02.004

Bradtmiller, L. I., Anderson, R. F., Sachs, J. P., & Fleisher, M. Q. (2010). A deeper respired carbon pool in the glacial equatorial Pacific Ocean. *Earth and Planetary Science Letters, 299*(3-4), 417-425. https://doi.org/10.1016/j.epsl.2010.09.022

Braz, C., Zahirovic, S., Salles, T., Flament, N., Harrington, L., & Müller, R. D. (2021). Modelling the role of dynamic topography and eustasy in the evolution of the Great Artesian Basin. *Basin Research, 33*(6), 3378-3405. https://doi.org/10.1111/bre.12606

Broecker, W. S. (2003). The oceanic $CaCO_3$ cycle. In H. D. Holland & K. K. Turekian (Eds.), *Treatise on Geochemistry* (pp. 529–549): Elsevier. https://doi.org/10.1016/B0-08-043751-6/06119-3

Broecker, W. S., & Peng, T.-H. (1982). *Tracers in the Sea* (Vol. 690): Lamont-Doherty Geological Observatory, Columbia University Palisades, New York. https://doi.org/10.1017/S0033822200005221

Broecker, W. S., & Peng, T. H. (1987). The role of $CaCO_3$ compensation in the glacial to interglacial atmospheric CO_2 change. *Global Biogeochemical Cycles, 1*(1), 15-29. https://doi.org/10.1029/GB001i001p00015

Campbell, S. M., Moucha, R., Derry, L. A., & Raymo, M. E. (2018). Effects of dynamic topography on the Cenozoic carbonate compensation depth. *Geochemistry, Geophysics, Geosystems, 19*(4), 1025-1034. https://doi.org/10.1002/2017GC007386

Cartapanis, O., Galbraith, E. D., Bianchi, D., & Jaccard, S. L. (2018). Carbon burial in deep-sea sediment and implications for oceanic inventories of carbon and alkalinity over the last glacial cycle. *Climate of the Past, 14*(11), 1819-1850. https://doi.org/10.5194/cp-14-1819-2018

Chavez, F. P., & Barber, R. T. (1987). An estimate of new production in the equatorial Pacific. *Deep Sea Research Part A. Oceanographic Research Papers, 34*(7), 1229-1243.

Chiarella, D., Longhitano, S. G., & Tropeano, M. (2017). Types of mixing and heterogeneities in siliciclastic-carbonate sediments. *Marine and Petroleum Geology, 88*, 617-627. https://doi.org/10.1016/j.marpetgeo.2017.09.010

Clift, P. D. (2017). A revised budget for Cenozoic sedimentary carbon subduction. *Reviews of Geophysics, 55*(1), 97-125. https://doi.org/10.1002/2016RG000531

Coffin, M. F., Pringle, M. S., Duncan, R. A., Gladczenko, T. P., Storey, M., Müller, R. D., & Gahagan, L. A. (2002). Kerguelen hotspot magma output since 130 Ma. *Journal of petrology, 43*(7), 1121-1137. https://doi.org/10.1093/petrology/43.7.1121

Cortese, G., Gersonde, R., Hillenbrand, C.-D., & Kuhn, G. (2004). Opal sedimentation shifts in the World Ocean over the last 15 Myr. *Earth and Planetary Science Letters, 224*(3-4), 509-527. https://doi.org/10.1016/j.epsl.2004.05.035

Cramer, B. S., Toggweiler, J. R., Wright, J. D., Katz, M. E., & Miller, K. G. (2009). Ocean overturning since the Late Cretaceous: Inferences from a new benthic foraminiferal isotope compilation. *Paleoceanography and Paleoclimatology, 24*(4). https://doi.org/10.1029/2008PA001683

Crowley, T. J. (1983). Calcium-carbonate preservation patterns in the central North Atlantic during the last 150,000 years. *Marine Geology, 51*(1-2), 1-14. https://doi.org/10.1016/0025-3227(83)90085-3

Dasgupta, R. (2013). Ingassing, storage, and outgassing of terrestrial carbon through geologic time. *Reviews in Mineralogy and Geochemistry, 75*(1), 183-229.

Davies, T. A., Kidd, R. B., & Ramsay, A. T. S. (1995). A time-slice approach to the history of Cenozoic sedimentation in the Indian Ocean. *Sedimentary Geology, 96*(1-2), 157-179. https://doi.org/10.1016/0037-0738(94)00131-D

Delaney, M. L., & Boyle, E. A. (1988). Tertiary paleoceanic chemical variability: Unintended consequences of simple geochemical models. *Paleoceanography & Paleoclimatology, 3*(2), 137-156. https://doi.org/10.1029/PA003i002p00137

Derry, L. A. (2022). Carbonate weathering, CO_2 redistribution, and Neogene CCD and pCO_2 evolution. *Earth and Planetary Science Letters, 597*, 117801. https://doi.org/10.1016/j.epsl.2022.117801

Dickens, G. R., & Owen, R. M. (1999). The latest Miocene–early Pliocene biogenic bloom: a revised Indian Ocean perspective. *Marine Geology, 161*(1), 75-91. https://doi.org/10.1016/S0025-3227(99)00057-2

Dummann, W., Hofmann, P., Herrle, J. O., Frank, M., & Wagner, T. (2023). The early opening of the Equatorial Atlantic gateway and the evolution of Cretaceous peak warming. *Geology, 51*(5), 476-480. https://doi.org/10.1130/G50842.1

Duncan, R. A. (2002). A time frame for construction of the Kerguelen Plateau and Broken Ridge. *Journal of Petrology, 43*(7), 1109-1119. https://doi.org/10.1093/petrology/43.7.1109

Dutkiewicz, A., & Müller, R. D. (2021). The carbonate compensation depth in the South Atlantic Ocean since the Late Cretaceous. *Geology, 49*(7), 873-878. https://doi.org/10.1130/G48404.1

Dutkiewicz, A., & Müller, R. D. (2022). The history of Cenozoic carbonate flux in the Atlantic Ocean constrained by multiple regional carbonate compensation depth reconstructions. *Geochemistry, Geophysics, Geosystems, 23*(11), e2022GC010667. https://doi.org/10.1029/2022GC010667

Dutkiewicz, A., Müller, R. D., Cannon, J., Vaughan, S., & Zahirovic, S. (2018). Sequestration and subduction of deep-sea carbonate in the global ocean since the Early Cretaceous. *Geology, 47*(1), 91-94. https://doi.org/10.1130/G45424.1

Dutkiewicz, A., Müller, R. D., Cannon, J., Vaughan, S., & Zahirovic, S. (2019). Sequestration and subduction of deep-sea carbonate in the global ocean since the Early Cretaceous. *Geology, 47*(1), 91-94. https://doi.org/10.1130/G45424.1

Dutkiewicz, A., Müller, R. D., Wang, X., O'callaghan, S., Cannon, J., & Wright, N. M. (2017). Predicting sediment thickness on vanished ocean crust since 200 Ma. *Geochemistry, Geophysics, Geosystems, 18*(12), 4586-4603. https://doi.org/10.1002/2017GC007258

Dutkiewicz, A., O'Callaghan, S., & Müller, R. (2016). Controls on the distribution of deep-sea sediments. *Geochemistry, Geophysics, Geosystems, 17*(8), 3075-3098.

Feely, R. A., Sabine, C. L., Lee, K., Berelson, W., Kleypas, J., Fabry, V. J., & Millero, F. J. (2004). Impact of anthropogenic CO_2 on the $CaCO_3$ system in the oceans. *Science, 305*(5682), 362-366. https://doi.org/10.1126/science.1097329

Filippelli, G. M. (1997). Intensification of the Asian monsoon and a chemical weathering event in the late Miocene–early Pliocene: implications for late Neogene climate change. *Geology, 25*(1), 27-30. https://doi.org/10.1130/0091-7613(1997)025%3C0027%3AIOTAMA%3E2.3.CO%3B2

Foppert, A., Rintoul, S. R., Purkey, S. G., Zilberman, N., Kobayashi, T., Sallèe, J. B., et al. (2021). Deep Argo reveals bottom water properties and pathways in the Australian-Antarctic Basin. *Journal of Geophysical Research: Oceans, 126*(12), e2021JC017935. https://doi.org/10.1029/2021JC017935Digital

Foster, G. L., Royer, D. L., & Lunt, D. J. (2017). Future climate forcing potentially without precedent in the last 420 million years. *Nature Communications, 8*(1), 14845. https://doi.org/10.1038/ncomms14845

Friedrich, O., Norris, R. D., & Erbacher, J. (2012). Evolution of middle to Late Cretaceous oceans—A 55 m.y. record of Earth's temperature and carbon cycle. *Geology, 40*(2), 107-110. https://doi.org/10.1130/G32701.1

Gerhardt, S., & Henrich, R. (2001). Shell preservation of Limacina inflata (Pteropoda) in surface sediments from the Central and South Atlantic Ocean: a new proxy to determine the aragonite saturation state of water masses. *Deep Sea Research Part I: Oceanographic Research Papers, 48*(9), 2051-2071. https://doi.org/10.1016/S0967-0637(01)00005-X

Gradstein, F. M., Ogg, J. G., Schmitz, M. D., & Ogg, G. M. (2020). *Geologic time scale 2020* (Vol. 1). Netherlands: Elsevier. https://doi.org/10.1016/C2020-1-02369-3

Gray, W. R., Rae, J. W. B., Wills, R. C. J., Shevenell, A. E., Taylor, B., Burke, A., et al. (2018). Deglacial upwelling, productivity and CO_2 outgassing in the North Pacific Ocean. *Nature Geoscience, 11*(5), 340-344. https://doi.org/10.1038/s41561-018-0108-6

Greene, S. E., Ridgwell, A., Kirtland Turner, S., Schmidt, D. N., Pälike, H., Thomas, E., et al. (2019). Early Cenozoic decoupling of climate and carbonate compensation depth trends. *Paleoceanography and paleoclimatology, 34*(6), 930-945. https://doi.org/10.1029/2019PA003601

Gupta, A. K., Yuvaraja, A., Prakasam, M., Clemens, S. C., & Velu, A. (2015). Evolution of the South Asian monsoon wind system since the late Middle Miocene. *Palaeogeography, Palaeoclimatology, Palaeoecology, 438*, 160-167. https://doi.org/10.1016/j.palaeo.2015.08.006

Hay, W. W. (1999). Carbonate sedimentation through the late Precambrian and Phanerozoic. *Zentralblatt für Geologie und Paläontologie/Teil 1, 1998*(5-6), 435-445.

Henehan, M. J., Hull, P. M., Penman, D. E., Rae, J. W., & Schmidt, D. N. (2016). Biogeochemical significance of pelagic ecosystem function: an end-Cretaceous case study. *Philosophical Transactions of the Royal Society B: Biological Sciences, 371*(1694). https://doi.org/10.1098/rstb.2015.0510

Henehan, M. J., Ridgwell, A., Thomas, E., Zhang, S., Alegret, L., Schmidt, D. N., et al. (2019). Rapid ocean acidification and protracted Earth system recovery followed the end-Cretaceous Chicxulub impact. *Proceedings of the National Academy of Sciences, 116*(45), 22500-22504. https://doi.org/10.1073/pnas.1905989116

Holbourn, A., Kuhnt, W., Kulhanek, D. K., Mountain, G., Rosenthal, Y., Sagawa, T., et al. (2024). Re-organization of Pacific overturning circulation across the Miocene Climate Optimum. *Nature Communications, 15*(8135). https://doi.org/10.1038/s41467-024-52516-x

Holbourn, A., Kuhnt, W., Lyle, M., Schneider, L., Romero, O., & Andersen, N. (2014). Middle Miocene climate cooling linked to intensification of eastern equatorial Pacific upwelling. *Geology, 42*(1), 19-22. https://doi.org/10.1130/G34890.1

Holbourn, A. E., Kuhnt, W., Clemens, S. C., Kochhann, K. G., Jöhnck, J., Lübbers, J., & Andersen, N. (2018). Late Miocene climate cooling and intensification of southeast Asian winter monsoon. *Nature Communications, 9*(1), 1584. https://doi.org/10.1038/s41467-018-03950-1

Hönisch, B., Royer, D. L., Breecker, D. O., Polissar, P. J., Bowen, G. J., Henehan, M. J., et al. (2023). Toward a Cenozoic history of atmospheric CO_2. *Science, 382*(6675), eadi5177. https://doi.org/10.1126/science.adi5177

Honjo, S. (1976). Coccoliths: production, transportation and sedimentation. *Marine Micropaleontology, 1*, 65-79. https://doi.org/10.1016/0377-8398(76)90005-0

Honjo, S., Manganini, S. J., Krishfield, R. A., & Francois, R. (2008). Particulate organic carbon fluxes to the ocean interior and factors controlling the biological pump: A synthesis of global sediment trap programs since 1983. *Progress in Oceanography, 76*(3), 217-285. https://doi.org/10.1016/j.pocean.2007.11.003

Imai, R., Farida, M., Sato, T., & Iryu, Y. (2015). Evidence for eutrophication in the northwestern Pacific and eastern Indian oceans during the Miocene to Pleistocene based on the nannofossil accumulation rate, Discoaster abundance, and coccolith size distribution of Reticulofenestra. *Marine Micropaleontology, 116*, 15-27. https://doi.org/10.1016/j.marmicro.2015.01.001

Isson, T. T., Planavsky, N. J., Coogan, L. A., Stewart, E. M., Ague, J. J., Bolton, E. W., et al. (2020). Evolution of the global carbon cycle and climate regulation on earth. *Global Biogeochemical Cycles, 34*(2), e2018GB006061. https://doi.org/10.1029/2018GB006061

Jenkyns, H. C. (2018). Transient cooling episodes during Cretaceous Oceanic Anoxic Events with special reference to OAE 1a (Early Aptian). *Philosophical Transactions of the Royal Society A: Mathematical, Physical and Engineering Sciences, 376*(2130), 20170073. https://doi.org/10.1098/rsta.2017.0073

Jenkyns, H. C., Dickson, A. J., Ruhl, M., & Van den Boorn, S. H. (2017). Basalt-seawater interaction, the Plenus Cold Event, enhanced weathering and geochemical change: deconstructing Oceanic Anoxic Event 2 (Cenomanian–Turonian, Late Cretaceous). *Sedimentology, 64*(1), 16-43. https://doi.org/10.1111/sed.12305

Jones, M. M., Sageman, B. B., Selby, D., Jacobson, A. D., Batenburg, S. J., Riquier, L., et al. (2023). Abrupt episode of mid-Cretaceous ocean acidification triggered by massive volcanism. *Nature Geoscience, 16*(2), 169-174. https://doi.org/10.1038/s41561-022-01115-w

Karlin, R., Lyle, M., & Zahn, R. (1992). Carbonate variations in the Northeast Pacific during the late Quaternary. *Paleoceanography and Paleoclimatology, 7*(1), 43-61. https://doi.org/10.1029/91PA03077

Keller, G., & Barron, J. A. (1983). Paleoceanographic implications of Miocene deep-sea hiatuses. *Geological Society of America Bulletin, 94*(5), 590-613. https://doi.org/10.1130/0016-7606(1983)94<590:PIOMDH>2.0.CO;2

Kent, D. V., & Muttoni, G. (2013). Modulation of Late Cretaceous and Cenozoic climate by variable drawdown of atmospheric pCO_2 from weathering of basaltic provinces on continents drifting through the equatorial humid belt. *Climate of the Past, 9*(2), 525-546. https://doi.org/10.5194/cp-9-525-2013

Kerr, J., Rickaby, R., Yu, J., Elderfield, H., & Sadekov, A. Y. (2017). The effect of ocean alkalinity and carbon transfer on deep-sea carbonate ion concentration during the past five glacial cycles. *Earth and Planetary Science Letters, 471*, 42-53. https://doi.org/10.1016/j.epsl.2017.04.042

Klages, J. P., Hillenbrand, C.-D., Bohaty, S. M., Salzmann, U., Bickert, T., Lohmann, G., et al. (2024). Ice sheet–free West Antarctica during peak early Oligocene glaciation. *Science, 385*, 322-327. https://doi.org/10.1126/science.adj3931

Kolla, V., Bé, A. W., & Biscaye, P. E. (1976). Calcium carbonate distribution in the surface sediments of the Indian Ocean. *Journal of Geophysical Research, 81*(15), 2605-2616. https://doi.org/10.1029/JC081i015p02605

Komar, N., Zeebe, R., & Dickens, G. R. (2013). Understanding long-term carbon cycle trends: The late Paleocene through the early Eocene. *Paleoceanography and Paleoclimatology, 28*(4), 650-662. https://doi.org/10.1002/palo.20060

Komar, N., & Zeebe, R. E. (2021). Reconciling atmospheric CO_2, weathering, and calcite compensation depth across the Cenozoic. *Science Advances, 7*(4), eabd4876. https://doi.org/10.1126/sciadv.abd4876

Kump, L. R., & Arthur, M. A. (1997). Global chemical erosion during the Cenozoic: Weatherability balances the budgets. In W. F. Ruddiman (Ed.), *Tectonic uplift and climate change* (pp. 399-426). Boston, MA: Springer. https://doi.org/10.1007/978-1-4615-5935-1_18

Ladant, J.-B., Poulsen, C. J., Fluteau, F., Tabor, C. R., MacLeod, K. G., Martin, E. E., et al. (2020). Paleogeographic controls on the evolution of Late Cretaceous ocean circulation. *Climate of the Past, 16*(3), 973-1006.

Lear, C. H., Elderfield, H., & Wilson, P. A. (2000). Cenozoic deep-sea temperatures and global ice volumes from Mg/Ca in benthic foraminiferal calcite. *science, 287*(5451), 269-272. https://doi.org/10.1126/science.287.5451.269

Leckie, R. M., Bralower, T. J., & Cashman, R. (2002). Oceanic anoxic events and plankton evolution: Biotic response to tectonic forcing during the mid-Cretaceous. *Paleoceanography and Paleoclimatology, 17*(3), 13-11-13-29. https://doi.org/10.1029/2001PA000623

Lee, G. H., Park, S. C., & Kim, D. C. (2000). Fluctuations of the calcite compensation depth (CCD) in the East Sea (Sea of Japan). *Geo-Marine Letters, 20*(1), 20-26. https://doi.org/10.1007/s003670000029

Li, L., Luo, Y., Kienast, M., Qi, D., & Tjiputra, J. (2022). On the sedimentary carbonate accumulation and dissolution in Western Pacific marginal basins. *Limnology and Oceanography, 67*(1), 26-38. https://doi.org/10.1002/lno.11972

Liang, D., & Liu, C. (2018). Coccolith assemblages and primary productivity variations in the central Western Pacific Warm Pool over the last 380 kyr. *Journal of Ocean University of China, 17*(3), 563-570. doi:https://doi.org/10.1007/s11802-018-3405-1

Litchman, E. (2007). Resource competition and the ecological success of phytoplankton. In P. G. Falkowski & A. H. Knoll (Eds.), *Evolution of Primary*

Producers in the Seas (pp. 351-375): Elsevier. https://doi.org/10.1016/B978-012370518-1/50017-5

Liu, S., Hernández-Molina, F. J., Rodrigues, S., & Van Rooij, D. (2023). Deep-water circulation in the northeast Atlantic during the mid-and Late Cretaceous. *Geology, 51*(6), 515-520. https://doi.org/10.1130/G50886.1

Lübbers, J., Kuhnt, W., Holbourn, A. E., Bolton, C. T., Gray, E., Usui, Y., et al. (2019). The middle to late Miocene "Carbonate Crash" in the Equatorial Indian Ocean. *Paleoceanography and Paleoclimatology, 34*(5), 813-832. https://doi.org/10.1029/2018PA003482

Lyle, M. (2002). Age-Depth Profiles for Pacific DSDP and ODP Drillsites. *Center for Geophysical Investigation of the Shallow Subsurface, Boise State University, Boise, Idaho*, 0-66.

Lyle, M. (2003). Neogene carbonate burial in the Pacific Ocean. *Paleoceanography and Paleoclimatology, 18*(3), 1-19. https://doi.org/10.1029/2002PA000777

Lyle, M., & Baldauf, J. (2015). Biogenic sediment regimes in the Neogene equatorial Pacific, IODP Site U1338: Burial, production, and diatom community. *Palaeogeography, Palaeoclimatology, Palaeoecology, 433*, 106-128. https://doi.org/10.1016/j.palaeo.2015.04.001

Lyle, M., Barron, J., Bralower, T. J., Huber, M., Olivarez Lyle, A., Ravelo, A. C., et al. (2008). Pacific Ocean and Cenozoic evolution of climate. *Reviews of Geophysics, 46*(2). https://doi.org/10.1029/2005RG000190

Lyle, M., Dadey, K. A., & Farrell, J. W. (1995). 42. The Late Miocene (11–8 Ma) Eastern Pacific Carbonate Crash: evidence for reorganization of deep-water Circulation by the closure of the Panama Gateway. In N. G. Pisas, L. A. Mayer, T. R. Janecek, Palmer-Julson, & T. H. van Andel (Eds.), *Proceedings of the Ocean Drilling Program, Scientific Results* (Vol. 138, pp. 821-838). College Station, TX: Ocean Drilling Program. https://doi.org/10.2973/odp.proc.sr.138.157.1995

Lyle, M., Drury, A. J., Tian, J., Wilkens, R., & Westerhold, T. (2019). Late Miocene to Holocene high-resolution eastern equatorial Pacific carbonate records: stratigraphy linked by dissolution and paleoproductivity. *Climate of the Past, 15*(5), 1715-1739. https://doi.org/10.5194/cp-15-1715-2019

Lyu, J., Auer, G., Bialik, O. M., Christensen, B., Yamaoka, R., & De Vleeschouwer, D. (2023). Astronomically-paced changes in paleoproductivity, winnowing, and mineral flux over broken ridge (Indian Ocean) since the early Miocene. *Paleoceanography and Paleoclimatology, 38*(12), e2023PA004761. https://doi.org/10.1029/2023PA004761

Ma, X., Tian, J., Ma, W., Li, K., & Yu, J. (2018). Changes of deep Pacific overturning circulation and carbonate chemistry during middle Miocene East Antarctic ice sheet expansion. *Earth and Planetary Science Letters, 484*, 253-263. https://doi.org/10.1016/j.epsl.2017.12.002

Mackenzie, F. T., & Morse, J. W. (1992). Sedimentary carbonates through Phanerozoic time. *Geochimica et Cosmochimica Acta, 56*(8), 3281-3295. https://doi.org/10.1016/0016-7037(92)90305-3

Martinot, C., Bolton, C. T., Sarr, A. C., Donnadieu, Y., Garcia, M., Gray, E., & Tachikawa, K. (2022). Drivers of late Miocene tropical sea surface cooling: A new perspective from the equatorial Indian Ocean. *Paleoceanography and Paleoclimatology, 37*(10), e2021PA004407. https://doi.org/10.1029/2021PA004407

Michel, J., Borgomano, J., & Reijmer, J. J. G. (2018). Heterozoan carbonates: When, where and why? A synthesis on parameters controlling carbonate production and occurrences. *Earth-Science Reviews, 182*, 50-67. https://doi.org/10.1016/j.earscirev.2018.05.003

Miller, K. G., Browning, J. V., Schmelz, W. J., Kopp, R. E., Mountain, G. S., & Wright, J. D. (2020). Cenozoic sea-level and cryospheric evolution from deep-sea geochemical and continental margin records. *Science Advances, 6*(20), eaaz1346. https://doi.org/10.1126/sciadv.aaz1346

Miller, K. G., Schmelz, W. J., Browning, J. V., Rosenthal, Y., Hess, A. V., Kopp, R. E., & Wright, J. D. (2024). Global mean and relative sea-level changes over the past 66 Myr: implications for early Eocene ice sheets. *Earth Science, Systems and Society, 4*(1), 10091. https://doi.org/10.3389/esss.2023.10091

Müller, R. D., Cannon, J., Williams, S., & Dutkiewicz, A. (2018). PyBacktrack 1.0: A tool for reconstructing paleobathymetry on oceanic and continental crust. *Geochemistry, Geophysics, Geosystems, 19*(6), 1898-1909. https://doi.org/10.1029/2017GC007313

Müller, R. D., Mather, B., Dutkiewicz, A., Keller, T., Merdith, A., Gonzalez, C. M., et al. (2022). Evolution of Earth's tectonic carbon conveyor belt. *Nature, 605*(7911), 629-639. https://doi.org/10.1038/s41586-022-04420-x

Nathan, S. A., & Leckie, R. M. (2009). Early history of the Western Pacific Warm Pool during the middle to late Miocene (~13.2–5.8 Ma): Role of sea-level change and implications for equatorial circulation. *Palaeogeography, Palaeoclimatology, Palaeoecology, 274*(3-4), 140-159. https://doi.org/10.1016/j.palaeo.2009.01.007

Norris, R. D., Wilson, P. A., Blum, P., Fehr, A., Agnini, C., Bornemann, A., et al. (2012). Paleogene Newfoundland sediment drifts. *Integrated Ocean Drilling Program Management International, Inc.* https://doi.org/10.2204/iodp.pr.342.2012

Omta, A. W., Ferrari, R., & McGee, D. (2018). An analytical framework for the steady state impact of carbonate compensation on atmospheric CO_2. *Global Biogeochemical Cycles, 32*(4), 720-735. https://doi.org/10.1002/2017GB005809

Opdyke, B. N., & Wilkinson, B. H. (1988). Surface area control of shallow cratonic to deep marine carbonate accumulation. *Paleoceanography and Paleoclimatology, 3*(6), 685-703. https://doi.org/10.1029/PA003i006p00685

Pälike, H., Lyle, M. W., Nishi, H., Raffi, I., Ridgwell, A., Gamage, K., et al. (2012). A Cenozoic record of the equatorial Pacific carbonate compensation depth. *Nature, 488*, 609-614. https://doi.org/10.1038/nature11360

Penman, D. E., Turner, S. K., Sexton, P. F., Norris, R. D., Dickson, A. J., Boulila, S., et al. (2016). An abyssal carbonate compensation depth overshoot in the aftermath of the Palaeocene–Eocene Thermal Maximum. *Nature Geoscience, 9*(8), 575-580. https://doi.org/10.1038/ngeo2757

Pennington, J. T., Mahoney, K. L., Kuwahara, V. S., Kolber, D. D., Calienes, R., & Chavez, F. P. (2006). Primary production in the eastern tropical Pacific: A review. *Progress in Oceanography, 69*(2-4), 285-317. https://doi.org/10.1016/j.pocean.2006.03.012

Peterson, L., & Backman, J. (1990). Late Cenozoic Carbonate Accumulation and the History of the Carbonate Compensation Depth in the Western Equatorial Indian Ocean. In R. A. Duncan, J. Backman, & L. Peterson (Eds.), *Proceedings of the Ocean Drilling Program, Scientific Results* (Vol. 115, pp. 467-507). College

Station, TX: Ocean Drilling Program. https://doi.org/10.2973/odp.proc.sr.115.163.1990

Peterson, L. C., Murray, D. W., Ehrmann, W. U., & Hempel, P. (1992). Cenozoic carbonate accumulation and compensation depth changes in the Indian Ocean. In R. A. Duncan, D. K. Rea, R. B. Kidd, U. v. Rad, & J. K. Weissel (Eds.), *In Synthesis of Results from Scientific Drilling in the Indian Ocean* (Vol. 70, pp. 311-333). Geophysical Monograph Series. https://doi.org/10.1029/GM070p0311

Phillips, H. E., Tandon, A., Furue, R., Hood, R., Ummenhofer, C. C., Benthuysen, J. A., et al. (2021). Progress in understanding of Indian Ocean circulation, variability, air–sea exchange, and impacts on biogeochemistry. *Ocean Science, 17*(6), 1677-1751. https://doi.org/10.5194/os-17-1677-2021

Pillot, Q., Suchéras-Marx, B., Sarr, A. C., Bolton, C., & Donnadieu, Y. (2023). A global reassessment of the spatial and temporal expression of the Late Miocene Biogenic Bloom. *Paleoceanography and Paleoclimatology, 38*(3), e2022PA004564. https://doi.org/10.1029/2022PA004564

Piotrowski, A. M., Banakar, V. K., Scrivner, A. E., Elderfield, H., Galy, A., & Dennis, A. (2009). Indian Ocean circulation and productivity during the last glacial cycle. *Earth and Planetary Science Letters, 285*(1-2), 179-189. https://doi.org/10.1016/j.epsl.2009.06.007

Plank, T., & Manning, C. E. (2019). Subducting carbon. *Nature, 574*(7778), 343-352. https://doi.org/10.1038/s41586-019-1643-z

Poulsen, C. J., Barron, E. J., Arthur, M. A., & Peterson, W. H. (2001). Response of the mid-Cretaceous global oceanic circulation to tectonic and CO_2 forcings. *Paleoceanography and Paleoclimatology, 16*(6), 576-592. https://doi.org/10.1029/2000PA000579

Prabhat, P., Rahaman, W., Lathika, N., Tarique, M., Mishra, R., & Thamban, M. (2022). Modern-like deep water circulation in Indian Ocean caused by Central American Seaway closure. *Nature Communications, 13*(1), 7561. https://doi.org/10.1038/s41467-022-35145-0

Preiss-Daimler, I., Zarkogiannis, S. D., Kontakiotis, G., Henrich, R., & Antonarakou, A. (2021). Paleoceanographic perturbations and the marine carbonate system during the middle to late Miocene carbonate crash—a critical review. *Geosciences, 11*(2), 94. https://doi.org/10.3390/geosciences11020094

Qin, B., Li, T., Xiong, Z., Algeo, T. J., Jia, Q., Nürnberg, D., & Shi, J. (2022). Influences of Atlantic Ocean thermohaline circulation and Antarctic ice-sheet expansion on Pliocene deep Pacific carbonate chemistry. *Earth and Planetary Science Letters, 599*, 117868. https://doi.org/10.1016/j.epsl.2022.117868

Rae, J. W. B., Zhang, Y. G., Liu, X., Foster, G. L., Stoll, H. M., & Whiteford, R. D. M. (2021). Atmospheric CO_2 over the past 66 million years from marine archives. *Annual Review of Earth and Planetary Sciences, 49*(1), 609-641. https://doi.org/10.1146/annurev-earth-082420-063026

Ragueneau, O., Tréguer, P., Leynaert, A., Anderson, R. F., Brzezinski, M. A., DeMaster, D. J., et al. (2000). A review of the Si cycle in the modern ocean: recent progress and missing gaps in the application of biogenic opal as a paleoproductivity proxy. *Global and Planetary Change, 26*(4), 317-365. https://doi.org/10.1016/S0921-8181(00)00052-7

Rea, D. K., Basov, I. A., & Krissek, L. A. (1995). Scientific results of drilling the North Pacific transect. In D. K. Rea, I. A. Basov, D. W. Scholl, & J. F. Allan (Eds.), *Proceedings of the Ocean Drilling Program, Scientific Results* (Vol. 145, pp. 577-596). College Station, TX: Ocean Drilling Program. https://doi.org/10.2973/odp.proc.sr.145.1995

Rea, D. K., & Leinen, M. (1986). Crustal Subsidence and Calcite Deposition in the South Pacific Ocean. In M. Leinen & D. K. Rea (Eds.), *Initial Reports of the Deep Sea Drilling Project* (Vol. 92, pp. 299-303). Washington, U.S: Government. Printing Office. https://doi.org/10.2973/dsdp.proc.92.112.1986

Rea, D. K., & Lyle, M. W. (2005). Paleogene calcite compensation depth in the eastern subtropical Pacific: Answers and questions. *Paleoceanography and Paleoclimatology, 20*(1), 1-9. https://doi.org/10.1029/2004PA001064

Renaudie, J., & Lazarus, D. B. (2025). Cenozoic pelagic accumulation rates and biased sampling of the deep-sea record. *Biogeosciences, 22*(8), 1929-1946. https://doi.org/10.5194/bg-22-1929-2025

Renaudie, J., Lazarus, D. B., & Diver, P. (2020). NSB (Neptune Sandbox Berlin): An expanded and improved database of marine planktonic microfossil data and deep-sea stratigraphy. *Palaeontologia Electronica, 23*(1), 1-28. https://doi.org/10.26879/1032

Ridgwell, A. (2007). Interpreting transient carbonate compensation depth changes by marine sediment core modeling. *Paleoceanography and Paleoclimatology, 22*(4). https://doi.org/10.1029/2006PA001372

Ridgwell, A., & Hargreaves, J. C. (2007). Regulation of atmospheric CO_2 by deep-sea sediments in an Earth system model. *Global Biogeochemical Cycles, 21*(2). https://doi.org/10.1029/2006GB002764

Ridgwell, A., & Zeebe, R. E. (2005). The role of the global carbonate cycle in the regulation and evolution of the Earth system. *Earth and Planetary Science Letters, 234*(3-4), 299-315. https://doi.org/10.1016/j.epsl.2005.03.006

Roth, J. M., Droxler, A. W., & Kameo, K. (2000). The Caribbean carbonate crash at the middle to late Miocene transition: Linkage to the establishment of the modern global ocean conveyor. In R. M. Leckie, H. Sigurdsson, G. D. Acton, & G. Draper (Eds.), *Proceedings of the Ocean Drilling Program, Scientific Results* (Vol. 165). College Station, TX: Ocean Drilling Program. https://doi.org/10.2973/odp.proc.sr.165.013.2000

Roth, P. H. (1989). Ocean circulation and calcareous nannoplankton evolution during the Jurassic and Cretaceous. *Palaeogeography, Palaeoclimatology, Palaeoecology, 74*(1-2), 111-126. https://doi.org/10.1016/0031-0182(89)90022-9

Sabine, C. L., Key, R. M., Feely, R. A., & Greeley, D. (2002). Inorganic carbon in the Indian Ocean: Distribution and dissolution processes. *Global Biogeochemical Cycles, 16*(4), 15-11-15-18. https://doi.org/10.1029/2002GB001869

Salles, T., Husson, L., Trung Nguyen, T., Vila-Concejo, A., Leonard, J., Da Silva, A. P., et al. (2025). Carbonate burial regimes, the Meso-Cenozoic climate, and nannoplankton expansion. *Proceedings of the National Academy of Sciences, 122*(49), e2516468122. https://doi.org/10.1073/pnas.2516468122

Sarma, V., Dileep Kumar, M., & Saino, T. (2007). Impact of sinking carbon flux on accumulation of deep-ocean carbon in the Northern Indian Ocean. *Biogeochemistry, 82*, 89-100.

Sarr, A.-C., Donnadieu, Y., Bolton, C. T., Ladant, J.-B., Licht, A., Fluteau, F., et al. (2022). Neogene South Asian monsoon rainfall and wind histories diverged due to topographic effects. *Nature Geoscience, 15*(4), 314-319. https://doi.org/10.1038/s41561-022-00919-0

Schneider, B., & Schmittner, A. (2006). Simulating the impact of the Panamanian seaway closure on ocean circulation, marine productivity and nutrient cycling. *Earth and Planetary Science Letters, 246*(3-4), 367-380. https://doi.org/10.1016/j.epsl.2006.04.028

Schott, F. A., Xie, S. P., & McCreary Jr, J. P. (2009). Indian Ocean circulation and climate variability. *Reviews of Geophysics, 47*(1). https://doi.org/10.1029/2007RG000245

Sclater, J. G., Abbott, D., & Thiede, J. (1977). Paleobathymetry and sediments of the Indian Ocean. In J. R. Heirtzler, H. M. Bolli, T. A. Davies, J. B. Saunders, & J. G. Sclater (Eds.), *Indian Ocean Geology and Biostratigraphy: Studies Following Deep-Sea Drilling Legs* (Vol. 9, pp. 25-59). Special Publications. https://doi.org/10.1029/SP009p0025

Sclater, J. G., Meinke, L., Bennett, A., & Murphy, C. (1985). The depth of the ocean through the Neogene. In J. P. Kennett (Ed.), *The Miocene Ocean: Paleoceanography and Biogeography* (Vol. 163, pp. 1-20): Geological Society of America Memoirs. https://doi.org/10.1130/MEM163-p1

Scotese, C. R., Vérard, C., Burgener, L., Elling, R. P., & Kocsis, A. T. (2025). The Cretaceous world: plate tectonics, palaeogeography and palaeoclimate. *Geological Society, London, Special Publications, 544*(1), 31-202. https://doi.org/10.1144/SP544-2024-28

Shi, J., Jia, Q., Nürnberg, D., Li, T., Xiong, Z., & Qin, B. (2022). Coupled nutricline and productivity variations during the Pliocene in the western Pacific warm pool and their paleoceanographic implications. *Global and Planetary Change, 212*, 103810. https://doi.org/10.1016/j.gloplacha.2022.103810

Si, W., & Rosenthal, Y. (2019). Reduced continental weathering and marine calcification linked to late Neogene decline in atmospheric CO_2. *12*, 833-838. https://doi.org/10.1038/s41561-019-0450-3

Silvano, A., Purkey, S., Gordon, A. L., Castagno, P., Stewart, A. L., Rintoul, S. R., et al. (2023). Observing Antarctic bottom water in the Southern Ocean. *Frontiers in Marine Science, 10*, 1221701. https://doi.org/10.3389/fmars.2023.1221701

Sleep, N. H., & Zahnle, K. (2001). Carbon dioxide cycling and implications for climate on ancient Earth. *Journal of Geophysical Research: Planets, 106*(E1), 1373-1399. https://doi.org/10.1029/2000JE001247

Slotnick, B. S., Lauretano, V., Backman, J., Dickens, G. R., Sluijs, A., & Lourens, L. (2015). Early Paleogene variations in the calcite compensation depth: new constraints using old borehole sediments from across Ninetyeast Ridge, central Indian Ocean. *Climate of the Past, 11*(3), 473-493. https://doi.org/10.5194/cp-11-473-2015

Sloyan, B. M., Wijffels, S. E., Tilbrook, B., Katsumata, K., Murata, A., & Macdonald, A. M. (2013). Deep ocean changes near the western boundary of the South Pacific Ocean. *Journal of Physical Oceanography, 43*(10), 2132-2141. https://doi.org/10.1175/JPO-D-12-0182.1

Sosdian, S. M., & Lear, C. H. (2020). Initiation of the Western Pacific Warm Pool at the Middle Miocene Climate Transition? *Paleoceanography and Paleoclimatology, 35*(12), e2020PA003920. https://doi.org/10.1029/2020PA003920

Stein, C. A., & Stein, S. (1992). A model for the global variation in oceanic depth and heat flow with lithospheric age. *Nature, 359*(6391), 123-129. https://doi.org/10.1038/359123a0

Steinig, S., Dummann, W., Hofmann, P., Frank, M., Park, W., Wagner, T., & Flögel, S. (2024). Controls on Early Cretaceous South Atlantic Ocean circulation and carbon burial–a climate model–proxy synthesis. *Climate of the Past, 20*(7), 1537-1558. https://doi.org/10.5194/cp-20-1537-2024

Steuber, T., Löser, H., Mutterlose, J., & Parente, M. (2023). Biogeodynamics of Cretaceous marine carbonate production. *Earth-Science Reviews, 238*, 104341. https://doi.org/10.1016/j.earscirev.2023.104341

Straume, E. O., Gaina, C., Medvedev, S., & Nisancioglu, K. H. (2020). Global Cenozoic paleobathymetry with a focus on the Northern Hemisphere oceanic gateways. *Gondwana Research, 86*, 126-143. https://doi.org/10.1016/j.gr.2020.05.011

Stuecker, M. F., & Zeebe, R. E. (2010). Ocean chemistry and atmospheric CO_2 sensitivity to carbon perturbations throughout the Cenozoic. *Geophysical Research Letters, 37*(3). https://doi.org/10.1029/2009GL041436

Suchéras-Marx, B., & Henderiks, J. (2014). Downsizing the pelagic carbonate factory: Impacts of calcareous nannoplankton evolution on carbonate burial over the past 17 million years. *Global and Planetary Change, 123*, 97-109. https://doi.org/10.1016/j.gloplacha.2014.10.015

Suchéras-Marx, B., Mattioli, E., Allemand, P., Giraud, F., Pittet, B., Plancq, J., & Escarguel, G. (2019). The colonization of the oceans by calcifying pelagic algae. *Biogeosciences, 16*(12), 2501-2510. https://doi.org/10.5194/bg-16-2501-2019

Sulpis, O., Boudreau, B. P., Mucci, A., Jenkins, C., Trossman, D. S., Arbic, B. K., & Key, R. M. (2018). Current $CaCO_3$ dissolution at the seafloor caused by anthropogenic CO_2. *Proceedings of the National Academy of Sciences, 115*(46), 11700-11705. https://doi.org/10.1073/pnas.1804250115

Sutherland, R., Dos Santos, Z., Agnini, C., Alegret, L., Lam, A., Westerhold, T., et al. (2022). Neogene mass accumulation rate of carbonate sediment across northern Zealandia, Tasman Sea, southwest Pacific. *Paleoceanography and Paleoclimatology, 37*(2), e2021PA004294. https://doi.org/10.1029/2021PA004294

Taylor, V. E., Westerhold, T., Bohaty, S. M., Backman, J., Dunkley Jones, T., Edgar, K. M., et al. (2023). Transient shoaling, over-deepening and settling of the calcite compensation depth at the Eocene-Oligocene transition. *Paleoceanography and Paleoclimatology, 38*(6), e2022PA004493. https://doi.org/10.1029/2022PA004493

Torfstein, A., & Steinberg, J. (2020). The Oligo–Miocene closure of the Tethys Ocean and evolution of the proto-Mediterranean Sea. *Scientific Reports, 10*(1), 13817. https://doi.org/10.1038/s41598-020-70652-4

Umling, N. E., & Thunell, R. C. (2018). Mid-depth respired carbon storage and oxygenation of the eastern equatorial Pacific over the last 25,000 years. *Quaternary Science Reviews, 189*, 43-56. https://doi.org/10.1016/j.quascirev.2018.04.002

Valsala, V., Sreeush, M., & Chakraborty, K. (2020). The IOD impacts on the Indian Ocean carbon cycle. *Journal of Geophysical Research: Oceans, 125*(11), e2020JC016485.

van Andel, T. H. (1975). Mesozoic/Cenozoic calcite compensation depth and the global distribution of calcareous sediments. *Earth and Planetary Science Letters, 26*(2), 187-194. https://doi.org/10.1016/0012-821X(75)90086-2

van der Ploeg, R., Boudreau, B. P., Middelburg, J. J., & Sluijs, A. (2019). Cenozoic carbonate burial along continental margins. *Geology, 47*(11), 1025-1028. https://doi.org/10.1130/G46418.1

Von Der Heydt, A. S., & Dijkstra, H. A. (2011). The impact of ocean gateways on ENSO variability in the Miocene. In R. Hall, M. A. Cottam, & M. E. J. Wilson (Eds.), *The SE Asian Gateway: History and Tectonics of the Australia-Asia Collision* (Vol. 355, pp. 305-318). The Geological Society of London: Geological Society, London, Special Publications. https://doi.org/10.1144/SP355.15

Wade, B. S., O'Neill, J. F., Phujareanchaiwon, C., Ali, I., Lyle, M., & Witkowski, J. (2020). Evolution of deep-sea sediments across the Paleocene-Eocene and Eocene-Oligocene boundaries. *Earth-Science Reviews, 211*, 103403. https://doi.org/10.1016/j.earscirev.2020.103403

Walker, J. C. G., Hays, P. B., & Kasting, J. F. (1981). A negative feedback mechanism for the long-term stabilization of Earth's surface temperature. *Journal of Geophysical Research: Oceans, 86*(C10), 9776-9782. https://doi.org/10.1029/JC086iC10p09776

Wallmann, K. (2001). Controls on the Cretaceous and Cenozoic evolution of seawater composition, atmospheric CO_2 and climate. *Geochimica et Cosmochimica Acta, 65*(18), 3005-3025. https://doi.org/10.1016/S0016-7037(01)00638-X

Wang, C., Hu, X., Huang, Y., Wagreich, M., Scott, R., & Hay, W. (2011). Cretaceous oceanic red beds as possible consequence of oceanic anoxic events. *Sedimentary geology, 235*(1-2), 27-37. https://doi.org/10.1016/j.sedgeo.2010.06.025

Westerhold, T., Marwan, N., Drury, A. J., Liebrand, D., Agnini, C., Anagnostou, E., et al. (2020). An astronomically dated record of Earth's climate and its predictability over the last 66 million years. *Science, 369*(6509), 1383-1387. https://doi.org/10.1126/science.aba6853

Wong, K., Mason, E., Brune, S., East, M., Edmonds, M., & Zahirovic, S. (2019). Deep carbon cycling over the past 200 million years: a review of fluxes in different tectonic settings. *Frontiers in Earth Science, 7*, 263. https://doi.org/10.3389/feart.2019.00263

Woodruff, F., & Savin, S. M. (1989). Miocene deepwater oceanography. *Paleoceanography and Paleoclimatology, 4*(1), 87-140. https://doi.org/10.1029/PA004i001p00087

Wright, J. D., Miller, K. G., & Fairbanks, R. G. (1991). Evolution of modern deepwater circulation: Evidence from the late Miocene Southern Ocean. *Paleoceanography and Paleoclimatology, 6*(2), 275-290. https://doi.org/10.1029/90PA02498

Wyrtki, K. (1973). Physical oceanography of the Indian Ocean. In B. Zeitzschel & S. A. Gerlach (Eds.), *The biology of the Indian Ocean* (Vol. 3, pp. 18-36). Berlin, Heidelberg: Ecological Studies, Springer. https://doi.org/10.1007/978-3-642-65468-8_3

Xiao, K., Hu, X., Jiang, J., & Wang, J. (2024). Unraveling the Cenozoic carbon cycle by reconstructing carbonate compensation depth (CCD). *Science China Earth Sciences, 67*(6), 1743-1758. https://doi.org/10.1007/s11430-023-1291-5

Xu, D., Yi, L., Yuan, H., & Chen, W. (2022). Geochronological evidence inferring carbonate compensation depth shoaling in the philippine sea after the mid-brunhes event. *Journal of Marine Science and Engineering, 10*(6), 745. https://doi.org/10.3390/jmse10060745

Yi, L. (2023). Diverse glacial ventilation in deep Pacific: An integrated record from Mariana Trench and Magellan Seamounts over last 1.2 Myr. *Global and Planetary Change, 230*, 104279. https://doi.org/10.1016/j.gloplacha.2023.104279

Yin, S., Hernández-Molina, F. J., Jutzeler, M., & Li, J. (2022). Progressive intensification of Pacific Deep Water circulation since the early Pliocene. *Geophysical Research Letters, 49*(9), e2022GL098051. https://doi.org/10.1029/2022GL098051

Yu, J., Anderson, R. F., Jin, Z., Rae, J. W., Opdyke, B. N., & Eggins, S. M. (2013). Responses of the deep ocean carbonate system to carbon reorganization during the Last Glacial–interglacial cycle. *Quaternary Science Reviews, 76*, 39-52. https://doi.org/10.1016/j.quascirev.2013.06.020

Yuwono, F. S., & Sato, T. (2020). *Miocene Sea Surface Dynamics in the Western Equatorial Pacific Based on Calcareous Nannofossil Records*. Paper presented at the IOP Conference Series: Earth and Environmental Science. https://doi.org/10.1088/1755-1315/618/1/012006

Zachos, J., Pagani, M., Sloan, L., Thomas, E., & Billups, K. (2001). Trends, rhythms, and aberrations in global climate 65 Ma to present. *Science, 292*(5517), 686-693.

Zachos, J. C., Dickens, G. R., & Zeebe, R. E. (2008). An early Cenozoic perspective on greenhouse warming and carbon-cycle dynamics. *Nature, 451*(7176), 279-283. https://doi.org/10.1038/nature06588

Zachos, J. C., Röhl, U., Schellenberg, S. A., Sluijs, A., Hodell, D. A., Kelly, D. C., et al. (2005). Rapid acidification of the ocean during the Paleocene-Eocene thermal maximum. *Science, 308*(5728), 1611-1615. https://doi.org/10.1126/science.1109004

Zeebe, R. E., & Westbroek, P. (2003). A simple model for the $CaCO_3$ saturation state of the ocean: The “Strangelove,” the “Neritan,” and the “Cretan” Ocean. *Geochemistry, Geophysics, Geosystems, 4*(12). https://doi.org/10.1029/2003GC000538

Zeebe, R. E., & Wolf-Gladrow, D. (2001). *CO2 in seawater: equilibrium, kinetics, isotopes* (Vol. 65). Amsterdam: Journal of Marine Systems.

Zhang, H., Che, H., Xia, J., Cheng, Q., Qi, D., Cao, J., & Luo, Y. (2022a). Sedimentary $CaCO_3$ accumulation in the deep West Pacific Ocean. *Frontiers in Earth Science, 10*(857260), 1-8. https://doi.org/10.3389/feart.2022.857260

Zhang, H., Luo, Y., Yu, J., Zhang, L., Xiang, R., Yu, Z., & Huang, H. (2022b). Indian Ocean sedimentary calcium carbonate distribution and its implications for the glacial deep ocean circulation. *Quaternary Science Reviews, 284*, 107490. https://doi.org/10.1016/j.quascirev.2022.107490

Zhang, M., Xu, S., & Sano, Y. (2024a). Deep carbon recycling viewed from global plate tectonics. *National Science Review, 11*(6), nwae089. https://doi.org/10.1093/nsr/nwae089

Zhang, R., Liu, Z., Jiang, D., Yu, Y., Zhang, Z., Yang, Y., et al. (2024b). Cenozoic Indo-Pacific warm pool controlled by both atmospheric CO_2 and paleogeography. *Science Bulletin, 69*(9), 1323-1331. https://doi.org/10.1016/j.scib.2024.02.028

A | Appendix

Supplement to Article 1

Regional carbonate compensation depth variability in the Pacific Ocean since the Oligocene

Dalvand, F., Dutkiewicz, A., Wright, N. M., Mather, B. R. & Müller, R. D
EarthBythe Group, School of Geosciences, University of Sydney, NSW, Australia

Published in *Frontiers in Earth Science* (2025)
DOI: https://doi.org/10.3389/feart.2025.1605906

Supplementary Data for

Regional Carbonate Compensation Depth variability in the Pacific Ocean since the Oligocene

Faranak Dalvand [1], Adriana Dutkiewicz [1], Nicky M. Wright [1], Ben R. Mather [1], R. Dietmar Müller [1]

[1] EarthByte Group, School of Geosciences, University of Sydney, Sydney, Australia

*** Correspondence:**

Corresponding Author

Faranak Dalvand (faranak.dalvand@sydney.edu.au)

Contents of this file
Supplementary Figures 1 & 2.
Supplementary Table 1.

Additional supplementary data comprising pyBacktrack 1.4 output data files are available via Zenodo at https://doi.org/10.5281/zenodo.15116747.

Introduction

The supplementary data in this paper provides data to enable readers to explore our research methodology, conduct further analyses, and replicate our results. Additionally, sharing this data promotes transparency, reproducibility, and collaboration within the scientific community.

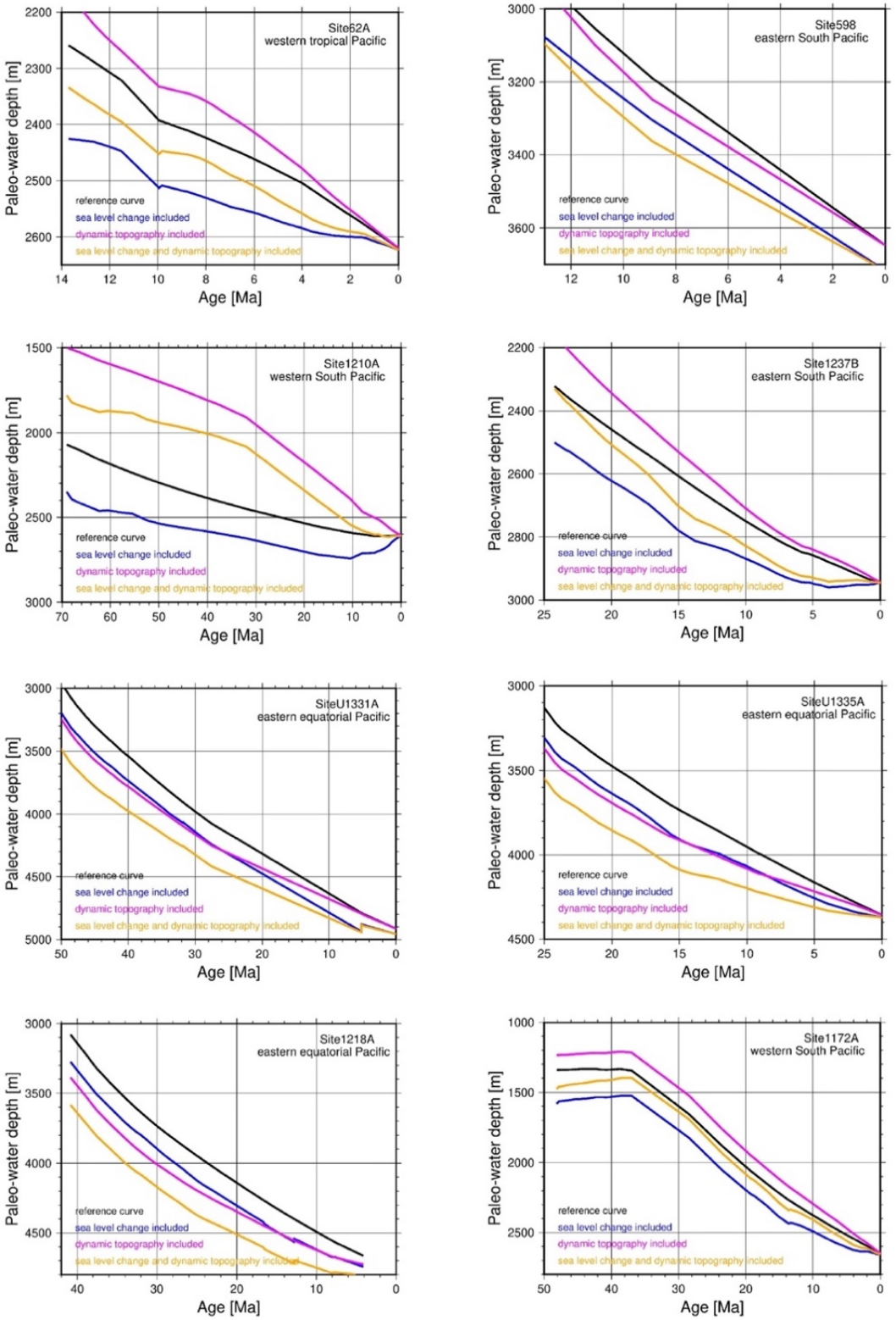

Supplementary Figure 7. Examples of backtracked paleo-water depths for deep-sea drill sites on ocean crust (Sites 598, U1331A, U1335A, and 1218A) and continental crust (Sites 62A, 1210A, 1237B, and 1172A). Each plot includes a black curve representing backtracking without the inclusion of dynamic topography and eustatic sea level. The blue curve shows backtracking incorporating sea level, while the purple curve incorporates dynamic topography only. The orange curve shows backtracking that includes both dynamic topography and sea level. Dynamic topography and sea level used in these examples are based on the M6 model from Müller et al. (2018).

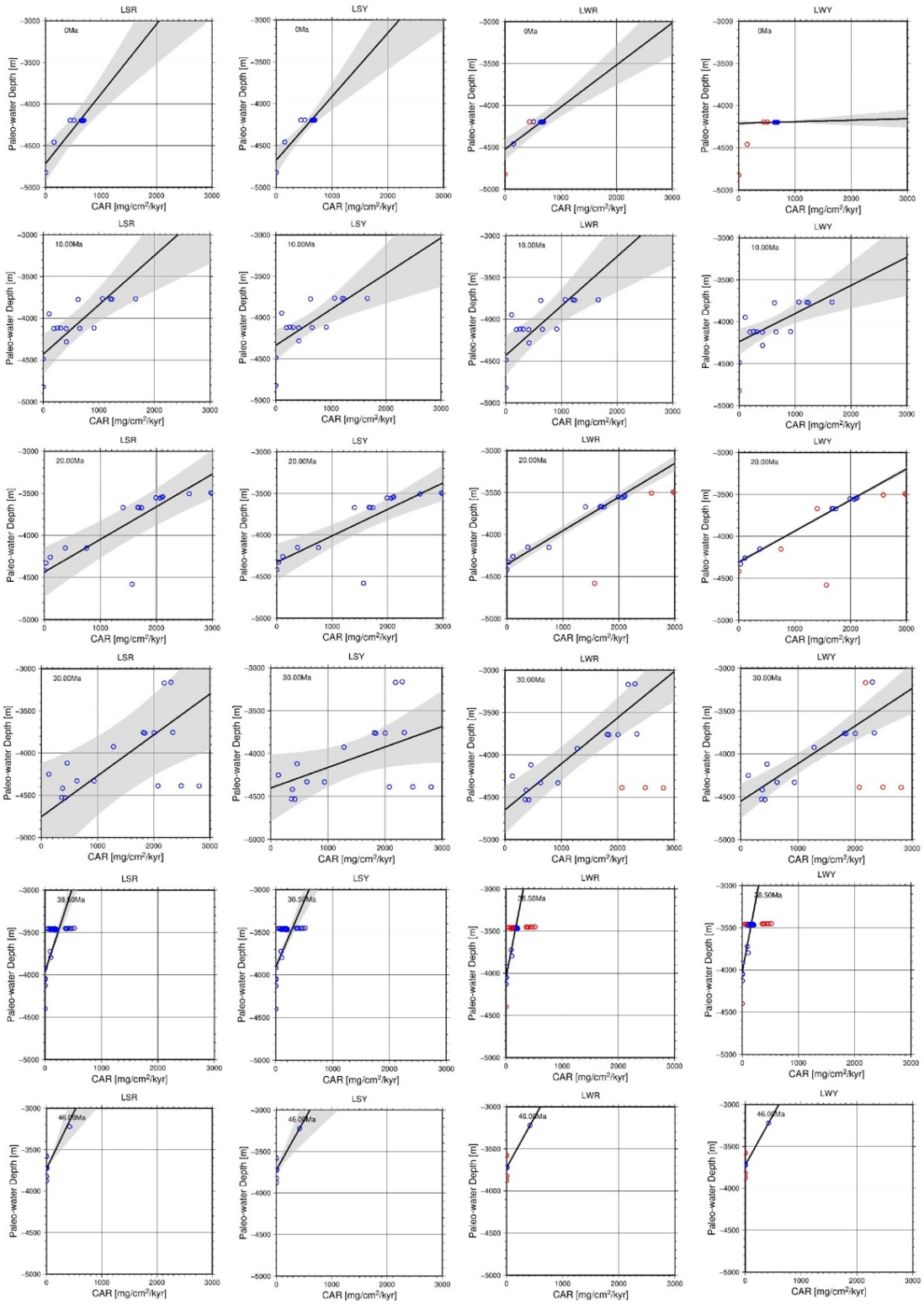

Supplementary Figure 2. Regression plots using the dataset of Pälike et al. (2012) to reconstruct the CCD based on four regression methods. The CCD is defined by the carbonate accumulation rate (CAR) values extrapolating to zero as a function of the paleo-water depth (i.e., the y-intercept). Data points (blue and red circles) represent various deep-sea drill sites at each time interval. Red circles indicate outliers. The gray envelope indicates uncertainty with 95% confidence. The regression

methods include LSR — least squares with reduced axis regression calculating errors on the x-axis (CAR) and the y-axis (paleo-water depth), LSY— least squares regression computing errors on the y-axis, LWR — weighted least squares with reduced axis regression and outlier detection, and LWY — weighted least squares with outlier detection and error computation on the y-axis.

Supplementary Table 1. Deep-sea drill sites from the Deep Sea Drilling Project (DSDP), Ocean Drilling Program (ODP), and Integrated Ocean Drilling Program (IODP) used in the study of the Regional Carbonate Compensation Depth variability in the Pacific Ocean since the Oligocene.
Note: Drill sites locality include EN for the eastern North Pacific, WN for the western North Pacific, EEQ for the eastern equatorial Pacific, WT for the western tropical Pacific, ES for the eastern South Pacific, and WS for the western South Pacific. NSB refers to Neptune Sandbox Berlin (NSB; https://nsb.mfn-berlin.de/, Renaudie et al., 2020).

Site name	Locality	Longitude (°)	Latitude (°)	Water depth (m)	Oceanic basement age (Ma)	Sediment thickness penetrated (m)	Basement reached	Depth below seafloor (m)	Age-depth model source
DSDP 5-33	EN	-127.5	39.5	4284	26.5	287	No	295	Lyle (2002)
DSDP 5-37	EN	-140.7	41.0	4682	27.8	30.6	Yes	30	Lyle (2002)
DSDP 6-55	WT	142.5	9.3	2850	154.4	119.1	No	130.8	Lyle (2002)
DSDP 7-62A	WT	141.9	1.9	2607	28.4	303.3	No	364	NSB
DSDP 7-65	WT	177.0	4.4	6142	137.7	130.5	No	145	Lyle (2002)
DSDP 8-70	EEQ	-140.4	6.3	5059	52.6	98	No	113	Lyle (2002)
DSDP 9-84	EEQ	-82.9	5.7	3096	10.5	213.3	No	253.9	Lyle (2002)
DSDP 16-158	EEQ	-85.2	6.6	1953	14.1	249.9	Yes	323	NSB
DSDP 17-170	WT	177.6	11.8	5792	147.3	30.7	Yes	196	NSB
DSDP 17-171	WT	-169.5	19.1	2290	113.3	173.3	Yes	464	NSB
DSDP 18-173	EN	-125.5	40.0	2927	20.6	196	Yes	333.5	NSB
DSDP 18-178	EN	-147.1	57.0	4218	39.4	212.5	Yes	794.5	NSB
DSDP 21-208	WS	161.2	-26.1	1545	-	255.4	No	594	NSB
DSDP 29-284	WS	167.7	-40.5	1166	-	166.8	No	208	Lyle (2002)
DSDP 30-289	WT	158.5	-0.5	2206	146.5	712.6	Yes	1271	NSB
DSDP 32-313	WT	-171.0	20.2	3484	111.8	220.5	Yes	606	NSB
DSDP 33-317B	WS	-162.3	-11.0	2598	125.4	308	No	943.5	NSB
DSDP 34-319	ES	-101.5	-13.0	4296	15.1	99.33	Yes	157	Lyle (2002)
DSDP 56-436	WN	145.6	39.9	5240	133.9	240.8	No	397.5	NSB
DSDP 58-446	WN	132.8	24.7	4980	76.9	197.1	No	420.5	Initial Report
DSDP 59-448	WT	134.9	16.3	3483	39.4	234	No	584.5	NSB
DSDP 59-451	WT	143.3	18.0	2060	6.5	280.1	No	930.5	Initial Report
DSDP 60-458	WT	146.9	17.9	3453	146	97.83	Yes	465.5	NSB
DSDP 60-459B	WT	147.3	17.9	4121	146.4	182.14	Yes	691.5	NSB
DSDP 62-463	WT	174.7	21.4	2525	150.4	301.8	No	822.5	NSB
DSDP 63-469	EN	-120.5	32.6	3790	17.4	170.2	No	453.5	NSB
DSDP 63-470	EN	-117.5	28.9	3549	15.1	90	Yes	168	NSB
DSDP 63-472	EN	-114.0	23.0	3831	13.9	65.11	Yes	137.5	NSB

Site name	Locality	Longitude (°)	Latitude (°)	Water depth (m)	Oceanic basement age (Ma)	Sediment thickness penetrated (m)	Basement reached	Depth below seafloor (m)	Age-depth model source
DSDP 68-503A	EEQ	-95.6	4.1	3672	9.9	138	No	235	NSB
DSDP 85-572A	EEQ	-113.8	1.4	3893	15.7	154.35	No	154	NSB
DSDP 85-572D	EEQ	-113.8	1.4	3893	15.7	258.87	Yes	479.5	NSB
DSDP 85-573	EEQ	-133.3	0.5	4301	37.0	159.4	No	158.6	NSB
DSDP 85-573B	EEQ	-133.3	0.5	4301	37.0	279.7	Yes	529	NSB
DSDP 85-574	EEQ	-133.3	4.2	4561	36.0	208.93	No	206.5	NSB
DSDP 85-574C	EEQ	-133.3	4.2	4561	36.0	197.35	Yes	532.5	NSB
DSDP 86-578	WN	151.6	33.9	6010	145.7	165.02	No	176.8	NSB
DSDP 86-579A	WN	153.8	38.6	5736.6	134.1	115.87	No	149.5	NSB
DSDP 86-581	WN	159.8	43.9	5476	126.3	77.59	Yes	352.5	NSB
DSDP 90-587	WS	161.3	-21.2	1101	-	88.81	No	147	NSB
DSDP 90-590B	WS	163.4	-31.2	1299	-	465.26	No	499.1	NSB
DSDP 90-591	WS	164.4	-31.6	2131	-	278.21	No	283.1	NSB
DSDP 90-594	WS	174.9	-45.5	1204	-	161.55	No	639.5	NSB
DSDP 92-597	ES	-129.8	-18.8	4157.1	27.2	42.1	Yes	54.7	Lyle (2002)
DSDP 92-598	ES	-124.7	-19.0	3699	18.1	41.2	No	52.4	Lyle (2002)
ODP 129-800A	WT	152.3	21.9	5686	160.8	150.73	Yes	544.4	NSB
ODP 130-803D	WT	160.5	2.4	3412.2	151.9	494.96	Yes	656	NSB
ODP 130-806B	WT	159.4	0.3	2519.9	148.3	666.36	No	743.1	NSB
ODP 130-807C	WT	156.6	3.6	2805.7	156.3	252.84	Yes	1528.4	NSB
ODP 133-823B	WT	146.8	16.9	1638.4	147	123.73	No	119.8	Lyle (2002)
ODP 138-844C	EEQ	-90.5	7.9	3414.5	17.3	189.34	No	180.1	NSB
ODP 138-845A	EEQ	-94.6	9.6	3704.2	15.9	292.63	No	291.6	NSB
ODP 138-846D	EEQ	-90.8	-3.1	3295.8	16.9	247.85	No	249.4	NSB
ODP 138-847B	EEQ	-95.3	0.2	3334.3	9.8	242.19	No	247	NSB
ODP 138-848B	EEQ	-110.5	-3.0	3855.6	9.5	97.75	No	93.8	NSB
ODP 138-849B	EEQ	-110.5	0.2	3839.1	10.5	343.78	No	350.5	NSB
ODP 138-850B	EEQ	-110.5	1.3	3786.1	10.8	393.58	No	399.8	NSB
ODP 138-851B	EEQ	-110.6	2.8	3760.3	11.7	318.05	Yes	320.5	NSB
ODP 138-852C	EEQ	-110.1	5.3	3859.8	10.2	107.1	No	117.3	NSB
ODP 138-853B	EEQ	-109.8	7.2	3715.5	8.6	77.68	Yes	72.4	NSB
ODP 144-871A	WT	172.3	5.6	1254.6	151.9	126.05	No	151.9	NSB
ODP 144-873B	WT	164.9	11.9	1334	176.3	53.83	No	69	NSB
ODP 145-881C	WN	161.5	47.1	5530.8	118.9	227.2	No	363.8	NSB
ODP 145-882A	WN	167.6	50.4	3243.8	114.7	411.2	No	398.3	NSB
ODP 145-883B	WN	167.8	51.2	2395.6	113.0	695	Yes	840.7	NSB
ODP 145-883E	WN	167.8	51.4	2385.5	113.0	344.3	Yes	856.5	NSB
ODP 145-884B	WN	168.3	51.5	3824.8	112.7	791.76	Yes	853.9	NSB
ODP 145-885A	EN	-168.2	44.7	5713.3	83.8	67.1	No	72.4	Initial Report
ODP 145-887C	EN	-148.4	54.4	3633.6	35.4	269.44	Yes	273.8	NSB

Site name	Locality	Longitude (°)	Latitude (°)	Water depth (m)	Oceanic basement age (Ma)	Sediment thickness penetrated (m)	Basement reached	Depth below seafloor (m)	Age-depth model source
ODP 181-1124C	WS	-176.5	-39.5	3962	127.5	473.1	No	583.7	Initial Report
ODP 189-1171C	WS	149.1	-48.5	2147.8	-	252.5	No	274.8	NSB
ODP 189-1171D	WS	149.1	-48.5	2147.8	-	711	No	959	NSB
ODP 189- 1172A	WS	149.9	-44.0	2620	-	508.9	No	552.6	NSB
ODP 191-1179C	WN	160.0	41.1	5563.9	132.7	287.4	Yes	292.9	NSB
ODP 198-1207A	WN	162.8	37.8	3100.8	138.1	243.4	No	223	NSB
ODP 198-1208A	WN	158.2	36.1	3345.7	140.1	392.3	No	392.3	NSB
ODP 198-1209A	WN	158.5	32.7	2387.2	146.2	263.6	No	259.6	NSB
ODP 198-1210A	WN	158.3	32.2	2573.5	146.7	251.2	No	241.4	NSB
ODP 198-1211A	WN	157.9	32.0	2907.5	147.2	169.9	No	158.9	NSB
ODP 198-1212A	WN	157.7	32.4	2682.5	146.9	101.6	No	101.6	NSB
ODP 199-1218A	EEQ	-135.4	8.9	4826.3	43.0	265.9	Yes	276.8	NSB
ODP 199-1219A	EEQ	-142.0	7.8	5063.4	56.0	236.8	Yes	250.8	NSB
ODP 199-1220A	EEQ	-142.8	10.2	5217.9	56.5	119.2	No	182.78	NSB
ODP 202-1236A	ES	-81.4	-21.4	1323	39.1	167.7	No	164.5	Initial Report
ODP 202-1237B	ES	-76.6	-16.1	3212	44.2	331.4	No	317.4	Initial Report
IODP 320-U1331A	EEQ	-142.2	12.1	5120.92	53.9	154.4	Yes	190.6	NSB
IODP 320-U1332A	EEQ	-141.0	11.9	4917.62	51.1	145.7	Yes	152.4	NSB
IODP 320-U1333A	EEQ	-138.4	10.5	4858.82	46.4	176.1	Yes	184.1	NSB
IODP 320-U1334A	EEQ	-132.0	8.0	4793.22	38.9	288.6	Yes	285.5	NSB
IODP 320-U1335A	EEQ	-126.3	5.3	4333.02	25.3	421.6	No	421.1	NSB
IODP 320-U1336A	EEQ	-128.3	7.7	4291.02	34.3	258.9	No	302.9	NSB
IODP 321-U1337A	EEQ	-123.2	3.8	4465.62	22.1	419.6	Yes	449.8	NSB
IODP 321-U1338A	EEQ	-118.0	2.5	4204.52	18.4	345.6	Yes	410	NSB

References

Lyle, M. (2002). Age-Depth Profiles for Pacific DSDP and ODP Drillsites. *Center for Geophysical Investigation of the Shallow Subsurface, Boise State University, Boise, Idaho*, 0-66.

Müller, R. D., Cannon, J., Williams, S., & Dutkiewicz, A. (2018). PyBacktrack 1.0: A tool for reconstructing paleobathymetry on oceanic and continental crust. *Geochemistry, Geophysics, Geosystems, 19*(6), 1898-1909. https://doi.org/10.1029/2017GC007313

Pälike, H., Lyle, M. W., Nishi, H., Raffi, I., Ridgwell, A., Gamage, K., et al. (2012). A Cenozoic record of the equatorial Pacific carbonate compensation depth. *Nature, 488*, 609-614. https://doi.org/10.1038/nature11360

Renaudie, J., Lazarus, D. B., & Diver, P. (2020). NSB (Neptune Sandbox Berlin): An expanded and improved database of marine planktonic microfossil data and deep-sea stratigraphy. *Palaeontologia Electronica, 23*(1), 1-28. https://doi.org/10.26879/1032

B | Appendix

Supplement to Article 2

Indian Ocean carbonate compensation depth since the Late Oligocene

Dalvand, F., Dutkiewicz, A., Wright, N. M. & Müller, R. D
EarthBythe Group, School of Geosciences, University of Sydney, NSW, Australia

Published in *Geo-Marine Letters* (2025)
DOI: https://doi.org/10.1007/s00367-025-00825-5

Supplementary Data for

Indian Ocean Carbonate Compensation Depth since the Late Oligocene

Faranak Dalvand [1], Adriana Dutkiewicz [1], Nicky M. Wright [1], R. Dietmar Müller [1]

[1] EarthByte Group, School of Geosciences, University of Sydney, Sydney, Australia

Corresponding Author:

Faranak Dalvand (faranak.dalvand@sydney.edu.au)

Contents of this file

Supplementary Figures 1, 2 & 3 and Tables 1 & 2.

Additional supplementary data comprising pyBacktrack 1.4 input and output data files are available via https://doi.org/10.5281/zenodo.17232379.

Introduction

The supplementary data provided in this paper equips readers with the resources to conduct further analyses and validate our findings. Moreover, the availability of this data enhances transparency, ensures reproducibility, and encourages collaboration within the scientific community.

Supplementary Figures

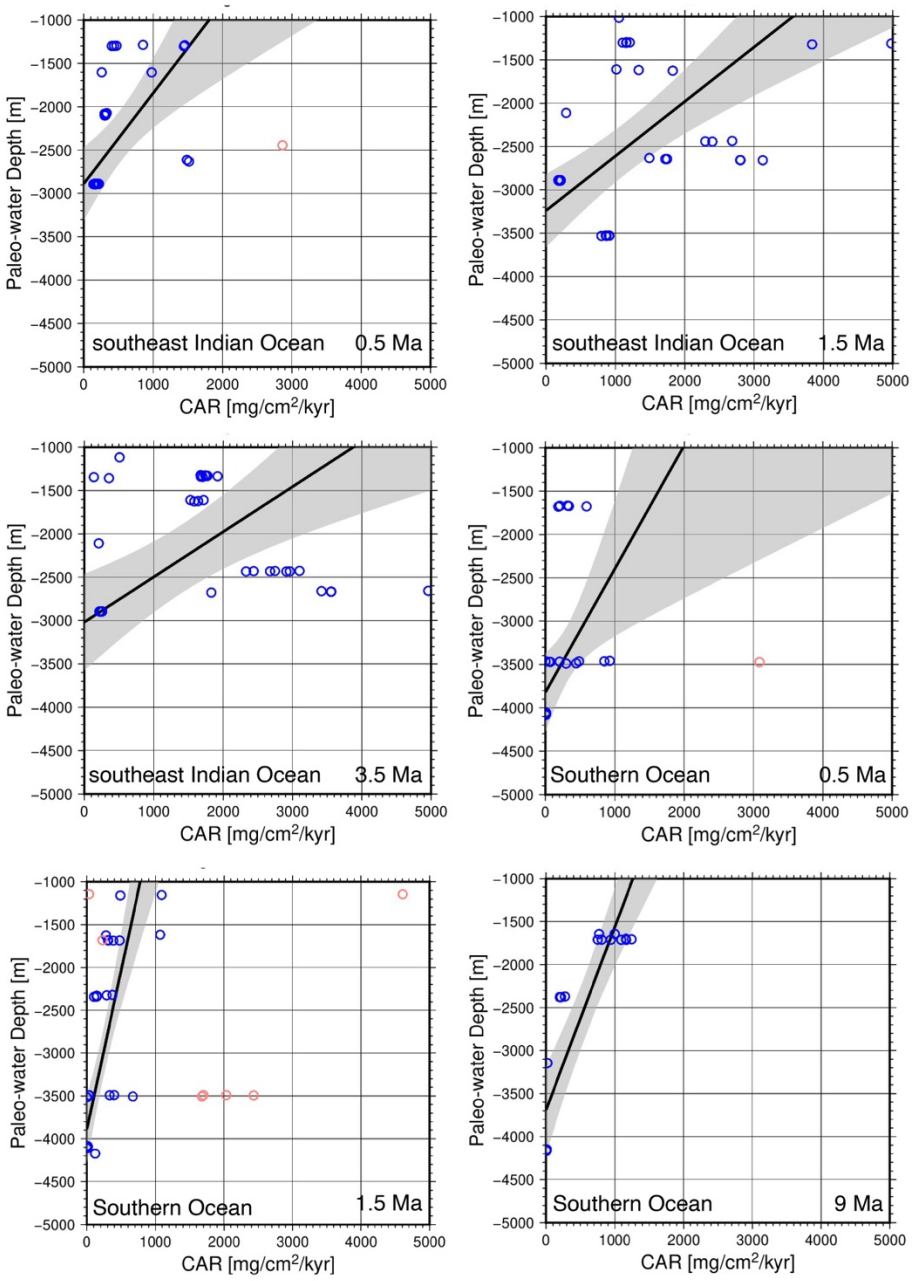

Figure 8 Examples of regression analysis for CCD computation across the southeast Indian Ocean and the Southern Ocean, accounting for outliers, which incorporates the dynamic topography model from Braz et al. (2021) and the eustatic sea-level model from Miller et al. (2024). The paleo-water depth at which the carbonate accumulation rate (CAR) values become negligible (approach zero) with increasing depth determines the CCD, corresponding to the y-intercept. Blue and red data points within each time window display data from multiple drill sites, with red circles indicating identified outliers. The 95% confidence envelope is depicted as a grey band.

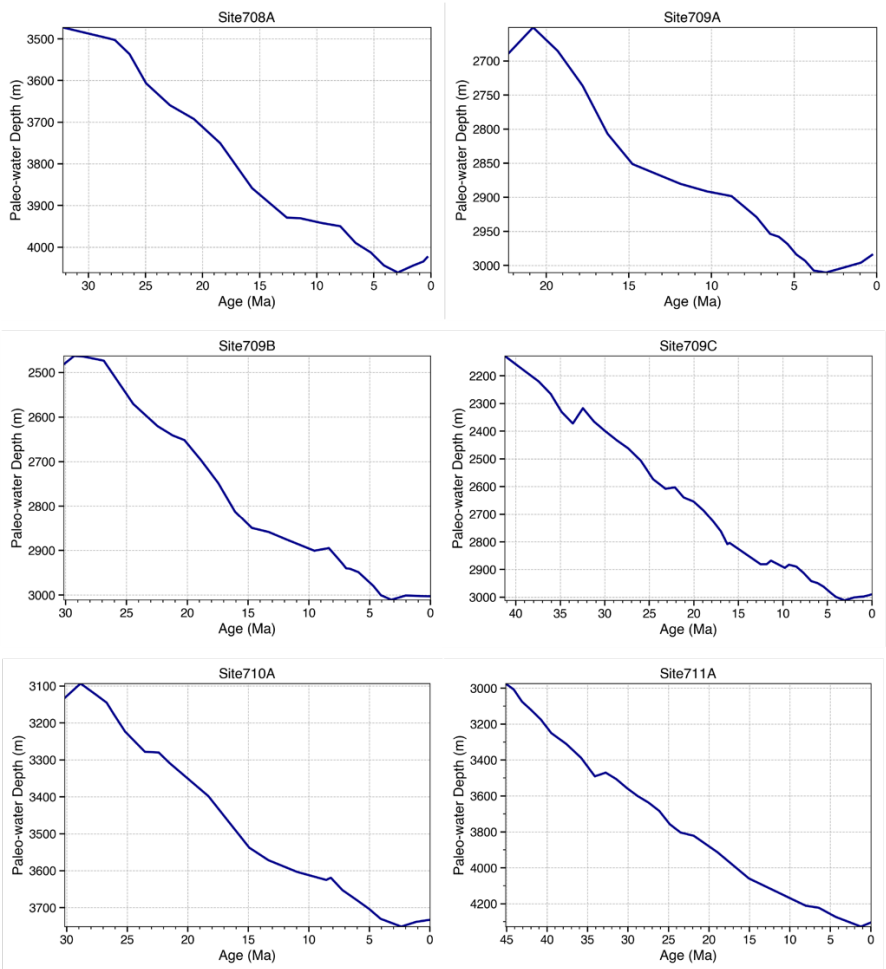

Figure 9 Examples of backtracked paleo-water depths through time for multiple drill sites from the western equatorial Indian Ocean, using pyBacktrack 1.4 software (Müller et al., 2018), as described in the Data and Method section. Dynamic topography and eustatic sea level models used in this study are based on Braz et al. (2021) and Miller et al. (2024), respectively.

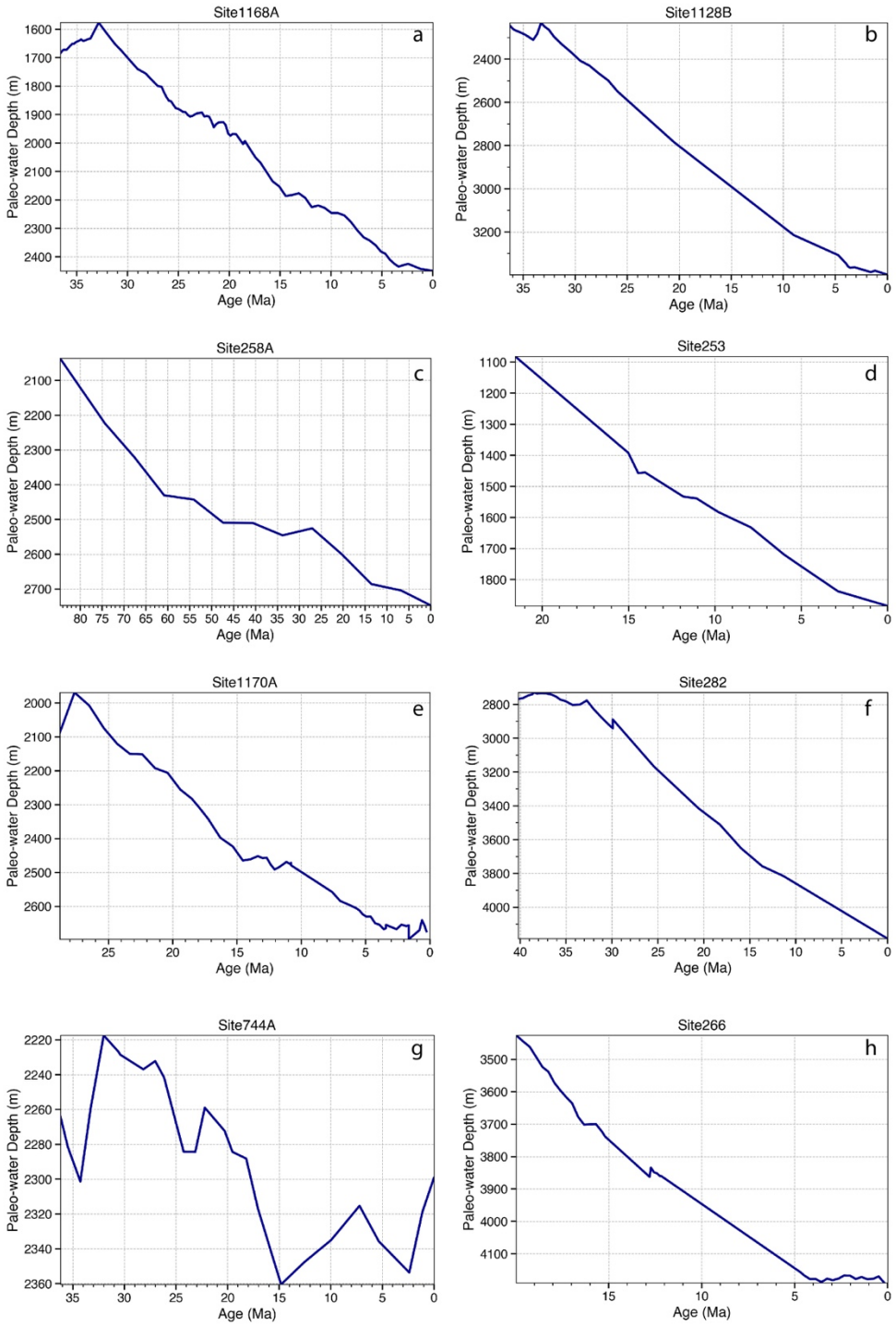

Figure 10 Examples of backtracked paleo-water depths through time for multiple drill sites from the southeastern Indian Ocean (panel a–f) and Southern Ocean (panel g–h), using pyBacktrack 1.4 software (Müller et al., 2018), as described in the Data and Method section. Refer to Figure 2 for details of dynamic topography and eustatic sea level models.

Supplementary Table 1. Deep-sea drill sites used in the reconstruction of the Indian Ocean carbonate compensation depth (CCD) since the late Oligocene from the Deep Sea Drilling Project (DSDP), Ocean Drilling Program (ODP), and International Ocean Discovery Program (IODP) across three defined regions: the western equatorial Indian (WEI), the southeast Indian Ocean (SEI) and the Southern Ocean (SO). Drill site information, including longitude, latitude, water depth, penetrated sediment thickness,

and basement reached, is sourced from initial reports archived in the DSDP, ODP, and IODP expeditions databases. Basement depths are computed using pyBacktrack 1.4 (Müller et al., 2018). Oceanic basement ages are derived from a combination of the oceanic crustal age grid of Seton et al. (2020) and the age-depth relationship of Stein and Stein (1992) to compute tectonic subsidence. For continental crust, stretching factors are obtained from the global grids of Müller et al. (2019) (available at https://www.earthbyte.org/webdav/ftp/Data_Collections/Muller_etal_2019_Tectonics/Muller_etal_2019_TotalStretchingFactors/) and the global plate tectonic model of Müller et al. (2019). CC — continental crust, NSB —Neptune Sandbox Berlin (NSB; https://nsb.mfn-berlin.de/, Renaudie et al., 2020), and SedST refers to SedS&T chronostratigraphic database (http://sedst.org/#/home).

Site name	Locality	Long (°)	Lat (°)	Water depth (m)	Oceanic basement age (Ma)	CC- Rift start (Ma)	CC- Rift end (Ma)	Sediment thickness penetrated (m)	Basement reached	Age-depth model source
DSDP 22-213	SEI	93.9	-10.2	5611	58.2			173.5	Yes	NSB
DSDP 23-219	WEI	72.9	9.0	1764	63.6			411	No	Initial Report
DSDP 23-220	WEI	71.0	6.5	4036	52.6			350	Yes	Initial Report
DSDP 23-221	WEI	68.4	8.0	4650	48.3			270	Yes	Initial Report
DSDP 24-235	WEI	52.7	3.2	5130	55.7			684	No	Initial Report
DSDP 24-236	WEI	57.6	-1.7	4487	59.6			327.5	Yes	NSB
DSDP 26-253	SEI	87.4	-24.9	1962	45.7			546.5	No	NSB
DSDP 26-258	SEI	112.5	-33.8	2793		161	130.1	123.5	No	NSB
DSDP 27-260	SEI	110.3	-16.1	5702	130.8			329.7	Yes	Initial Report
DSDP 27-261	SEI	117.9	-12.9	5667	153.2			570.89	Yes	Initial Report
DSDP 28-265	SO	109.9	-53.5	3581	13.9			462	Yes	NSB
DSDP 28-266	SO	110.1	-56.4	4173	22.4			384	Yes	NSB
DSDP 28-267	SO	104.5	-59.3	4522	23.7			290	Yes	NSB
DSDP 28-282	SEI	143.5	-42.2	4202		161	34	311.5	Yes	Initial Report
ODP 115-708A	WEI	59.9	-5.5	4109.3	55.3			236.2	Yes	Initial Report
ODP 115-709A,B,C	WEI	60.6	-3.9	3047	55.2			353.7	No	NSB
ODP 115-710A	WEI	61.0	-4.3	3822.5	52.9			209.7	No	NSB
ODP 115-711A	WEI	61.2	-2.7	4439	51.8			249.6	No	NSB
ODP 117-712	WEI	73.4	-4.2	2904.3	52.4			115.3	Yes	Initial Report
ODP 117-713	WEI	73.4	-4.2	2920	52.4			191.7	Yes	NSB & Initial Report
ODP 116-717C	WEI	81.4	-0.9	4734.7	80.1			828.2	No	Initial Report
ODP 116-718C	WEI	81.4	-1.0	4730.2	79.9			935	No	Initial Report
ODP 116-719A	WEI	81.4	-1.0	4736.8	80.0			460.2	No	Initial Report
ODP 119-738B,C	SO	82.8	-62.7	2252.7	128.3			533.8	No	NSB
ODP 119-744A	SO	80.6	-61.6	2307.3	124.1			176.1	No	NSB
ODP 119-745B	SO	85.9	-59.6	4082.5	127.7			215	No	NSB
ODP 119-746A	SO	85.9	-59.6	4059.5	127.8			280.8	No	NSB
ODP 120-747A,C	SO	76.8	-54.8	1695	116.3			350	No	NSB
ODP 120-748A,B,C	SO	79.0	-58.4	1290		161	126	935	Yes	NSB
ODP 120-749B	SO	76.4	-58.7	1069.5		161	126	123.8	No	NSB
ODP 120-751A	SO	79.8	-57.7	1988	130.4			166.2	No	NSB

Site name	Locality	Long (°)	Lat (°)	Water depth (m)	Oceanic basement age (Ma)	CC- Rift start (Ma)	CC- Rift end (Ma)	Sediment thickness penetrated (m)	Basement reached	Age-depth model source
ODP 121-752A	SEI	93.6	-30.9	1086.3	51.4			308	No	NSB
ODP 121-753A	SEI	93.6	-30.8	1176.1	52.7			62.8	No	Initial Report
ODP 121-754A	SEI	93.6	-30.9	1063.6	50.3			172.1	No	Initial Report
ODP 121-756B	SEI	87.6	-27.4	1518.1	47.3			395.6	No	Initial Report
ODP 121-757B	SEI	88.2	-17.0	1650.2	51.0			369.3	Yes	NSB
ODP 121-758A	SEI	90.4	5.4	2923.6	78.1			527.1	Yes	NSB
ODP 122-761B	SEI	115.5	-16.7	2188.8		161	155	286	No	NSB
ODP 122-762B,C	SEI	112.3	-19.9	1360		161	155	940	No	NSB, SedST
ODP 122-763A,B	SEI	112.2	-20.6	1367.5		161	155	653.5	No	NSB, SedST
ODP 122-764A	SEI	115.5	-16.6	2698.6		161	155	69	No	Initial Report
ODP 123-766A	SEI	110.5	-19.9	3997.5	153.2			471	No	NSB
ODP 182-1128	SEI	127.6	-34.4	3876		161	34	280.7	No	Initial Report
ODP 183-1133B	SEI	128.9	-33.5	1037.2		161	34	152.1	No	Initial Report, SedST
ODP 183-1135A	SO	84.3	-59.7	1566.6		161	126	526	No	Initial Report
ODP 183-1136A	SO	84.8	-59.7	1930		161	126	128	Yes	Initial Report
ODP 183-1137A	SO	68.1	-56.8	1004.5		161	126	228.4	Yes	Initial Report
ODP 183-1138A	SO	76.0	-53.6	1141.4	114.0			698.1	Yes	NSB
ODP 183-1139A	SO	63.9	-50.2	1415.3	73.0			469.9	No	Initial Report
ODP 183-1140A	SO	68.5	-46.3	2394.1	42.8			237.3	Yes	Initial Report
ODP 189-1168A	SEI	144.4	-42.6	2463.3		161	34	883.5	No	NSB
ODP 189-1169A	SEI	145.2	-47.1	3568		161	37.1	246.3	No	Initial Report
ODP 189-1170A,D	SEI	146.0	-47.2	2704.7		161	34.0	464.3	No	NSB
IODP 369-U1514A,C	SEI	113.1	-33.1	3838.2		161	129.4	515.59	No	Proceeding Report
IODP 369-U1516A,C	SEI	112.8	-34.3	2676.46		161	126.9	540.1	No	Proceeding Report

Supplementary Table 2. Comparison between previously published present-day CCD reconstructions and this study. The Indian Ocean is divided into distinct regions, as identified in various studies listed in this table, each based on differing criteria and objectives. CIB — Central Indian Basin, WB — Wharton Basin, SWIB — Southwest Indian Basin, and SAB — South Australia Basin. n.d. — not determined.

Defined regions/ CCD	Sclater et al. (1977)	van Andel et al. (1975)	Campbell et al. (2018)	Peterson and Backman (1990)	Zhang et al. (2022)	Sulpis et al. (2018)	This study
Indian Ocean	~4.5 km - 0 Ma	~5.3 km - 0 Ma	**n.d.**	**n.d.**	**n.d.**	**n.d.**	**n.d.**
Central Indian Ocean	**n.d.**	~5.1 km - 0 Ma	**n.d.**	**n.d.**	**n.d.**	~4.4±0.3 km - 0 Ma	**n.d.**
Western equatorial Indian Ocean	**n.d.**	**n.d.**	~4.8±0.1 km- 0.5 Ma	~5 km – 0 Ma	**n.d.**	**n.d.**	~4.2±0.4 km- 0.5 Ma
CIB and WB	**n.d.**	**n.d.**	**n.d.**	**n.d.**	~4.8 km - 0 Ma	**n.d.**	**n.d.**
SWIB and SAB	**n.d.**	**n.d.**	**n.d.**	**n.d.**	~5 km - 0 Ma	**n.d.**	**n.d.**
Western Indian Ocean	**n.d.**	**n.d.**	**n.d.**	**n.d.**	**n.d.**	~4.7±0.2 km - 0 Ma	**n.d.**
Eastern Indian Ocean	**n.d.**	**n.d.**	**n.d.**	**n.d.**	**n.d.**	~5.1±0.2 km - 0 Ma	**n.d.**

Southern Ocean	**n.d.**	**n.d.**	**n.d.**	**n.d.**	**n.d.**	~4.1±0.3 km - 0 Ma	~3.8±0.5 km-0 Ma
Southeast Indian Ocean	**n.d.**	**n.d.**	**n.d.**	**n.d.**	**n.d.**	**n.d.**	~2.8±0.4 km-0 Ma

References

Braz, C., Zahirovic, S., Salles, T., Flament, N., Harrington, L., & Müller, R. D. (2021). Modelling the role of dynamic topography and eustasy in the evolution of the Great Artesian Basin. *Basin Research, 33*(6), 3378-3405. https://doi.org/10.1111/bre.12606

Campbell, S. M., Moucha, R., Derry, L. A., & Raymo, M. E. (2018). Effects of dynamic topography on the Cenozoic carbonate compensation depth. *Geochemistry, Geophysics, Geosystems, 19*(4), 1025-1034. https://doi.org/10.1002/2017GC007386

Miller, K. G., Schmelz, W. J., Browning, J. V., Rosenthal, Y., Hess, A. V., Kopp, R. E., & Wright, J. D. (2024). Global mean and relative sea-level changes over the past 66 Myr: implications for early Eocene ice sheets. *Earth Science, Systems and Society, 4*(1), 10091. https://doi.org/10.3389/esss.2023.10091

Müller, R. D., Cannon, J., Williams, S., & Dutkiewicz, A. (2018). PyBacktrack 1.0: A tool for reconstructing paleobathymetry on oceanic and continental crust. *Geochemistry, Geophysics, Geosystems, 19*(6), 1898-1909. https://doi.org/10.1029/2017GC007313

Müller, R. D., Zahirovic, S., Williams, S. E., Cannon, J., Seton, M., Bower, D. J., et al. (2019). A global plate model including lithospheric deformation along major rifts and orogens since the Triassic. *Tectonics, 38*(6), 1884-1907. https://doi.org/10.1029/2018TC005462

Peterson, L., & Backman, J. (1990). Late Cenozoic Carbonate Accumulation and the History of the Carbonate Compensation Depth in the Western Equatorial Indian Ocean. In R. A. Duncan, J. Backman, & L. Peterson (Eds.), *Proceedings of the Ocean Drilling Program, Scientific Results* (Vol. 115, pp. 467-507). College Station, TX: Ocean Drilling Program. https://doi.org/10.2973/odp.proc.sr.115.163.1990

Renaudie, J., Lazarus, D. B., & Diver, P. (2020). NSB (Neptune Sandbox Berlin): An expanded and improved database of marine planktonic microfossil data and deep-sea stratigraphy. *Palaeontologia Electronica, 23*(1), 1-28. https://doi.org/10.26879/1032

Sclater, J. G., Abbott, D., & Thiede, J. (1977). Paleobathymetry and sediments of the Indian Ocean. In J. R. Heirtzler, H. M. Bolli, T. A. Davies, J. B. Saunders, & J. G. Sclater (Eds.), *Indian Ocean Geology and Biostratigraphy: Studies Following Deep-Sea Drilling Legs* (Vol. 9, pp. 25-59). Special Publications. https://doi.org/10.1029/SP009p0025

Seton, M., Müller, R. D., Zahirovic, S., Williams, S., Wright, N. M., Cannon, J., et al. (2020). A global data set of present-day oceanic crustal age and seafloor spreading parameters. *Geochemistry, Geophysics, Geosystems, 21*(10), e2020GC009214. https://doi.org/10.1029/2020GC009214

Stein, C. A., & Stein, S. (1992). A model for the global variation in oceanic depth and heat flow with lithospheric age. *Nature, 359*(6391), 123-129. https://doi.org/10.1038/359123a0

Sulpis, O., Boudreau, B. P., Mucci, A., Jenkins, C., Trossman, D. S., Arbic, B. K., & Key, R. M. (2018). Current $CaCO_3$ dissolution at the seafloor caused by anthropogenic CO_2. *Proceedings of the National Academy of Sciences, 115*(46), 11700-11705. https://doi.org/10.1073/pnas.1804250115

van Andel, T. H., Heath, G. R., & Moore, J., Theodore Carlton. (1975). Cenozoic tectonics, sedimentation and paleoceanography of the central equatorial Pacific. In T. H. van

Andel, G. R. Heath, & J. Moore, Theodore Carlton (Eds.), *Cenozoic History and Paleoceanography of the Central Equatorial Pacific Ocean* (Vol. 143): Geological Society of America Memoris. https://doi.org/10.1130/MEM143-p1

Zhang, H., Luo, Y., Yu, J., Zhang, L., Xiang, R., Yu, Z., & Huang, H. (2022). Indian Ocean sedimentary calcium carbonate distribution and its implications for the glacial deep ocean circulation. *Quaternary Science Reviews, 284*, 107490. https://doi.org/10.1016/j.quascirev.2022.107490

C | Appendix

Supplement to Article 3

Cretaceous to Cenozoic Carbonate Burial Variability Across the Atlantic, Pacific and Indian Oceans

Dalvand, F., Dutkiewicz, A., Wright, N. M. & Müller, R. D

EarthBythe Group, School of Geosciences, University of Sydney, NSW, Australia

Submitted to the Journal of *Marine Geology* in February 2026

Supplementary Data for

Cretaceous to Cenozoic Carbonate Burial Variability Across the Atlantic, Pacific and Indian Oceans

Faranak Dalvand[1], Adriana Dutkiewicz[1], Nicky M. Wright[1], R. Dietmar Müller[1]

[1]EarthByte Group, School of Geosciences, University of Sydney, Sydney, Australia

Corresponding Author:

Faranak Dalvand (faranak.dalvand@sydney.edu.au)

Contents of this file

Supplementary Figures 1, 2, 3 & 4 and Tables 1, 2 & 3.

Additional supplementary data of global data files containing carbonate accumulation rate (CAR) and carbonate percent input and output data files are available via https://doi.org/10.5281/zenodo.18755594.

Introduction

The supplementary figures, tables and datasets enable independent validation of the results and analysis. Making these data publicly available enhances transparency, reinforces reproducibility, and promotes collaborative engagement within the scientific community.

Supplementary Figures

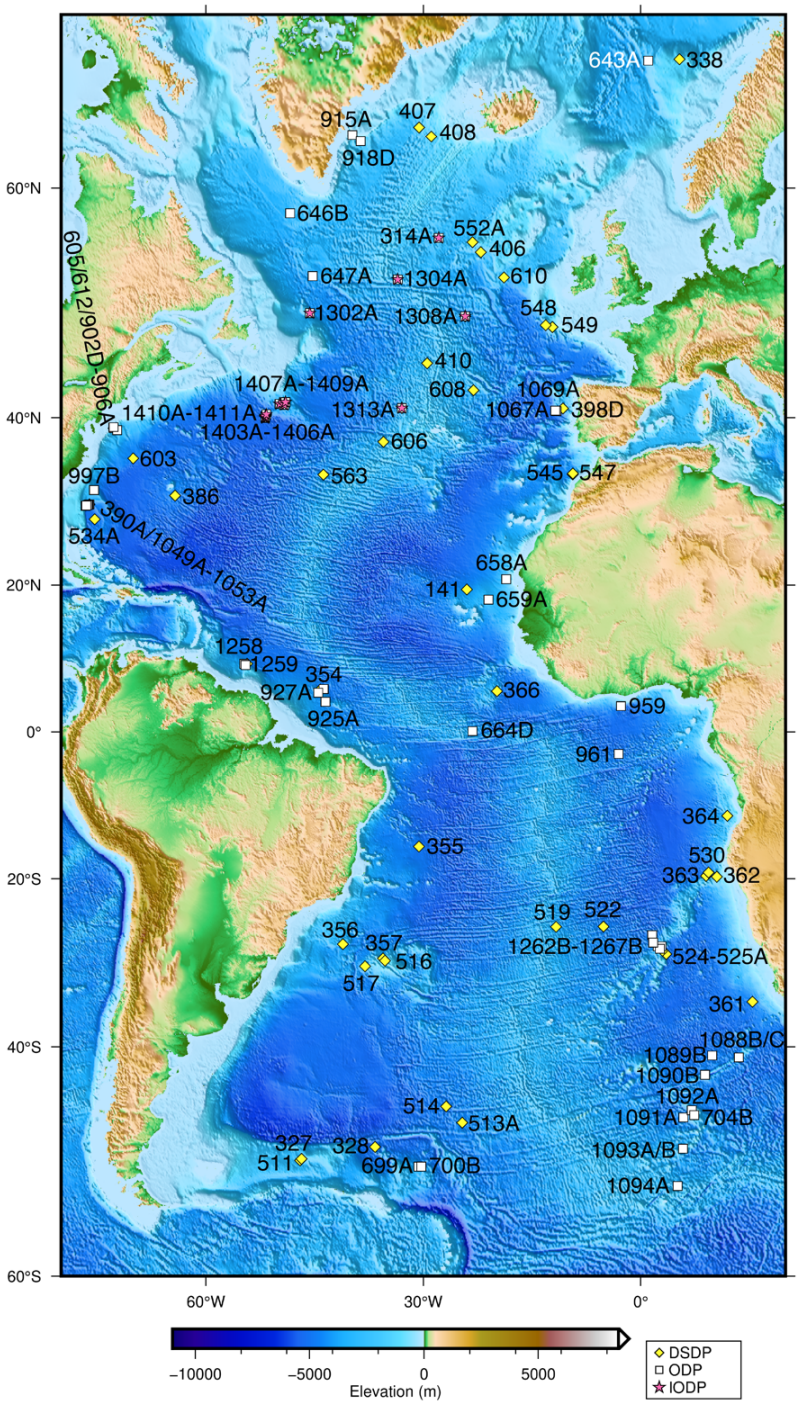

Figure 11. Drill holes in the Atlantic Ocean used in this study. The map incorporates elevation from the ETOPO1 global relief model (https://www.ngdc.noaa.gov/mgg/global/; Amante & Eakins, 2009). Mercator projection.

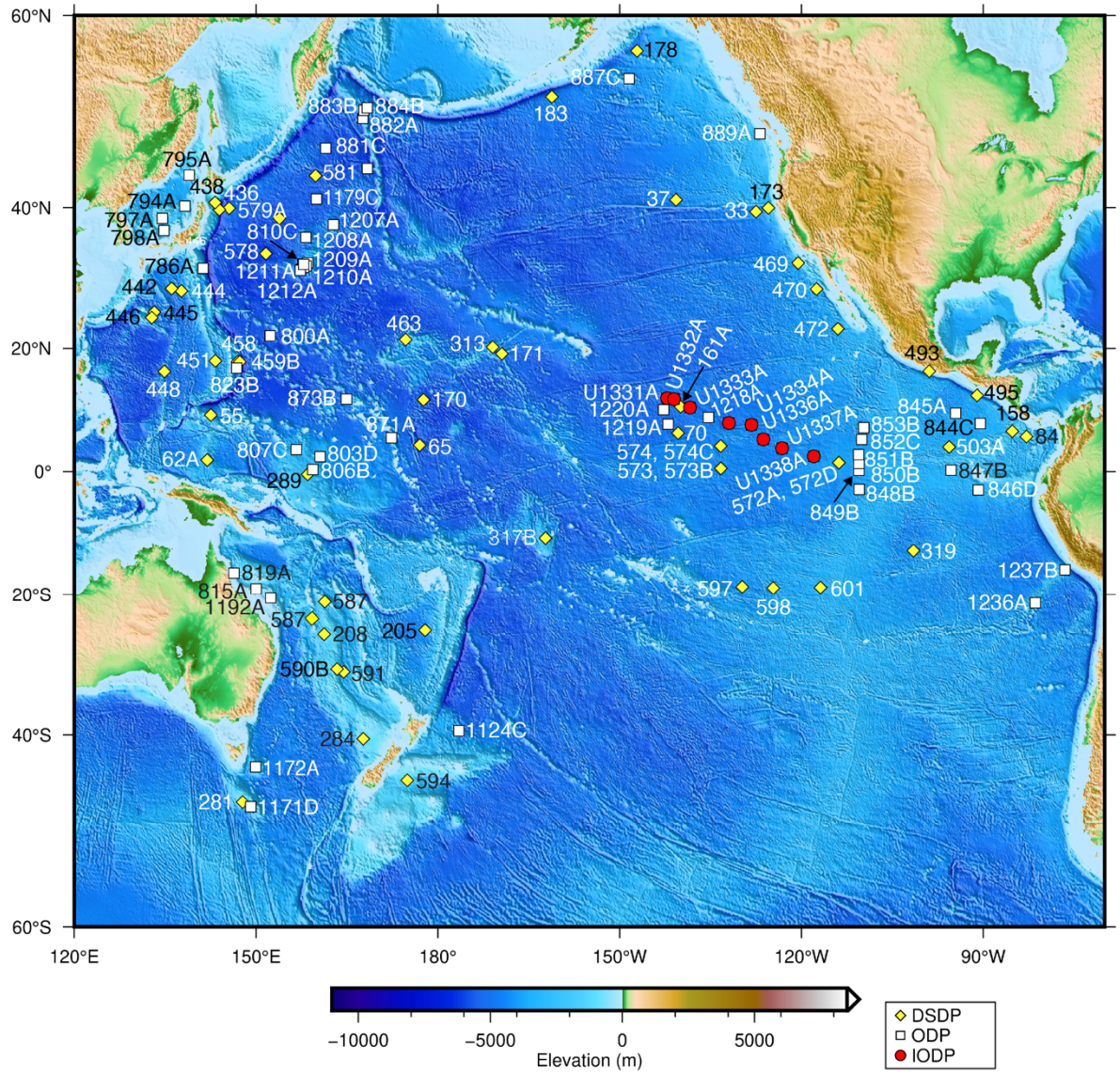

Figure 12. Drill holes in the Pacific Ocean used in this study. The map incorporates elevation from the ETOPO1 global relief model (https://www.ngdc.noaa.gov/mgg/global/; Amante & Eakins, 2009). Mercator projection.

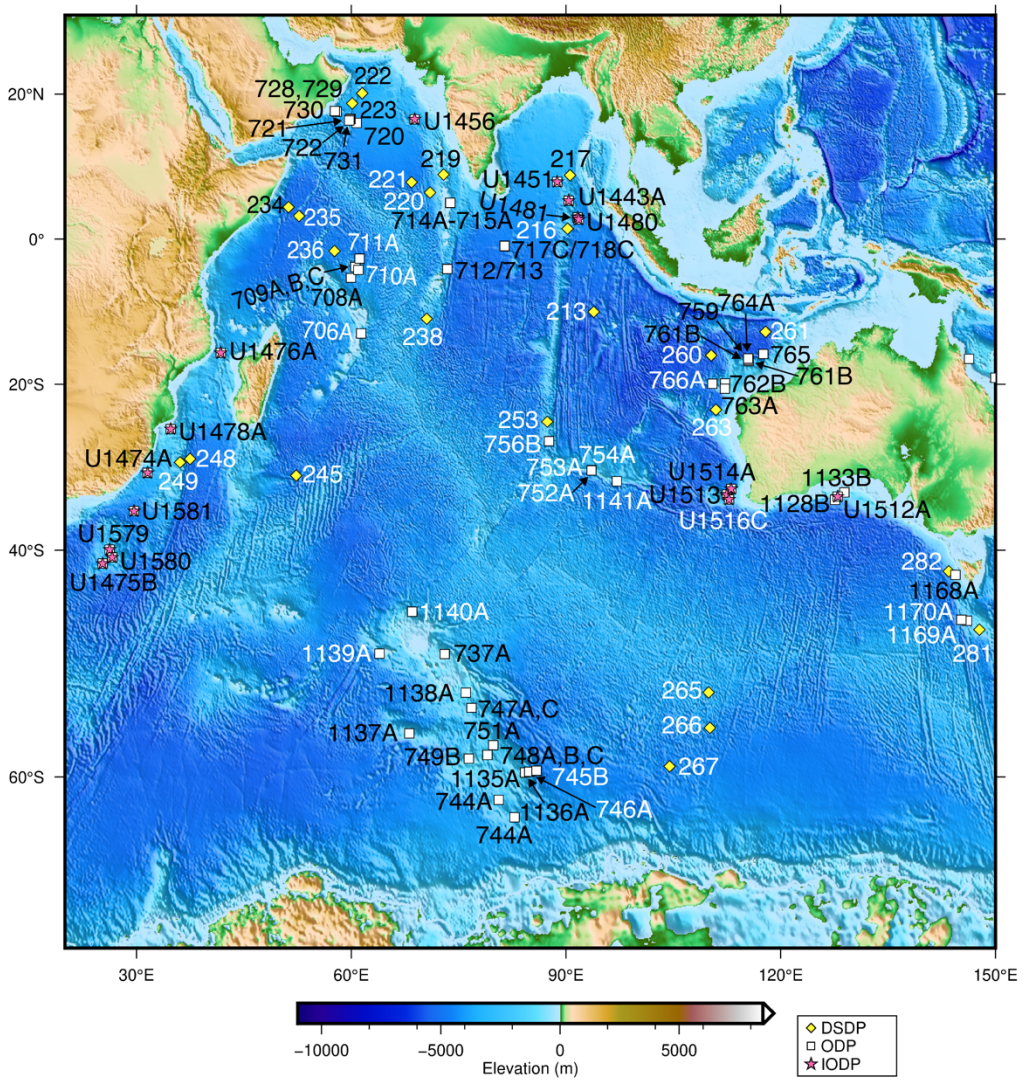

Figure 13. Drill holes in the Indian Ocean used in this study. The map incorporates elevation from the ETOPO1 global relief model (https://www.ngdc.noaa.gov/mgg/global/; Amante & Eakins, 2009). Mercator projection.

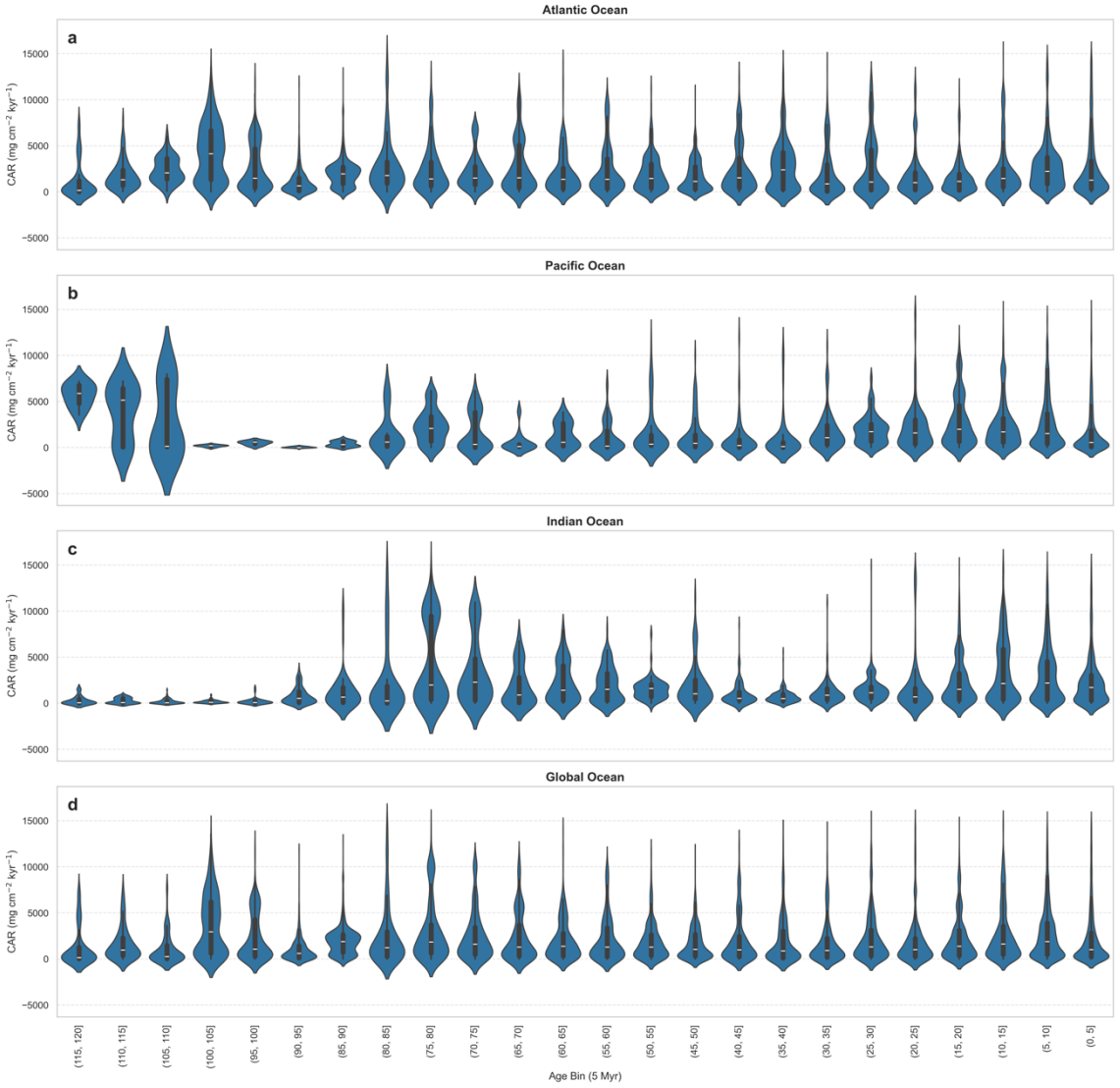

Figure 14. Violin plots showing distribution of carbonate accumulation rates (CAR) resolved in 5 Myr age bins from 0 to 120 Ma for the Atlantic (a), Pacific (b), Indian (c), and Global (d) oceans. Violin plots summarize the full probability density of CAR values (mg cm^{-2} kyr^{-1}) within each bin, where violin width reflects the relative concentration at a given accumulation rate. Narrow violins indicate temporally stable carbonate burial with limited dispersion, whereas broader violins and elongated upper tails signify increased variability and episodic high-accumulation events.

Supplementary Tables

Table 1. Deep-sea drill sites used in this study from the Deep Sea Drilling Project (DSDP), Ocean Drilling Program (ODP), and International Ocean Discovery Program (IODP) across the Atlantic Ocean. Drill site information, including longitude, latitude, water depth, penetrated sediment thickness, and basement reached, is sourced from initial reports archived in the DSDP, ODP, and IODP expeditions databases. Basement depths are calculated utilizing pyBacktrack 1.4 (Müller et al., 2018). Oceanic basement ages are constrained using the oceanic crustal age grid of Seton et al. (2020) combined with the age-depth relationship of Stein and Stein (1992) to compute tectonic subsidence. For continental crust, stretching factors are obtained from the global grids of Müller et al. (2019) (available at https://www.earthbyte.org/webdav/ftp/Data_Collections/Muller_etal_2019_Tectonics/Muller_etal_20

19_TotalStretchingFactors/) and the global plate tectonic model of Müller et al. (2019). NN–Northent North Atlantic, CN–Central North Atlantic, SA– South Atlantic.

Site name	Locality	Longitude (°)	Latitude (°)	Water depth (m)	Sediment thickness penetrated (m)	Oceanic basement age (Ma)	CC- Rift start (Ma)	CC- Rift end (Ma)	Basement reached
DSDP 14-141	CN	-24.0	19.4	4148	298	134.2			Yes
DSDP 36-327A	SA	-46.8	-50.9	2400	469.5		151	126	No
DSDP 36-328	SA	-36.7	-49.8	5095	397	127.0			No
DSDP 38-338	NN	5.4	67.8	1297	427.5	58.9			Yes
DSDP 39-354	CN	-44.2	5.9	4052	900	71.4			Yes
DSDP 39-355	SA	-30.6	-15.7	4901	461.5	80.5			Yes
DSDP 39-356	SA	-41.1	-28.3	3175	741	101.3			No
DSDP 39-357	SA	-35.6	-30.0	2086	797	92.6			No
DSDP 40-361	SA	15.4	-35.1	4549	1314	131.0			No
DSDP 40-362	SA	10.5	-19.8	1325	1081	126.0			No
DSDP 40-363	SA	9.0	-19.6	2248	715	115.7			No
DSDP 40-364	SA	12.0	-11.6	2448	1086	123.5			No
DSDP 41-366/366A	CN	-19.9	5.7	2853	850.5	78.4			No
DSDP 43-384	NN	-51.7	40.4	3909	195.3	129.6			Yes
DSDP 43-386	CN	-64.2	31.2	4782	973.8	118.4			Yes
DSDP 44-390A	CN	-76.1	30.1	2665	142.5	179.6			No
DSDP 47-398D	NN	-10.7	41.0	3910	1298		201	121	No
DSDP 48-406	NN	-22.1	55.3	2907	489.5		121	56	No
DSDP 49-407	NN	-30.6	63.9	2472	439.5	33.8			Yes
DSDP 49-408	NN	-28.9	63.4	1624	361	19.5			Yes
DSDP 49-410	CN	-29.5	45.5	2975	387.5	11.1			Yes
DSDP 71-511	SA	-47.0	-51.0	2589	632		151	126	No
DSDP 71-513A	SA	-24.6	-47.6	4373	380.5	34.9			Yes
DSDP 71-514	SA	-26.9	-46.0	4318	150.8	36.2			No
DSDP 72-516/516F	SA	-35.3	-30.3	1313	1270.6	92.1			Yes
DSDP 72-517	SA	-38.0	-30.9	2963	50.9	98.8			No
DSDP 73-519	SA	-11.7	-26.1	3769	151.6	12.3			Yes
DSDP 73-522	SA	-5.1	-26.1	4441	146.7	35.0			No
DSDP 73-524	SA	3.5	-29.5	4796	348.5	92.7			No
DSDP 74-525A	SA	3.0	-29.1	2467	574.6	88.3			Yes
DSDP 75-530	SA	9.4	-19.2	4629	996	117.1			No
DSDP 76-534A	CN	-75.4	28.3	4971	1666.5	169.7			No
DSDP 79-545	CN	-9.4	33.7	3142	701		241	155	No
DSDP 79-547A	CN	-9.3	33.8	3938	744.5		241	155	No
DSDP 80-548	NN	-12.2	48.9	1251	211		201	84	No
DSDP 80-548A	NN	-12.2	48.9	1251	345.5		201	84	Yes
DSDP 80-549A	NN	-13.1	49.1	2515	196		201	84	No
DSDP 81-552A	NN	-23.2	56.0	2301	183.5	60.5			Yes

Site name	Locality	Longitude (°)	Latitude (°)	Water depth (m)	Sediment thickness penetrated (m)	Oceanic basement age (Ma)	CC- Rift start (Ma)	CC- Rift end (Ma)	Basement reached
DSDP 82-563	CN	-43.8	33.6	3786	382.5	33.5			Yes
DSDP 93-603	CN	-70.0	35.5	4633	832.6	162.1			No
DSDP 93-605	CN	-72.6	38.7	2194	816.7	188.7			No
DSDP 94-607	NN	-33.0	41.0	3427	284.4	23.2			No
DSDP 94-608	NN	-23.1	42.8	3526	530.9	38.6			Yes
DSDP 94-609	NN	-24.2	49.9	3884	399.4	34.1			No
DSDP 94-610	NN	-18.9	53.2	2417	259.2		201	123.3	No
DSDP 94-606	CN	-35.5	37.3	3007	165.75	18.9			No
DSDP 95-612	CN	-72.8	38.8	1386	675.3	189.7			No
ODP 104-643A	NN	1.0	67.7	2769	565.2	48.5			No
ODP 105-646B	NN	-48.4	58.2	3440	766.7	55.2			No
ODP 105-647A	NN	-45.3	53.3	3869	716.6	54.0			Yes
ODP 108-658A	CN	-18.6	20.7	2264	300.4	180.3			No
ODP 108-659A	CN	-21.0	18.1	3071	273.8	153.3			No
ODP 108-664D	CN	-23.2	0.1	3802	296.8	10.4			No
ODP 114-699A	SA	-30.7	-51.5	3705.5	518.1	79.8			No
ODP 114-700B	SA	-30.3	-51.5	3601	489	78.2			No
ODP 114-704B	SA	7.4	-46.9	2532.3	671.7	67.8			No
ODP 150-902D	CN	-72.8	38.9	808	740.1	190.5			No
ODP 150-903A	CN	-72.8	38.9	444	702.8	190.6			No
ODP 150-903C	CN	-72.8	38.9	446	1149.7	190.6			No
ODP 150-904A	CN	-72.8	38.9	1123	576.7	190.0			No
ODP 150-905A	CN	-72.3	38.6	2698	910.6	186.8			No
ODP 150-906A	CN	-72.8	39.0	913	602.4	190.7			No
ODP 151-911A	NN	8.2	80.5	902	505.8		69	19	No
ODP 151-913B	NN	-6.9	75.5	3318	684.3	53.4			No
ODP 152-915A	NN	-39.8	63.5	533	209.4		80	56	Yes
ODP 152-918A	NN	-38.6	63.1	1869	332.7	55.0			No
ODP 152-918D	NN	-38.6	63.1	1868	1012.8	55.0			Yes
ODP 154-925A	CN	-43.5	4.2	3042	930.4	76.7			No
ODP 154-927A	CN	-44.5	5.5	3314	312.5	72.7			No
ODP 154-929A/929E	CN	-43.7	6.0	4358	527.5	69.3			No
ODP 164-997A	CN	-75.5	31.8	2770	434.3	183.3			No
ODP 164-997B	CN	-75.5	31.8	2770	750.7	183.3			No
ODP 171-1049A	CN	-76.1	30.1	2656	191.9	179.6			No
ODP 171-1050C	CN	-76.2	30.1	2297	606	179.8			No
ODP 171-1051A	CN	-76.4	30.1	1983	644.6	179.9			No
ODP 171-1052A	CN	-76.6	30.0	1345	174.5	180.2			No
ODP 171-1052E	CN	-76.6	30.0	1344	684.8	180.2			No
ODP 171-1053A	CN	-76.5	30.0	1630	183.2	180.1			No

Site name	Locality	Longitude (°)	Latitude (°)	Water depth (m)	Sediment thickness penetrated (m)	Oceanic basement age (Ma)	CC- Rift start (Ma)	CC- Rift end (Ma)	Basement reached
ODP 173-1067A	NN	-11.6	40.7	5021	855.6		201	123.1	Yes
ODP 173-1068A	NN	-11.6	40.7	5044	955.8		201	124.0	Yes
ODP 173-1069A	NN	-11.8	40.7	5075	959.3		201	127.5	No
ODP 177-1088B/1088C	SA	13.6	-41.1	2081.2	233.4	109.0			No
ODP 177-1089B	SA	9.9	-40.9	4623.8	264.9	100.9			No
ODP 177-1090B	SA	8.9	-42.9	3699.4	397.5	92.2			No
ODP 177-1091A	SA	5.9	-47.1	4360.5	310.9	54.3			No
ODP 177-1092A	SA	7.1	-46.4	1976.3	188.5	66.6			No
ODP 177-1093A/1093B	SA	5.9	-50.0	3623.9	597.7	43.0			No
ODP 177-1094A	SA	5.1	-53.2	2807.6	158.6	23.9			No
ODP 208-1262B	SA	1.6	-27.2	4753.6	209.9	70.6			No
ODP 208-1263A	SA	2.8	-28.5	2717.1	345.6	87.6			No
ODP 208-1264A	SA	2.8	-28.5	2507	280.7	87.8			No
ODP 208-1265A	SA	2.6	-28.8	3059.8	321	87.0			No
ODP 208-1266A/1266C	SA	2.3	-28.5	3796.6	334.2	85.7			No
ODP 208-1267B	SA	1.7	-28.1	4355.1	329	71.0			No
IODP 303-U1302A	NN	-45.6	50.2	3569	107.1		201	84	No
IODP 303-U1304A	NN	-33.5	53.1	3069	239	12.0			No
IODP 303-U1308A	NN	-24.2	49.9	3871	341.1	34.1			No
IODP 306-U1313A	NN	-33.0	41.0	3412	308.6	23.2			No
IODP 306-U1314A	NN	-27.9	56.4	2799	258.4	38.9			No
IODP 342-U1403A	NN	-51.8	39.9	4944	253.3	127.1			No
IODP 342-U1404A	NN	-51.8	40.0	4742	308.8	127.6			No
IODP 342-U1405A	NN	-51.8	40.1	4286	308.6	128.6			No
IODP 342-U1406A	NN	-51.7	40.4	3815	283.3	129.4			No
IODP 342-U1407A	NN	-49.8	41.4	3073	308.7	129.9			No
IODP 342-U1408A	NN	-49.8	41.4	3022	246.5	129.9			No
IODP 342-U1410A	NN	-49.2	41.3	3387	259.8	126.4			No
IODP 342-U1411B	NN	-49.0	41.6	3299	254.2	129.5			No

Table 2. Deep-sea drill sites used in this study from the Deep Sea Drilling Project (DSDP), Ocean Drilling Program (ODP), and Integrated Ocean Drilling Program (IODP) across the Pacific Ocean. Drill site information, including longitude, latitude, water depth, penetrated sediment thickness, and basement reached, is sourced from initial reports archived in the DSDP, ODP, and IODP expeditions databases. Basement depths are calculated utilizing pyBacktrack 1.4 (Müller et al., 2018). Oceanic basement ages are constrained using the oceanic crustal age grid of Seton et al. (2020) combined with the age-depth relationship of Stein and Stein (1992) to compute tectonic subsidence. For continental crust, stretching factors are obtained from the global grids of Müller et al. (2019) (available at https://www.earthbyte.org/webdav/ftp/Data_Collections/Muller_etal_2019_Tectonics/Muller_etal_2019_TotalStretchingFactors/) and the global plate tectonic model of Müller et al. (2019). EN–Eastern North Pacific, WN–Western North Pacific, EEQ–Eastern Equatorial Pacific, WT–Western Tropical Pacific, ES–Eastern South Pacific, WS–Western South Pacific.

Site name	Locality	Longitude (°)	Latitude (°)	Water depth (m)	Sediment thickness penetrated (m)	Oceanic basement age (Ma)	CC- Rift start (Ma)	CC- Rift end (Ma)	Basement reached
DSDP 5-33	EN	-127.5	39.5	4284	287	26.5			No
DSDP 5-37	EN	-140.7	41.0	4682	30.6	27.8			Yes
DSDP 6-55	WT	142.5	9.3	2850	119.1	154.4			No
DSDP 7-62A	WT	141.9	1.9	2607	303.3	28.5			No
DSDP 7-65	WT	177.0	4.4	6142	130.5	137.7			No
DSDP 8-70	EEQ	-140.4	6.3	5059	98	52.8			No
DSDP 9-84	EEQ	-82.9	5.7	3096	213.3	10.3			No
DSDP 16-158	EEQ	-85.2	6.6	1953	249.9	14.0			Yes
DSDP 16-161	EEQ	-140.0	10.7	4939	245.1	49.1			Yes
DSDP 17-170	WT	177.6	11.8	5792	30.7	147.3			Yes
DSDP 17-171	WT	-169.5	19.1	2290	173.3	113.8			Yes
DSDP 18-173	EN	-125.5	40.0	2927	196	20.5			Yes
DSDP 18-178	EN	-147.1	57.0	4218	212.5	39.3			Yes
DSDP 19-183	EN	-161.2	52.6	4708	344	54.6			Yes
DSDP 21-205	ES	177.9	-25.5	4320	42.1	29.8			Yes
DSDP 21-208	WS	161.2	-26.1	1545	255.4		101	59	No
DSDP 29-284	WS	167.7	-40.5	1166	166.8		101	59	No
DSDP 30-289	WT	158.5	-0.5	2206	712.6	146.5			Yes
DSDP 32-305	WN	157.9	32.0	2903	631	147.2			No
DSDP 32-313	WT	-171.0	20.2	3484	220.5	111.9			Yes
DSDP 33-317B	WS	-162.3	-11.0	2598	308	125.4			No
DSDP 34-319	ES	-101.5	-13.0	4296	99.33	15.1			Yes
DSDP 56-436	WN	145.6	39.9	5240	240.8	134.0			No
DSDP 57-438A	WN	143.2	40.6	1558	878		31.3	0	No
DSDP 57-440	WN	143.9	39.7	4509	814		22	0	No
DSDP 58-442A	WN	136.1	29.0	4649	313.5	19.9			No
DSDP 58-444	WN	137.7	28.6	4852	91.5	17.0			No
DSDP 58-445	WN	133.2	25.5	3377	892	82.2			No
DSDP 58-446	WN	132.8	24.7	4980	197.1	77.0			No
DSDP 59-448	WT	134.9	16.3	3483	234	83.9			No
DSDP 59-451	WT	143.3	18.0	2060	280.1	75.0			No
DSDP 60-458	WT	146.9	17.9	3453	97.83	67.1			Yes
DSDP 60-459B	WT	147.3	17.9	4121	182.14	67.1			Yes
DSDP 62-463	WT	174.7	21.4	2525	301.8	150.2			No
DSDP 63-469	EN	-120.5	32.6	3790	170.2	17.3			No
DSDP 63-470	EN	-117.5	28.9	3549	90	15.1			Yes
DSDP 63-472	EN	-114.0	23.0	3831	65.11	13.9			Yes
DSDP 66-493	EEQ	-98.9	16.4	645	556.5		37.7	0	Yes
DSDP 67-495	EEQ	-91.0	12.5	4140	446.5	24.6			Yes
DSDP 68-503A	EEQ	-95.6	4.1	3672	138	10.0			No

Site name	Locality	Longitude (°)	Latitude (°)	Water depth (m)	Sediment thickness penetrated (m)	Oceanic basement age (Ma)	CC- Rift start (Ma)	CC- Rift end (Ma)	Basement reached
DSDP 85-572A	EEQ	-113.8	1.4	3893	154.35	15.6			No
DSDP 85-572D	EEQ	-113.8	1.4	3893	258.87	15.6			Yes
DSDP 85-573	EEQ	-133.3	0.5	4301	159.4	37.0			No
DSDP 85-573B	EEQ	-133.3	0.5	4301	279.7	37.0			Yes
DSDP 85-574	EEQ	-133.3	4.2	4561	208.93	35.9			No
DSDP 85-574C	EEQ	-133.3	4.2	4561	197.35	35.9			Yes
DSDP 86-577	WN	157.7	32.4	2675	118.8	146.9			No
DSDP 86-578	WN	151.629	33.9	6010	165.02	140.5			No
DSDP 86-579A	WN	153.8	38.6	5736.6	115.87	134.1			No
DSDP 86-581	WN	159.8	43.9	5476	77.59	126.5			Yes
DSDP 90-587	WS	161.3	-21.2	1101	88.81		101	59	No
DSDP 90-588	WS	161.2	-26.1	1533	236		101	59	No
DSDP 90-590B	WS	163.4	-31.2	1299	465.26		101	59	No
DSDP 90-591	WS	164.4	-31.6	2131	278.21		101	59	No
DSDP 90-594	WS	174.9	-45.5	1204	161.55		41	0	No
DSDP 92-597	ES	-129.8	-18.8	4157.1	42.1	27.3			Yes
DSDP 92-598	ES	-124.7	-19.0	3699	41.2	18.1			No
DSDP 92-601	ES	-116.9	-18.9	3433	20.4	4.9			No
ODP 125-786A	WN	141.2	31.9	3058.1	166.5	134			Yes
ODP 127-794A	WN	138.2	40.2	2811	351.3		201	0	No
ODP 127-795A	WN	139.0	44.0	3300.2	364.9	27.2			Yes
ODP 127-797B	WN	134.5	38.6	2862.2	495.7		201	0	Yes
ODP 128-798A	WN	134.8	37.0	903.1	495.7		201	0	Yes
ODP 129-800A	WT	152.3	21.9	5686	150.73	160.8			Yes
ODP 130-803D	WT	160.5	2.4	3412.2	494.96	151.9			Yes
ODP 130-806B	WT	159.4	0.3	2519.9	666.36	148.2			No
ODP 130-807C	WT	156.6	3.6	2805.7	252.84	156.3			Yes
ODP 132-810C	WN	157.8	32.4	2623	136.1	146.8			No
ODP 133-815A	WS	150.0	-19.2	465.5	473.5		123	48	No
ODP 133-819A	WS	146.3	-16.6	565.2	400		123	48	No
ODP 133-823B	WT	146.8	16.9	1638.4	123.73	69.5			No
ODP 138-844C	EEQ	-90.5	7.9	3414.5	189.34	17.3			No
ODP 138-845A	EEQ	-94.6	9.6	3704.2	292.63	15.9			No
ODP 138-846D	EEQ	-90.8	-3.1	3295.8	247.85	16.9			No
ODP 138-847B	EEQ	-95.3	0.2	3334.3	242.19	9.9			No
ODP 138-848B	EEQ	-110.5	-3.0	3855.6	97.75	9.5			No
ODP 138-849B	EEQ	-110.5	0.2	3839.1	343.78	10.5			No
ODP 138-850B	EEQ	-110.5	1.3	3786.1	393.58	10.8			No
ODP 138-851B	EEQ	-110.6	2.8	3760.3	318.05	11.7			Yes
ODP 138-852C	EEQ	-110.1	5.3	3859.8	107.1	10.2			No

Site name	Locality	Longitude (°)	Latitude (°)	Water depth (m)	Sediment thickness penetrated (m)	Oceanic basement age (Ma)	CC- Rift start (Ma)	CC- Rift end (Ma)	Basement reached
ODP 138-853B	EEQ	-109.8	7.2	3715.5	77.68	8.7			Yes
ODP 144-871A	WT	172.3	5.6	1254.6	126.05	152.0			No
ODP 144-873B	WT	164.9	11.9	1334	53.83	176.3			No
ODP 145-881C	WN	161.5	47.1	5530.8	227.2	118.9			No
ODP 145-882A	WN	167.6	50.4	3243.8	411.2	114.6			No
ODP 145-883B	WN	167.8	51.2	2395.6	695	113.0			Yes
ODP 145-883E	WN	167.8	51.4	2385.5	344.3	112.6			Yes
ODP 145-884B	WN	168.3	51.5	3824.8	791.76	112.6			Yes
ODP 145-885A	EN	-168.2	44.7	5713.3	67.1	83.7			No
ODP 145-887C	EN	-148.4	54.4	3633.6	269.44	35.3			Yes
ODP 146-889A	EN	-126.9	48.7	1311.2	325.8	20.5			No
ODP 181-1124C	WS	-176.5	-39.5	3962	473.1	127.5			No
ODP 184-1143A	WT	113.3	9.4	2772	325.8		41	0	No
ODP 189-1171C	WS	149.1	-48.5	2147.8	252.5		161	34	No
ODP 189-1171D	WS	149.1	-48.5	2147.8	711		161	34	No
ODP 189- 1172A	WS	149.9	-44.0	2620	508.9		161	34	No
ODP 191-1179C	WN	160.0	41.1	5563.9	287.4	132.7			Yes
ODP 194-1192A	WS	152.4	-20.6	4126	242.5		123	50	No
ODP 198-1207A	WN	162.8	37.8	3100.8	243.4	138.1			No
ODP 198-1208A	WN	158.2	36.1	3345.7	392.3	140.2			No
ODP 198-1209A	WN	158.5	32.7	2387.2	263.6	146.1			No
ODP 198-1210A	WN	158.3	32.2	2573.5	251.2	146.7			No
ODP 198-1211A	WN	157.9	32.0	2907.5	169.9	147.1			No
ODP 198-1212A	WN	157.7	32.4	2682.5	101.6	146.9			No
ODP 199-1218A	EEQ	-135.4	8.9	4826.3	265.9	43.0			Yes
ODP 199-1219A	EEQ	-142.0	7.8	5063.4	236.8	56.0			Yes
ODP 199-1220A	EEQ	-142.8	10.2	5217.9	119.2	56.6			No
ODP 202-1236A	ES	-81.4	-21.4	1323	167.7	39.2			No
ODP 202-1237B	ES	-76.6	-16.1	3212	331.4	44.2			No
IODP 320-U1331A	EEQ	-142.2	12.1	5120.92	154.4	54.0			Yes
IODP 320-U1332A	EEQ	-141.0	11.9	4917.62	145.7	51.0			Yes
IODP 320-U1333A	EEQ	-138.4	10.5	4858.82	176.1	46.3			Yes
IODP 320-U1334A	EEQ	-132.0	8.0	4793.22	288.6	38.9			Yes
IODP 320-U1335A	EEQ	-126.3	5.3	4333.02	421.6	25.3			No
IODP 320-U1336A	EEQ	-128.3	7.7	4291.02	258.9	34.4			No
IODP 321-U1337A	EEQ	-123.2	3.8	4465.62	419.6	22.1			Yes
IODP 321-U1338A	EEQ	-118.0	2.5	4204.52	345.6	18.5			Yes

Table 3. Deep-sea drill sites used in this study from the Deep Sea Drilling Project (DSDP), Ocean Drilling Program (ODP), and International Ocean Discovery Program (IODP) across the Indian

Ocean. Drill site information, including longitude, latitude, water depth, penetrated sediment thickness, and basement reached, is sourced from initial reports archived in the DSDP, ODP, and IODP expeditions databases. Basement depths are calculated utilizing pyBacktrack 1.4 (Müller et al., 2018). Oceanic basement ages are constrained using the oceanic crustal age grid of Seton et al. (2020) combined with the age-depth relationship of Stein and Stein (1992) to compute tectonic subsidence. For continental crust, stretching factors are obtained from the global grids of Müller et al. (2019) (available at https://www.earthbyte.org/webdav/ftp/Data_Collections/Muller_etal_2019_Tectonics/Muller_etal_2019_TotalStretchingFactors/) and the global plate tectonic model of Müller et al. (2019). WN–Western North Indian, EE–Eastern Equatorial Indian, WE–Western Equatorial Indian, ES–Eastern South Indian, WS– Western South Indian, SO–Southern Ocean.

Site name	Locality	Longitude (°)	Latitude (°)	Water depth (m)	Sediment thickness penetrated (m)	Oceanic basement age (Ma)	CC- Rift start (Ma)	CC- Rift end (Ma)	Basement reached
DSDP 22-213	ES	93.9	-10.2	5611	173.5	58.2			Yes
DSDP 22-216	WE	90.2	1.5	2262	477.5	71.6			Yes
DSDP 22-217	WE	90.5	8.9	3030	614	83.2			No
DSDP 23-219	WE	72.9	9.0	1764	411	65.0			No
DSDP 23-220	WE	71.0	6.5	4036	350	53.0			Yes
DSDP 23-222	WN	61.5	20.1	3546	1300	63.3			No
DSDP 23-223	WN	60.1	18.7	3633	740	61.2			No
DSDP 23-221	WE	68.4	8.0	4650	270	47.8			Yes
DSDP 24-234	WE	51.2	4.5	4721	247	129.6			No
DSDP 24-235	WE	52.7	3.2	5130	684	56.9			No
DSDP 24-236	WE	57.6	-1.7	4487	327.5	60.8			Yes
DSDP 24-238	WE	70.5	-11.2	2832	586.5	34.1			Yes
DSDP 25-245	SW	52.3	-31.5	4857	396.5	61.0			Yes
DSDP 25-248	WS	37.5	-29.5	4994	434	130.1			Yes
DSDP 25-249	WS	36.1	-29.9	2088	412	129.7			Yes
DSDP 26-253	ES	87.4	-24.9	1962	546.5	45.7			No
DSDP 26-258	ES	112.5	-33.8	2793	123.5		161.00	130.1	No
DSDP 27-260	ES	110.3	-16.1	5702	329.7	130.7			Yes
DSDP 27-261	ES	117.9	-12.9	5667	570.89	153.1			Yes
DSDP 27-263	ES	111.0	-23.3	5048	746	132.8			No
DSDP 28-265	SO	109.9	-53.5	3581	462	13.8			Yes
DSDP 28-266	SO	110.1	-56.4	4173	384	22.4			Yes
DSDP 28-267	SO	104.5	-59.3	4522	290	35.3			Yes
DSDP 29-281	ES	147.8	-48.0	1591	169		161.00	34	No
DSDP 29-282	ES	143.5	-42.2	4202	311.5		161.00	34	Yes
ODP 115-706A	WE	61.4	-13.1	2504.3	47.5	46.2			No
ODP 115-708A	WE	59.9	-5.5	4109.3	236.2	56.6			Yes
ODP 115-709A,B,C	WE	60.6	-3.9	3047	353.7	55.4			No
ODP 115-710A	WE	61.0	-4.3	3822.5	209.7	53.4			No
ODP 115-711A	WE	61.2	-2.7	4439	249.6	51.2			No

Site name	Locality	Longitude (°)	Latitude (°)	Water depth (m)	Sediment thickness penetrated (m)	Oceanic basement age (Ma)	CC- Rift start (Ma)	CC- Rift end (Ma)	Basement reached
ODP 115-712	WE	73.4	-4.2	2904.3	115.3	52.8			Yes
ODP 115-713	WE	73.4	-4.2	2920	191.7	52.8			Yes
ODP 115-714A	WE	73.8	5.1	2042	233	64.6			No
ODP 115-715A	WE	73.8	5.1	2266.3	287.8	64.8			Yes
ODP 116-717C	WE	81.4	-0.9	4734.7	828.2	80.7			No
ODP 116-718C	WE	81.4	-1.0	4730.2	935	80.5			No
ODP 116-719A	WE	81.4	-1.0	4736.8	460.2	80.5			No
ODP 117-720A	WN	60.7	16.1	4037.5	414.3	57.8			No
ODP 117-721A	WN	59.9	16.7	1955.3	86.4	58.4			No
ODP 117-721B	WN	59.9	16.7	1944.8	424.2	58.4			No
ODP 117-722A	WN	59.8	16.6	2027.8	280	58.2			No
ODP 117-728A	WN	57.8	17.7	1427.8	346.4	31.4			No
ODP 117-729A	WN	58.0	17.6	1398.5	109.1	32.0			No
ODP 117-730A	WN	57.7	17.7	1065.8	403.9	31.2			No
ODP 117-731A	WN	59.7	16.5	2365.8	409	57.0			No
ODP 119-737A	WN	73.0	-50.2	574.5	273.2	76.7			No
ODP 119-738B,C	SO	82.8	-62.7	2252.7	533.8	128.3			No
ODP 119-744A	SO	80.6	-61.6	2307.3	176.1	124.2			No
ODP 119-745B	SO	85.9	-59.6	4082.5	215	127.7			No
ODP 119-746A	SO	85.9	-59.6	4059.5	280.8	127.7			No
ODP 120-747A,C	SO	76.8	-54.8	1695	350	116.4			No
ODP 120-748A,B,C	SO	79.0	-58.4	1290	935		161.00	126	Yes
ODP 120-749B	SO	76.4	-58.7	1069.5	123.8		161.00	126	No
ODP 120-751A	SO	79.8	-57.7	1988	166.2	130.4			No
ODP 121-752A	ES	93.6	-30.9	1086.3	308	51.3			No
ODP 121-753A	ES	93.6	-30.8	1176.1	62.8	53.6			No
ODP 121-754A	ES	93.6	-30.9	1063.6	172.1	51.3			No
ODP 121-756B	ES	87.6	-27.4	1518.1	395.6	47.4			No
ODP 121-757B	ES	88.2	-17.0	1650.2	369.3	50.8			Yes
ODP 121-758A	ES	90.4	5.4	2923.6	527.1	78.1			Yes
ODP 122-760A	ES	115.5	-16.9	1969.7	284.9		161.00	155	No
ODP 122-761B	ES	115.5	-16.7	2188.8	286		161.00	155	No
ODP 122-762B,C	ES	112.3	-19.9	1360	940		161.00	155	No
ODP 122-763A,B	ES	112.2	-20.6	1367.5	653.5		161.00	155	No
ODP 122-764A	ES	115.5	-16.6	2698.6	69		161.00	155	No
ODP 123-766A	ES	110.5	-19.9	3997.5	471	154.5			No
ODP 182-1128	ES	127.6	-34.4	3876	280.7		161.00	34	No
ODP 183-1133B	ES	128.9	-33.5	1037.2	152.1		161.00	34	No
ODP 183-1135A	SO	84.3	-59.7	1566.6	526		161.00	126	No

Site name	Locality	Longitude (°)	Latitude (°)	Water depth (m)	Sediment thickness penetrated (m)	Oceanic basement age (Ma)	CC- Rift start (Ma)	CC- Rift end (Ma)	Basement reached
ODP 183-1136A	SO	84.8	-59.7	1930	128		161.00	126	Yes
ODP 183-1137A	SO	68.1	-56.8	1004.5	228.4		161.00	126	Yes
ODP 183-1138A	SO	76.0	-53.6	1141.4	698.1	114.0			Yes
ODP 183-1139A	SO	63.9	-50.2	1415.3	469.9	73.1			No
ODP 183-1140A	SO	68.5	-46.3	2394.1	237.3	43.0			Yes
ODP 183-1141A	ES	97.1	-32.2	1196.9	185.6	45.5			Yes
ODP 189-1168A	ES	144.4	-42.6	2463.3	883.5		161.00	34	No
ODP 189-1169A	ES	145.2	-47.1	3568	246.3		161.00	36.8	No
ODP 189-1170A,D	ES	146.0	-47.2	2704.7	464.3		161.00	34	No
IODP 353-U1443A	EE	90.4	5.4	2929.45	344	78.1			No
IODP 354-U1451	EE	88.7	8.0	3607.28	582.1	82.3			No
IODP 355-U1456	WN	68.8	16.6	3639.23	426.6	64.9			No
IODP 361-U1474A	WS	31.5	-31.2	3033.82	254.1	139.5			No
IODP 361-U1475B	WS	25.3	-41.4	2669.46	243.9	90.2			No
IODP 361-U1476A	WS	41.8	-15.8	2165.71	224.2	148.1			No
IODP 361-U1478A	WS	34.8	-25.8	487.94	248.4	150.4			No
IODP 362-U1480	WS	91.6	3.0	4147.51	815	68.0			YES
IODP 362-U1481A	WS	91.8	2.8	4178.32	1500	67.5			No
IODP 369-U1512A	ES	128.0	-34.0	3070.87	700.8		161.00	34	No
IODP 369-U1513	ES	112.5	-33.8	2789.19	292.5		161.00	130.1	YES
IODP 369-1514A	ES	113.1	-33.1	3838.2	515.59		161.00	129.1	No
IODP 369-U1516C	ES	112.8	-34.3	2676.46	540.1		161.00	127.4	No
IODP 392-U1579	ES	26.2	-40.0	2492.92	1165.4	104.3			YES
IODP 369-U1580	ES	26.6	-40.8	2560.33	611.7	94.8			YES
IODP 369-U1581	ES	29.7	-35.7	4591.35	1297.6	109.3			No

References

Amante, C., & Eakins, B. W. (2009). *ETOPO1 arc-minute global relief model: procedures, data sources and analysis*. Retrieved from National Geophysical Data Center, NOAA: https://repository.library.noaa.gov/view/noaa/1163

Müller, R. D., Cannon, J., Williams, S., & Dutkiewicz, A. (2018). PyBacktrack 1.0: A tool for reconstructing paleobathymetry on oceanic and continental crust. *Geochemistry, Geophysics, Geosystems, 19*(6), 1898-1909. https://doi.org/10.1029/2017GC007313

Müller, R. D., Zahirovic, S., Williams, S. E., Cannon, J., Seton, M., Bower, D. J., et al. (2019). A global plate model including lithospheric deformation along major rifts and orogens since the Triassic. *Tectonics, 38*(6), 1884-1907. https://doi.org/10.1029/2018TC005462

Seton, M., Müller, R. D., Zahirovic, S., Williams, S., Wright, N. M., Cannon, J., et al. (2020). A global data set of present-day oceanic crustal age and seafloor spreading

parameters. *Geochemistry, Geophysics, Geosystems, 21*(10), e2020GC009214. https://doi.org/10.1029/2020GC009214

Stein, C. A., & Stein, S. (1992). A model for the global variation in oceanic depth and heat flow with lithospheric age. *Nature, 359*(6391), 123-129. https://doi.org/10.1038/359123a0